Table of Contents

VOLUME 2

APPENDICES

Index of Tables

Index of Figures

Chapter 1. Introduction

1.1 Problem Overview

Residential construction represents a $200-250 billion per year industry accounting for approximately 50% of the overall construction expenditures in the United States. While concrete, masonry, and steel are used in residential construction, the above-grade structures are made of wood in more than 90 percent of new housing starts (NAHB 1996). Between one and two million new homes are built in the U.S. every year, predominantly out of dimension lumber framing. More efficient and improved utilization of wood, a renewable, energy efficient material is in need to help reduce some of the costs associated with residential construction. High economic losses in housing are caused by two major reasons: bio-deterioration and natural hazards. This study is focused on the response of light-frame buildings to lateral forces caused by natural hazards like hurricanes and earthquakes.

Walls as components of a building lateral force resisting system (Figure 1. 1) are referred to as *shear walls*. In light-frame buildings, shear walls typically consist of lumber framing and panel sheathing attached with dowel type fasteners (usually nails, staples, or screws). If designed to resist high wind and/or seismic forces, walls at each story often require mechanical fasteners, such as tie-down anchors and shear bolts, to provide continuous and complete load paths from the top of the building to the foundation. In this dissertation, the engineered walls are referred to as fully-anchored or anchored walls. Non-engineered walls, referred to as conventional walls, are secured to underlying structures by nails or shear bolts only.

The amount of material used in buildings is influenced by structural requirements to resist vertical loads (gravity) and lateral forces (wind and earthquake). Design of structures for gravity is generally well understood. At the same time, the performance of structures during recent natural disasters such as Hurricanes Andrew and Hugo and the Loma Prieta and Northridge earthquakes uncovered the immediate need for research into improving the high-wind and seismic design and construction of houses. Economic losses from just these four disasters were approximately $50 billion.

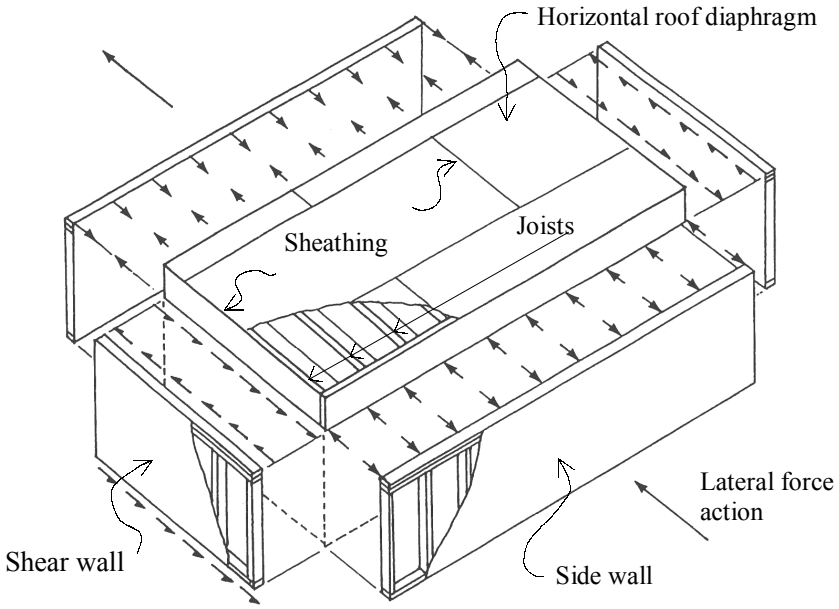

Figure 1. 1. Lateral force resisting system of a light-frame building (Diekmann 1995).

Southern states, such as Mississippi, Louisiana, Texas, and Florida, bordering the coastline suffer from hurricanes most of all. Historically, the most frequent forms of hurricane damage were related to roofing and roof sheathing, windows, and interior finish. After the 1992 Hurricane Andrew, the American Plywood Association (APA) increased requirements for roof sheathing attachment aiming at reduction of premature failures of roofs during high winds. Consequently, the forces from roofs and diaphragms will be transferred to walls, which should be designed and constructed to resist their share of the lateral load.

Americans are accustomed to thinking that earthquakes are something that only Californians have to worry about. That's a potentially lethal mistake. In fact, about 90 percent of the nation's population live in seismically active areas. More than 3,500 earthquakes have been recorded east of the Mississippi River since 1700, and a few of them have been significant. In 1886, Charleston, S.C. experienced a massive quake, variously estimated at between 7.1 and 7.5 in Richter's scale that leveled much of the city and killed 60 people. Two large New Madrid, MO, quakes in 1811 and 1812 have been estimated as 8-plus level in the Richter scale, which would be 1000 times stronger than the San Francisco 1906 earthquake. Two hundred years ago, the New Madrid area was mostly wilderness. Today, in the worst-case scenario, a magnitude 8 quake would wreak

havoc over a densely populated five-state area. Particularly at risk is Memphis, TN, 35 miles west of the epicenter of a 6.8 quake in 1843. A 1990 federal disaster drill projected as many as 2,200 dead and 18,000 injured and $40 billion of property damage. The environmental and economic losses will impact a large territory of the country far beyond the five-state area.

Light-frame wood buildings have exhibited varying performance in past earthquakes, depending on details of construction and plan and elevation configurations. In Table 1. 1, attributes of buildings exhibiting good and poor response are summarized. Timber framed structures generally perform well, because of light mass, which reduces inertial lateral forces, and because of a large number of redundancies, which allow load sharing between the elements (Deam, 1997). Most connections in wood structures provide ductility and dissipate large amounts of energy through hysteretic damping and friction. Slackness of connections appears to increase the natural period of vibration, therefore effectively reduces the maximum forces in structural elements (Dean *et al.*, 1986).

Table 1. 1. Performance of light-frame shear walls in past earthquakes.

Result	**Characteristic**	**Symptom**
Good performance	High specific strength of wood	Light mass of building
	Light mass of the building	Reduced inertia forces
	Multiple elements (redundancy)	Load share
	Ductile connections	Energy dissipation
	Slackness of the assembly	Increase natural period of vibration
	Simple symmetric shape of building	No torsion effects
	Adequate anchorage and connections	Continuous load paths
	Small windows and doors	Uniform stiffness, continuous load paths
Poor performance	Gypsum sheathing	Poor cyclic performance
	Deformational incompatibility	Unexpected collapse mechanism
	Large windows and doors	Interrupted load paths, torsion effects
	Horizontal and vertical irregularity	Torsion effects
	Inadequate anchorage and connections	Interrupted load paths, unexpected collapse mechanism
	Exceeded design loads	Collapse

Buildings have performed adequately if they worked as a unit, had adequate shear walls, and were reasonably symmetric in plan and elevation. Limited damage occurred to houses with simple rectangular configurations, continuous floors, and small door and window openings (Soltis and Falk, 1992). Structures with wood sheathing, straight laid or diagonally laid boards, or plywood on the walls have exhibited good to excellent performance. Structures which relied on other materials (such as gypsum wallboard) for bracing the walls have demonstrated poor performance and partial collapse (Zacher, 1994).

The primary cause of overall building damage has been improper design resulting in inadequate lateral support, particularly near large openings such as garage or patio doors of two-story houses. Another reason for structural failures has been improper installation of hold-down devices and/or lack of lateral bracing between building components. However, there have been a number of failures in walls with properly installed hold-down devices. These failures may have been caused by overload when the force levels exceeded the design levels, or were due to deformation incompatibilities between the hold-down devices and the wall sheathing, which has been observed during cyclic testing (Zacher, 1994).

Over the past several decades, the APA has supplied shear wall design information. Current design values for shear walls were proposed by the APA based on static monotonic tests on 2.4-m (8-ft.) square walls fully restrained against overturning. The tests were performed according to ASTM standards E 72 and E 564 using static unidirectional (i.e. monotonic) loading applied in several stages at a uniform rate of displacement. After experimental evaluation, equal shear performance characteristics were assigned to various structural sheathing materials -- such as plywood, oriented strandboard (OSB), and COM-PLY -- having the same thickness and span rating. The design capacity of other sheathing materials, such as interior drywall panels, was considered additive to the capacity of structural exterior sheathing.

Design values were established based on these tests as ultimate unit shear divided by a factor of safety or as a unit shear at a certain story drift. The factor of safety is a product of several factors, which take into account various conditions. The components

of the safety factor have not been published yet (Line 1998). The monotonic test results continue to be the standard by which all residential construction is designed. However, it is acknowledged that monotonic tests are insufficient for qualifying shear walls for use in seismic design.

Inspection of structural damage after the earthquakes and wind storms has resulted in emotional and reactionary rulings that have reduced allowable design values for light-frame construction unless the values are based on cyclic tests (Skaggs and Rose, 1996). The cyclic and dynamic responses of shear walls are not well studied and appear to be different from monotonic results. Some tests (Oliva, 1990, Schmidt *et al.*, 1994, Rose, 1998) indicated that the current design values might not be adequate for use if new performance criteria are considered such as displacement design instead of force design. Information such as the strength, ductility capacity, and anchorage requirements based on cyclic tests must be provided to evaluate safe and acceptable design values for light-frame walls.

In recent years, researchers proposed numerous cyclic and dynamic test procedures aimed at obtaining more realistic information on shear wall response to seismic loading. However, no standard cyclic or dynamic test protocol has yet been adopted in the US or internationally. Therefore, the monotonic test procedures remain an important means for testing high-wind resistance, comparing various wall configurations, and for calibrating alternative test protocols. Among the cyclic test procedures proposed to date in the US, the so-called *sequential-phased displacement* (SPD) procedure may be the most used. The SPD protocol is a sequence of a large number of reversed cycles generated at a constant frequency with gradually increasing amplitudes between phases, which include "decay" cycles (i.e., cycles with smaller amplitudes). This procedure was reported by Porter (1987) and adopted by the Structural Engineers Association of Southern California (SEAOSC 1997b).

Some investigators claim that it is imperative that a standard protocol for cyclic testing be developed so that seismic response and methods for preventing earthquake damage in the future are learned (Zacher, 1994). Other investigators think that as long as the cyclic test protocol is conservative and can be used for all materials, the performance

of various construction materials can be easily compared. It is also imperative that an acceptable analytical method be developed for converting experimental results from cyclic tests to design values.

The ideal approach to gain a better understanding of dynamic response of timber structures and to improve their performance is a comprehensive research plan that coordinates experimental and analytical approaches (Foliente, 1994). Results of the research would be a mechanics-based methodology that allows engineers to design shear walls of various configurations and boundary conditions. A few of the topics that a comprehensive research plan should address are geometry, openings, and construction detailing.

1.2 Research Needs

As Diekmann (1997) wittily remarked, our human lifestyle makes windows and doors in walls an inevitable fact of life. Narrow wall segments near corners, windows, and doors obstruct response of the whole lateral force resisting system.

Modern residential buildings represent a variety of plan layouts and construction practices. Consequently, the lateral force resisting system of a structure incorporates a number of shear walls of various lengths with openings; or put differently, a number of shear wall segments separated by openings of various size. Horizontal irregularities of residential buildings with intricate layouts of walls cause torsional effects, which are difficult to account for without knowing the force distribution among the walls. Indeed, the distribution depends on rigidity of horizontal diaphragms and the relative stiffness of the walls. Figure 1. 2 shows some typical examples of horizontal irregularity of residential buildings where intricate layouts of walls cause torsion effects which are difficult to account for without knowing the force distribution among the walls. Yet, before a rigid or flexible diaphragm is assumed, a designer needs to estimate maximum shear loads the walls can resist. It is reasonable to assume that maximum unit shear and deformational properties of shear walls depend on their aspect ratio, sheathing fastener density, amount of openings, and overturning restraint. The influence of these wall conditions on shear wall performance is not well studied.

The wall aspect ratio (ratio of height to length) may have an effect on the magnitude of the overturning moment and on the stress distribution experienced by the wall. For equivalent load, a tall narrow wall, with a large height to length ratio, is expected to generate a higher overturning moment than one with a smaller aspect ratio, which would influence the design of the overturning anchorage connections. In addition, as the length of the wall increases, the effect of shear distribution becomes greater, which may affect the magnitude of the deformations experienced by the assembly and may change the mode of failure. The effect of aspect ratio on shear wall performance was analyzed numerically by White and Dolan (1995). Experimental validation of the numerical investigation is needed.

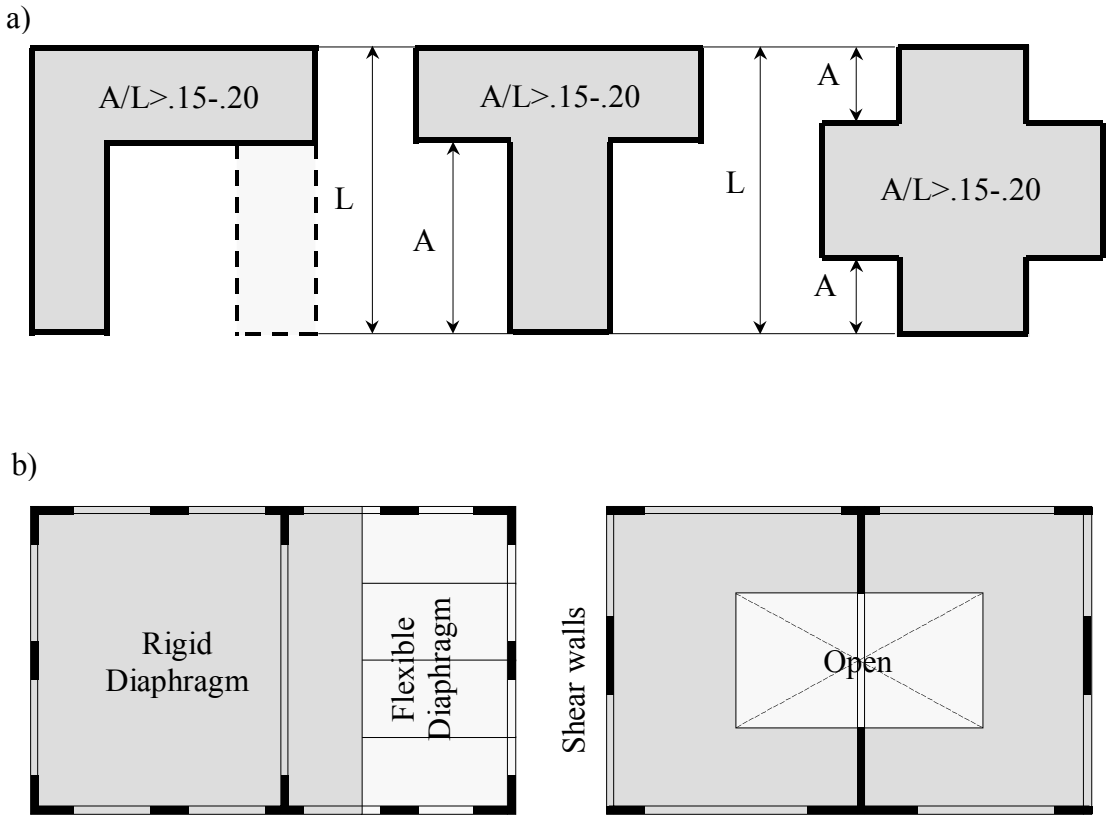

Figure 1. 2. Building plan irregularities (Adapted from BSSC 1998):
a) Geometry; b) Discontinuity in diaphragm stiffness and shear walls with openings

Windows, doors, and other large openings progressively reduce strength and stiffness of shear walls as the size of opening increases. The design resistance of a wall with openings is assumed equal to the sum of base shears in fully-sheathed segments of

the wall being uniformly distributed among these segments. This assumption has historically been made before any studies had been completed for shear walls with openings subjected to cyclic or seismic loading. There are different methodologies to account for the reduction of the strength and stiffness of the walls with openings. One such method to gain reasonable acceptance is the perforated shear wall method (AF&PA, 1996), in which the sum of the unit shears is reduced by an empirical factor. The factor was derived using Sugiyama's and Matsumoto's (1994) equation based on monotonic racking tests.

Different construction practices and detailing requirements exist in different regions. Typical engineering practice for shear wall construction requires mechanical anchor connections to be placed at the ends of each fully-sheathed shear wall segment. In conventional construction, it is common that walls are attached to the base by means of nails or shear bolts. The nails working in withdrawal provide little resistance to uplift of the wall. When bottom plates of walls are attached to the base by the shear bolts, the uplift is resisted by the bolts through washers and nuts and by shearing of sheathing fasteners. Currently, there is no agreed upon design methodology to determine capacity of shear walls without hold-down anchors.

To produce accurate design of modern shear walls, engineers need to have both performance and prescriptive provisions with distinct rules accounting for:

1. Length of shear wall segments (aspect ratio);
2. Openings (doors, windows, non-structural sheathing);
3. Overturning restraint (nails, shear bolts, tie-down anchors).

This goal can be achieved by developing a mechanics-based design methodology using analytical modeling verified and validated through a limited number of shear wall tests.

Dolan has initiated a series of projects to address the above-described needs. In 1989, Dolan developed finite-element models to simulate monotonic, cyclic, and dynamic response of shear walls. He performed a series of experimental tests to

determine the load-deflection characteristics of nail connections between framing and sheathing. These characteristics were used in the program to analyze shear walls. To verify the models, he tested 2.4 × 2.4 m (8 × 8 ft) shear wall specimens under static, cyclic, and historical earthquake loading.

Under Dolan's direction at Virginia Tech, Gutshall (1994) tested nail and bolted connections under monotonic and cyclic loading to quantify their performance parameters. White (1995) modified the analysis program and performed a parametric study to determine the effect of configuration on the response of shear walls to monotonic and seismic loading. The effect of large openings on 2.4 × 12.0 m (8 × 40 ft) shear walls was studied experimentally by Johnson (1997). Heine (1997) continued the testing program of the long shear walls to study the effect of hold-down restraint on the performance of light-frame wood shear walls.

1.3 Objectives

This study was intended to continue the previous studies and supplement the results with additional experimental and mathematical investigations to improve the methodology of shear wall design. The following complementary objectives comprise the purpose of the study:

1. Determine performance characteristics of light-frame shear walls with various aspect ratios and overturning restraint under monotonic and reverse cyclic loading. The following parameters were evaluated: capacity and maximum shear strength, elastic stiffness and shear modulus, ductility ratio, and equivalent viscous damping ratio. In addition, cyclic shear stiffness was determined during cyclic tests.

2. Develop a mechanics-based model to predict the shear wall strength with account for the effects of the wall aspect ratio and overturning restraint. For validation of the model, the experimental results were used.

3. Develop a method to predict the deflections of shear walls under lateral load using sheathing-to-framing connection test results, mechanical properties of component materials, and various anchorage conditions.

Results of the study will serve as supporting information for building codes and design specifications, and will lead to improved methods for design of shear walls.

1.4 Significance

A substantial amount of research has been conducted on the subject of shear walls. Nevertheless, some areas remain with inadequate knowledge. Costs associated with developing information on the dynamic response of light-frame buildings would be enormous if only an experimental approach is used. A method was developed in this study to translate sheathing-to-framing connection test results to full-scale shear wall response. Such approach will minimize the expense because connection tests are less complicated and less expensive to conduct than full-scale wall tests. The use of analytical modeling to predict the response of structures will produce more general information and will allow different wall configurations to be simulated to determine the critical configurations.

Most failures of shear walls during an earthquake or hurricane are initiated in the connections of walls to substructures. Information obtained in this study improves the understanding of force distribution in shear walls with and without tie-down anchorage. A method is provided to accurately estimate the stiffness and capacity of shear walls while accounting for the presence of anchors and the pattern of sheathing attachment. Considering the damage and life loss experienced in natural disasters, and the fact that majority of the nation's population lives in hurricane prone regions (along the Gulf of Mexico and Atlantic Ocean), the importance of improving the design and construction of light-frame construction becomes evident. The results of the investigation will lead to developing design and construction methods to enhance durability, serviceability, and safety performance of houses in the 21st century.

1.5 Overview of the Dissertation

Background presented in Chapter 2 begins with general information about modern light-frame shear wall structures and a brief historic overview of research related to the topic. Further, experimental studies that have been completed in the past are discussed. Special attention is given to test methods and loading regimes. This discussion provides background for development of testing procedures used in this study. Next, a brief overview of pertinent literature is included with emphasis to most recent publications. Specific discussions of previous research results are incorporated in subsequent chapters of the dissertation.

In Chapter 3, an experimental plan for testing shear walls is presented. Characteristics of wall specimens are discussed and justified based on past research. The discussion includes description of construction details, test procedures, and instrumentation.

Chapter 4 provides information on the material properties of the component materials, such as OSB sheathing, framing lumber, and sheathing nails, used in the shear wall specimens. Then, background information, test procedures and results of monotonic tests of sheathing-to-framing connections are presented and discussed. The performance parameters of the connections are used for analytical modeling of shear walls described in Chapter 6.

Chapter 5 starts with definitions of performance parameters of shear walls under monotonic and reverse cyclic loading. Then, results of shear wall tests are presented and discussed. Conclusions are drawn about effects of aspect ratio, number of panels, hold-down restraint, wood density, quality of sheathing attachment, and load regime on the performance of shear walls.

In Chapter 6, analytical models of light-frame shear walls are discussed. An overview of past research includes closed-form and finite-element models. The development of the elastic and the ultimate strength models for unrestrained single-panel and multi-panel shear walls is presented. The simple formula is proposed to predict the shear wall strength. Then, the methods of predicting deflections of shear walls with and

without tie-down anchors are advanced. The predictions are compared with the test results on the full-size shear walls.

In conclusion, Chapter 7 presents an overview of the research objectives, methods, and achieved results. Recommendations are given for future research and validation of the proposed formulae.

1.6 Scope and Limitations

The study deals with light-frame wood shear walls used for platform construction. Walls that are considered as part of a building lateral force resisting system subject to wind or seismic forces are the focus. Improved wind and seismic design is the goal of the experimental and analytical investigation.

Experimental testing of full-size shear walls included monotonic one-directional loading and reverse cyclic (quasi-static) loading. No shake table or pseudo-dynamic experiments were conducted. Walls were tested in horizontal position; consequently, dead load was not applied in the wall plane. Anchorage conditions varied from a full restraint against overturning (representative of engineered design) to a near minimum overturning restraint (representative of conventional practice). One type of tie-down anchor was used. One type and size of framing, sheathing, and fastener schedule was used in the experimental tests of walls and connections. The sheathing was attached on one side of the wall; effects of double-sided sheathing and interaction of different types of sheathing were not considered.

Two-dimensional mechanics-based models were used for analytical modeling. No 3D modeling was undertaken. Hold-down effects of adjacent transverse walls or corner walls were neglected. The mechanical model is capable of predicting magnitudes and distribution of forces between shear wall segments subjected to static loading in the plane of the wall.

Conclusions and recommendations are supported by a limited number of experimental and mathematical examinations; therefore, further validation using other variables and techniques is anticipated and strongly advised.

Chapter 2. Background

2.1 General

Light-frame shear walls are an efficient means of enclosing residential and commercial space. They provide the resistance to gravity loads, transverse wind loads, and in-plane lateral forces imposed by wind and seismic loading. Therefore, shear walls must have sufficient strength and rigidity to carry these loads. The lateral forces can be either transferred from roof or floor diaphragms to the shear wall elements, or directly applied to shear walls themselves.

Modern light-frame shear walls typically consist of three major components: lumber frame, sheathing, and connections that attach the framing together, the sheathing to the framing, and the framing to the base. Frame elements (plates and studs) are usually made of 38×89 mm or 38×140 mm (2×4 in. or 2×6 in. nominal) lumber. Studs are spaced 410 mm or 610 mm (16 in. or 24 in.) on center. For exterior sheathing, structural panel products such as plywood and oriented strandboard (OSB) are most commonly used. Gypsum wallboard, or drywall, is mainly used for interior sheathing. Sheathing panels are manufactured in 1.2×2.4 m (4×8 ft.) sheets and applied either vertically or horizontally. The sheathing is attached to the framing with dowel-type fasteners such as nails, screws, or staples, although adhesives are sometimes used.

From structural point of view, a light-frame wall is a very efficient system. Due to the large number of closely spaced members and fasteners, the system is highly redundant. It is capable of resisting vertical loads and lateral forces. Frame members without sheathing have no lateral resistance at all. For lateral resistance, shear strength and stiffness of sheathing are essential. In addition, the structural sheathing improves load sharing among the frame elements. However, the most important effect on shear wall performance is introduced by fasteners connecting the sheathing edges to the frame and, to a lesser extent, the connection between framing members. All the connections (dowel-type fasteners) are known to perform in a nonlinear manner. Consequently, the displacement response of shear walls to varying loads is nonlinear too.

Another important aspect in lateral resistance of shear walls is the means of hold-down restraint applied to prevent shear wall overturning. The hold-down restraint is partially provided by the weight of upper structures. However, considering a shear wall parallel to floor joists and sharing dead load between multiple interior walls, the effect of the gravity loads supported by exterior shears wall should not be overestimated.

The overturning moments are resisted effectively when mechanical devices are attached to the studs to transfer the uplift forces to the foundation. In engineered seismic design, the mechanical restraint is represented by tie-down anchors, which are typically applied at the ends of each fully-sheathed segment of the wall. In high wind design (AF&PA 1996), an alternative method allows placement of tie-down anchors at the ends of the entire wall only, leaving intermediate wall segments near door and window openings mechanically unrestrained against overturning.

Conventional construction practices do not require mechanical hold-down of shear walls. The *International Residential Code* (ICC 2000) requires just one 16d nail every 406 mm (16 in.) to attach the sole plate to underlying structures. At the first floor, sills of non-engineered walls are fastened to the foundation by anchor bolts at not more than 1219 mm (4 ft.) according to *NEEHRP* (BSSC 1998). However, this anchorage does not provide overturning restraint *per se* and serves to resist horizontal shear forces only. Further, the anchor bolts attaching the wall sill plate to the platform are referred to as *shear bolts*.

2.2 Historic Overview

Substantial amount of experimental and numerical research has been completed on the structural performance of light-frame shear walls. Extensive bibliographies have been written by Carney (1975), Peterson (1983), Wolfe and Moody (1991), and Foliente and Zacher (1994).

Research of wood-based shear walls dates back to 1927 (Peterson, 1983). Most of the research before 1930 dealt with urgent problems related to earthquake damage analysis. During the next decade, more attention was given to the investigation of the structural properties of wood buildings. During this period, a basic understanding of the

mechanics of wood products and providing a standard for design and manufacture was investigated.

Until the mid-1940's conventional light-frame structures used so-called "let-in" corner bracing or diagonal lumber sheathing to provide shear resistance. Even after panel-type sheathing became popular, diagonal bracing remained standard. Panel sheathing began to be used for shear walls in the late 1940's. In 1949, a guideline was issued for the acceptance of panel sheathing in place of "let-in" corner bracing, which formed the basis of subsequent standards for construction.

During the 1950's and 1960's, researchers took advantage of previous information to enrich the knowledge in this field. The majority of the work was experimental in nature and focused on the influence of parameters such as sheathing type and orientation, fastener type and spacing, and wall geometry. Analyses were simplified, differences between static and dynamic response of the walls were not well understood. Many full-size shear walls and even full-scale houses had been tested. Up to that time, research work and design guidelines for shear walls were mostly based on experience and testing results.

The rapid development of computers in early 1950's provided the opportunity to use advanced analytical methods to study the performance of structures. Since the mid-1960's, the finite-element method had been used for the analysis of wood shear walls. In 1967, Amana and Booth published the results of theoretical studies on nailed and glued plywood stressed skin components. They introduced the concept of nail modulus to account for fastener stiffness. In 1972, a group of researchers at Oregon State University, in cooperation with the lumber industry, used the finite-element method to predict deflection, stress, and the ultimate load capacity of walls (Polensek, 1976). During this period, many formulae and models for wood shear walls were developed. Some researchers began to study the nonlinear behavior of shear wall connections and started to consider the wood shear wall members as orthotropic materials (Foschi, 1977). The results of the numerical investigations were generally experimentally verified.

During the last two decades, significant progress has been made in the study of shear wall performance. Computer technology made possible to develop new testing techniques such as reverse cyclic, pseudo-dynamic, and shake table tests. Data acquisition systems were developed to collect and analyze results of cyclic and dynamic tests with high frequency sampling. Researchers made great efforts to develop new analysis tools to simulate the performance of structures. Advanced principles of mechanics were applied to overcome drawbacks of earlier studies, which used simple beam theory. Now, numerical analysis methods such as finite-element method combined with a variation approach are used extensively. Recent studies tend to gradually shift from linear to nonlinear modeling; from static one-directional loading to reversed-cyclic and dynamic loading; from plane deformation to 3D deformation; and from structures without openings to those with openings.

Several workshops and meetings have been held in the last two decades to discuss the state-of-the-art and research needs in the seismic design of timber structures. Reports and proceedings have been published by ATC (1980), Gupta (1981), Itani and Faherty (1984), Ceccotti (1990), RILEM (1994), and Foliente (1994, 1997).

2.3 Test Methods and Loading Regimes

2.3.1 Current ASTM Methods (Static Monotonic Tests)

In the US, test methods for various materials, connections, and assemblies are standardized by the American Society for Testing and Materials (ASTM). Standard test methods and practices for mechanical fasteners in wood, structural panels, and framed shear walls are established in ASTM D1761, E72, and E564, respectively. ASTM D1761 is applied to testing single fasteners such as nails, staples, screws, bolts, nail plates, and joist hangers. ASTM E72 is applied to specific configurations of wall, floor, and roof panels under various load conditions. In particular, racking load is imposed to 2.4×2.4 m (8×8 ft.). The test is intended to assess and compare resistance of various sheet materials attached to a standard frame. For measuring structural performance of complete walls, method ASTM E564 is recommended. This method allows testing of

any structural light-frame wall configuration on a rigid support to determine the shear stiffness and strength of the wall.

All three methods were originally intended to evaluate performance under static monotonic loads only. In method ASTM D1761, load is applied at a uniform rate of 2.54 mm (0.10 in.)/min ± 25%. Special loading methods, such as cycling or pulsating, are only mentioned in Section 10.3 of ASTM D1761 but no specific procedure is recommended. (A standard test method for cyclic properties of connections assembled with mechanical fasteners is being proposed as an ASTM standard and is discussed in the next subsection.)

In method ASTM E72, the load is applied at a uniform rate of motion "such that the loading to 3.5 KN (790 lbf.) total load shall be completed in not less than 2 min from the start of the test". The specimen is loaded in three stages to 3.5, 7.0, and 10.5 KN (790, 1570, and 2360 lbf.), each stage followed by unloading. After that, the specimen is loaded to failure or until the total deflection of the panel becomes 100 mm (4 in.).

In ASTM E564, a static load test and an optional cyclic loading test are offered. In this former test, a preload of approximately 10% of estimated ultimate load is applied, maintained for five minutes, and removed. After that, one third and two thirds of estimated ultimate load are applied, and so on until ultimate load is reached. At each increment, load is maintained at least one minute before load and deflection readings are recorded, then the load is removed and readings are made after a five-minute pause. The cyclic test also begins with the 10% pre-load. Consequently, five reversed cycles at each load or displacement increment are applied until failure of the assembly occurs. The rates of loading and increment levels are not specified in this procedure.

In addition to the loading regimes, there are differences in hold-down provisions in the two standards. ASTM E72 method requires that "hold-down rods shall be tightened prior to load application so that the total force in each rod does not exceed 90 N (20 lbf.)" as shown in Figure 2. 1. In construction practice, other means of tie-down are used (if any); therefore, the test is applicable for comparison of different panel products, not for evaluation of various wall systems. In ASTM E 564 procedure, the wall "shall be

attached to the test base with anchorage connections simulating those that will be used in service." This allows performance evaluation of different kinds of walls. However, size of specimens remains constant: 2.4×2.4 m (8×8 ft.). To study effects of aspect ratio and/or openings, the test procedures need to be modified.

Results of static monotonic tests are helpful but not adequate to assess performance characteristics (strength, stiffness, deformation capacity, and energy dissipation) of connections and assemblies under seismic conditions.

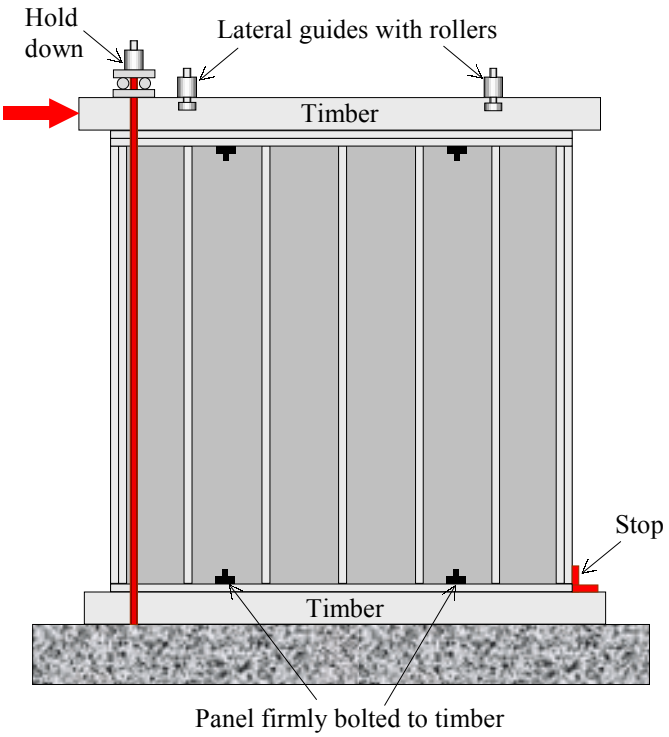

Figure 2. 1. Racking load assembly according to ASTM E72

2.3.2 Cyclic Test Methods (Quasi-Static Testing) [1)]

First reverse cyclic tests of sheathed timber framed shear walls were reported by Medearis and Young (1964) in U.S. and later Thurston and Flack (1980) in New Zealand. The loading procedures consisted of small number of cycles (4-5) with gradually increasing amplitudes until failure.

[1)] Cyclic tests conducted at frequencies below 1.0 Hz are considered quasi-static because they do not induce inertial effects in the system response. Any harmonic excitation at higher frequencies is considered pseudo-dynamic tests as opposed to dynamic tests based on random excitations.

In New Zealand, researchers continued developing cyclic testing procedures relying on small number of cycles. Stewart (1987) applied four pairs of reversed cycles in testing 2.4-m (8-ft.) square walls at a rate 5 mm/min (0.2 in./min) in the following pattern: 100%, 200%, 300%, and 400% of initial amplitude of 15 mm (0.6 in.). Dean (1988) applied six sets of three cycles in testing of nailed sheathing joints using the following pattern: 100%, 120%, 140%, 160%, 180%, and 200% of nominal nail strength. He compared load-controlled and what he called 'displacement-controlled' regimes. In the latter, the first cycle of each set was load-controlled; the other two repeated the amplitude of the fist cycle. Deam (1997) reported tests of multi-story plywood sheathed shear walls under quasi-static loading using a similar approach. The first cycle was load-controlled to determine deflection at design load; the rest of the cycles had progressively increasing amplitudes in the pattern similar to that used by Stewart (1987). The walls had survived 6 to 18 cycles. Each test took several days.

Several protocols for reversed cyclic tests of connections and assemblies have been proposed and used by researchers in other countries. EN TC 124.117 (CEN 1995) protocol is one of a series of European standards for testing joints with mechanical fasteners. It includes two procedures: a general one (CEN Long), when determination of the complete cyclic load-slip performance is required, and a particular one (CEN Short), when main performance characteristics at a pre-determined ductility level are determined. The CEN Long procedure consists of a number of cycle groups of three cycles each (except for the first and the second cycle groups which consist of a single cycle.) The increments are 25%, 50%, 75%, 100%, 200%, 400%, and so on, of the yield slip (Δ_{yield}) until failure or a slip of 30 mm (1.2 in.) is reached. The CEN Short procedure consists of three identical cycles, after which a unidirectional load is applied to the joint until failure. The maximum amplitude of loading is determined as a product of ductility and yield slip ($D \times \Delta_{yield}$).

Yield slip is determined by the intersection of two lines. The first line is drawn through the points on the load-slip curve between $0.1P_{max}$ and $0.4P_{max}$. The second line is the tangent to the curve having a slope of 1/6 of the first line. The maximum slip (Δ_u) is taken as either the displacement when the load has dropped to 80% of the maximum load,

or a slip of 30 mm (1.2 in.) whichever occurs first in the test. A constant rate of slip, between 0.02 and 0.2 mm/sec (0.05 and 0.5 in./min), is recommended for the cyclic test.

FCC-Forintek protocol (Karacabeyli, 1996) consists of a sequence of triangular sinusoidal cycle groups, with each cycle group containing three identical cycles. Amplitude of each cycle group is taken as a percentage of the nominal yield slip (Δ_{yield}) with alternating increase and decrease of the amplitude until specimen failure. Nominal yield slip is defined as the displacement at a load equal to half of the maximum load obtained during a monotonic test. The maximum slip (Δ_u) is defined at the maximum load. Load is applied with frequency of 0.5 Hz. A similar procedure without degrading cycles was used by Karacabeyli and Ceccotti (1996) for testing of 2.4×4.9 m (8×16 ft.) shear walls using ASTM E564 setup.

In Germany, Reyer and Oji (1991) proposed two loading regimes, which where used by Canadian researchers Chui and Ni (1997) for testing load-embedment response of wood under dowel-type fasteners. One of the regimes was a reversed cyclic loading function with increasing amplitudes in each cycle in proportion to yield displacement as follows: 25%, 50%, 75%, 100%, 150%, 200%, 300%, and so on until failure or a displacement of 10 mm (0.4 in.) was reached. The value of yield displacement was 0.1 mm (0.004 in.) determined from monotonic tests. Two rates of loading were used for comparison: 0.25 Hz and 0.5 Hz.

Another load regime proposed by Reyer and Oji (1991) was aimed at study pre-loading history effects. It was a phased sequential loading function, having twenty cycles of loading in each phase. Within each phase, there were six initial cycles with increasing amplitudes, followed by eight cycles of constant amplitude, and then six final cycles of decreasing amplitudes. The sequence of peak amplitudes in the loading phases followed the pattern of the first regime with a loading rate of 0.25 Hz.

A number of different test protocols have been proposed and used in the USA during last two decades (e.g. Zacher and Gray, 1989; Dolan, 1989; Hanson, 1990), but none of them had been established as ASTM standard.

Zacher and Gray (1989)[1)] tested standard size panels using displacement-controlled pattern at 2.0 Hz. Each test consisted of 15 sinusoidal cycles with three cycles each approximately 5%, 10%, 25%, 40%, 60%, and 100% of maximum displacement. The maximum displacement was pre-selected for each test (not exceeding 3 in. due to limitations of the equipment used).

Dolan (1989) applied ASTM E564 setup to test standard size walls at a rate of displacement 30 mm/min (1.2 in./min). The loading procedure was three sets of four cycles: 100%, 200%, and 400% of initial displacement of 13 mm (0.5 in.)

Hanson (1990) used ASTM E72 test setup and applied the following loading schedule: ten cycles at ± 75%, 100%, and 150% of design load, and five cycles at ± 250%, and 300% of design load at a rate of 0.05 Hz for all the cycles.

A standard method for determining dynamic properties of connections assembled with mechanical fasteners is proposed as ASTM standard (ASTM, 1995). This test method can be applied to any type, size, and number of fastenings in any building material or combinations of materials. The loading method incorporates the Sequential Phased Displacement (SPD) procedure proposed by Porter (1987) and modified by Dolan. The original procedure was developed by a joint U.S. and Japan Technical Coordinating Committee on Masonry Research and is commonly referred to as the TCCMAR procedure.

The displacement is a triangular sinusoidal ramp function at a frequency of 0.5 Hz, which is in the range expected during an earthquake or a high-wind event. The procedure begins with at least three sets of three cycles each before the first yield or another inelastic behavior. The amplitude of each set gradually increases by a fraction of the yield displacement. Once yielding or the first major event (FME) occurs, three cycles with decreasing amplitudes are added. The amplitude of each consecutive decay cycle decreases by 25% of the maximum amplitude of the phase. The decay cycles are followed by minimum of three stabilization cycles at the amplitude of the initial cycle.

[1)] The authors named the tests dynamic, which was not exactly so. Although the rate of loading was sufficiently high, the excitation was harmonic displacement controlled function, but not random vibration.

The set of initial, decay, and stabilization cycles represents a phase in the displacement pattern. Phases are repeated sequentially with the initial cycle amplitude increasing in proportion to the yield displacement until the connection fails. The increment of increased amplitude is proposed to be 100% of the yield displacement for ductile connections and 25% - for brittle ones.

In 1996, the Structural Engineers Association of Southern California (SEAOSC) adopted standard methods for testing shear walls, connectors, and anchors for buildings (SEAOSC, 1996 and 1997a, b), which incorporated the SPD procedure. Test setup for walls is similar to ASTM E564.

In 1995, APA – The Engineered Wood Association started an extensive multi-year test program to investigate problems related to the cyclic tests. In particular, it was planned to compare ASTM E72, ASTM E564, and SEAOC load tests on matched specimens (Skaggs and Rose, 1996). In addition, so called 'simplified' and 'modified' TCCMAR procedures were used in preliminary tests of walls and nail connections (Rose, 1996, and Ficcadenti *et al* 1995). In simplified procedure, decay cycles were omitted, while modified procedure consisted only of the initial and decay cycles. This was done to look into effects of the load history on the response of the nailed structures.

2.3.3 Pseudo-Dynamic and Shake Table Tests

The pseudo-dynamic test method (PSD) was originally developed in Japan (Takanashi 1975). In this test, a computer-controlled actuator attached to the top of a shear wall specimen applies the load, which is calculated using a time-history analysis of the shear wall for a specified seismic ground motion record. The incremental stiffness of the specimen is returned to the analysis to calculate the load at the next time-step. The appropriate value of equivalent damping ratio has to be determined in advance.

Theoretically, the method is versatile and allows testing of large full-scale multi-degree-of-freedom systems with realistic load distribution. However, a large number of actuators are needed for testing such systems, which is not practical. Furthermore, conventional PSD test requires a hold period for computation at each step. This is a major limitation in application to wood structures, where failure mechanism is dependent

on rate-of-loading. This limitation can be solved if a continuous PSD procedure is developed where real-time application of earthquake load is possible (Donea *et al.*, 1996). To date, the PSD method has found very limited application for testing light-frame shear walls. To author's knowledge, only Kamia (1988) and Kamia *et al.* (1996) in Japan have reported pseudo dynamic tests of single-story light-frame shear walls.

Shake table tests produce the most realistic type of seismic loading. A specimen with additional mass on top is mounted on the table, which simulates a real-time earthquake acceleration record. Depending on the shake table, it can produce 3D accelerations. Close to the real response of the structure and failure modes can be monitored in this test. Dolan (1989) and Stewart (1987) tested 2.4×2.4 m (8×8 ft.) walls on shake tables.

Disadvantages of this method are as follows: the size of specimen is limited by size and capacity of the shake table; the tables are few, expensive, and complex in maintenance and control; definition of forces involves approximate calculations through measured accelerations; results need interpretation to conventional terms of forces and relative displacements. The choice of loading record may be critical to results and results may be applicable to the input load used in the test (Foliente, 1996).

2.3.4 Discussion of Test Methods

As opposed to natural disasters, laboratory testing allows direct monitoring of structural performance under controlled load conditions. Results provide information that can be used to (1) develop, refine or calibrate analytical models and perform dynamic analysis, and (2) improve new and existing products and design procedures (Foliente, 1997).

All existing test methods possess their advantages and limitations, which were many times discussed by researchers[1)]. Foliente (1996) summarized: "None of the methods… can be selected as the "best" by itself alone… [T]he tests complement each other – one method's weakness is another method's strength and vice versa." Some

[1)] See also *Earthquake Spectra's* Theme Issue: Experimental Methods (Feb 1996, Vol.12)

researchers (Stewart 1987 and Dolan 1989) used both quasi-static and shake-table tests in their studies of shear wall performance.

Until recently, the majority of tests were performed using ASTM standards to study static monotonic response. Design values were established based on these tests as ultimate unit shear divided by a factor of safety or unit shear at a certain story drift. Now, it is acknowledged that strength and stiffness determined monotonically might be adequate for wind design, but not for seismic design. Furthermore, information gathered from a monotonic test is insufficient to describe seismic response, such as load history effects and ability of a structure to dissipate energy (structural damping).

Cyclic testing can provide such information. When performed at rates slow enough that inertial effects do not effect the results it is referred to as a 'quasi-static' test. Now it is the most common testing method in structural earthquake engineering and will likely remain being so because of its relative simplicity and cost-effectiveness compared to pseudo-dynamic or shake table tests (Foliente, 1996). Quasi-static tests are capable of providing sufficient information (strength, stiffness, ductility, and damping) for all practical purposes: design codes, pseudo-dynamic tests, analytical modeling, and cooperative exchange of data. The problem of the method is the lack of a standard procedure, which would allow effective realization of its potential.

The pseudo-dynamic procedure is a hybrid of time-history response analysis and loading test of the structure conducted simultaneously. It is rarely used for testing of timber structures because rate of loading affects their response, the procedure is rather complicated, and interpretation of results is difficult. In shake table tests, ground motion is simulated in the most realistic manner, which allows monitoring true failure modes. However, these tests are expensive, shake tables are few. It is unlikely that a standard procedure will be adopted for a narrow party of potential users. Size of specimens is limited by size of tables, and information is dependent on loading regime used.

2.4 Overview of Past Experimental Studies

A vast body of standard and non-standard shear wall tests has been performed all over the world. Until the 1980's, most of the tests used ASTM or similar monotonic

loading procedures. These tests provided information for wind design, because in high wind conditions, buildings are subjected to loads, which act primarily in one direction. A comprehensive summary of monotonic shear wall tests conducted by American Plywood Association since 1965 was reported by Tissell (1990). Wolfe and Moody (1991) summarized available test data on structural performance of low-rise wood-frame building systems published by North American researchers during 40 years. In last decade, cyclic and shake table test data obtained in different parts of the world became available. Foliente and Zacher (1994) made an updated overview of test data. The latest findings were reported at International Wood Engineering Conference in New Orleans, LA, (Gopu 1996) and Forest Products Society annual meeting in Vancouver, Canada (FPS 1998).

Foliente (1997) summarized typical cyclic response of timber joints and structural systems as follows:

a) "Nonlinear, inelastic load-displacement relationship without a distinct yield point;
b) Progressive loss of lateral stiffness at each loading cycle (stiffness degradation);
c) Degradation of strength when cyclically loaded to the same or with increasing displacement level (strength degradation); and
d) Pinched hysteresis loops (i.e., thinner loops in the middle than near extreme ends)."

Varying structural parameters and their effect on shear wall performance had been examined more or less. One or more researchers have come to the following conclusions:

- Sheathing (type, thickness, and orientation):

1. There is no significant difference in static and dynamic performance of walls sheathed with OSB, plywood, and waferboard. Addition of gypsum wallboard (drywall) increases stiffness and strength of shear walls but reduces ductility; ultimate resistance occurs at smaller displacements. Under cyclic loading, drywall exhibits a more brittle failure at lower loads than under static monotonic loading.

2. Thickness of structural sheathing affects shear stiffness and mode of failure of walls and performance of fasteners. Nails pull or tear through thinner panels, and fatigue or withdraw in case of thicker ones.

3. Vertical and horizontal orientations of wood-based composites sheathing are equivalent if adequate blocking is provided, while gypsum sheathing exhibits higher racking strength when oriented horizontally.

- Framing (blocking, bracing, and stud spacing and width):

1. Omission of blocking at the horizontal joint between sheathing panels changes shear load path and decreases strength of the wall.

2. Let-in bracing contributes to monotonic racking strength of walls with gypsum sheathing.

3. Thinner panels tend to buckle when fastened to studs spaced 610 mm (24 in.) o. c. or greater.

4. Thicker studs are needed to prevent wood splitting when sheathing nails are closely spaced.

- Fasteners (type, size, and schedule, use of adhesives):

1. Sheathing connections generally govern overall behavior of the assemblies. Nails and staples provide high ductility and good energy dissipation while screws and adhesives exhibit high stiffness and brittle failure.

2. Ductility of sheathing connections depends on sheathing thickness ratio and framing penetration ratio[1)]. Higher density of nailing increases stiffness and strength of walls.

- Geometry (aspect ratio, openings):

1. Racking resistance and shear stiffness of shear walls under monotonic loading is proportional to wall length if height-to-length aspect ratio does not exceed limit of 2:1; greater aspect ratios result in stud bending contributions to story drift.

2. Distribution of shear forces and overturning moments is dependent on length of the wall and opening configuration, and is not well studied.

[1)] Sheathing thickness ratio = (sheathing thickness) / (nail diameter); framing penetration ratio = (framing penetration) / (nail diameter). (Dean, 1988).

3. Openings alter load paths affecting strength, stiffness, and ductility of the structure. Currently, strength is estimated as a cumulative strength of fully sheathed wall segments reduced by an empirical factor (≤ 1.0) depending on amount of openings and anchorage conditions.

- Overturning restraint (anchorage, intercomponent connections):

1. Anchorage conditions strongly affect response of shear walls by providing higher strength and stiffness; effect on ductility depends on geometry of the wall.

2. When testing isolated narrow shear walls, test set-ups do not reflect conditions of actual construction. Cross walls, floors, and roof or ceiling provide additional restraint and affect the response.

Few attempts have been made to systematically explore effects of wall length and overturning restraint under monotonic loading. Among those, are reports by Sugiyama and Suzuki (1975a and 1975b) and by Tissell and Rose (1994). Commins and Gregg from *Simpson Strong-Tie Co.* (1994) tested three narrow shear walls with a 3.5:1 aspect ratio to full design load under cyclic loading for 90 cycles and to 140% of design load for another 90 cycles. The testing was performed at frequency 2 Hz and 15 Hz. The walls were sheathed with plywood on one side. Three types of hold-down devices were used. In 1996, the same authors tested four 2.4 m (8 ft.)-tall walls with hold-down restraint and aspect ratios 4:1, 2:1, 4:3, and 1:1 using SPD protocol. The test series assigned a first major event (FME) to the system at 20 mm (0.8 in.). These are the only references found to date for cyclic testing and effects of overturning restraint in conjunction with wall aspect ratio.

Formerly, effects of intercomponent connections were underestimated or ignored. Now it is acknowledged that these connections are one of the most important, and the least understood, links in the load path (Foliente, 1997). Recent earthquakes demonstrated urgent need to address these issues. A number of seismic performance tests of full-size buildings have been performed in Japan. Sugiyama *et al.* (1988) found that the racking resistance of walls in full-scale houses under cycling loading was about one and a half times that of isolated shear walls of the same type. Perhaps, this was due to the

smaller uplift in the actual house than in the shear wall racking test performed similar to ASTM E72.

Tests of whole buildings are useful for better understanding the load sharing mechanisms between components, validation of 2D tests of isolated components, and identification of "ideal" or acceptable failure mechanisms. However, these tests are expensive and unaffordable for most laboratories. In the author's opinion, carefully designed tests of shear walls with attached components (narrow cross walls and/or diaphragms) could be reasonably economical and practical alternative to 3D tests of buildings in studying system effects. Nevertheless, effects of intercomponent connections are left out of the scope of the present research.

2.5 Conclusions

General performance of modern light-frame shear walls, historic outline, test procedures and summary of past experimental studies in this field have been presented. The following conclusions can be drawn:

- Laboratory tests are needed because they allow close monitoring of structural performance under controlled loading conditions and can be used to improve construction technology and design provisions.

- Current standard tests employ monotonic loading of 2.4-m (8-ft.) square walls with hold-down anchorage to provide information for design of shear walls restrained against overturning. This information is acknowledged to be insufficient for seismic design of shear walls and walls without overturning restraint.

- Quasi-static procedures appear to be the only methods where standardization is availing for general seismic performance evaluation if a common cyclic testing standard is adopted.

- A standard procedure should provide a consistent basis for exchange of data and cooperative research for the development of models and design methodologies for building codes (Foliente and Zacher, 1994). Critical aspects for development of such a standard are purpose of the test, load history, and data interpretation.

- Investigation of effects of various factors on shear wall performance is needed, among those: loading type; size and aspect ratio; openings; anchorage systems; boundary conditions (Foliente and Zacher, 1994).

In the author's opinion, a procedure proposed by Dolan (1994) for mechanical connections, or similar procedures adopted by SEAOSC (1997a) for framed walls, structural connectors, and anchors, are the most promising to become a national standard despite criticism expressed by some parties at engineering forums (e.g. Foliente, 1996). At least two arguments if favor of above-mentioned procedures are:

Universalism: allow examination and comparison of existing and novel systems made of various materials and fastenings and detect potential slackness of those;

Conservatism: filter out brittleness, fatigue and other negative effects unseen by shorter procedures. If historic earthquakes did not present us with fatigue failures (yet), what about the luck of salvaged buildings in the next big one?

Chapter 3. Design of Shear Wall Tests

3.1 Introduction

Experimental testing of full-size shear walls is a crucial part of this study. The tests help better understanding shear wall performance under lateral loads. Test results are used to validate the analytical models, to improve design methodology of shear walls, and to check current design values.

The objective of the shear wall tests was to obtain and compare performance characteristics of shear wall segments with various aspect ratios and overturning restraint. Results can be compared with previous findings to determine effects of wall length and anchorage conditions on overall shear wall performance and distribution of forces between shear wall segments.

Research hypothesis of the experiment was as follows: Response of shear walls to lateral excitation varies depending on aspect ratio, amount of overturning restraint, and type of loading.

In this chapter, parameters of tested wall specimens are discussed and justified. The discussion includes description of construction details, test procedures, instrumentation, and data acquisition system.

3.2 Aspect Ratios

In this study, wall specimens are regarded as fully sheathed full-height segments of shear walls in platform construction. The segments can be located next to the ends of walls or between openings (e.g., windows or doors). To facilitate further discussion, the reader is referred to Table 3. 1 and Table 3. 2 where the geometry of specimens, rationale for testing, and pertinent background information are summarized. General appearance of wall specimens with full anchorage is shown in Figure 3. 1.

Deciding upon the upper bound of aspect ratios for testing, it appeared reasonable to start with the ratio 4:1. Although it is beyond the minimum code requirements (3.5:1), architects often use it to accommodate garage doors and wide ‘view’ windows. Many

failures in past earthquakes proved this was a not-safe practice (Andreason and Rose, 1994, Zacher, 1994). To quantify the effect of the high aspect ratio and to seek possible improvement in hold-down restraint of such walls is the purpose of this test series.

Table 3. 1. Selection of wall size and aspect ratio

Aspect ratio	**Wall size** *m (ft.)*	**Rationale**
4:1	2.4×0.6 (8×2)	Often used for wide windows and garage doors; Many failures in historic earthquakes; Beyond minimum prescriptive code requirements.
2:1	2.4×1.2 (8×4)	Minimum prescriptive code requirements; Typical size of intermediate and corner walls.
1:1	2.4×2.4 (8×8)	Standard *ASTM* specimen size; Link to design values and wealth of past research.
2:3	2.4×3.6 (8×12)	Maximum considered size of a fully sheathed wall segment; Link to data obtained by *Heine (1997)*.

APA – The Engineered Wood Association reported tests of full size walls with aspect ratios 6:1, 4:1, and 3:1 with OSB sheathing using ASTM E564 monotonic procedure (Tissell and Rose, 1994). They gave recommendations on design and detailing of narrow-width braced walls. Earlier, Sugiyama and Suzuki (1975) used ratios 2.7, 1.3, and 0.9 in monotonic racking tests of full size walls with plywood and gypsum board sheathing. They compared effects of ASTM E72 and so-called 'non-rod' methods of anchorage on the response of these walls.

To date, only a few cyclic tests of full size walls with aspect ratios larger than 1:1 have been reported. These are reports by Commins and Gregg (1994 and 1996) who tested three narrow shear walls with a 3.5:1 aspect ratio to full design load under cyclic loading, and four 2.4 m (8 ft.)-tall walls with hold-down restraint and aspect ratios 4:1, 2:1, 4:3, and 1:1 using SPD protocol.

Table 3. 2. Previous research considered in selection of wall size and aspect ratio.

Aspect ratio	**Wall size** *m (ft.)*	**Reference**	**Test method**	**Type of sheathing**	**# tests**
6:1 **4:1** **3:1**	2.4×0.4 (8×1.3) 2.4×0.6 (8×2) 2.4×0.8 (8×2.7)	*Tissell and Rose (1994)*	Monotonic: E564	OSB, GWB, Plywood	20
3.5:1 **4:1** **2:1** **4:3** **1:1**	2.4×0.7 (8×2.3) 2.4×0.6 (8×2) 2.4×1.2 (6×4) 2.4×1.8 (8×6) 2.4×2.4 (8×8)	*Commins and Gregg (1994, 1996)*	Cyclic: 2 Hz, 15 Hz Cyclic: SPD	Plywood	3 1 1 1 1
3:1 **4:3** **1:1**	2.4×0.9 (8×3) 2.4×1.8 (8×6) 2.4×2.7 (8×9)	*Sugiyama & Suzuki (1975)*	Monotonic: E72 vs. 'no-rod'	Plywood, GWB	12 12 12
1:1	2.4×2.4 (8×8)	*Tissell (1990)*	Monotonic: E72, E564	Plywood, OSB, GWB	524
1:1	2.4×2.4 (8×8)	*Rose (1998)*	Cyclic: SPD, 'simplified' SPD	Plywood, OSB, +GWB	11
1:1	2.4×2.4 (8×8)	*Dolan (1987)* *Stewart (1989)*	Monotonic, cyclic, shake table	Plywood, waferboard	55 12
1:1	2.4×2.4 (8×8)	*Dinehart & Shenton (1998)*	Monotonic: E564, Cyclic: SPD	Plywood, OSB	4 8
1:1	2.4×2.4 (8×8)	*Merrick (1999)*	Cyclic: 0.2 Hz	Plywood, OSB, GWB	7
2:3	2.4×3.6 (8×12)	*Heine (1997)*	Cyclic: SPD	OSB+GWB	4
1:2	2.4×4.9 (8×16)	*Karacabeyli & Ceccotti(1996)*	Cyclic 'Forintek'	Plywood, OSB,GWB	6
1:2	2.4×4.9 (8×16)	*Deam (1997)*	Cyclic: BRANZ	GWB	4
1:1 **1:2** **1:3**	2.4×2.4 (8×8) 2.4×4.9 (8×16) 2.4×7.3 (8×24)	*Wolfe (1983)*	Monotonic: E564	GWB	30
1:3	2.4×7.3 (8×24)	*Falk & Itani (1989)*	Monotonic, forced & free vibration	Plywood, GWB	4
1:3	2.4×7.3 (8×24)	*He(1997)*	Cyclic: SPD, CEN, 'Forintek'	OSB	13
1:5	2.4×12 (8×40)	*Johnson (1997)* *Heine (1997)*	Monotonic and Cyclic: SPD	Plywood, OSB,GWB	6 12
1:1 **1:2** **1:3** **1:4**	0.6×0.6 (2×2) 0.6×1.2 (2×4) 0.6×1.8 (2×6) 0.6×2.4 (2×8)	*Patton-Mallory et al. (1984)*	Monotonic: 0.5 cm/min. (0.2 in./min.)	Plywood, GWB	200

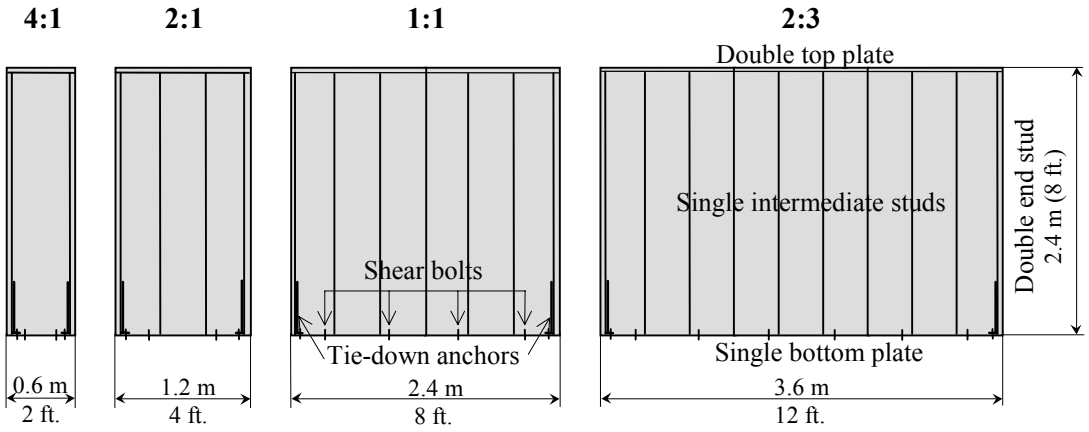

Figure 3. 1. General appearance of wall specimens with full anchorage:

Next is a series of tests on 2:1 aspect ratio. It represents the minimum 1.2-m (4-ft.) width of conventional 2.4-m (8-ft.) high wall allowed by U.S. model codes to resist wind or seismic loads. It is the most typical width of fully sheathed wall segments used to fill the space between windows and doors in residential construction.

Ratio of 1:1 was included in the test program as it represented standard ASTM specimen size – 2.4×2.4 m (8×8 ft.) – and procedure, which was used by APA to establish current design values. A vast body of experiments has been performed on square walls of this size. Tissell (1990) summarized experimental data obtained by APA since 1965 using ASTM E72 monotonic racking tests. Recently, APA started a multi-year testing program using SEAOSC (1997) reversed cyclic load method. Rose (1998) reported first results of these experiments, which included different kinds and thickness of sheathing. TCCMAR and 'simplified' TCCMAR load protocols were applied with FME at 20 mm (0.8 in.). Test results of the eleven shear walls revealed that FME occurred at an average displacement of 12 mm (0.48 in.) (Rose, 1998). Among earlier studies, it is important to consider monotonic, cyclic, and shake-table tests performed by Dolan (1989) and Stewart (1987). The series of tests performed by the author on walls with the standard aspect ratio serves as a point of reference and a link to past tests. This is one of the means to validate data obtained in this study.

For longer walls, it is a well-established practice to consider their response proportional to their length. Nonetheless, it is reasonably argued that distribution of overturning forces in longer walls differs from that in narrow walls and needs

experimental verification. In a modern house, it is unlikely that fully sheathed segments of a wall with opening(s) exceed 3.6 m (12 ft.) in length. Given the conventional height of the wall 2.4 m (8 ft.), the range of aspect ratios under investigation was limited by 2:3 on the lower bound.

Other aspect ratios, which were considered but not included in the experimental plan, are listed in Table 3. 2. Reasons for rejection were as follows:

- Priority in this study is given to narrow walls since their response is least studied and design is least conservative.
- Long walls without openings cause the least problems in performance; if openings are present, their effect in long wall segments is less pronounced, and the response is closer to that envisioned at design.
- It is unlikely that fully sheathed segments in walls with openings in residential buildings are longer than 3.6 m (12 ft.); the force distribution is assumed uniform in longer walls.
- It is possible to make correlation between previous findings and present study without repetition of tests.

3.3 Anchorage conditions

As already mentioned, the amount of overturning restraint and anchorage for shear depends upon methods of construction. Minimum restraint is provided in conventional construction by nails attaching the sill plate to the platform. In engineered buildings designed for seismic regions, the end studs of each fully-sheathed wall segment are fastened to the foundation by mechanical tie-down devices, and the bottom plate is attached to the foundation by uniformly spaced anchor bolts. This method provides the maximum restraint against wall overturning. To prevent cross-grain bending and to ensure effective transfer of load, 64×64 mm (2.5×2.5 in.) steel plates should be placed between the sill plate and the nut according to IBC (ICC 2000). The so-called perforated

shear wall method (AF&PA 1996) determines design values for shear walls with tie-down devices at the ends (corners) of the wall only.

Very often in construction practice an intermediate solution is applied: the bottom plates of the first story walls are attached to the foundation by shear bolts while tie-down devices at the end studs are omitted. Although the shear bolts are designed to resist the base shear, this method can be considered partially-engineered only.

Most prior experiments with shear walls were performed on walls secured to foundation by mechanical hold-down anchorage as required by ASTM E72 or ASTM E564. Debates concentrated about methods of modeling tie-down restraint in the standard tests (NAHB 1990; Leiva, 1994; Skaggs and Rose 1996). Performance of conventional walls, where such restraint is absent, has not been effectively explored.

Along with rational arguments, Table 3. 3 summarizes the anchorage conditions, which were examined in this study. Three series with various anchorage conditions were tested with the purpose to estimate the change in racking performance of shear walls due to varying construction practices. Engineered design with maximum overturning restraint was represented by walls with 'full anchorage' (**FA**): 15.9-mm (5/8-in.) diameter A307 anchor (shear) bolts at 610 mm (24 in.) o. c. attaching sill plate to the foundation and Simpson Tie-down HTT22 devices nailed to both end studs with thirty-two 16d sinker nails (ASTM F 1667 NL SK-09 C). The tie-down devices were anchored to the base with 15.9-mm (5/8-in.) diameter instrumented bolts to measure uplift forces in the end studs. The shear bolts were secured by nuts with the use of 64×64 mm (2.5×2.5 in.) wide and 6 mm (0.25 in.) thick steel plate washers as required by seismic design provisions. Johnson (1997) and Heine (1997) used the same detailing for similar walls. This series of tests serves as a link to many previous studies.

The 'no anchorage' (**NA**) series introduced a condition at near minimum overturning restraint where specimens were attached through the bottom plate to the rigid foundation[1)] by 16d bright common nails (ASTM F 1667 NL CM S-11 B). The

[1)] A double 38×89 mm (2×4 in., nominal) wood sill plate bolted to reinforced-concrete foundation.

'intermediate anchorage' (**IA**) condition was modeled by attaching the bottom plate of the shear wall to the base with 15.9-mm (5/8-in.) diameter bolts at 610 mm (24 in.) o. c.

Table 3. 3. Anchorage conditions

Series		Description	Rationale
FA	Full anchorage (maximum restraint)	5/8 in. bolts at 24 in. o. c., Simpson Tie-down HTT22 with 32 16d sinker nails and 5/8-in. bolt.	Typical engineered construction practice; Maximum hold-down restraint possible; Possibility to compare with previous tests according to ASTM E564.
NA	No anchorage (minimum restraint)	16d bright common nails	Typical conventional construction; Minimum hold-down restraint possible.
IA	Intermediate anchorage	5/8 in. bolts at 24 in. o. c.	Often used in practice; Represent intermediate restraint.

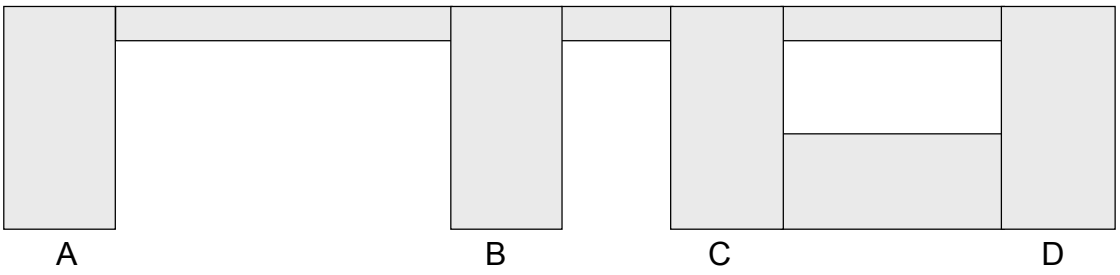

Figure 3. 2. Shear wall with openings: garage door, pedestrian door, and window.

Another factor that changes the response of shear wall segments is their location relative to the corners and openings. For example, consider a wall with openings as is shown in Figure 3. 2. It is safe to assume that the behavior of corner wall segments **A** and **D** will be different from intermediate segments **B** and **C**. The difference will be due to uneven distribution of overturning forces along the length of the wall, which in turn depends on support conditions, presence of anchors, and foundation rigidity. Furthermore, the response of the outer segments may be considerably controlled through connection with transverse (corner) walls, which produce additional hold-down restraint to the wall. Finally, segments above and below openings adjacent to the full-height segments will provide partial restraint.

Structural details of specimen anchorage conditions are portrayed in Figure 3. 3. For fully restrained walls, similar configuration is given in *Guidelines for Wood Diaphragms and Shear Walls* (SEAOC 1997). For walls with no anchorage, the number

of nails attaching the bottom plate to the base was determined to provide sufficient uplift resistance to the wall before it reached the shear capacity. The detailed information on the nailing schedules is provided in Chapter 5 and in the Appendix (Walls 04NAm).

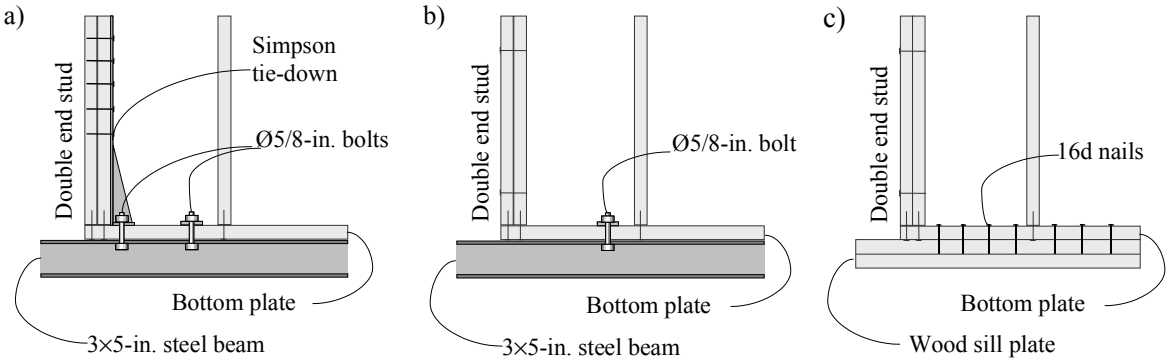

Figure 3. 3. Details of shear wall anchorage conditions:
a) 'Full anchorage', b) 'Intermediate anchorage', c) 'No anchorage'.

3.4 Fabrication of Specimens

The fabrication details of the shear wall specimens are summarized in Table 3. 4 and are illustrated in Figure 3. 4. The framing for each specimen consisted of 38×89 mm (2×4 in.-nominal) spruce-pine-fir (SPF) stud grade members spaced 406 mm (16 in.) on centers. Exception was made for the walls with the aspect ratio of 4:1, in which studs were spaced 533 mm (21 in.) on centers. End studs consisted of two members fastened by two 16d (∅4.1×89 mm) common nails every 0.6 m (2 ft.). The studs were attached to the single bottom plate and the double top plate with two 16d common nails at each end. A single layer of OSB sheathing, 11 mm (7/16 in.) thick, was attached to one wall side by power-driven 8d (∅3.3×63.5 mm) common SENCO® nails at 152 mm (6 in.) on centers along the edges and 305 mm (12 in.) on centers along intermediate studs. The long dimension of the sheathing was oriented parallel to the studs.

Table 3. 4. Structural details of wall specimens

Component	**Fabrication and materials**
Framing	Spruce-Pine-Fir, Stud grade, S-Dry, 38×89 mm (2×4 in.-nominal); Intermediate studs at 406 mm (16 in.) o. c.; Double studs at the ends of wall segments; Single bottom plate, double top plate.
Sheathing	Structural oriented strandboard (OSB), 11 mm (7/16 in.) thick, 122×243 mm (4×8 ft.) sheets installed with the long side parallel to studs; Attached on one side.
Framing attachment	Plate to plate: Two 16d (∅4.1×89 mm) bright common nails per foot; Stud to stud: Two 16d bright common per foot; Plate to stud: Two 16d bright common each end.
Sheathing attachment	Power driven 8d (∅3.3×63.5 mm) SENCO® nails at 152 mm (6 in.) o. c. (edge), 305 mm (12 in.) o. c. (field).
'Full anchorage' 'No anchorage' 'Intermediate anchorage'	Simpson HTT 22 Tie-down, nailed to end studs with 32 16d (∅3.8×82.6 mm) sinker nails; 15.9-mm (5/8-in.) diameter A307 bolt to connect to foundation; 15.9-mm (5/8-in.) diameter A307 bolts at 610 mm (24 in.) o. c. with 64×64×6.4 mm (2.5×2.5×0.25 in.) steel plate washers. Three rows of 16d (∅4.1×89 mm) common nails at 76 mm (3 in.) o. c.; 15.9-mm (5/8-in.) diameter A307 bolts at 610 mm (24 in.) o. c. with 64×64×6.4 mm (2.5×2.5×0.25 in.) steel plate washers.

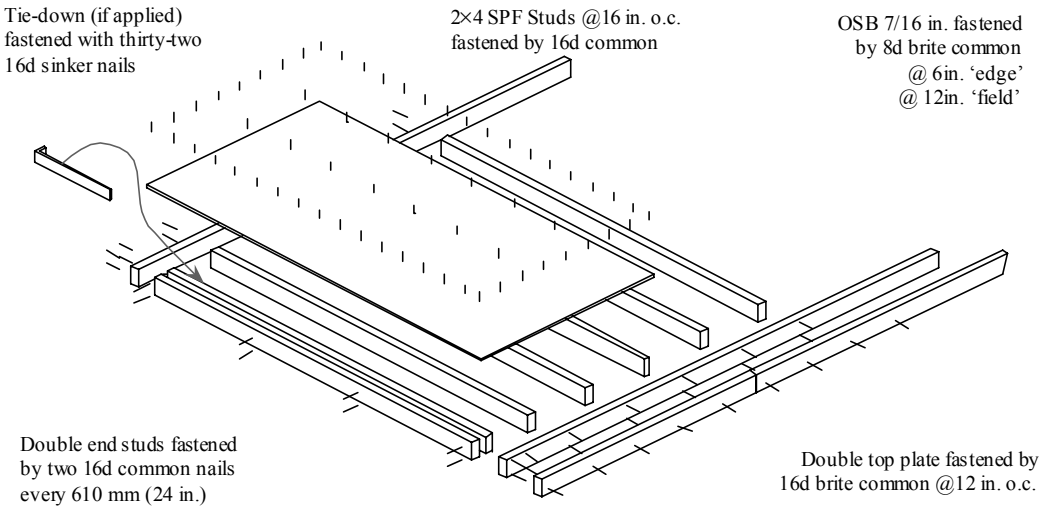

Figure 3. 4. Wall assembly (Courtesy of C. Heine).

An important factor affecting the shear wall performance is the quality and fabrication tolerances for sheathing-to-framing attachment. Although importance of this issue is emphasized in ASTM E 72, researchers often do not report what edge distances they used in manufacturing test specimens. Note that the height of the standard test

specimen allows convenient attachment of the sheathing to the bottom plate at an edge distance of 19 mm (3/4 in.), which is limited by the 38-mm (1.5-in.) typical framing thickness. However, the typical wall height in North American platform construction is 2467 mm (97-1/8 in.), which is 30 mm (1-3/16 in.) longer than the standard sheathing panel. This leaves an edge distance of approximately 10 mm (3/8 in.) for nailing if 2353-mm (92-5/8-in.) long studs are used.

Current design provisions require fasteners to be placed at least 3/8 in. (10 mm) from ends and edges of boards and sheets (BSSC 1998). As is shown in Chapter 4, monotonic tests of sheathing-to-framing nailed connections have revealed a 40% reduction of the connection deformation capacity (ultimate displacement) in direction perpendicular-to-grain when the edge distance was reduced from 19 mm (3/4 in.) to 10 mm (3/8 in.). Therefore, it is important to account for the edge-distance effects during shear wall tests. However, the author is unaware of any other recent studies of the influence of the nail-edge distance on connection and/or shear wall performance.

In this study, most of the specimens had sheathing fastened to the framing with 19-mm (3/4-in.) edge distance along the top and bottom plates. Eight specimens were intentionally nailed with the reduced edge distance to represent the minimum allowable by current design provisions specified in NEHRP (BSSC 1998). No interior sheathing was applied.

Prior to testing, the specimens were stored in the laboratory for at least two weeks to allow for wood relaxation around the nails.

3.5 Test Setup

Specimens were tested in a horizontal position, as is shown in Figure 3. 5. In this setup, no dead load was applied in the plane of the wall, which conservatively represented a wall parallel to floor joists. Walls **FA** and **IA** were supported by 76×127-mm (3×5-in.) steel beam attached to the bottom plate as shown in Figure 3. 3a and b. To eliminate any interference of the support with the sheathing displacements, the narrow face of the beam was oriented towards the plates. Walls **NA** were attached to a wood sole plate made of two 2×4 members as shown in Figure 3. 3c. The steel support

beam and the wood sole plate were secured to the reinforced-concrete foundation by ∅15.9-mm (5/8-in.) anchor bolts.

Another 76×127-mm (3×5-in.) steel beam was attached at the top plate with ∅15.9-mm (5/8-in.) bolts spaced 610-mm (24-in.) o. c. distributing the racking load from a programmable hydraulic actuator. To reduce the amount of the wall slip along the support during the test, the oversize of holes for the shear bolts was minimized. The holes in the supporting beams were only 0.8 mm (1/32 in.) larger than the bolt diameter, the holes in the top and bottom plates were drilled without oversize. On the contrary, the holes for the anchor bolts in walls **FA** were drilled regular size ∅17.5 mm (11/16 in.) and then elongated 13 mm (1/2 in.). It was done to minimize the interference of the anchor bolts into shear resistance and to minimize the shear force effects on the tension force measurements in the instrumented bolts.

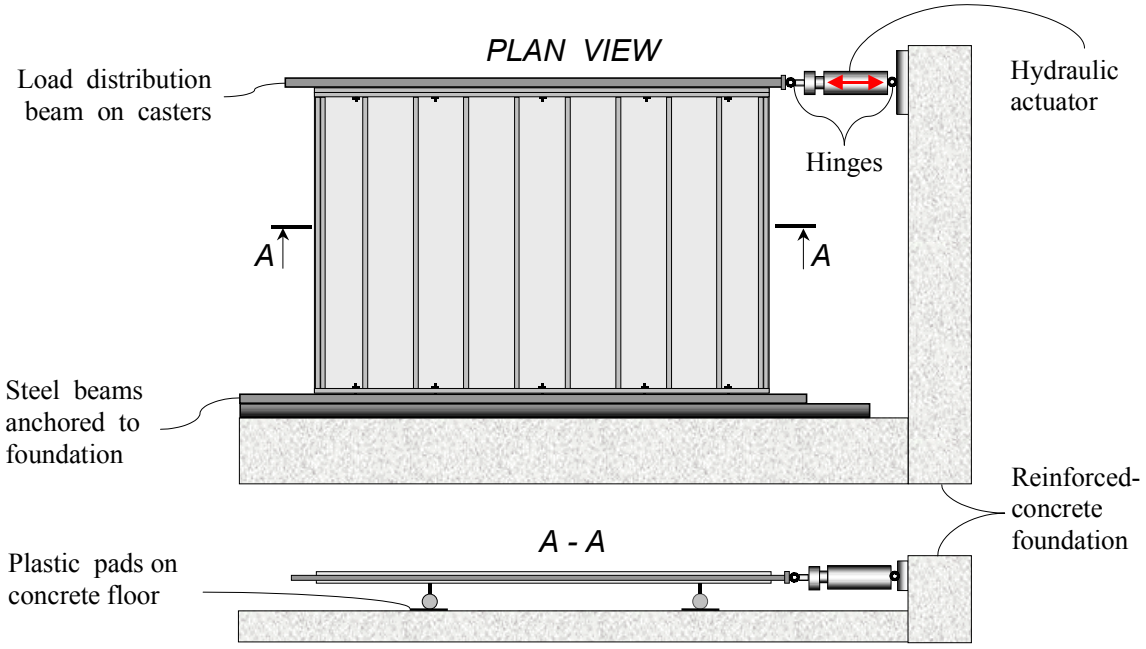

Figure 3. 5. Test setup for shear wall with aspect ratio 2:3.

The actuator, with a displacement range of ±152 mm (6 in.) and a capacity of 245 KN (55 Kips), was secured between the support and the distribution beam by means of the hinged connections shown in Figure 3. 5. If these hinges were omitted, the separation of the wall framing during the test would be restrained by the weight of the

equipment, and the load measurement would be biased by the induced moment. Two casters were fixed to the load distribution beam, to allow free movement of the top of the specimen in a parallel direction to the applied load. The casters rolled along the greased surface of plastic pads laid on the floor to reduce any friction induced by the wall weight.

3.6 Load Regimes

All walls were tested monotonically and cyclically. In the absence of a standard cyclic test procedure, researchers in the USA and other countries perform cyclic tests using different protocols. They have noticed that fatigue failure of fasteners caused by SPD tests and other "long" protocols generally is not observed during seismic events. The fatigue of fasteners is due to significantly greater energy demands imposed by these procedures than experienced during historic earthquakes (Karacabeyli and Ceccotti 1998). On the other hand, "short" cyclic protocols that produce realistic failure modes do not reveal the effects of load history on shear wall performance. This information is important for rehabilitation of the buildings surviving severe earthquakes and for establishing multiple performance levels of structures in future design codes.

In the SPD procedure, phase increments are a function of the *first major event* (FME), defined as "the first significant limit state to occur" (SEAOSC 1997a). Since the response of wood shear walls in the elastic range is nonlinear and the deflections are small, the value of FME is difficult to measure. Researchers determine the FME differently and arrive at values varying between 2.5 and 20.3 mm (0.1 and 0.8 in.). In the recently proposed ISO protocol for timber joints (ISO 1998), the phase increments are determined as a function of the ultimate displacement obtained from monotonic tests. The ultimate displacement corresponds to failure displacement, a displacement corresponding to 20% load decrease after the peak load, or a limiting displacement, whichever occurs first (ISO 1998). This approach allows more consistent interpretation of the test procedure, which provides an advantage in comparison with the FME definition. However, unlike the SPD test, the ISO test is performed at a constant rate of displacement, which is further removed from seismic load conditions.

In the search for harmony between obtaining the maximum information and realistic failure modes, the author used a hybrid of the SPD and the ISO protocols during these cyclic tests. According to the SPD procedure, a constant frequency of the wall excitation was used. Decay cycles were eliminated, allowing reduction of the energy demand without affecting the wall response (Rose 1998). The pattern of cycling was set using the ISO approach, while being consistent with the FME definition.

Displacement history plots for monotonic and cyclic test procedures are shown in Figure 3. 6. Each test was stopped when the specimen fully exhausted its ability to resist load. Monotonic load was applied at 15 mm/min (0.6 in./min.) in a single stage. Unlike the specifications in ASTM E72 and E564, unloading phases were omitted: the load was progressively increased from zero to maximum until failure of the specimen. The unloading phases were eliminated in the monotonic procedure because of the limited information provided onset.

Cyclic load was applied at a frequency of 0.25 Hz with three cycles in each phase following three initial phases of single cycles. The amplitudes of the phases were 2.5, 5.0, 7.5, 10, 20, 30 percent, etc. of the ultimate monotonic displacement. The average ultimate displacement of 76 mm (3.0 in.) was observed during the monotonic tests of walls with sheathing attached at the minimum edge distance. In terms of the SPD procedure, the same pattern of cycling would correspond to the FME of 7.6 mm (0.3 in.), which conservatively fit the observed results.

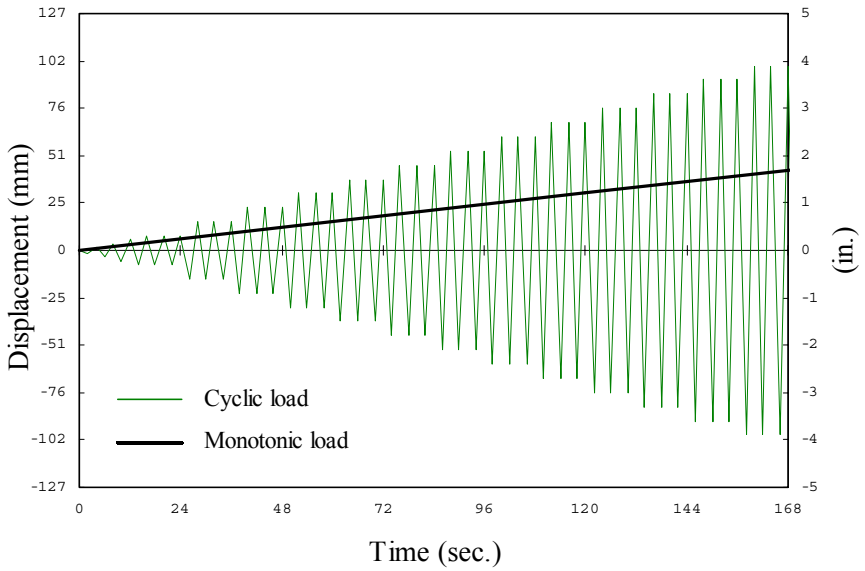

Figure 3. 6. Displacement pattern of monotonic and cyclic loading procedures.

3.7 Instrumentation and Measurements

Careful instrumentation is extremely important for interpretation of test results. Regrettably, many reports provide little detail (if any at all) describing the measurement systems used. This prohibits evaluation of accuracy and, sometimes, correctness of data, and minimizes the benefit that readers could obtain from their predecessors' achievements and/or mistakes. When developing the instrumentation setup, advantages and flaws of that used by Heine (1997) were considered and some improvements assumed.

The data acquisition system used during the tests is portrayed in Figure 3. 7. The maximum 16 channels of data acquisition were employed. The hydraulic actuator contained the internal LVDT (channel #1) and the load cell (channel #2) that supplied information on the applied force and displacement. These two transducers supplied the basic data for the load-deflection analysis of the tests. Other transducers provided supplementary information that allowed detailed monitoring of the specimen performance during the test.

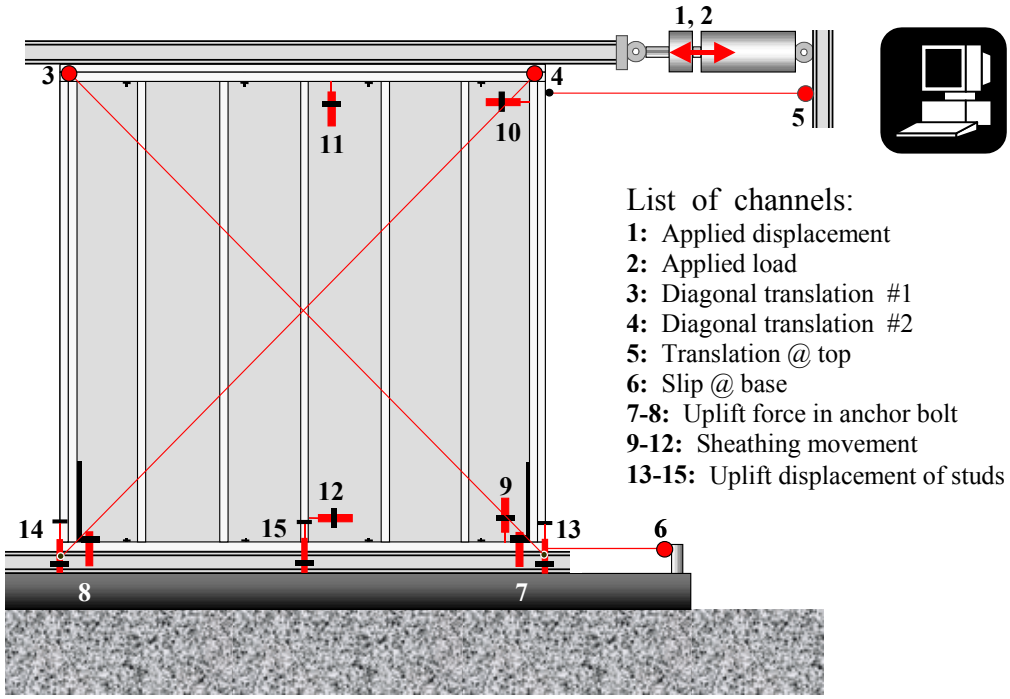

Figure 3. 7. Instrumentation of shear wall test specimen

Resistance potentiometers (pots) #3 and #4 measured diagonal elongation of the wall between the top and bottom plates. The diagonal measurements were taken to obtain information on pure shear deformation of the wall assuming the specimen distorted as a parallelogram (according to ASTM E564). However, this assumption was valid only until separation of the studs from top and/or bottom plates started. Pot #5 attached to a rigid foundation measured lateral translation of the top of the right end stud. The difference between readings of channel #1 and #5 illustrated the separation of the stud from the top plate or slip of the top plate with respect to the load distribution beam during the test. Pot #6 recorded the horizontal slip of the wall relative to the foundation.

Channels #7 and #8 represent anchor bolts instrumented with strain gages for direct measuring of tension forces experienced in the anchors during loading. These channels were in use only when full anchorage conditions were tested.

LVDT's (channels #13 and #14) were mounted on the base to measure uplift displacement of the end studs relative to the foundation. The information was used to account for rotation when determining true racking (shear) deformation of walls. Heine (1997) followed Johnson (1997) and used for this purpose brackets protruding outside the

wall frame. Consequently, the readings were amplified depending on the method of anchorage and required additional assumptions for interpreting the data. In our tests, LVDT's were aligned with the stud edges to produce more reliable and unbiased results. Walls with aspect ratios of 1:1 and 2:3 accommodated additional LVDT's (#15) and (#15 and #16), respectively to measure uplift of intermediate studs. These observations were used in determining rotational points of the walls.

To measure the displacement of sheathing relative to the frame, one sheathing panel in each wall accommodated four LVDT's (#9 to #12) near the panel corners. The LVDT probes were rested against polished steel plates attached to the studs to reduce friction when the probe moved along the stud. It was assumed that channels #9 and #11 measured only vertical translation components and channels #10 and #12 – the horizontal components. When Heine (1997) used this system in his tests, it appeared too delicate and failed occasionally causing confusion during data processing. In two tests, the LVDT's were replaced by resistance potentiometers in a hope to obtain a better system. The idea was declined, because the data collected with the pots included both horizontal and vertical translation components, which was not feasible to separate.

The resolution of the measuring tools and possible errors of measurements are presented in Table 3. 5. Due to wide range of anticipated deformations, adequate precision could not be achieved in measuring wall deflections and movements of sheathing at small displacements. Beyond 2.5-mm (0.1-in.) translation of the load cell, the equipment was capable of providing sufficiently precise measurements. For example, the error of measuring the wall deflection did not exceed 2.0%.

During the monotonic tests, data was recorded at a frequency 15 times per second; during the cyclic tests, data was recorded at a frequency 25 times per second. Heine (1997) concluded that higher frequency of sampling did not ensure better accuracy but slowed data processing greatly.

Table 3. 5. Resolution of measuring tools and possible errors of measurements.

Measuring tool			**Measurement**		
Name	Range	Resolution	Application	Range	Error, % [1)]
Tape measure	8 m 25 ft.	1.6 mm .0625 in.	Manufacture of wall, installation of pots, LVDT's, and bolts	127-3700 mm 3-144 in.	1.0 0.2
Load cell	245 KN 55 Kips	0.12 KN 27 lbf.	Measure applied load	1.3-27 KN 300-6000 lbf.	4.5 0.2
LVDT #1 (Actuator)	±152 mm ±6 in.	$\pm 7.4 \times 10^{-2}$ mm $\pm 2.9 \times 10^{-3}$ in.	Measure load cell movement	0.6-127 mm 0.025-5.0 in.	11.6 0.06
LVDT's #9 to #16	±25.4 mm ±1.0 in.	$\pm 1.2 \times 10^{-2}$ mm $\pm 4.9 \times 10^{-4}$ in.	Measure movement of studs and sheathing	0.13-25.4 mm 0.005-1.0 in.	2.0 0.05
Pots #3, 4, 5	±152 mm ±6 in.	$\pm 7.4 \times 10^{-2}$ mm $\pm 2.9 \times 10^{-3}$ in.	Measure racking displacement	0.6-127 mm 0.025-5.0 in.	11.6 0.06
Pot #6	±25.4 mm ±1.0 in.	$\pm 1.2 \times 10^{-2}$ mm $\pm 4.9 \times 10^{-4}$ in.	Measure slip at base	0.13-25.4 mm 0.002-0.8 in.	24.5 0.06
Instr. bolts #7 and #8	±44 KN ±10 Kips	±0.022 KN ±4.9 lbf.	Measure forces in anchors	0.45-22 KN 100-5000 lbf.	2.5 0.05

[1)] In numerator is maximum possible error, in denominator – minimum error

3.8 Classification of the Experiment

A three-way cross-classification of the experiment is displayed in Table 3. 6. Four wall configurations (4:1, 2:1, 1:1, and 2:3) were tested using two load procedures: monotonic and reversed cyclic. Three anchorage conditions were examined representing different construction practices and location of the segment in a wall: 'Full anchorage' (**FA**), 'Intermediate anchorage' (**IA**), and 'No anchorage' (**NA**). According to ASTM E564, it was planned to perform each test twice unless load-displacement relationships do not agree within 15%. In this case, a third identical test would be conducted. During the tests, the number of replications was changed: in some cases more than two specimens were tested, in other cases one specimen was considered sufficient. The deviations from the plan and the test results are discussed in Chapter 5. The amount of component materials for wall assembly and for the entire project is estimated in Table 3. 7.

Table 3. 6. Three-way cross-classification of the experiment.

Aspect ratio and wall size	**Load**	**Number of tests**			**Total**
		Full anchorage	**Intermediate anchorage**	**No anchorage**	
4:1 2.4×0.6 m (8×2 ft.)	*Monotonic*	2	2	-	4
	Cyclic	2	2	-	4
2:1 2.4×1.2 m (8×4 ft.)	*Monotonic*	2	2	2	6
	Cyclic	2	2	2	6
1:1 2.4×2.4 m (8×8 ft.)	*Monotonic*	2	2	2	6
	Cyclic	2	2	2	6
2:3 2.4×3.6 m (8×12 ft.)	*Monotonic*	2	2	2	6
	Cyclic	2	2	2	6
Total		12	16	16	44

Table 3. 7. Estimated amount of materials for shear wall tests.

Aspect ratio and wall size	**Type** [1] **number of walls**	**Materials per wall**						
		OSB 7/16 in. 8×4 ft.	**Frame 2×4 in. SPF**	**Anchors Simpson HTT22**	**Bolts 5/8in.**	**Nails**		
						8d [2]	**16d** [3]	**16d** [4]
4:1 2.4×0.6 m (8×2 ft.)	**NA** -	-	-	-	-	-	-	-
	IA 4	1/2	5	-	2	38	34	-
	FA 4	1/2	5	2	2	38	34	64
2:1 2.4×1.2 m (8×4 ft.)	**NA** 4	1	8	-	-	62	80	-
	IA 4	1	8	-	2	62	44	-
	FA 4	1	8	2	2+2	62	44	64
1:1 2.4×2.4 m (8×8 ft.)	**NA** 4	2	12	-	-	124	132	-
	IA 4	2	12	-	2+2	124	60	-
	FA 4	2	12	2	4+2	124	60	64
2:3 2.4×3.6 m (8×12 ft.)	**NA** 4	3	17	-	-	186	184	-
	IA 4	3	17	-	4+2	186	76	-
	FA 4	3	17	2	6+2	186	76	64
Total	**44**	**76**	**484**	**32**	**72** [5]	**4768**	**824**	**1024**

[1] **NA**: No anchorage series, **IA**: Intermediate anchorage series, **FA**: Full anchorage series.

[2] *SENCO*® bright common nails ASTM F 1667 NL CM S – 07 B.

[3] Bright common nails ASTM F 1667 NL CM S – 11 B.

[4] Sinker nails ASTM F 1667 NL SK– 09 C.

[5] Instrumented bolts are not included in total number of bolts.

3.9 Summary

An experimental program and the rationale for testing full-size shear wall segments have been presented. Objectives of the experiment are to obtain the performance characteristics of shear walls with various aspect ratios and anchorage conditions. A minimum of 44 full-size shear walls of four aspect ratios (4:1, 2:1, 1:1, and

2:3) were planned to be tested using two load procedures: monotonic and reversed cyclic. The three types of anchorage conditions utilized in the tests represented different construction practices and location of the segment in a wall. The test setup and the system of measurements, including up to 16 channels of electronic data acquisition, were developed, which provided satisfactory accuracy. The number of components for assembly of each specimen and for the entire project was shown.

In the next chapter, physical and mechanical properties of wall components are presented. Results of the shear wall tests are discussed in Chapter 5.

Chapter 4. Material Properties

4.1 General

In this chapter, physical and mechanical properties of shear wall components, such as OSB sheathing, framing lumber, sheathing nails, and sheathing-to-framing connections, are discussed. This information is used in the analysis of test results on shear walls and as input data for analytical models of shear walls. It is also useful for future comparisons with materials used in other shear wall tests.

4.2 Sheathing Panels

Oriented strandboard (OSB) panels manufactured by Georgia Pacific were purchased locally. The panels were 11-mm (7/16-in., nominal) thick, rated 24/16 Exposure 1 sheathing. The label from the wrapper on one packet of OSB is shown in Figure 4. 1.

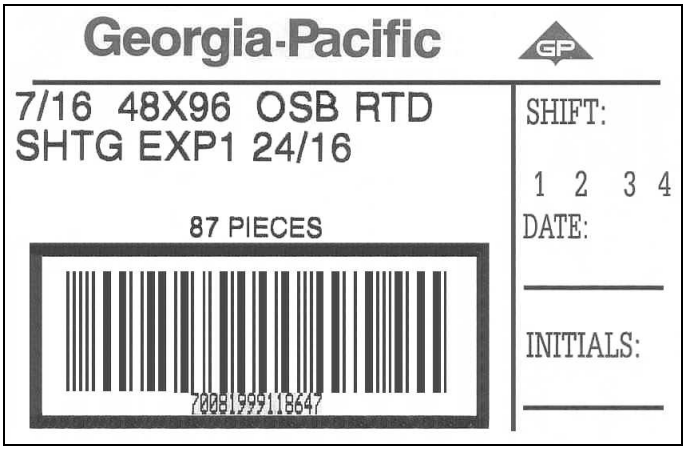

Figure 4. 1. Wrapper's label of OSB panels.

Stiffness properties of the OSB panels are listed in Table 4. 1. These values are based on the APA published design values (APA 1995) with the adjustment for the panel grade and construction.

Table 4. 1. Mechanical properties of OSB panels.

Mechanical Property	Units	Stress applied parallel to strength axis	Stress applied perpendicular to strength axis
Panel bending stiffness, *EI*	KN-mm^2/m width	734,000	152,000
	lb-in^2/ft. width	78,000	16,000
Panel axial stiffness, *FA*	KN/m	55,400	42,300
	lb./ft.	3,800,000	2,900,000
Panel rigidity through thickness, $G_v t_v$	N/mm of depth	14,700	14,700
	lb./in. of depth	83,700	83,700

4.3 Framing Elements

The SPF stud grade lumber produced by Canadian company CANFOR was purchased from the local Lowe's retail store. Two types of 2 by 4 dimension lumber were obtained: 2438-mm (96-in.) long studs (Figure 4. 2) and 2353-mm (92 5/8-in.) long studs (Figure 4. 2b). The first dimension was used in the top and bottom plates; the second was used in stud elements. All elements were cut to length and then stored outside in two stacks (Figure 4. 3) covered by a tarp two weeks before wall manufacture.

a) b)

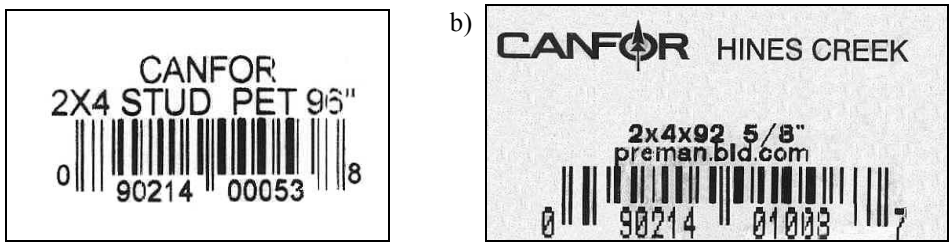

Figure 4. 2. Lumber manufacturer's packet labels: a) 96-in. studs, b) 92 5/8-in. studs.

Prior to wall assembly, every stud and 2.4-m (8-ft.) long plate member was tested using *Metriguard* system to determine the dynamic modulus of elasticity (MOE) on flat side (both flat sides were tested). In a shear wall, the framing is bent about the flat side; therefore, the tests should have produced reasonably accurate estimate of the MOE for use in numerical analysis. The advantage of using this method is the ability to obtain results instantaneously. The test setup is shown in Figure 4. 4. The method is based on determination of natural frequency of free vibration of the beam, which is related to its

stiffness and mass assuming single-degree-of-freedom system. The natural frequency is governed by the following equation:

Figure 4. 3. Lumber storage.

$$\omega^2 = \frac{48EI}{mL^3} \tag{4. 1}$$

where, EI = stiffness of the beam,

m = mass of the beam,

L = span of the beam.

Rearranging the terms, the value for MOE is found:

$$E = \frac{mL^3}{48I} \cdot \omega_n^2 \tag{4. 2}$$

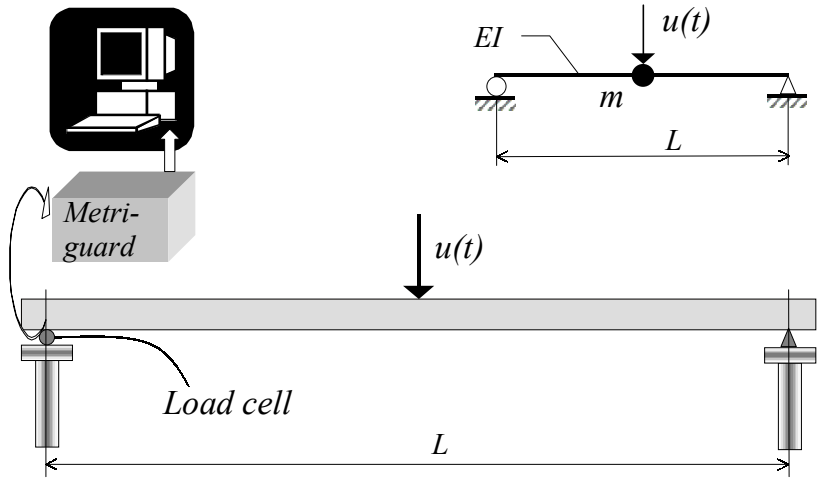

Figure 4. 4. Test setup for determining dynamic MOE of lumber.

The *Metriguard* system allowed estimating the wood density in kg/cm^3 by measuring the mass (weight) of the beam. The moisture content (MC) of wood was measured using electric moisture meter with 6-mm (1/4-in.) long needles. Certainly, these measurements produced the MC near the lumber surface and did not reflect the average MC of the wood. The MC data served as a check for the uniformity of MC for the lumber in stock.

To estimate the static MOE and to check the correlation between the dynamic and the static MOE, a number of additional tests were performed using static load. Similar to the *Metriguard* test, the beam was loaded on the flat side at the center of the 2285-mm (90-in.) span. The load was applied in two steps of 222 KN (50 lbf.). The increase of deflection between the first and the second steps was measured at the mid-span using a dial gage with 0.025-mm (0.001-in.) resolution. The measurement was repeated during unloading and the absolute values of the deflections were averaged for the record. Then, the opposite side of the beam was tested. The static MOE was calculated using the formula:

$$E = \frac{PL^3}{48I\Delta} \tag{4. 3}$$

where, P = 50 lbf.,

Δ = average deflection during uploading and unloading.

The static test is more time consuming than the *Metriguard* test. Therefore, it was conducted on a sample of randomly selected pieces of lumber. The minimum sample size was initially estimated using the formula (Ott, 1992):

$$n = \frac{(z_{1-\alpha/2})^2\sigma^2}{\varepsilon^2} = \frac{1.645^2 \cdot (3.0\times10^5)^2}{(6\times10^4)^2} \approx 68 \tag{4. 4}$$

where, ε = 0.05×1.2x10^6 psi, tolerable error; limited by the range of error due to measurements, assumed 5% of allowable design value for SPF Stud Grade,

σ = $0.25 \times 1.2 \times 10^6$ psi, standard deviation; for MOE of lumber assumed 25% of allowable design value for SPF Stud Grade,

$z_{1-\alpha/2}$ = 1.645, quintile of normal distribution for $\alpha = 0.10$.

The results of regression analysis based on 120 observations (60 studs tested on two sides) are illustrated in Figure 4. 5. The data show sufficiently good correlation ($R^2 = 0.888$) between the static and the dynamic MOE with linear regression coefficient equal 0.927. The standard deviation was within 18% in both data sets.

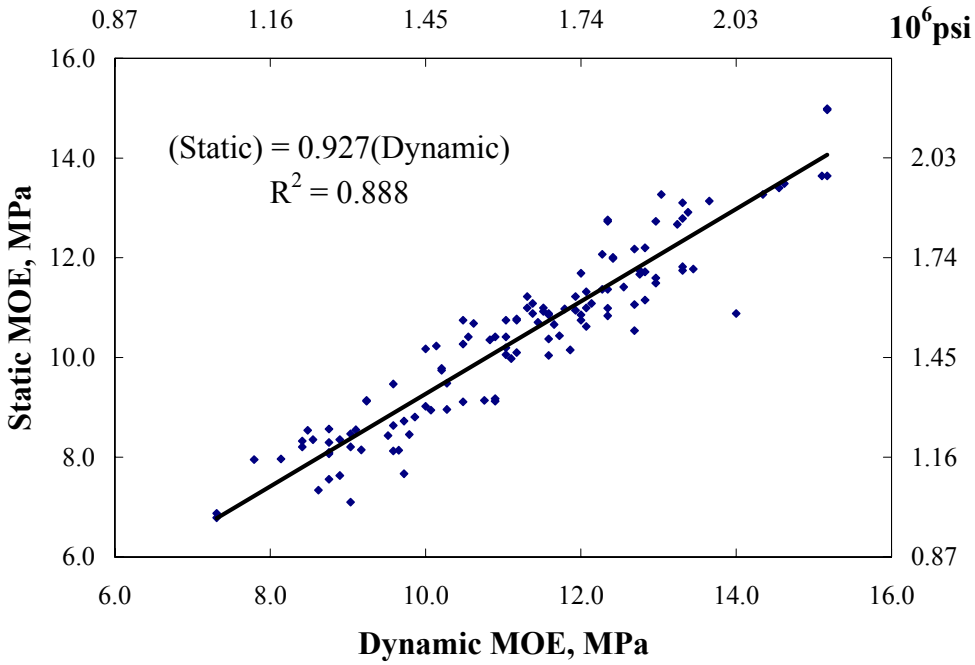

Figure 4. 5. Linear regression between dynamic and static MOE.

Table 4. 2 presents the statistical summary of *Metriguard* tests, moisture content measurements, and conversion of the dynamic MOE into the static MOE based on the results of regression analysis. Analysis of variation (*t*-test) revealed a significant statistical difference between the properties of lumber used for studs and plates. The plates appeared approximately 15% more dense and stiff than the studs; therefore, the data should be used with discretion during numerical modeling of the shear walls.

Table 4. 2. Summary of lumber parameters.

Parameter	Statistic	Studs	Plates
Dynamic MOE	Mean, MPa Mean, 10^6psi C.O.V., %	10.9 1.57 17.6	12.6 1.83 14.9
Static MOE	Mean, MPa Mean, 10^6psi	10.1 1.46	11.7 1.70
Density	Mean, kg/cm^3 C.O.V., %	0.478 10.9	0.547 10.5
Moisture content	Mean, % Standard Deviation	10.2 1.3	12.4 1.7
Number of observations[1]		638	130

[1] Each piece of lumber was tested on two sides.

4.4 Sheathing Nails

OSB sheathing was attached to framing by 8d SENCO® steel wire common nails using a pneumatic gun. Parameters of these fasteners correspond to the following ASTM specification: F 1667 NLCMS–07B, i.e., steel wire, flat head, diamond point, round smooth shank, bright; shank diameter D = 3.3 mm (0.131 in.), length L = 63.5 mm (2 ½ in.), and head diameter H = 7.1 mm (0.281 in.).

A sample of 10 nails from the manufacturing lot was tested to determine the nail bending strength according to ASTM 1575. The MTS servo-hydraulic testing machine was used with the 2.2-KN (500-lbf.) load cell. The load was applied at a constant rate of displacement in the middle of the 38-mm (1 ½-in.) span. Digital load-deflection data were recorded during the tests and the bending resistance parameters of the nails were determined using an Excel program. The yield point was found at the intersection of the load-deflection curve and a straight line representing the initial tangent modulus offset 5% of the nail diameter as shown in Figure 4. 6. The low variability of results allowed establishing the nail bending properties based on a small sample size of 10 replications. Table 4. 3 shows statistics of the yield point, elastic stiffness, and the ultimate strength of the nails in the sample.

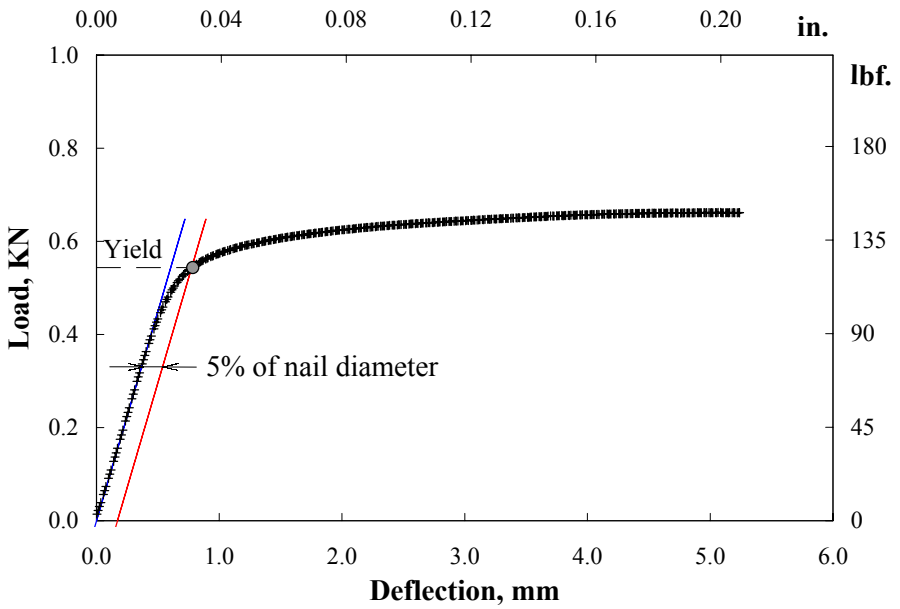

Figure 4. 6. Typical load-deflection curve to determine the yield point of nail.

Table 4. 3. Summary of sheathing nail parameters.

Parameter	Units	Mean	C.O.V.
Yield strength σ_{yield}	MPa	827	4.61%
	Ksi	120	
Deflection at yield point Δ_{yield}	mm	0.765	3.75%
	in.	0.030	
Elastic stiffness EI	KN·mm^2	1027	2.75%
	lbs·in^2	358	
Ultimate strength σ_{max}	MPa	1022	1.33%
	Ksi	148	

4.5 Sheathing-to-Framing Connections

4.5.1 Introduction

Racking performance of shear walls is governed by characteristics of sheathing-to-framing connections. It is well known that yielding of nails between sheathing and framing is the main source of ductility in typical shear walls. When other means of connection are used, such as screws and/or adhesive, the ductility and the failure mode can change significantly. Therefore, any analytical model of a shear wall includes characteristics of sheathing-to-framing connections. It is desirable to approximate the connection performance by a function, which allows closed-form mathematical solution.

To obtain characteristics of the sheathing-to-framing connections for further use in analytical modeling, thirty monotonic tests were performed on sheathing connections representing the performance of a single nail in a shear wall. The following paragraphs provide background information on the models of the nonlinear load-slip performance of nailed connections used in this study. Then, the influence of load direction and the sheathing edge distance in sheathing-to-framing connections is discussed. The test procedure and the test results of the sheathing-to-framing connections are followed by the concluding remarks.

4.5.2 Background

Ehlbeck (1979) provided extended overview of the nailed joints' performance. In recent years, numerous empirical models have been proposed for describing non-linear load-slip relationship of nailed connections, including hysteretic models for predicting the dynamic performance (e.g., Wen 1980, Stewart 1987, Dolan 1989, Ceccotti and Vignoli 1990, Foliente 1995, Chui et al 1998, etc.). It was not a goal of this study to propose a new model but to utilize the most popular and practical solutions.

One of the most often cited is the model developed by Foschi (1974) for a nail on an elastic-plastic foundation expressed as:

$$F_n = (P_0 + K_1\delta)\left[1 - \exp(\frac{-K_0\delta}{P_0})\right] \quad (4.5)$$

The physical meaning of the constants K_0, K_1, and P_0 is illustrated in Figure 4. 7. Constants K_0 and K_1 determine the initial and post-yield stiffness of the connection and P_0 is the load-intercept of the post-yield stiffness asymptote.

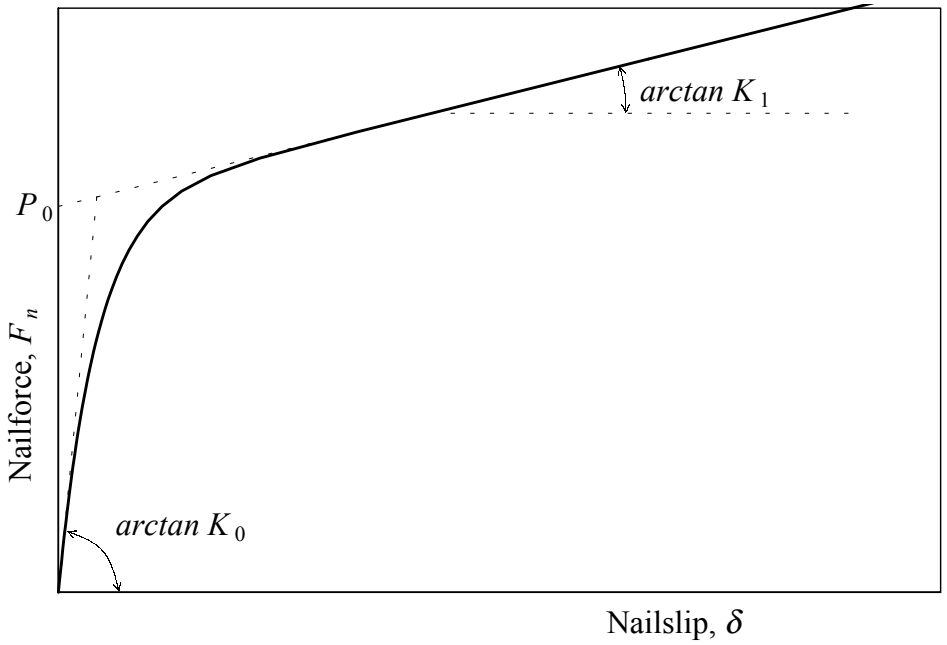

Figure 4. 7. Foschi load-slip curve.

Foschi (1977) applied this relationship in finite-element analysis of diaphragms and trusses under static loads. Dolan (1989) modified the Foschi equation by adding post-capacity degradation slope:

$$F_n = (P_0 + K_1\delta)\left[1 - \exp(\frac{-K_0\delta}{P_0})\right] - K_2(\delta - \delta_{peak}) \quad (4.6)$$

where, K_2 defines the slope for deformations greater than δ_{peak} as is shown in Figure 4. 8.

Dolan incorporated the modified equation into his hysteresis model of the sheathing-to-framing connector and used it in his finite-element model of shear wall for dynamic analysis.

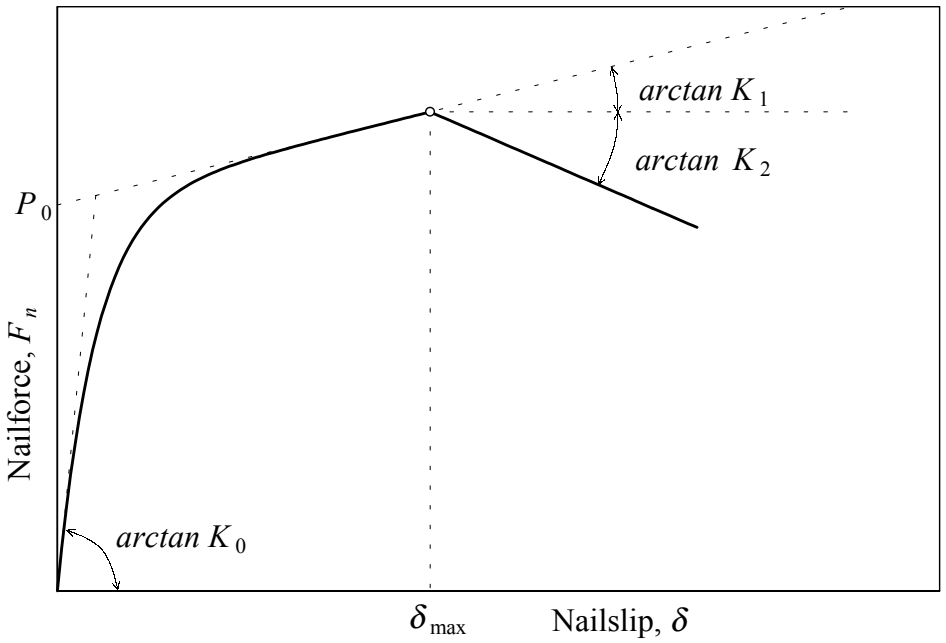

Figure 4. 8. Modified Foschi load-slip curve (Dolan 1989).

McCutcheon (1985) showed several non-linear functions that could be applied for predicting the racking deformation of shear walls using energy method. Patton-Mallory and McCutcheon (1987) conducted an experimental study on single-fastener connections and small-scale shear walls with plywood and gypsum panels. After fitting power, logarithmic, asymptotic, and hyperbolic tangent functions, the authors concluded that the asymptotic fastener curve produced the best predictions of shear wall performance up to peak loads:

$$F_n = \frac{A_0 \cdot \delta}{A_1 + \delta} \tag{4. 7}$$

Parameters A_0 and A_1 have physical meanings: A_0 represents the asymptotic strength of the connection and A_1 represents the slip at half the asymptotic strength. A_1 can also be represented as a factored service slip (Deam 1997) as is shown in Figure 4. 9:

$$F_n = \frac{F_a \cdot \delta}{1.5\delta_s + \delta} \tag{4. 8}$$

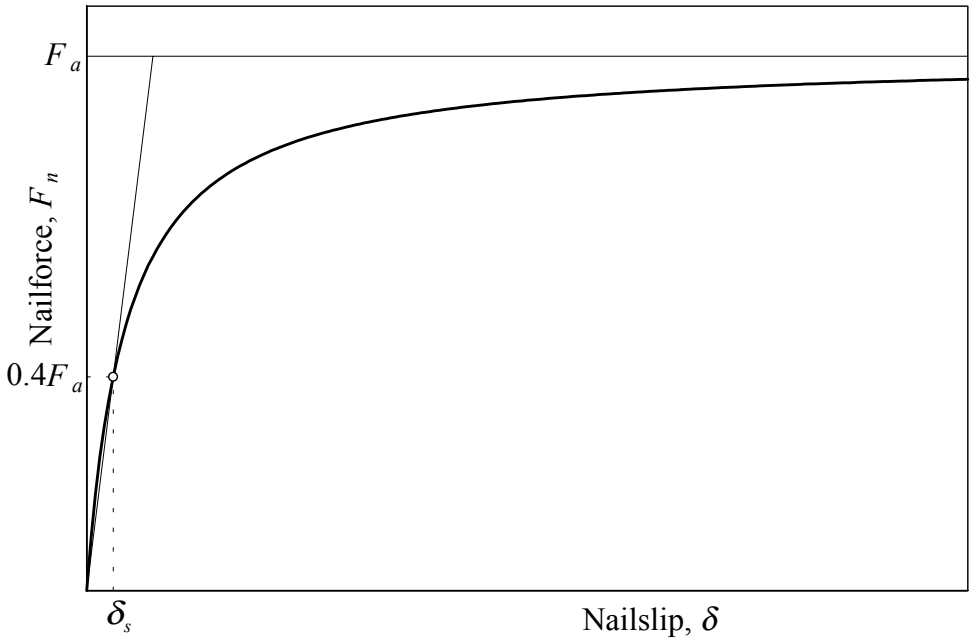

Figure 4. 9. Asymptotic approximation of load-slip curve.

Commercial finite element analysis program SAP®2000 (CSI 1997) uses simplified Wen's (1976) model for dynamic analysis of structures with so-called nonlinear link elements. The load-slip relationship of the link elements is represented independently in two orthogonal directions and is expressed as follows:

$$F_n = ratio \cdot K \cdot \delta + (1 - ratio) \cdot yield \cdot z \tag{4. 9}$$

where, K = elastic spring constant;

ratio = ratio of post-yield stiffness to elastic stiffness;

yield = yield force;

z = internal hysteretic variable, $|z| \le 1$, determined as:

$$z = \frac{K}{yield} \begin{cases} \delta \cdot \left(1 - |z|^{exp}\right) & if \quad \delta z > 0 \\ \delta & otherwise \end{cases} \tag{4. 10}$$

The shape of the load-slip relationship and physical meaning of the constants are illustrated in Figure 4. 10.

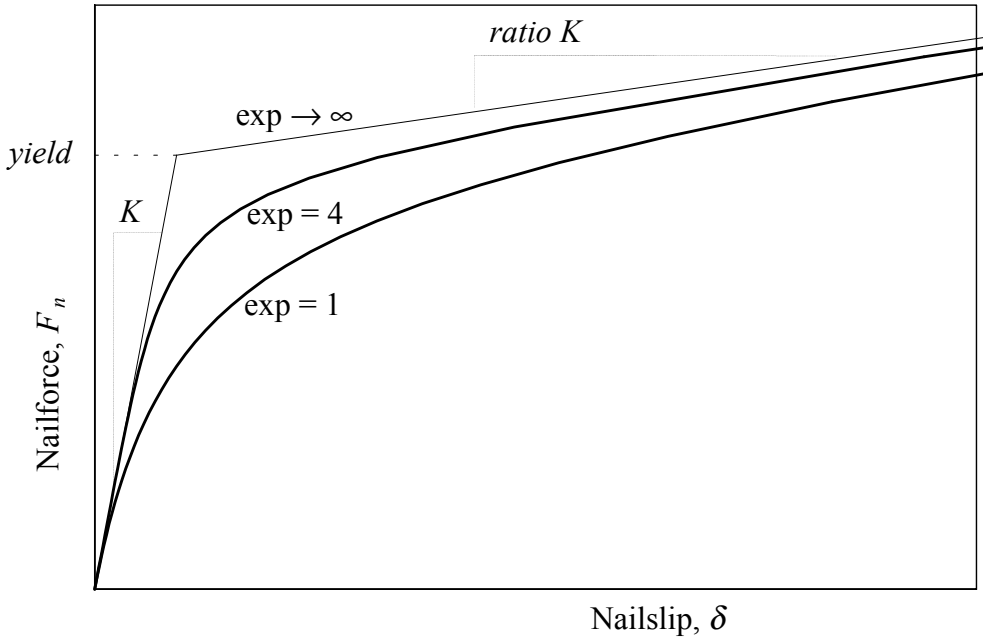

Figure 4. 10. Parameters of nonlinear link element in SAP2000 (SCI 1997).

More advanced and sophisticated models including so-called pinching effects in nailed connections under cyclic loading have been proposed recently by Foliente (1995) and Chui et al (1998). These models are not discussed here because the cyclic tests of sheathing-to-framing connections were not conducted during this study.

Dolan (1994) proposed an ASTM standard test method for dynamic properties of connections assembled with mechanical fasteners. In this method, the nonlinear performance of the connection is approximated by a bilinear equivalent energy elastic-plastic curve (EEEP) as is shown in Figure 4. 11. The EEEP curve represents an ideal elastic-plastic connection dissipating an equivalent amount of energy with the real connection. This definition of the EEEP curve can be used for both monotonic and cyclic tests.

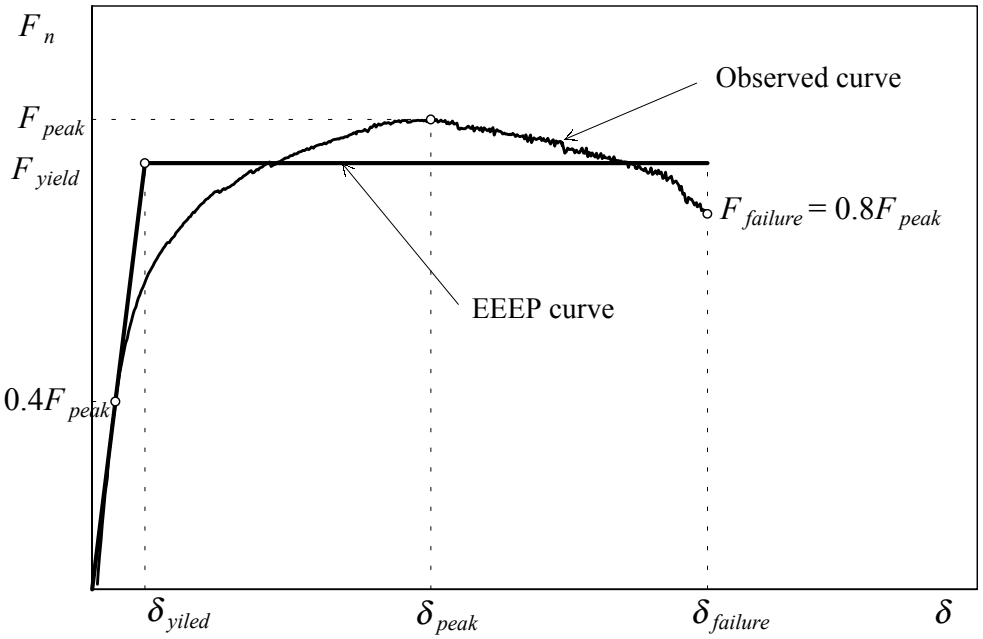

Figure 4. 11. EEEP curve parameters.

The elastic portion of the EEEP curve represents the elastic stiffness, K_e. The plastic portion of the EEEP curve is a horizontal line positioned so that the area under the EEEP curve equals the area under the response curve from zero to deflection at failure, $\delta_{failure}$. The deflection at failure corresponds to the point on the curve where force decreases to a value of 80% of the peak force, F_{peak}. The yield point (F_{yield}, δ_{yield}) is found at the intersection of the elastic and plastic lines of the EEEP curve. Equating the areas under the response curve and the EEEP curve, the yield force can be expressed as (Heine 1997):

$$F_{yield} = \frac{-\delta_{failure} \pm \sqrt{\delta_{failure}^2 - \frac{2A}{K_e}}}{-\frac{1}{K_e}} \tag{4. 11}$$

where: A = area under the response curve between zero and $\delta_{failure}$;

$$K_e = 0.4F_{peak}/\delta@0.4F_{peak}$$

The ductility ratio of the connection is found from the EEEP curve:

$$D = \frac{\delta_{failure}}{\delta_{yield}} \tag{4. 12}$$

In this study, parameters of Foschi-Dolan, Wen, asymptotic, and EEEP curves were determined during the analysis of the sheathing-to-framing connections.

4.5.3 Load Direction and Edge Distance Effects

In the *National Design Specification for Wood Construction*, NDS (AF&PA 1991), *American Plywood Association*, APA, publications, and other literature, it is accepted that there is no difference in performance of nailed connections loaded parallel- and perpendicular- to-grain. However, a minute look at the shear wall construction and performance reveals differences in boundary conditions between nails working in parallel-to-grain direction and across the grain.

Figure 4. 12 illustrates typical distortion pattern of an engineered fully-anchored shear wall under the racking load. Assuming infinitely rigid framing elements, the ratio of the vertical and horizontal components of the sheathing nails distortion at the corners equals the aspect ratio (height-to-length) of the sheathing panel (McCutcheon 1978). Assuming a finite stiffness of the chords, Stewart (1987) and Murakami *et al* (1999) have demonstrated that the ratio is lower. Perhaps, it is safe to assume that there is a little difference in the loading conditions, and therefore the response, of nails along the plates and the chords in fully-anchored shear walls.

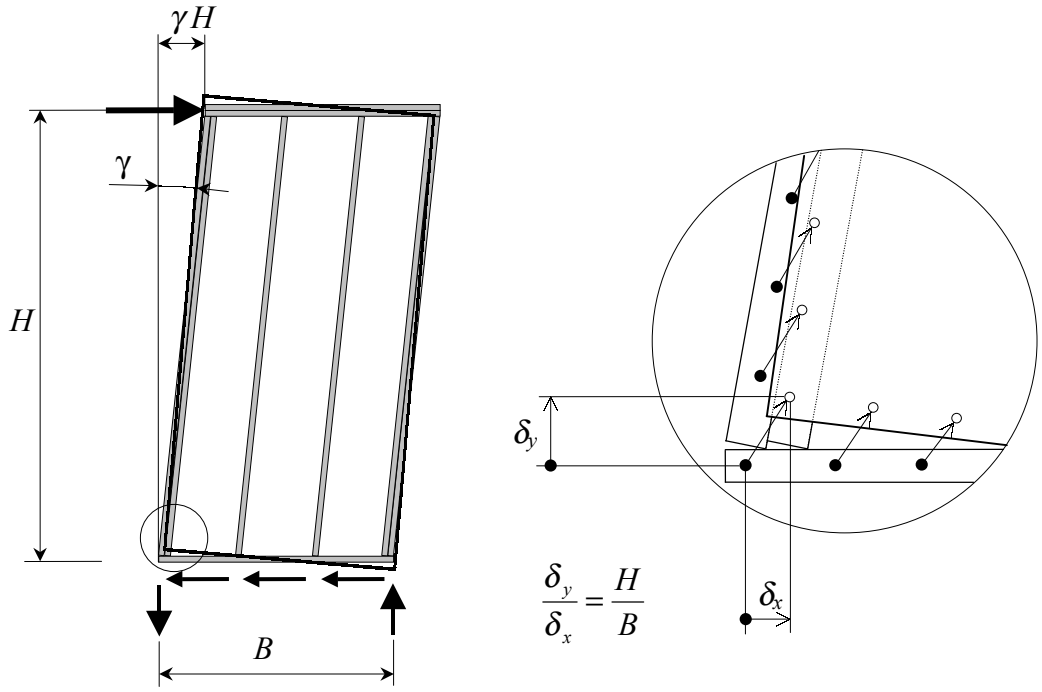

Figure 4. 12. Distortion of fully-anchored wall.

Distortion of a conventional shear wall without dead load in the plane of the wall is shown in Figure 4. 13. The close-up view displays the pattern of the nail distortion observed during the tests of such shear walls. The nails at the top and bottom plates work predominantly across the grain, and the nails along the studs – parallel-to-grain. The nails in the studs have effectively unlimited edge distance[1)] in the direction of loading while the nails along the bottom plate have a small edge distance, often less than 12.5 mm (1/2 in.), which is often determined by the construction method and how the sheathing panel is attached. In platform construction, if 2353-mm (92 5/8-in.)-long studs are used, the edge distance at the bottom plate is likely to be 10 mm (3/8 in.) or less. The predominant failure mode of the walls is nail tear through the sheathing edge (so-called 'unzipping') across the bottom plate. In this case, perpendicular-to-grain loading of sheathing connections is critical for the shear wall performance.

[1)] Edge distance – here, distance from the edge of sheathing to the center of the nail.

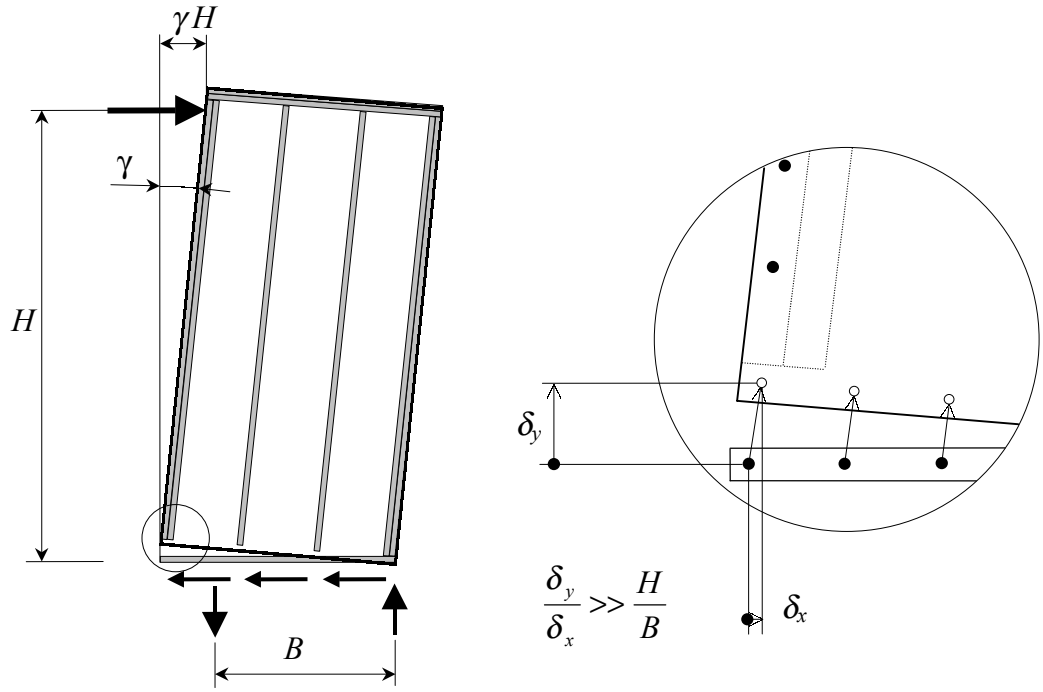

Figure 4. 13. Distortion of non-anchored shear wall.

The only study concerning the edge distances for plywood shear walls is found in the Douglas Fir Plywood Association (1948) publication. Some 650 monotonic tests on nailed connections of Douglas Fir plywood and Douglas Fir lumber were conducted on various nail sizes, panel thickness, wood moisture content, and edge distances relative to the panel and relative to the studs. The criterion of performance was the ultimate load (strength) of the connection. It was concluded that there was no consistent or predictable difference in the loads applied parallel, perpendicular, or at 45 degrees to the face-ply grain. However, the tests showed that the strength of connections decreased as the edge distance was decreased from, so-called standard edge distance. It was acknowledged that in majority of cases, when sheathing is applied to the framing, the available edge distances are less than the standard values for both plywood and stud. Consequently, the connection strength is reduced. For example, the ultimate strength of 9.5-mm (3/8-in.)-thick plywood and a 2 by 4 lumber connection with 8d nail is reduced 72.5% when the edge distance is decreased from 16 mm (5/8 in.) to 10 mm (3/8 in.).

Since 1948, the new sheathing product, OSB, has gained market share. The author is not aware of any publications with regard to the effect of edge distances for the

OSB panels. Nevertheless, design codes (e.g., BSSC 1998) still use 10-mm (3/8-in.) distance as the required minimum for sheathing-to-framing attachment.

4.5.4 Test Methods

The objective of the nailed connections tests was to obtain performance characteristics, such as strength, stiffness, ductility, and load-deflection relationship, of the sheathing-to-framing connections used in the shear wall tests (Chapters 3 and 5). These data were used for analytical modeling of shear wall racking performance (Chapter 6). In this study, only the static model was considered; therefore, only monotonic tests of connections were conducted. The complementary goal of the tests was to test the differences in performance of the connections loaded parallel- and perpendicular-to-grain with various sheathing edge distances.

The following three series of connection tests were performed:

1. **LM**: Connection with the sheathing edge distance 51 mm (2 in.) under monotonic load applied parallel-to-grain of the stud;
2. **PM**: Connection with the edge distance 19 mm (3/4 in.) under monotonic load applied perpendicular-to-grain of the stud;
3. **PMR**: Connection with the edge distance 10 mm (3/8 in.) under monotonic load applied perpendicular-to-grain of the stud;

To produce the specimens for the connection tests, the same materials and methods used to construct the shear wall specimens were applied: 11-mm (7/16-in.) OSB, 2×4 S-P-F studs, and 8d *SENKO*® nails. The nails were power-driven with a pneumatic gun using a jig to control edge distances of the connections. Five studs with similar specific gravity and modulus of elasticity were selected using the *Metriguard* test. Three groups of ten specimens were cut from clear wood of the studs. The specimens were matched so that each group contained two specimens from the same stud and the numbers of the specimens corresponded to the stud number. The matching allowed minimizing the influence of specific gravity in comparisons of the connection performance.

The tests were conducted according to the ASTM 1761 standard using a fixture described in the proposed ASTM (1995) method for testing connections with mechanical fasteners. Sizes and configurations of the specimens and principle setup are shown in Figure 4. 14. Figure 4. 15 shows the general view of the setup for LM series. The fixture prevents out-of-plane movement of the side element while allowing it to slide along the pin rollers during loading. The main member is fixed to the base at the top and the bottom. Although, the pin rollers induce a little friction, they restrain the separation of the elements during the test. Consequently, the setup provides conditions for the connection performance that are more rigid than in shear wall specimens, where the sheathing is not restrained.

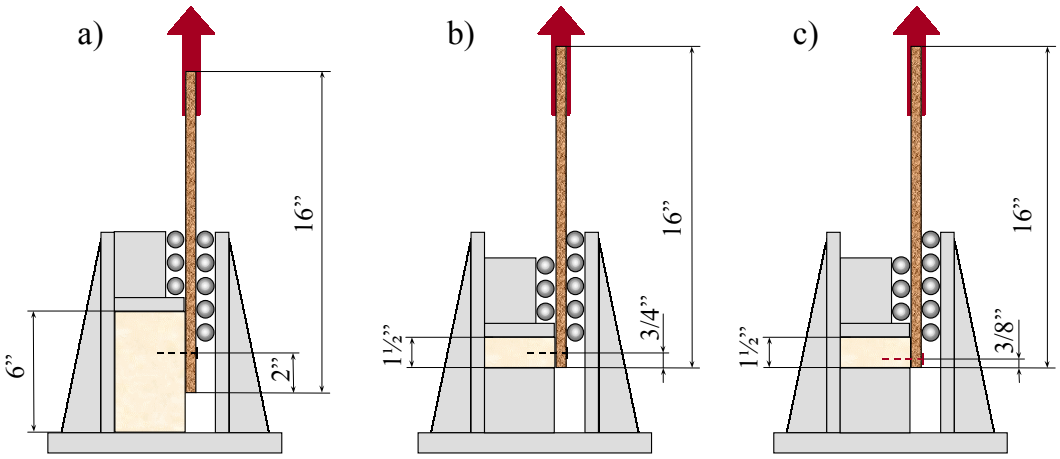

Figure 4. 14. Test setup for sheathing-to-framing connections:
a) LM series, b) PM series, c) PMR series (1 in. = 25.4 mm).

The fixture provides a fixed support on both ends of the specimen, which requires careful alignment of the fixture and the specimen relative to the load cell in order to avoid imposing any moment on the system. Given the variability in lumber sizes and curvature in side elements, it was almost impossible to eliminate the moment in every test. Therefore, it has to be realized that an error due to equipment was present in load readings. The error is estimated as large as 5% of maximum load on connections with low resistance.

Figure 4. 15. General view of the test setup for LM series.

The fixture was attached to the MTS hydraulic testing machine as shown in Figure 4. 15. The specimens were loaded at constant rate of displacement 2.5 mm/min. (0.1 in./min.). Each specimen was loaded until at least 25-mm (1-in.) displacement was reached or until failure. Load and displacement data were recorded with the 4450-N (1000-lbf.) load cell and the built-in LVDT at a frequency 10 times per second using *LabTech* software. At least 10 thousand data points were recorded in each test. Resolution of load and displacement readings was 3 N (0.7 lbf.) and 0.08 mm (0.003 in.) respectively.

Each series included 10 specimens[1)]. The sample size was based on the number of specimens recommended by ASTM 1761. Moisture content and specific gravity of wood members were determined immediately following the tests using gravimetric methods. The average specific gravity of the wood specimens was 0.40 (based on oven-dry volume) with 8% variation. The average wood moisture content was 12.4±1.2%

[1)] LM Series contained 9 specimens. The data was lost due to an error in data acquisition setup.

4.5.5 Test Results

Figure 4. 16 illustrates the average observed load-slip curves of the tested connections by series. Table 4. 4 summarizes statistics of strength and stiffness parameters of the tested connections by series. The elastic stiffness and yield point were determined using the equivalent energy elastic-plastic method for each specimen and then averaged. From a statistical point of view, the tests represented complete randomized block design. General linear model procedures were used to compare each parameter of Table 4. 4 between the series. Table 4. 5 shows results of analysis of variance obtained using SAS® software. (The numbers in the table represent *p*-values.)

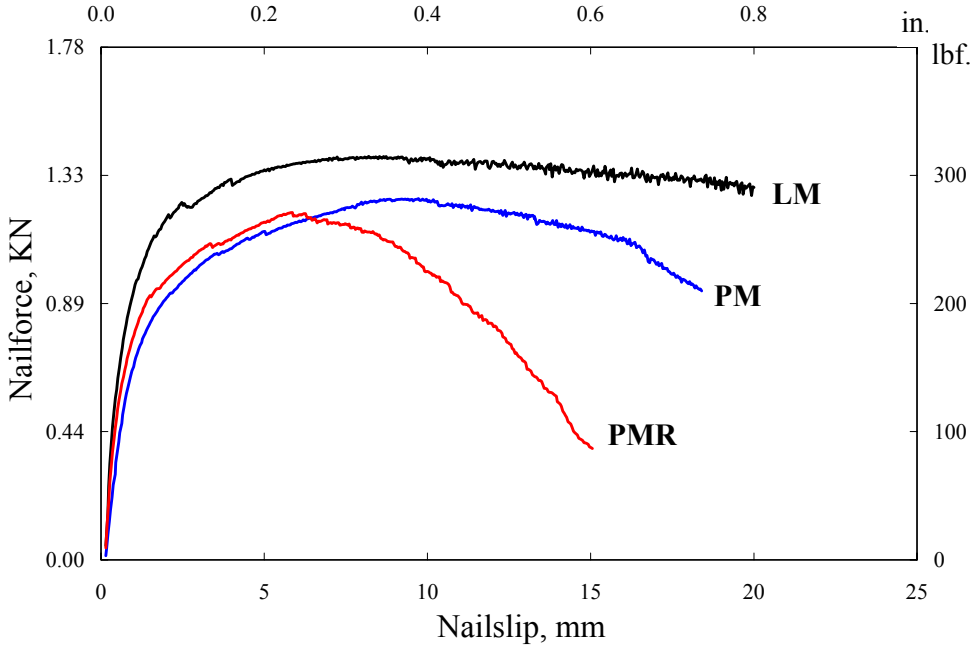

Figure 4. 16. Average observed load-slip curves.

Due to high variation in slip values, there was no significant statistical difference in the elastic slip (δ@ $0.4F_{peak}$) and yield slip (δ_{yield}) between the series. Nevertheless, the elastic stiffness and strength of connections parallel-to-grain were significantly higher than in both perpendicular-to-grain series. Connections loaded parallel-to-grain (**LM**) were, on average, 15% stronger than those loaded perpendicular-to-grain. The parallel-to-grain deformation at the peak load was not statistically different from that of connections loaded perpendicular-to-grain (**PM**) with 19-mm (3/4-in.) edge distance.

Table 4. 4. Strength and EEEP parameters.

Parameter	Units	LM Series			PM Series			PMR Series		
		AVG	**STD**	**COV**	**AVG**	**STD**	**COV**	**AVG**	**STD**	**COV**
F_{peak}	lbf.	331	46.7	14.1%	289	31.4	10.9%	284	25.3	8.9%
δ_{peak}	in.	0.486	0.326	67.1%	0.426	0.100	23.5%	0.245	0.132	53.7%
F_{yield}	lbf.	294	45.8	15.6%	253	27.1	10.7%	247	17.3	7.0%
δ_{yield}	in.	0.042	0.007	16.1%	0.058	0.011	18.7%	0.049	0.027	55.5%
$F_{failure}$	lbf.	265	37.3	14.1%	231	25.1	10.9%	227	20.2	8.9%
$\delta_{failure}$	in.	0.884	0.167	18.9%	0.685	0.108	15.8%	0.449	0.095	21.3%
$0.4F_{peak}$	lbf.	132	18.7	14.1%	116	12.6	10.9%	113	10.1	8.9%
$\delta @ 0.4F_{peak}$	in.	0.019	0.003	15.8%	0.027	0.005	18.6%	0.022	0.012	53.9%
K_e	lbf./in.	7129	1045.7	14.7%	4459	883.9	19.8%	5934	2114.7	35.6%
$D = \delta_{fail}/\delta_{yield}$		21.35	3.3	15.6%	12.22	3.5	28.8%	10.23	2.8	27.1%

Note: 1 in. = 25.4 mm, 1 lbf. = 4.45 N

Table 4. 5. Statistical comparison of connection parameters (ANOVA).

Contrasts	P_{peak}	δ_{peak}	$\delta @ 0.4P_{peak}$	P_{yield}	δ_{yield}	$\delta_{failure}$	K_e	D
LM vs. rest	0.0026 **S**	0.235 **NS**	0.0839 **NS**	0.0011 **S**	0.1885 **NS**	0.0001 **S**	0.0048 **S**	0.0001 **S**
LM vs. PM	0.0110 **S**	0.990 **NS**	0.0489 **M**	0.0075 **S**	0.0982 **NS**	0.002 **S**	0.0010 **S**	0.0001 **S**
LM vs. PMR	0.0048 **S**	0.0443 **S**	0.2868 **NS**	0.0011 **S**	0.5032 **NS**	0.0001 **S**	0.0998 **NS**	0.0001 **S**
PM vs. PMR	0.7081 **NS**	0.0362 **S**	0.3026 **NS**	0.3432 **NS**	0.260 **NS**	0.0012 **S**	0.0349 **S**	0.8903 **NS**
PMR vs. rest	0.0524 **M**	0.0194 **S**	0.9636 **NS**	0.0092 **S**	0.8165 **NS**	0.0001 **S**	0.7873 **NS**	0.0058 **S**

Note: **S**: Statistically significant difference (P-value < 0.05);
NS: Statistically non-significant difference (P-value < 0.05);
M: Marginal (P-value ≈ 0.05).

Surprisingly, the connection strength in perpendicular-to-grain direction did not appear lower when the edge distance was reduced. Note that the variation in specific gravity (8%) was comparable with the variation in the peak loads (9 to 11%), which

might be one of the reasons for uncertainty in this comparison. On the other hand, the variation in specific gravity was not high enough to reveal significant effects on the connection strength. In addition, misalignment of a specimen during the test might affect the results considerably.

Most important differences were found in the slip at peak load and slip at failure, which affected the connection ductility. The deformation at peak load and failure decreased more than 40% when the edge distance was reduced from 19 to 10 mm (3/4 to 3/8 in.). The corresponding deformations decreased 50% when the edge distance was reduced from 51-mm (2-in.) to 10-mm (3/8-in.).

Figure 4. 17 illustrates the failure modes of the connections and helps explaining the reasons for the early degradation of the connections with reduced edge distance. Connections with 51-mm (3/4-in.) edge distance loaded parallel-to-grain failed when the nail pulled head through the sheathing at deflections well beyond 20 mm (0.8 in.). Connections with 10-mm (3/8-in.) edge distance loaded perpendicular-to-grain failed predominantly by tearing through the sheathing edge. Connections with 19-mm (3/4-in.) edge distance exhibited a combination of both failure modes, which was likely dependent on the wood density. From comparison of Figure 4. 17b and c it is clear that the reduced edge distance effectively reduced the deformation capacity of the connection. This information indicated that the minimum allowable edge-distance requirements might not be sufficient to provide the desired ductile resistance of shear walls under lateral loads.

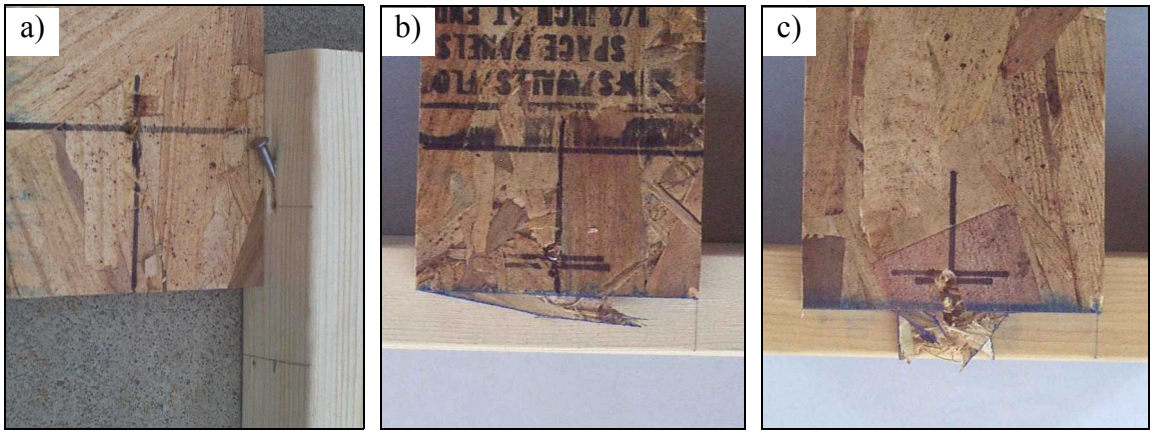

Figure 4. 17. Typical failure modes: a) LM series, b) PM series, c) PMR series.

4.5.6 Curve Fitting

4.5.6.1 Foschi-Dolan Curve

Equation (4.6) consists of two parts. The first part is the Foschi Equation (4.5) that is valid up to δ_{peak}. Average displacement at the peak load for each series ($\delta_{peak\ avg}$) was considered as a limiting point for the Foschi curve. First, individual equations were fit for each specimen using the observed data. Then, one hundred data points for each specimen were generated using the individual equations. At each data point, the predicted values of load and displacement were averaged within the series and the standard errors[1)] were found to determine the 95% confidence intervals. Then, the equation was fit to the predicted average, lower limit, and upper limit data again. Therefore, three equations for each series were obtained to predict the average response of the connections along with the lower and upper bounds with 95% confidence. The procedure was suggested by Birch (1998).

Since each individual specimen had a different δ_{peak}, fitting the second part of Equation (4.6) for individual specimens was not feasible keeping $\delta_{peak\ avg}$ as a common peak point. Besides, variation in the 'tail' portion of the response curves exceeded any reasonable need for the individual approach. Therefore, the full equation (4.6) for the deflections exceeding $\delta_{peak\ avg}$ was fitted for the average observed curves only. For the regression analysis, *TableCurve 2D* software was used. The resulting curves are shown in Figure 4. 18. The equation parameters are listed in Table 4. 6.

Table 4. 6. Average and 95% confidence interval parameters of Foschi-Dolan curves.

Para-meter	Units	LM			PM			PMR		
		Avg	Lower limit	Upper limit	Avg	Lower limit	Upper limit	Avg	Lower limit	Upper limit
P_0	lbf.	294	208	383	231	170	292	209	496	291
K_0	lbf./in.	8386	4841	12122	5445	3753	7159	7419	2244	14344
K_1	lbf./in.	44.2	1.20	82.4	132	104	160	257	-700	105
K_2	lbf./in.	100	-	-	361	-	-	700	-	-
δ_{peak}	in.	0.426	-	-	0.423	-	-	0.247	-	-

Note: 1 in. = 25.4 mm, 1 lbf. = 4.45 N

[1)] Student quintiles $t_{n-1}(1-\alpha/2)$ were used to obtain 95% confidence intervals ($\alpha = 0.05$).

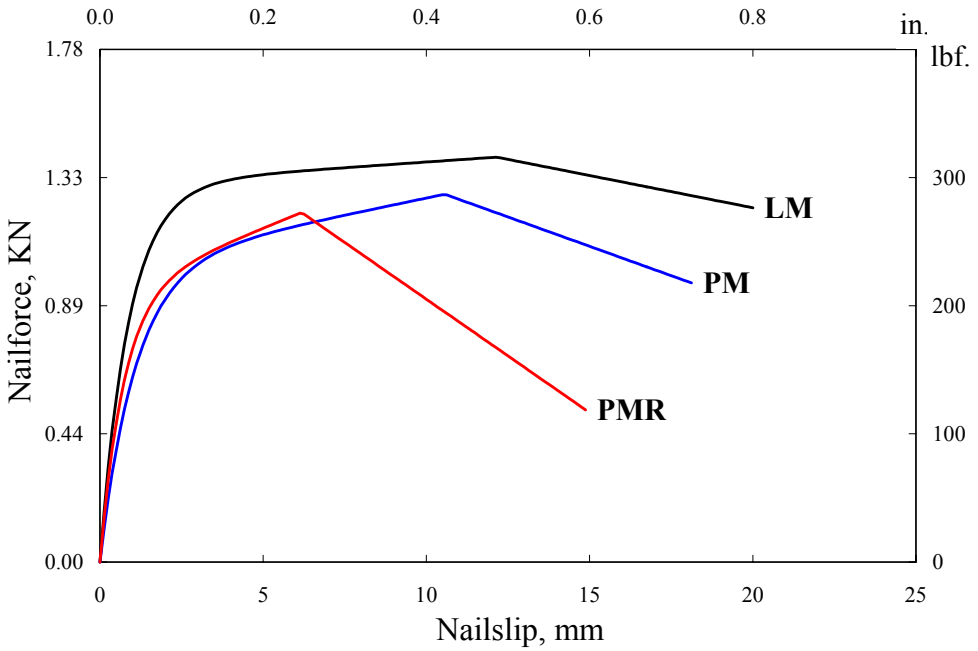

Figure 4. 18. Average Foschi-Dolan curves.

4.5.6.2 Asymptotic-Circle Curve

During the analysis, it was obvious that if the connection slip was not limited by the peak deflection, the predictions of the connection and the shear wall capacities would be overestimated. Furthermore, the deflections at the maximum load and failure of the wall could not be predicted. To describe the connection performance more accurately, the degradation portion was added to the load-slip curve. Due to high variation, the form of the degradation portion is not important as long as it does not complicate the mathematical solution during shear wall analysis. The circular curve shown in Figure 4. 19. meets this requirement and fits the test results with sufficient accuracy:

$$F_n = F_{peak}\sqrt{1-\frac{(\delta-\delta_{peak})^2}{\delta_0^2}} \tag{4. 13}$$

The physical meaning of δ_0 is the additional slip of the connection beyond δ_{peak} until zero force is reached. Therefore, the connection slip is limited by the following condition:

$$\delta \le \delta_{peak} + \delta_0 \tag{4. 14}$$

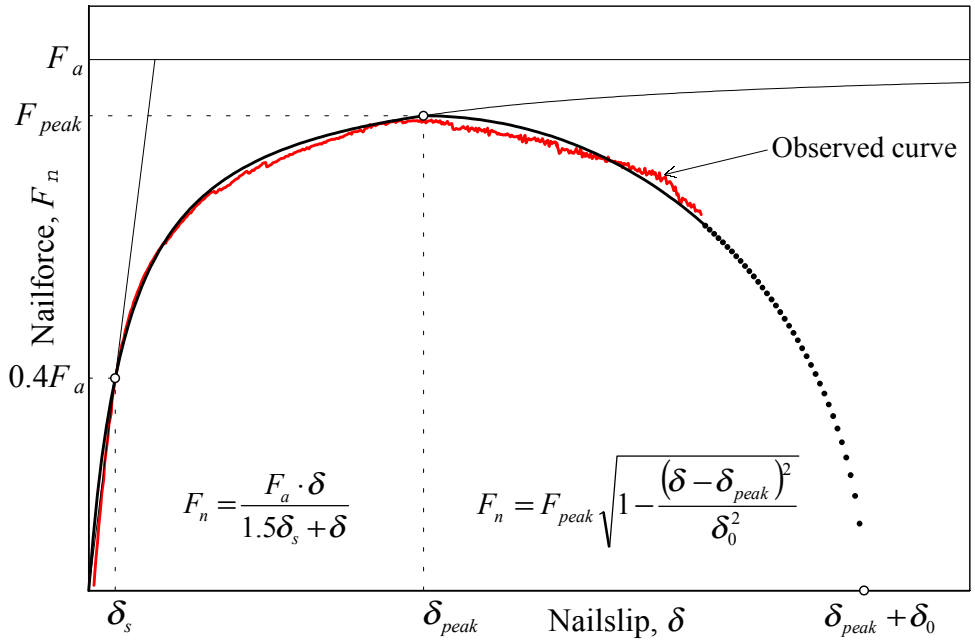

Figure 4. 19. Asymptotic-circle approximation of load-slip curve.

The results of curve fitting are given in Table 4. 7 and the average curves for each series are shown in Figure 4. 20.

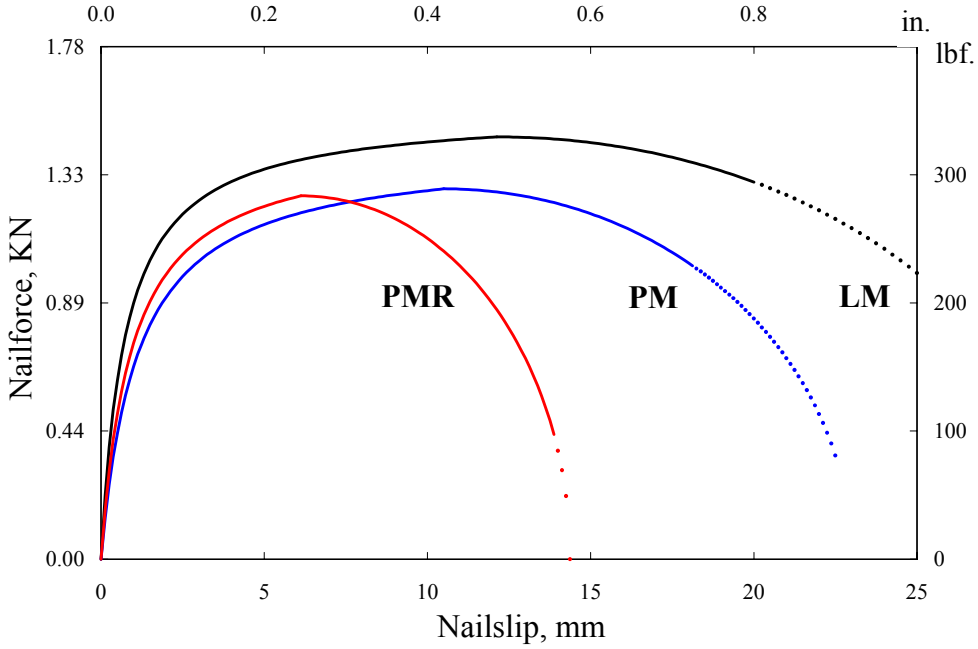

Figure 4. 20. Average asymptotic-circle curves for series LM, PM, and PMR.

Table 4. 7. Average and observed lower limit parameters of asymptotic-circle curves.

Parameter	Units	LM		PM		PMR	
		Average	Lower limit	Average	Lower limit	Average	Lower limit
F_a	lbf.	350	325	320	290	327	320
δ_s	in.	0.02	0.021	0.03	0.035	0.025	0.032
F_{peak}	lbf.	330	330	289	258	284	260
δ_{peak}	in.	0.485	0.485	0.42	0.42	0.245	0.21
δ_0	in.	0.70	0.70	0.50	0.25	0.34	0.27
K=04F_a/δ_s	lbf./in.	7000	6190	4267	3314	5232	4000

Note: 1 in. = 25.4 mm, 1 lbf. = 4.45 N

The last row in Table 4. 7 shows the values of elastic stiffness determined at $0.4F_a$. These values are in good agreement with the corresponding values determined from EEEP curves (see Table 4. 4). This confirmed again that the asymptotic function gives reasonable, yet simple approximation of the connection load-slip relationship.

4.5.6.3 Wen Model (SAP2000)

Parameters for Equation (4.9) were selected such that the resulting curve repeated the shape of the corresponding average Foschi curve found in Section 4.5.6.1. Although both functions are determined by the initial and secondary asymptotes, the asymptotic parameters are not identical. Since the nail-slip in Wen's model is a function of the hysteretic variable z, direct curve fitting was not feasible. Parameters were selected by trial and error such that their values were close to their physical meanings. The results are listed in Table 4. 8 and the average curves for each series are shown in Figure 4. 21. These data were used for nonlinear SAP2000 analysis of shear walls (Chapter 6).

Table 4. 8. Average and observed lower limit parameters of Wen model for SAP2000.

Parameter	Units	LM		PM		PMR	
		Average	Lower limit	Average	Lower limit	Average	Lower limit
yield	lbf.	330	311	289	276	290	285
ratio		0.0043	0.0024	0.0070	0.0045	0.0038	0.0025
K	lbf./in.	7000	6190	4276	3314	5232	4000
exp		2.3	2.3	2.3	2.3	2.7	2.7

Note: 1 in. = 25.4 mm, 1 lbf. = 4.45 N

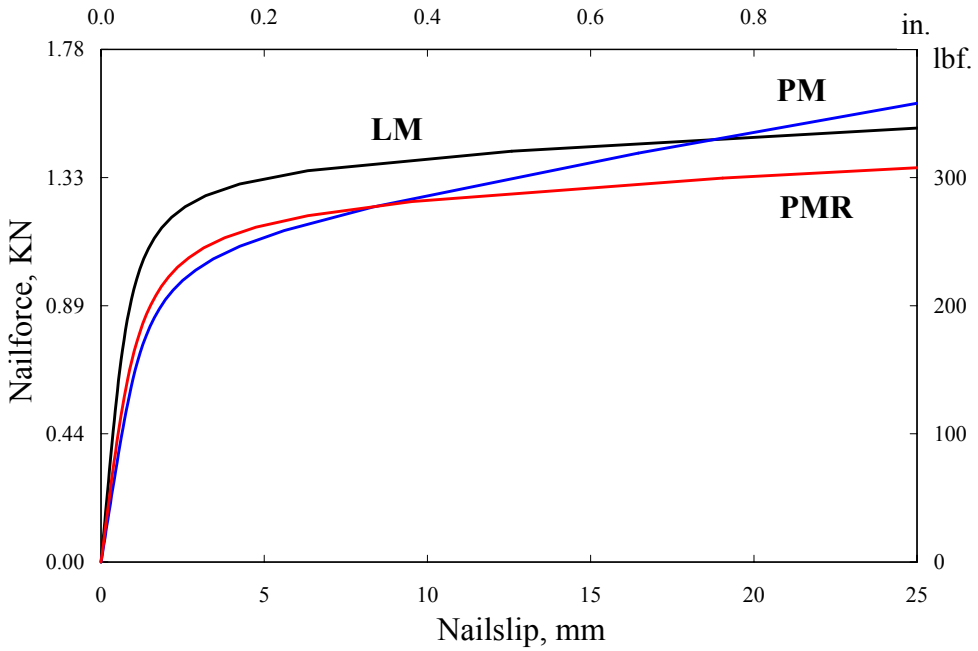

Figure 4. 21. Average Wen curves for series LM, PM, and PMR.

4.5.7 Concluding Remarks on Sheathing-to-Framing Connections

Thirty monotonic tests on sheathing-to-framing connections were conducted to determine strength and stiffness parameters of connections used in the shear wall specimens (Chapter 5). Three different configurations of the connections were tested: a) 51-mm (2-in.) edge distance, loaded parallel-to-grain, b) 19-mm (3/4-in.) edge distance, loaded perpendicular-to-grain, and c) 10-mm (3/8-in.) edge distance, loaded perpendicular to grain. In the analysis of load-deflection relationships, several models were considered. Parameters of Foschi-Dolan, asymptotic-circle, Wen, and EEEP models were determined.

Experimental results revealed that the deformations at peak load of connections with 51-mm edge distance loaded parallel-to-grain were not statistically different from those of connections with 3/4-in. edge distance loaded perpendicular-to-grain. The deformations at peak load and at failure were reduced more than 40% when the edge distance was reduced from 19 to 10 mm (3/4 to 3/8 in.), although the reduction in the edge distance did not affect the connection strength. The corresponding deflections were reduced 100% when the edge distance was reduced from 51 to 10-mm (2-in. to 3/8-in.).

This information indicated that the minimum allowable edge-distance requirements might not be sufficient to provide the desired ductile resistance of shear walls under lateral loading conditions. In light of these findings, additional connection tests should be performed in order to revise the current design specifications.

The curve fitting was conducted in order to use the obtained parameters in analytical modeling of shear walls. When selecting a function for modeling the nonlinear load-slip relationship of the connections, it is desirable to account for the limited deflection capacity of connections loaded perpendicular-to-grain. It can be done either using Dolan's modification of the Foschi curve or adding the circular tail to the asymptotic function as it is proposed herein.

4.6 Summary

In this chapter, characteristics of shear wall components have been discussed. Mechanical properties of OSB panels were cited from APA (1995) technical data. Density and dynamic modulus of elasticity (MOE) of each framing member were measured using *Metriguard* system. The dynamic MOE was correlated to the static MOE via supplementary tests on matched specimens. Bending characteristics of sheathing nails were determined according to ASTM 1575 standard.

Strength and stiffness parameters of sheathing-to-framing connections were determined through monotonic tests on thirty single-fastener specimens. The direction of loading and the edge distance represented conditions similar to the connections in shear walls. Several functions were used to fit the load-slip relationships observed during the tests.

The information from this chapter is used in the analysis of test results on shear walls and as input data for analytical models of shear walls. It is also useful for future comparisons with materials used in other shear wall tests.

Chapter 5. Results of Shear Wall Tests

5.1 General

Fifty-six specimens were constructed and tested during this study. The tests were organized into twenty-two test series, each representing a group of specimens with the same configuration and applied load regime. The number of tests performed in each series and the keys to their basic nomenclature (in bold characters) are displayed in Table 5. 1. In further discussion, the test specimens are identified by the abbreviation that includes the wall length in feet (**02**, **04**, **08**, or **12**), restraint conditions (**FA**, **IA**, or **NA**), load regime (**m** or **c**), and the replication number (**1**, **2**, etc.). For example, **08FAm1** designates the first replication of the monotonic test on 8-ft. wall with full anchorage; **04IAc2** stands for the second replication of the cyclic test on 4-ft. wall with intermediate anchorage.

Detailed information on each test specimen is provided in the Appendix. The Appendix consists of twenty-two sections, each representing a test series. Each section contains the following information:

1. Schematic drawing of the specimen configuration and the load direction.

2. Name tag of each specimen in the series, the date of manufacture and the date of the test, MOE and density of framing elements, and the reference file names. The data files are available from the Brooks Forest Products Research Center at Virginia Polytechnic Institute and State University (VPI&SU). Notes are made on special manufacturing and testing conditions.

3. Commentary section, including observations of the performance and failure mode of each specimen, rationale for repetitive tests (if applicable), notes on performance of hardware and data acquisition system, and general comments comparing performance of the specimens and equipment. This part of the report is very important because it contains original notes taken on the day of the test and provides insight on the peculiarities of the testing procedures.

For each specimen:

4. Data summary table, including performance parameters as discussed in Section 5.2.

5. Graph with the observed load-deflection curve. The scale of the graph is uniform for monotonic and cyclic tests of the specimens of the same configuration, but varies otherwise.

6. For monotonic tests: graph of the unit load-deflection curve and EEEP approximation curve. For cyclic tests: initial and stabilized envelope curves, EEEP, and SEAOSC approximation curves. The scale of these graphs is uniform through the entire report for comparison purposes.

7. Graph of the vertical displacement of studs[1)]. For monotonic tests: observed curves are shown. For cyclic tests: initial envelopes are shown. Observed hysteresis curves in Excel format can be obtained from the Brooks Forest Products Research Center at VPI&SU.

8. Graph of the sheathing displacement relative to the framing. For monotonic tests: observed curves are shown. For cyclic tests: initial envelopes are shown. Observed hysteresis curves in Excel format can be obtained from the Brooks Forest Products Research Center at VPI&SU.

9. Graph of the tension forces in the anchor bolts (where applicable). For monotonic tests: observed curves are shown. For cyclic tests: initial envelopes are shown. Observed hysteresis curves in Excel format can be obtained from the Brooks Forest Products Research Center at VPI&SU.

10. For cyclic tests: Load- and displacement-time record. Variable scale is used.

In the following discussion, the test results are related to the effects of the aspect ratio, the overturning restraint conditions, and the load regime. The influence of the

[1)] Although the specimens were tested in a horizontal position, the in-plane displacements of the studs normal to the plates are referred in the text to as vertical (upward and downward) displacements of studs.

density of framing lumber and the edge distance of sheathing-to-framing connections is emphasized.

Table 5. 1. List of test series.

Series name	**Wall length**, ft.[1)]	**Restraint conditions**	**Load regime**	**Number of tests**
12FAm	**12**	**F**ull **A**nchorage	**m**onotonic	2
12FAc			**c**yclic	2
12IAm		**I**ntermediate **A**nchorage	**m**onotonic	2
12IAc			**c**yclic	4
12NAm		**N**ails	**m**onotonic	1
12NAc			**c**yclic	1
08FAm	**8**	**F**ull **A**nchorage	**m**onotonic	2
08FAc			**c**yclic	2
08IAm		**I**ntermediate **A**nchorage	**m**onotonic	5
08IAc			**c**yclic	4
08NAm		**N**ails	**m**onotonic	1
08NAc			**c**yclic	1
04FAm	**4**	**F**ull **A**nchorage	**m**onotonic	2
04FAc			**c**yclic	3
04IAm		**I**ntermediate **A**nchorage	**m**onotonic	2
04IAc			**c**yclic	3
04NAm		**N**ails	**m**onotonic	5
04NAc			**c**yclic	2
02FAm	**2**	**F**ull **A**nchorage	**m**onotonic	3
02FAc			**c**yclic	2
02IAm		**I**ntermediate **A**nchorage	**m**onotonic	3
02IAc			**c**yclic	4
Total				56

[1)] 1 ft. = 304.8 mm

5.2 Definitions of Shear Wall Performance Parameters

Analysis of shear wall performance is based on the definitions introduced in this section. Load-deflection data collected during the shear wall tests was used to determine strength, stiffness, ductility, and damping characteristics according to the SEAOSC (1997) guidelines and proposed ASTM (1995) method. Alternative definitions are proposed for some of the variables, because there is no universal agreement on standard definitions. However, the definitions used provide consistent measure of performance and the ability to compare the performance between specimens. The parameters are summarized in the Appendix for each specimen and can be reanalyzed once the variable definitions are standardized.

In addition to the parameters introduced in this section, the Appendix includes graphs of sheathing displacements relative to the framing, vertical displacements of studs, and uplift forces resisted by anchor bolts (where applicable). The digital and graphical data are accompanied with observational comments on performance and failure mode of each specimen.

5.2.1 Load-Deflection Curves

Load-deflection curves were generated for each specimen based on data produced by channels #1 and #2 (Figure 3.12). Usually, *story drift* is determined as the difference between horizontal movement at the top of the wall (channel #1) and at the bottom plate (channel #6). However in these tests, to compare the performance of walls with various anchorage conditions, the horizontal slip of the bottom plate was not deducted. In this case, fewer random and systematic errors related to measurements were involved in computation of wall parameters. On one hand, this allowed obtaining more consistent results and more accurate estimation of energy dissipation. On the other hand, the results conservatively ignored the amount of slip at the top and bottom plates, which varied from 0.1 mm (0.005 in.) at proportional limit to 1 mm (0.04 in.) at peak loads. The error due to ignoring this slip is negligible (less than 2%).

For comparison of walls with various aspect ratios, the recorded load data were normalized by the wall length, and the subsequent analysis was made in terms of unit shear load, v, KN/m (Kips/ft.):

$$v = F/L \tag{5. 1}$$

where: F = recorded load, KN (Kips),

L = length of wall, m (ft.).

For analysis of monotonic tests, observed response curves were used. For analysis of cyclic tests, so-called *envelope response curves* were generated. A typical response curve of shear walls during the cyclic loading is shown in Figure 5. 1. It is a series of hysteresis loops corresponding to each cycle of negative and positive deflections of the wall. From the hysteresis loops, complete (negative and positive) envelope, or 'backbone' curves were determined by producing the line of best fit through the maximum force and associated displacement for each cycle. Two types of envelope curves were obtained. The *'initial' envelope curve* accommodated peak loads from the first cycle of each phase of the loading; the so-called *'stabilized' envelope curve* contained peak loads from the last (third) cycle of each phase.

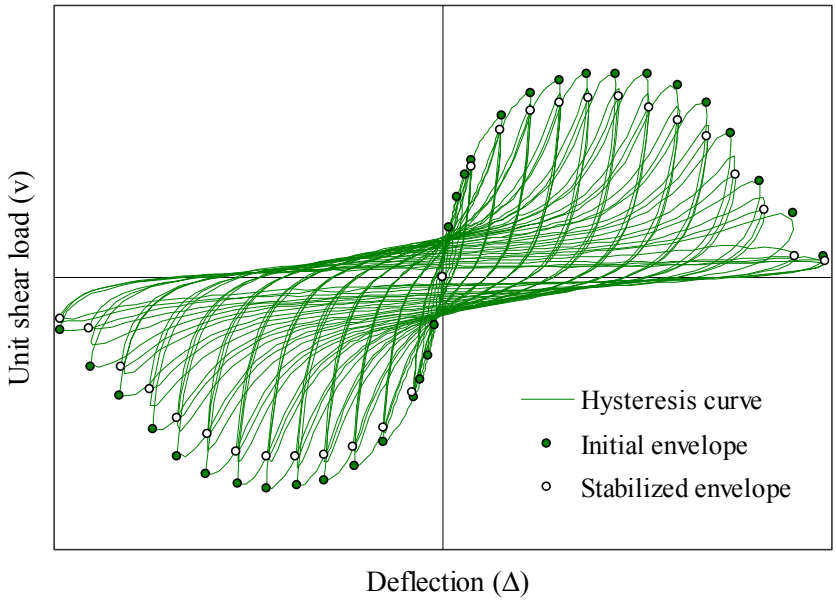

Figure 5. 1. Typical hysteresis and envelope curves.

The envelope curves of light-frame shear walls resemble the shape of monotonic response curves. The differences between these curves allow quantifying the strength and stiffness degradation of the structure due to repeated reversed loading. Since the envelope curves include reversed sides, the absolute values of parameters of the negative and the positive curves are averaged during the analysis. The averaging is based on the assumption that the structure may have to survive fully reversed cycles of equally large amplitude during a seismic event.

For a brief digital representation of the load-deflection relationship, four reference points were found in each curve at the following distortion angles: 1) 1/300, 2) 1/200, 3) 1/100, and 4) 1/60. In our tests, these points correspond to the following deflections: 1) 8.1 mm (0.32 in.), 2) 12.2 mm (0.48 in.), 3) 24.2 mm (0.96 in.), and 4) 40.6 mm (1.6 in.). The reference points are quoted in the Appendix for each specimen and are useful for future reference with the tests reported by other researchers and for calculations of secant and cyclic stiffness parameters.

5.2.2 Equivalent Energy Elastic-Plastic Curve

Figure 5. 2 reveals how strength and stiffness parameters are defined from a load-deflection or envelope curve using the energy calculations. Wall strength (v_{peak}), deflection at capacity (Δ_{peak}), deflection at $0.4v_{peak}$, and failure point ($v_{failure}$, $\Delta_{failure}$) are determined for each monotonic, initial, and stabilized response curve using a plot similar to that shown in Figure 5. 2. The failure point is considered to occur at $0.8\ v_{peak}$ (i.e., when a 20% decrease in resistance occurs). The deflection at this point is also called the *ultimate deflection* (ISO 1998). The area under the curve limited by the failure point approximates the work that can be done by the wall during a monotonic test. Using these data points, the *equivalent energy elastic-plastic* (EEEP) curve is derived for each specimen, as is shown in Figure 5. 2.

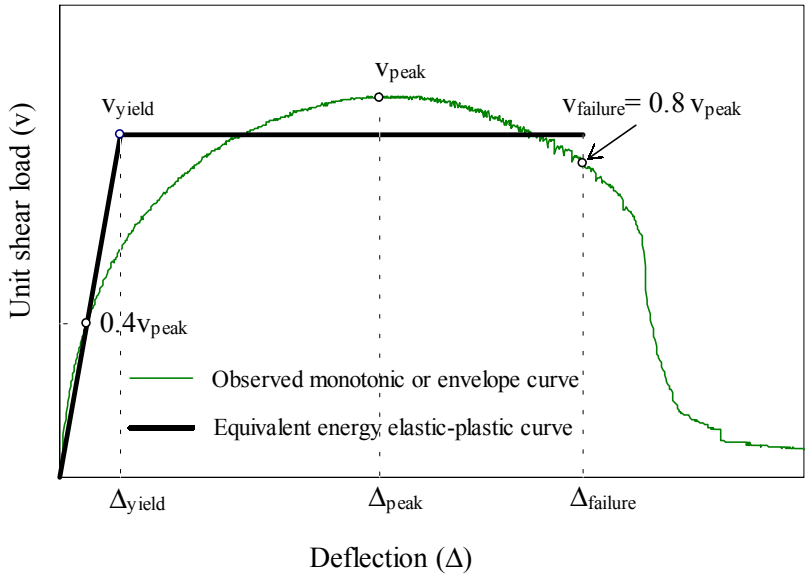

Figure 5. 2. Performance parameters of shear walls.

This artificial curve depicts how an ideal perfectly elastic-plastic wall would perform dissipating an equivalent amount of energy. This definition of the EEEP curve is used for both monotonic and cyclic tests. Note that the total energy dissipated by walls during cyclic tests is significantly greater than that determined from the envelope curve because hysteresis loops overlap. This definition is used for comparison purposes only. The bilinear EEEP curves obtained this way allow comparing the parameters of the nonlinear performance of different walls on an equivalent energy basis.

The elastic portion of the EEEP curve contains the origin and has a slope equal to the *unit elastic stiffness*, k_e. The plastic portion of the EEEP curve is a horizontal line positioned so that the area under the EEEP curve equals the area under the response curve from zero deflection to $\Delta_{failure}$. The yield point (v_{yield}, Δ_{yield}) is found at the intersection of the elastic and plastic lines of the EEEP curve. Equating the areas under the response curve and the EEEP curve, the yield strength can be expressed (Heine 1997):

$$v_{yield} = \frac{-\Delta_{failure} \pm \sqrt{\Delta_{failure}^2 - \frac{2A}{k_e}}}{-\frac{1}{k_e}} \qquad (5.2)$$

where: A = area under the response curve between zero and $\Delta_{failure}$.

In this dissertation, the unit elastic stiffness, k_e, is defined as the slope of the line passing through the origin and the point on the response curve where the load equals 40% of v_{peak}:

$$k_e = 0.4v_{peak} / \Delta_{@0.4v_{peak}} \quad (5.3)$$

The *shear modulus*, G, is obtained from the unit elastic stiffness as follows:

$$G = k_e \times H \quad (5.4)$$

where: H = 2440 mm (96 in.), height of shear wall.

The definition of elastic stiffness at $0.4v_{peak}$ is based on the proposed ASTM (1995) standard for cyclic tests of mechanical connections, and it is a compromise reached in an effort to harmonize the ASTM test standard and the CEN standard. The variable may be adjusted once an agreement on the definition is reached. This definition also affects the values determined for other variables, such as ductility, that use the initial stiffness directly or indirectly. In cyclic tests, this stiffness represents a good estimate of the stiffness that shear walls would exhibit after being loaded a number of times at low to moderate amplitudes.

5.2.3 SEAOSC Parameters

In this subsection, performance parameters proposed in SEAOSC (1997) standard are introduced. According to this standard, two characteristic points corresponding to the *yield limit state* (YLS) and the *strength limit state* (SLS) are found in the response curve. The yield limit state (v_{yls}, Δ_{yls}), or FME, is defined as the last point in the load-deflection curve where the difference in forces between the initial and the stabilized cycle, at the same amplitude, does not exceed 5%. The strength limit state (v_{sls}, Δ_{sls}) is found at the point corresponding to the maximum displacement for the peak force attained by the system. These two points determine two bilinear segments approximating the shear wall response shown in Figure 5.3. The shear moduli, G'_{yls} and G'_{sls}, corresponding to each limit state are determined from:

$$G' = (F/\Delta) \cdot (H/L) \quad (5.\ 5)$$

where: F = shear load recorded at the point of interest (YLS or SLS), KN (Kip),

Δ = corresponding deflection, mm (in.).

Note that the SEAOSC method does not require averaging parameters of the positive and negative sides of the hysteresis curve. It specifies the YLS and SLS that can belong to either side of the curve. On one hand, it is useful to estimate the minimum FME and the maximum shear strength of the structure. On the other hand, it can overestimate the capacity of the structure, especially if the structure develops unsymmetrical response to a symmetrical excitation. The illustration of the results may be confusing if the YLS occurs on one side of the curve and the SLS occurs on the opposite side, which typically happens. To eliminate the confusion and to collect all useful information from the test data, the limit states for both sides of the hysteresis curve as is shown in Figure 5. 3 were determined and reported in the Appendix. The data allow evaluating whether the structure is able to produce symmetrical response or starts degrading immediately after the maximum strength is reached. Unlike the EEEP method, the SEAOSC approach does not analyze the post-SLS performance of the structure. As Figure 5. 3 illustrates, the structure may have a significant reserve of strength and energy dissipation beyond the SLS point. Many researchers agree that this aspect of the structural performance should not be ignored.

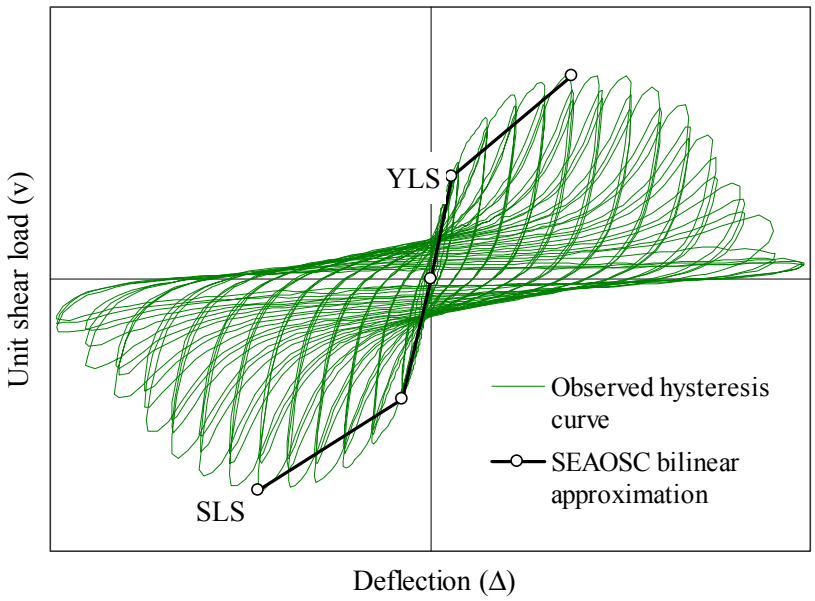

Figure 5. 3. Example of SEAOSC bilinear curves.

5.2.4 Ductility

Ductility is a very important characteristic of structural seismic resistance that represents the ability of the structure to yield and deform inelastically without failure. Several ratios can be introduced to measure ductility. Most commonly used is the *ductility ratio*, D, which quantifies the ability of the structure to yield until the load capacity is reached. In terms of the EEEP parameters, the ductility ratio can be expressed as follows:

$$D = \Delta_{peak} / \Delta_{yield} \tag{5. 6}$$

An alternative measure of ductility proposed by Dolan (ASTM 1995) and supported by some other researchers can be called the *ultimate ductility ratio*, D_u. This value represents the maximum displacement that the structure can undergo beyond the yield point until failure:

$$D_u = \Delta_{failure} / \Delta_{yield} \tag{5. 7}$$

The rationale for this measure is as follows. Most ductile structures, including light-frame shear walls, are able to yield far beyond Δ_{peak}. When the structural component is unable to resist additional load, it transfers the load onto other components.

During analysis of systems with such ductile components, it appears important to know the ultimate displacement capacity of each component to predict the collapse mechanism more realistically.

Interchangeably with the ultimate ductility ratio, the so-called *toughness index*, D_f, can be introduced to measure the toughness of failure, in other words, to indicate the amount of deflection capacity remaining in the structure at the peak load:

$$D_f = \Delta_{failure} / \Delta_{peak} \tag{5. 8}$$

Together with the ductility ratio, the toughness index is a convenient measure of shear wall performance, which provides sufficient information to determine the ultimate ductility ratio. From the NEHRP Provisions prospective, D_f index can also provide some useful information.

5.2.5 Damping

Another important characteristic of cyclic performance of structural systems is their ability to dissipate the strain energy, or damping. Damping energy, W_D, dissipated per cycle by the wall is calculated by integrating the area enclosed by the hysteresis loop at the corresponding displacement (as shown in Figure 5. 4). The strain energy, U_0, equals the area enclosed by the triangle *ABC* in Figure 5. 4. To compare damping properties of the walls, *equivalent viscous damping ratio*, ζ_{eq}, for each initial and stabilized cycle and work to failure, $W_{failure}$, are estimated:

$$\zeta_{eq} = \frac{1}{4\pi} \frac{W_D}{U_0} \tag{5. 9}$$

Since hysteresis loops are not ideally symmetric, the areas of triangles *ABC* and *ADE* in Figure 5. 4 are averaged to approximate the value of the strain energy U_0 in Equation (5.9). The value of the equivalent viscous damping ratio varies during the test. Reported in the Appendix are the values at the peak load.

Work to failure, or energy dissipation, reported in the Appendix was measured as the total area enclosed by hysteresis loops until failure in cyclic tests, or the area under the load-deflection curve until failure in monotonic tests.

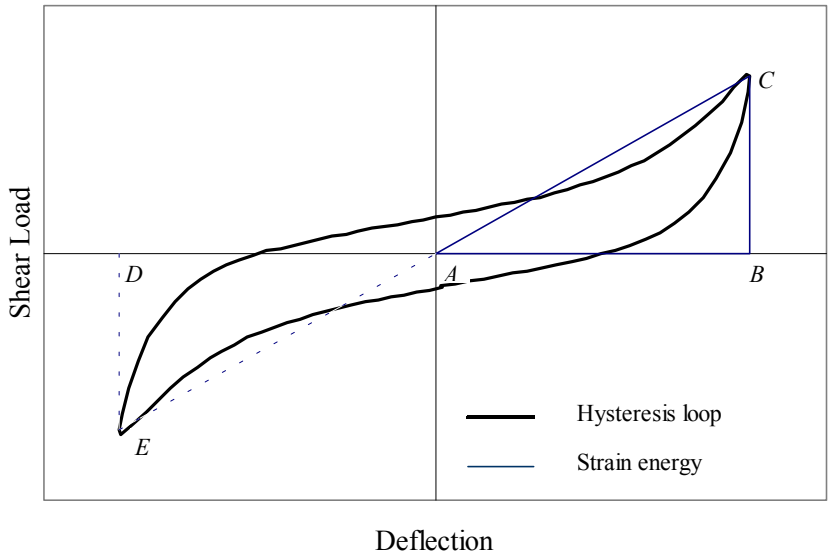

Figure 5. 4. Damping and strain energy of a cycle.

5.3 Monotonic Tests on Walls with Full Anchorage (Walls FAm)

Eight **FA** walls were tested monotonically. (Recall that historically the monotonic tests on 2.4-m (8-ft.) square walls anchored to the foundation served as a basis for establishing design values.) The sheathing was attached to the frame at 19 mm (3/4 in.) from the edge. Therefore, the test results obtained in **08FAm** series set the basis for comparison with all other tests conducted during this study.

The curves in Figure 5. 5 represent the monotonic response of walls with the average wood density of studs 510 kg/m^3. It can be concluded that walls 1.2-m (4 ft.) and longer exhibited similar responses: They reached peak loads at deflections exceeding 64 mm (2.5 in.), and then gradually degraded. The 20% decrease in resistance occurred past 105-mm (4.1-in.) deflections. Walls 2.4-m (8-ft.) and 3.6-m (12-ft.) long developed the average strength of 9.9 KN/m (0.68 Kip/ft.). The strength of the 1.2-m wall was 12% lower, although a lower wood density might have been the reason for that. Narrow walls, 0.6-m (2-ft.) long, developed deflections exceeding 152 mm (6 in.) without noticeable strength degradation. However, due to significant contribution of stud bending they were 50% more flexible and weak relative to the longer walls. At a deflection of 64 mm (2.5 in.), they resisted only 6.4 KN/m (0.44 Kip/ft.).

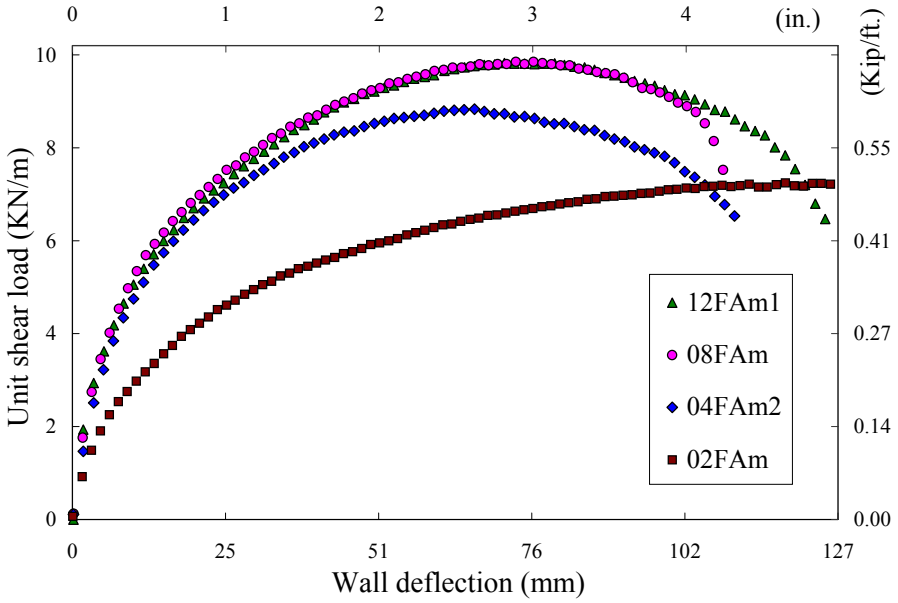

Figure 5. 5. Response curves of **FAm** walls.

The walls exhibited significant amount of racking. Figure 5. 6 shows a graph of sheathing displacements relative to the framing near the corners of the first panel in **12FAm1** wall. The distribution of the displacements was almost symmetric. At the peak loads, the displacements in the corners reached 5 to 10 mm (0.2 to 0.4 in.). Similar displacements were observed in **08FAm** walls. This information indicated that the sheathing panel rotated approximately around the center, all sheathing nails along the perimeter contributed the shear wall resistance, and the wall segment developed its full capacity. The displacements in walls with one sheathing panel (**04FAm** and **02FAm**) were not uniform. The displacements at the top were less than a half of those at the bottom. The load capacity of the narrow walls might have been reduced because of the uneven distribution of work between the nails.

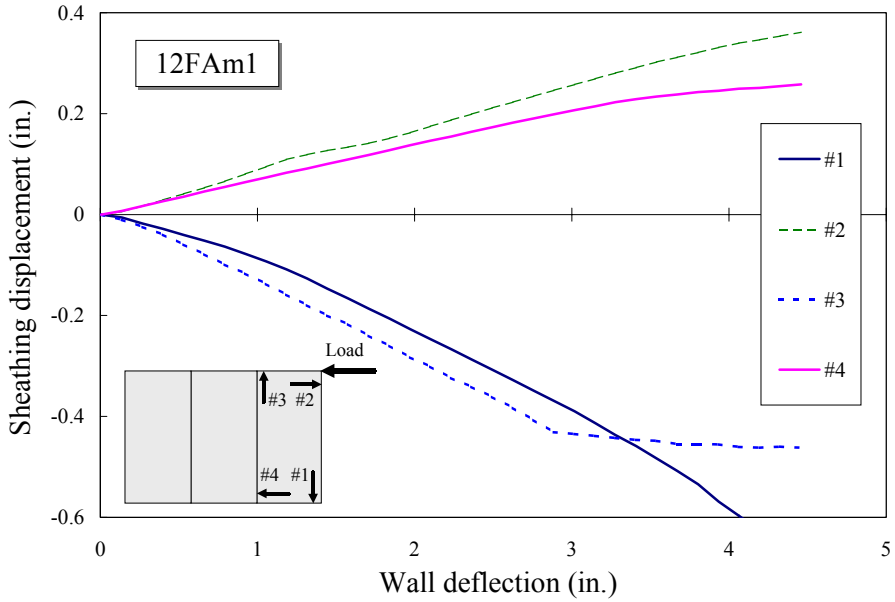

Figure 5. 6. Sheathing displacements in **12FAm1** wall.

As is shown in Figure 5. 7, the vertical displacements of the end studs were typically equal and opposite of each other. At the peak loads, the displacements were approximately 5 mm (0.2 in.). The uplift displacement of the end studs was limited by the tie-down restraint.

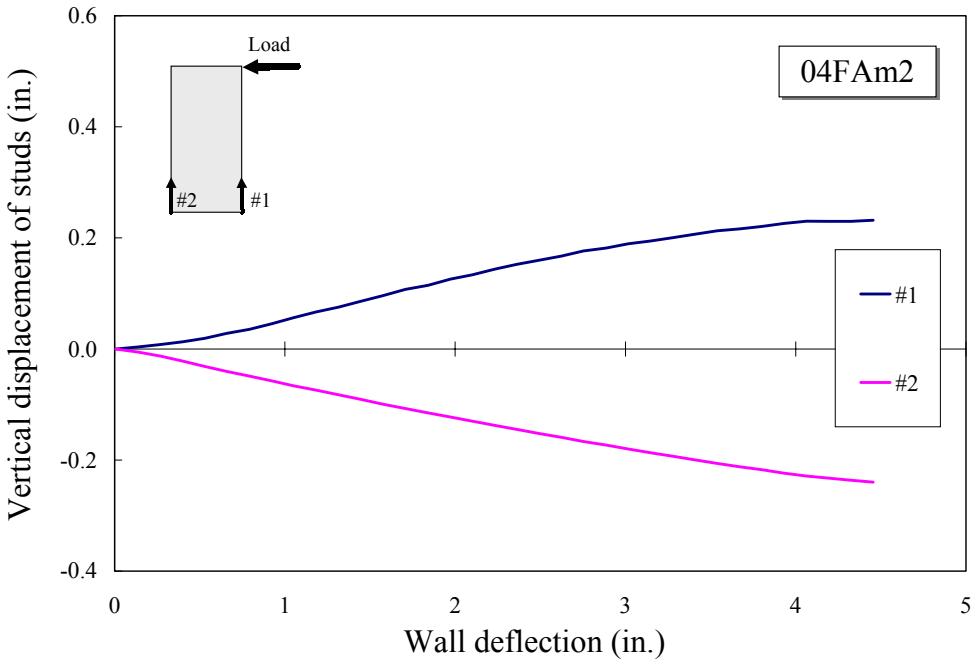

Figure 5. 7. Vertical displacements of studs in **FAm** walls.

At typical failure (Figure 5. 8), the right end stud separated from the top plate and the sheathing panels unzipped arbitrarily along the top and/or bottom plates with the sheathing nails tearing through the panel edges. Usually, the sheathing unzipped along one of the studs with the nails pulling heads through the sheathing. Adjacent edges of sheathing panels in 2.4 and 3.6-m (8 and 12-ft.) walls crushed into each other and exerted significant friction. It is likely that the bearing and friction forces lead to the higher energy dissipation of these walls relative to the 1.2-m (4-ft.) walls.

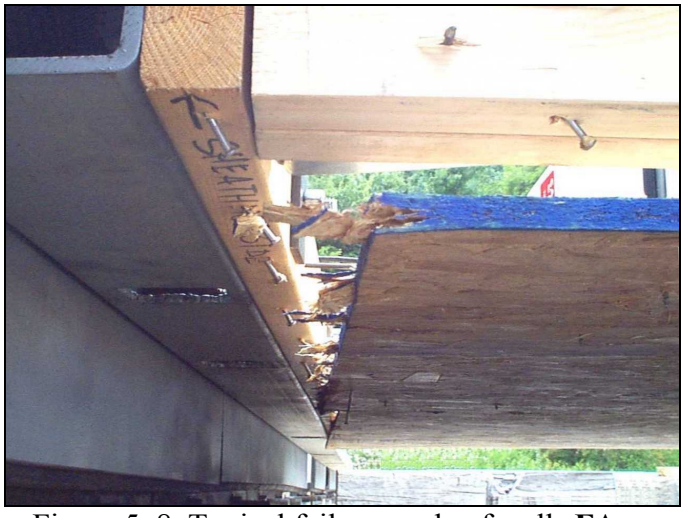

Figure 5. 8. Typical failure mode of walls **FAm**.

Walls **04FAm1** and **12FAm2** are discussed separately because their performance deviated from the general trend. The response curves are shown in comparison with the matched walls in Figure 5. 9. Although the elastic stiffness and the load capacity of the matched walls differed less than 10%, there was at least 35% reduction in deflections at the peak and failure loads. These walls dissipated 50% less energy than typical walls. In other words, the ductility and toughness of these two walls were significantly reduced when compared to the typical walls.

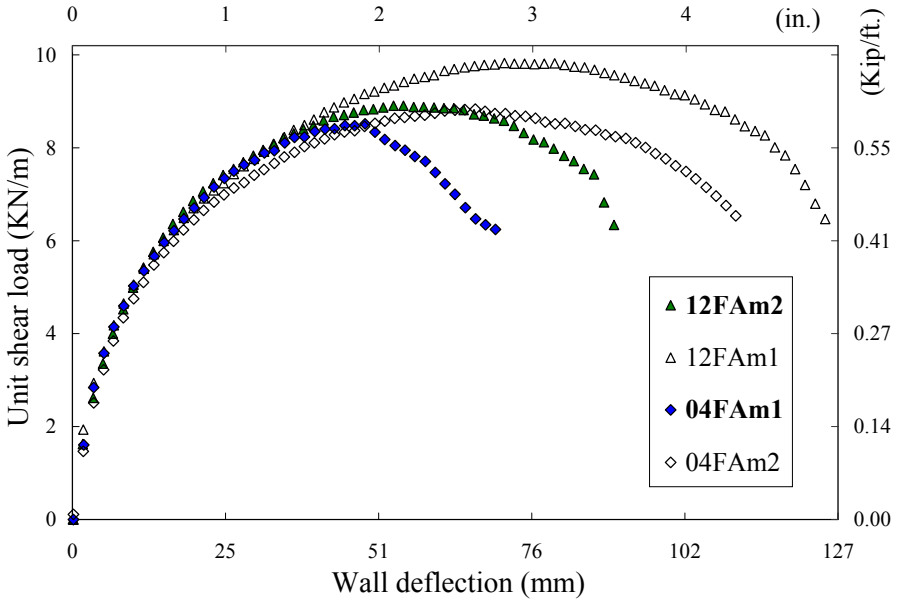

Figure 5. 9. Response curves of walls **12FAm2** and **04FAm1**.

Figure 5. 10 illustrates the predominant failure mode of the wall **04FAm1**. Similar failure was experienced by wall **12FAm2**: the sheathing nails along the right end stud were pulled out. The failure mode and the information on the wood density of studs suggested that among possible reasons for the ductility reduction was the lower density of the framing lumber. The wood density data recorded during the wall manufacture revealed that the right end studs in walls **04FAm1** and **12FAm2** had wood density 445 and 393 kg/m^3 respectively. The density of the corresponding studs in walls **04FAm2** and **12FAm1** was 520 and 556 kg/m^3 respectively. It is not surprising that the entire row of nails along the low-density end stud did not provide the adequate resistance and pulled out.

Figure 5. 11 shows the sheathing displacements of wall **04FAm1**. A similar graph was recorded for wall **12FAm2**. The sheathing translation was not symmetrical: displacements at the bottom were 3 to 4 times larger than at the top. This information indicates that the most of the work was done by the nails at the bottom plate. Although the edge distance along the top and bottom plates was 19 mm (3/4 in.), the lack of the connection resistance along the end stud (due to low density) overloaded these nails and caused the early strength degradation of the entire shear wall.

Figure 5. 10. Failure mode of wall **04FAm1**.

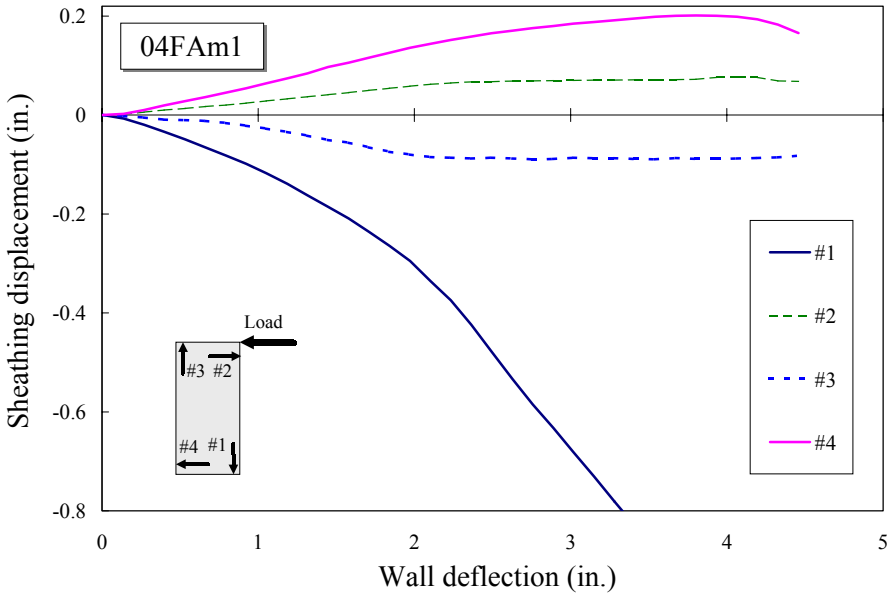

Figure 5. 11. Sheathing displacements of wall **04FAm1**.

5.4 Cyclic Tests on Walls with Full Anchorage (Walls FAc)

Ten **FA** walls were tested cyclically. The average initial envelope response curves are shown in Figure 5. 12. The corresponding stabilized response envelopes are shown in Figure 5. 13. The envelope curves are smooth and resembling the shape to the monotonic curves shown in Figure 5. 5. However, the peak loads and the corresponding deflections were somewhat lower. The average initial cyclic strength of 1.2-m (4-ft.) and longer walls varied between 7.8 and 9.2 KN/m (0.54 to 0.63 Kips/ft.) and developed between 46 and 53-mm (1.8 and 2.1-in.) amplitudes. The resistance degraded gradually and usually dropped 20% percent only during the 76-mm (3-in.) amplitude displacements. Walls **02FAc** exhibited trends similar to the corresponding **02FAm** walls. They deflected over 102 mm (4 –in.) without strength degradation; however the shear modulus was 50% lower than for other walls, and at 53-mm (2.1-in.) amplitudes, only 6.1 KN/m (0.42 Kip/ft.) load was sustained. Note that the average wood density of studs in **FAc** series was 9% lower than in **FAm** series, and the walls with higher wood density developed higher strength.

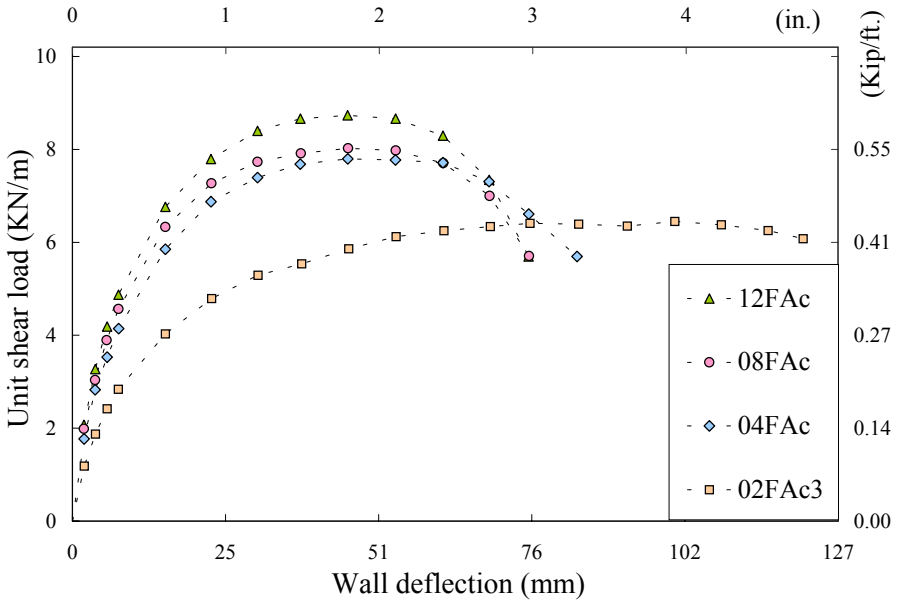

Figure 5. 12. Average initial envelope response curves of **FAc** walls.

As usual, the stabilized envelopes repeated the shape of the initial envelopes at a 13% lower resistance level. All major events (yield, strength, and failure) in the stabilized envelopes were found at the same amplitudes as in the initial envelopes.

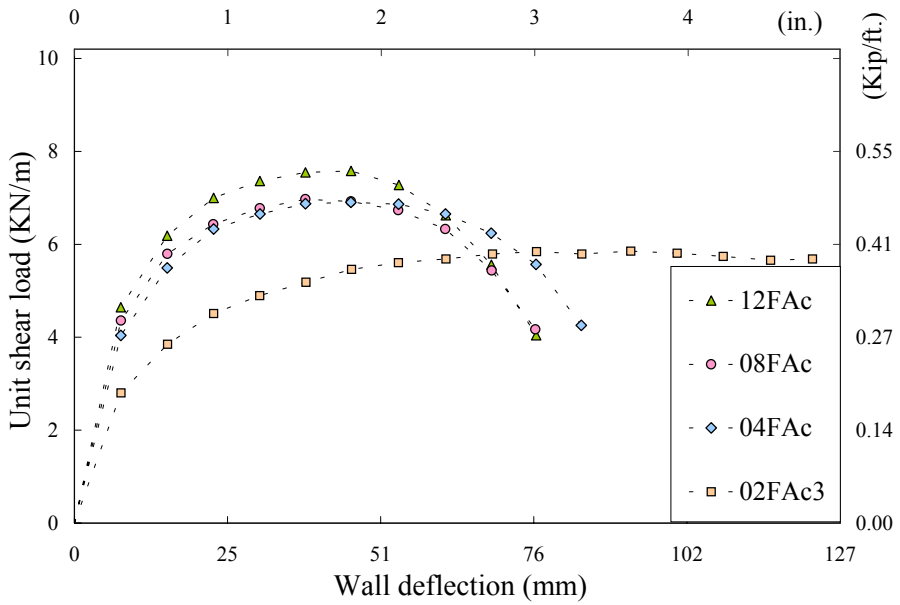

Figure 5. 13. Average stabilized envelope response curves of **FAc** walls.

Figure 5. 14 represents initial envelopes of the sheathing displacements relative to the framing near the corners of the first panel in a **12FAc** wall. It illustrates that the wall developed significant amount of racking typical of **FAm** walls where all sheathing nails contributed the wall resistance. During cycling, the sheathing panel rotated about the center and the displacements at the corners reached 5 to 8 mm (0.2 to 0.3 in.) at the strength limit state. Similar displacements were observed in **08FAc** walls.

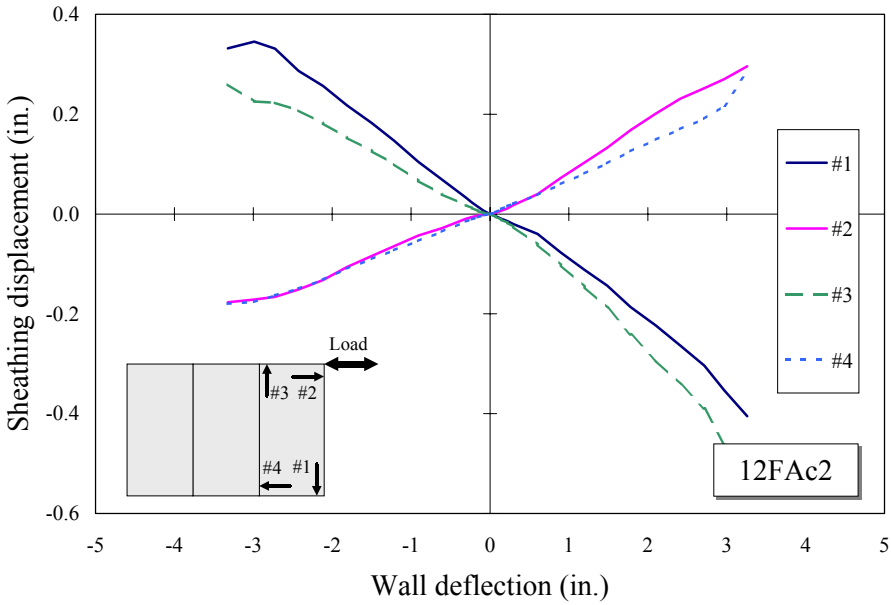

Figure 5. 14. Sheathing displacements in **FAc** walls (initial envelope).

The distribution of the sheathing displacements in **04FAc2** wall was uniform. Walls **04FAc1** and **04FAc3** exhibited the distribution of the sheathing displacements typical of the corresponding monotonic tests: the nails at the bottom were loaded twice as much as those at the top (see Figure 5. 15). (Note, among the three 1.2-m (4-ft.) long walls, **04FAc2** wall was the strongest.)

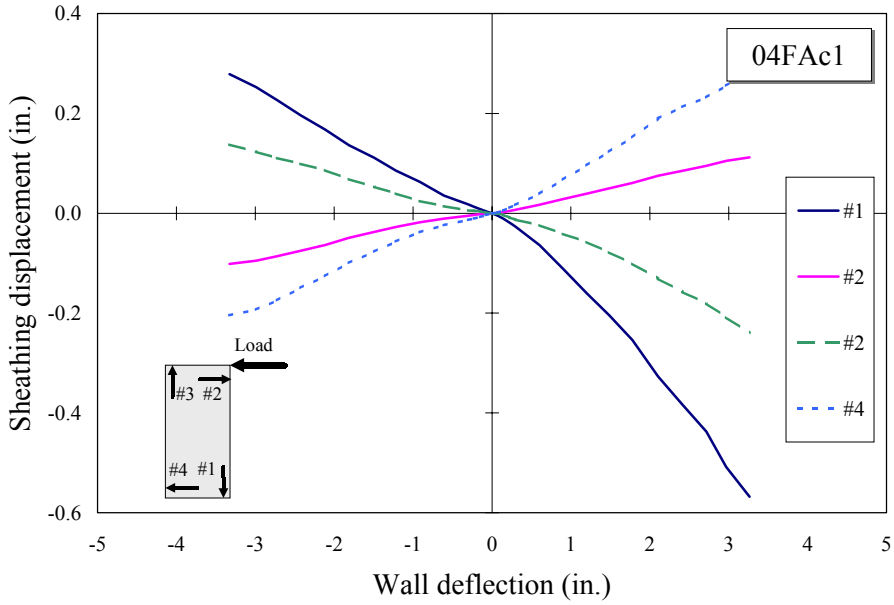

Figure 5. 15. Sheathing displacements in **04FAc1** wall (initial envelope).

Figure 5. 16 illustrates the initial envelopes of the stud vertical displacements in a typical **FAc** wall. The upward and downward displacements of the end studs during the reversed cycling were nearly symmetrical in all **FAc** walls. Similar to **FAm** walls, the tie-down anchors limited the uplift of the end studs to 5 mm (0.2 in.). Therefore, the end studs always separated from the top plate at failure. The intermediate studs might separate arbitrarily from the top or the bottom plates at failure together with the sheathing.

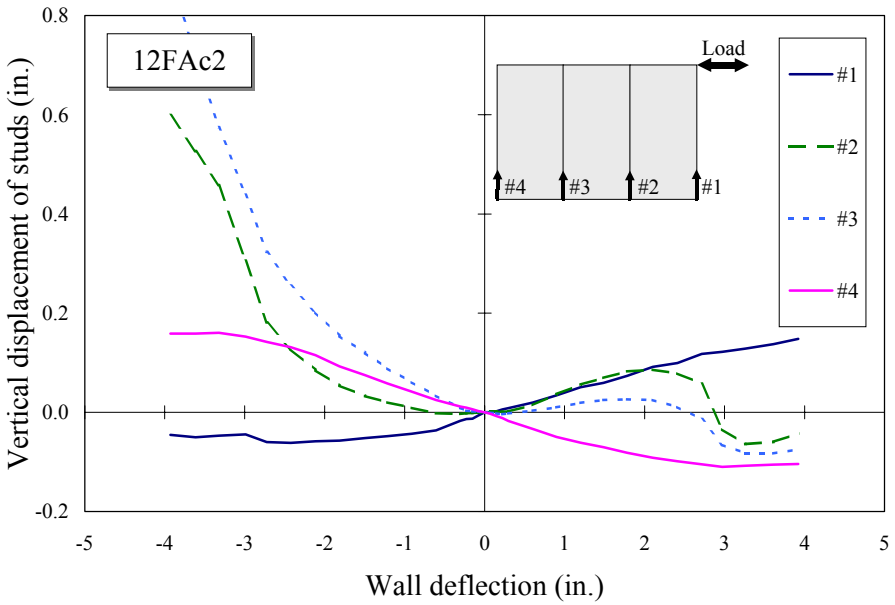

Figure 5. 16. Vertical displacements of studs in **FAc** walls (initial envelope).

Failure modes of **FAc** walls were more complex than failures of **FAm** walls. During reversed cycling, the sheathing nails always started withdrawal from the studs. By the end of the test, depending on the wood density, quality of sheathing attachment, and the wall size, the nails might fail in fatigue, pull out of wood, pull through of head or tear through the sheathing edge. Typically, it was a combination of all failure modes. The row of nails along the bottom plate usually failed in fatigue as is shown in Figure 5. 17, because the bottom plate was rigidly secured to the base. The nails along the top plate often tore through the edge near the panel corners and pulled heads through the sheathing in the middle. The shorter edge distance more likely resulted in the tear through the edge similar to shown in Figure 5. 18.

It was noticed that the nail fatigue was predominant in stiff walls **08FAc** and **12FAc** with the uniform sheathing displacements. In the walls with the single panel, **04FAc**, the nails near corners were often pulled out of wood as shown in Figure 5. 19. In narrow walls **02FAc,** the sheathing displacements were only half of those with the full size panel. Therefore, they did not experience nail fatigue unless subjected to multiple cycles above 127-mm (5-in.) amplitudes.

Figure 5. 17. Nail fatigue along the bottom plate in **FAc** wall.

Figure 5. 18. Nails tear through the edge at the top plate.

Figure 5. 19. Nails pull out of wood near the corner.

5.5 Conclusions on Walls with Full Anchorage

Based on eighteen monotonic and cyclic tests on walls with the full anchorage, the following conclusions were made:

1. Walls 1.2 m (4 ft.) and longer developed the same strength, on unit length basis, provided the wood density of studs was equal. Uniform wood density allowed the uniform distribution of sheathing displacements relative to the framing and the development of full load capacity of the sheathing-to-framing connections.

2. When sheathing nails withdrew from the wood because of low wood density and/or cyclic loading, it reduced the shear wall ductility and energy dissipation up to 50%.

3. Walls 0.6-m (2-ft.) long had 50% lower stiffness and strength relative to the long walls. However, their strength did not degrade at high deflections due to small displacement demand on sheathing-to-framing connections.

4. During cyclic loading, the load resistance of walls decreased on average 13% between the initial and stabilized cycles.

5.6 Monotonic Tests on Walls with Intermediate Anchorage (Walls IAm)

Twelve monotonic tests were conducted on **IA** walls. In seven of these walls, the sheathing panels were attached with 19-mm (¾-in.) edge distance along the top and bottom plates. Three walls were built with 10-mm (3/8-in.) edge distance on the perimeter. Two of these walls were repaired after the first test and re-tested. The discussion of the test results is divided into three subsections. For comparison purposes, the graphs are presented at a uniform scale throughout the discussion. Although the loading of the specimens typically continued beyond 127 mm (5 in.), most of the specimens failed significantly earlier. For clarity of illustration, the load-deflection curves are shown until the failure point (80% F_{peak}).

5.6.1 IAm Walls with 19-mm (3/4-in.) Edge Distance

The average response curves of these walls are shown in Figure 5. 20. Analysis of the graphs suggested that the performance of **IAm** walls was dependent on the aspect ratio and the number of panels in the wall.

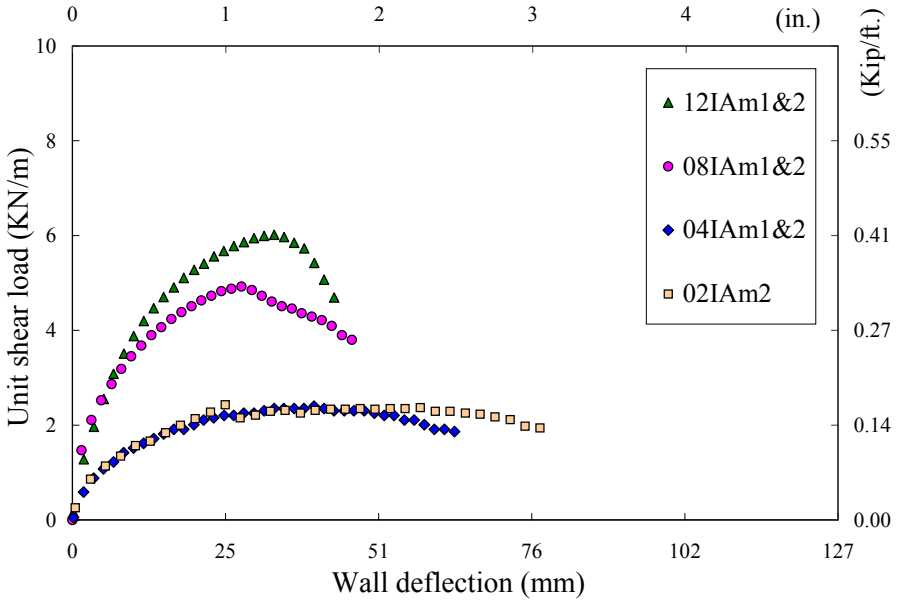

Figure 5. 20. Response curves of **IAm** walls with 19-mm edge distance.

12IAm walls were the strongest but the least ductile. The average strength, 6.0 KN/m (0.41 Kip/ft.), was reached at 34 mm (1.3 in.) and was followed by a quick degradation. The resistance decreased 20 % at 43-mm (1.7-in.) deflection. The strength was 60% and the ultimate ductility ratio, D_u, was only half of the observed in the corresponding **FAm** tests. Consequently, **IAm** walls dissipated 1/5 of the energy until failure when compared to **FAm** walls. Walls **08IAm** were 18% weaker (per unit length) than **12IAm** walls. The average strength 4.9 KN/m (0.34 Kip/ft.) was reached at 28-mm (1.1-in.) deflection, but the degradation slope was less steep. The 20% decrease of resistance occurred at 45-mm (1.8-in.) deflection.

The strength of **04IAm** and **02IAm** walls (per unit length) was approximately half of the **08IAm** walls. Similar to other walls in the series, the peak resistance was observed between 27 and 33-mm (1.1 and 1.3-in.) deflections but the strength degradation was

significantly lower. Walls **04IAm** decreased 20% of peak resistance at 62-mm (2.4-in.) deflection, and **02IAm** wall – at 74-mm (2.9-in.) deflection.

The significant differences in the performance of **IAm** walls and **FAm** walls, and the differences in the performance of **IAm** walls of various sizes can be explained by comparing the sheathing displacements relative to the framing. Figure 5. 21 shows the sheathing displacements in the first panel of a **12IAm** wall. In comparison with the typical **FAm** wall (see Figure 5. 6), the racking of the panel was insignificant. Most of the work was done by the sheathing nails along the bottom plate. The nails along the studs displaced less than 1 mm (0.04 in.) and the nails along the top plate, less than 1.8 mm (0.07 in.). In **08IAm** walls, the corresponding displacements were less than 0.8 mm (0.03 in) and in **02IAm** walls – less than 0.5 mm (0.02 in.). It follows from the measurements that the shorter the **IAm** wall was, the less racking it developed.

The performance of **02IAm** and **04IAm** walls with a single panel was completely controlled by the sheathing connections along the bottom plate. In **08IAm** walls, the interaction between two panels contibuted to the higher wall racking resistance. In **12IAm** walls, the third panel further improved the wall racking resistance. This statement is supported by the illustartion of the vertical displacements of studs in the **12IAm** wall in Figure 5. 22. The wall rotated about point #3 until the load capacity was reached. It is an indication of the 'anchoring' role of the third panel in the beginning of the test. When the load capacity was exceeded, the point of rotation shifted towards the wall corner and by the end of the test, the wall rotated about the point 300 mm (1 ft.) away from the left corner. Analysis of the stud displacements in **08IAm** walls showed that the center of rotation in the elastic region was near the middle of the second panel. From this information, it can be assumed that the second and the third panels developed more racking than was observed in the first panel.

Charactristic of the **IAm** walls performance was the bending of the right end of the bottom plate (between the end stud and the shear bolt) due to work of sheathing nails. At peak load, the end of the bottom plate split under the first sheathing nail and gradually straightened out while the nails pulled through the sheathing.

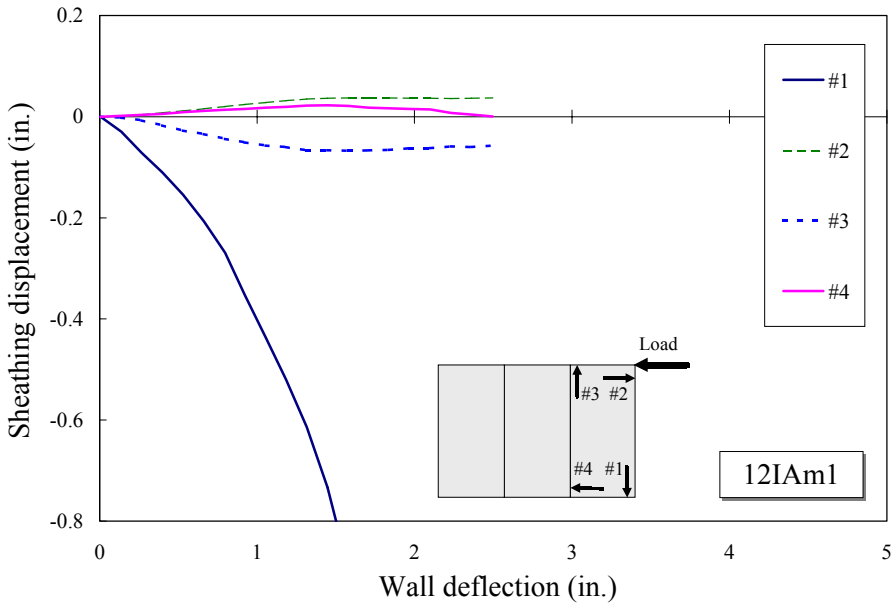

Figure 5. 21. Sheathing displacements in **12IAm** wall.

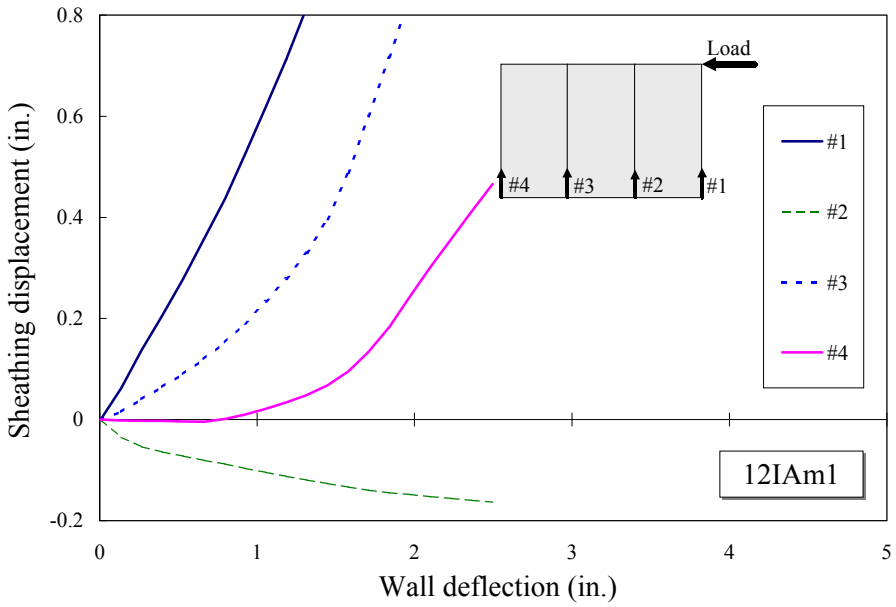

Figure 5. 22. Vertical displacements of studs in 12IAm wall.

Figure 5. 23 shows a **12IAm** wall after the test. It is a typical failure mode of **IAm** walls with full-size sheathing panels. The wall rotates about the left corner as a rigid body, without visible racking displacements. The sheathing is unzipped along the bottom plate with the nails torn through the panel edges.

Figure 5. 23. Typical failure mode of **IAm** wall.

The **02IAm** wall failed differently. The split of the bottom plate under the first sheathing nail caused the immediate resistance drop. Then, the resistance gradually degraded but the wall deflection was not sufficient for the sheathing connections to unzip due to the short length of the wall.

5.6.2 IAm Walls with 10-mm (3/8-in.) Edge Distance.

Two additional **08IAm** walls and **02IAm1** wall were built with 10-mm (3/8-in.) edge distance along the top and bottom plates. The test results of these walls were different from the walls discussed above. Therefore, a separate discussion of the edge distance effects is given here.

The response curves are shown in comparison with the matched walls in Figure 5. 24. The load capacity of **08IAm3&4** and **02IAm1** walls with the reduced edge distance was at least 19% less than that of **08IAm1&2** and **02IAm2** walls, respectively. The deflections at peak loads were approximately the same as before – 27 mm (1.1 in.) – but the deflections at failure decreased by 30%. Consequently, the toughness was 30% less and the work to failure was only half of that observed for the walls with 19-mm (3/4-in.) edge distance. Note that the wood density of framing in **08IAm1&2** walls was lower than the density in **08IAm3&4** walls. Therefore, the reduction in strength and toughness could be attributed to the edge distance effects mainly.

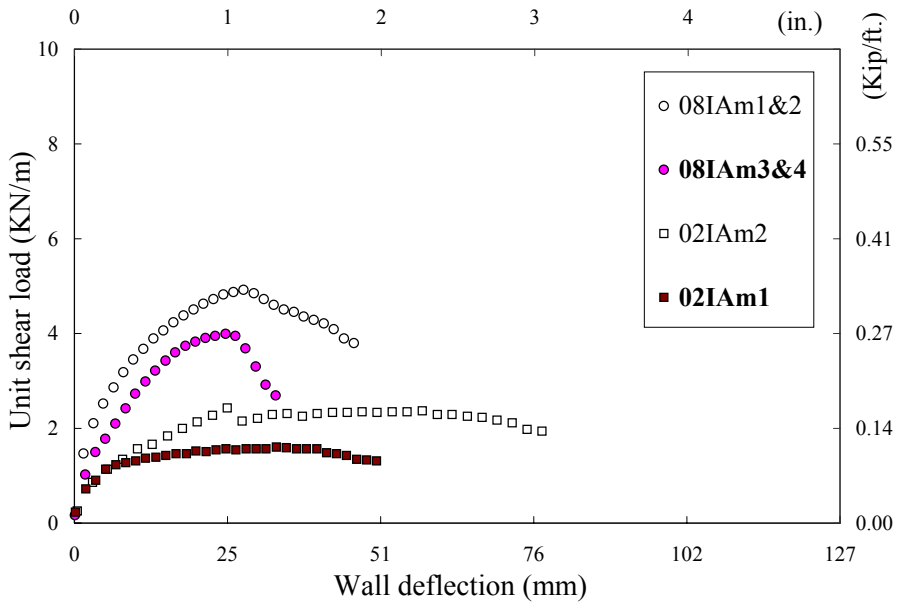

Figure 5. 24. Response curves of **IAm** walls with 10-mm edge distance.

The failure mode of **08IAm** walls with the reduced edge distance did not change, in principle. The sheathing unzipped along the bottom in the same way. Only the separation took place at lower deflections and was more brittle in character. Figure 5. 25 helps explain the lower deflection capacity of these walls: Obviously, it took less translation to unzip the 10-mm (1/8-in.) edge than 19-mm (3/4-in.) edge. The peak load was observed as soon as the first nail tore through the edge. The failure modes of **02IAm** walls were also similar to each other: the bottom plate split under the first sheathing nail but the nails did not tear through the sheathing.

Figure 5. 25. Failure mode of **08IAm** wall with 10-mm edge distance.

5.6.3 Repaired IAm Walls

After the tests, **IAm** walls with the reduced edge distance received little visible damage except for along the bottom plate. The measured sheathing displacements along the perimeter of the first panel did not exceed 0.7 mm (0.03 in.), and it was suggested that the walls be repaired and tested again to estimate the performance of the retrofitted walls.

Immediately after the first test, **08IAm4** wall was repaired by replacing the bottom plate and attaching the sheathing at 152 mm (6 in.) o. c. with 1/2-in. edge distance. The **08IAm4r** wall was tested one hour after the repair. Wall **02IAm1** was repaired one week after the test. The bottom plate was not replaced and old nails were not removed. Instead, the density of the nailing was increased: additional nails attached the sheathing to the bottom plate at 76 mm (3 in.) o. c. with 19-mm (3/4-in.) edge distance. Wall **02IAm1re** was tested one hour after the repair.

The response curves of the repaired walls are shown in comparison with the other tests in this series. The repaired walls were able of carrying at least the same load and they failed at larger deflections. The improvement was achieved due to the larger edge distance and, maybe, due to the fresh nailing. However, the improvement was not as high as one might expect looking at the performance of the other walls with the large edge distance.

The reason for the low performance of **08IAm4r** wall was the low wood density of the new bottom plate. The density of the original bottom plate in **08IAm4** wall was 610 kg/m^3, while the density of the new bottom plate was only 453 kg/m^3. Due to the low wood density, the strength of the sheathing-to-framing connection along the bottom plate was reduced. Consequently, the center of rotation of **08IAm4r** wall was shifted to the left corner, and the second panel of the wall contributed minimum to the racking displacements.

The split in the bottom plate played the critical role in the resistance of **02IAm1re** wall. Since the first nail in the row was excluded from work during the first test, the stiffness of the wall was very low. The split in the bottom plate increased during the second test, and the wall barely reached the original strength. The high density of nailing

made the situation worse: by the end of the test, the bottom pate was split almost in half (see Figure 5. 27).

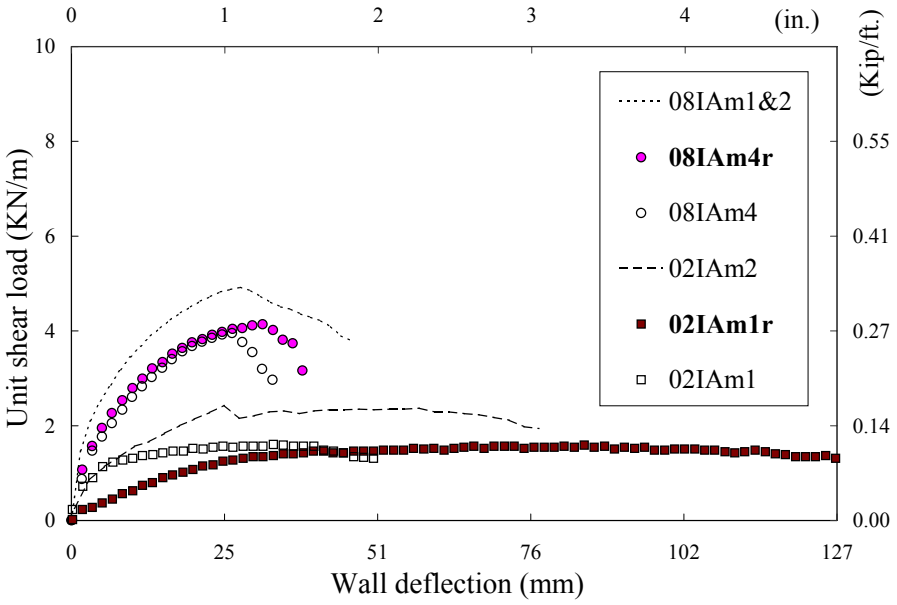

Figure 5. 26. Response curves of repaired **IAm** walls.

Figure 5. 27. Failure mode of **02IAm1re** wall.

To accumulate more data on performance of retrofitted walls it was decided to continue testing retrofitted walls under the cyclic tests described in the next section.

5.7 Cyclic Tests on Walls with Intermediate Anchorage (Walls IAc)

Fifteen cyclic tests were conducted on **IA** walls. Eight walls were built and tested according to the plan, with the sheathing attached at 152 mm (6 in.) o. c. with the edge distance 10 to 19 mm (3/8 to 3/4 in.) along the top and bottom plates. The walls did not exhibit visible racking and appeared undamaged after the test, except for the bottom plate area. Therefore, it was possible to replace the bottom plate and re-test the walls to estimate the residual capacity and other performance parameters of the retrofitted walls. In three of these walls, the sheathing was attached to the new bottom plate with the regular 152-mm (6-in.) spacing and 19-mm (3/4-in.) edge distance. In the other four walls, the nail spacing along the bottom plate was reduced to 76 mm (3 in.) o. c. Increasing the density of nailing was considered a reasonable means of retrofitting the walls because the row of nails along the bottom plate appeared controlling the performance of **IA** walls. The results of these tests are discussed in the following three subsections.

5.7.1 IAc Walls with Regular Nailing Schedule

The average initial envelope response curves are shown in Figure 5. 28. In general, the shape of these curves repeated the shape of the corresponding monotonic curves shown in Figure 5. 20. Walls **12IAc** were the strongest and the most rigid. Walls **02IAc** were the least strong but the most ductile. The average initial cyclic strength of **12IAc** walls was 5.4 KN/m (0.37 Kip/ft.). The initial cyclic strength of **08IAc** walls was 18% lower than that of the **12IAc** walls. The initial strength of **04IAc** walls was 45% lower than that of **08IAc** walls. Similar strength ratios were observed during the corresponding monotonic tests, which supported the assumption about the contribution of adjacent panels to the racking resistance. Wall deflections at the peak loads and failure were typically smaller than that observed during the corresponding monotonic tests. The similar trend was observed when comparing **FAm** and **FAc** walls, where the earlier strength degradation was related to the withdrawal of sheathing nails from wood.

The stabilized response envelopes for **IAc** walls are shown in Figure 5. 29. The stabilized resistance parameters determined from these envelopes were, on average, 15% lower than the initial ones.

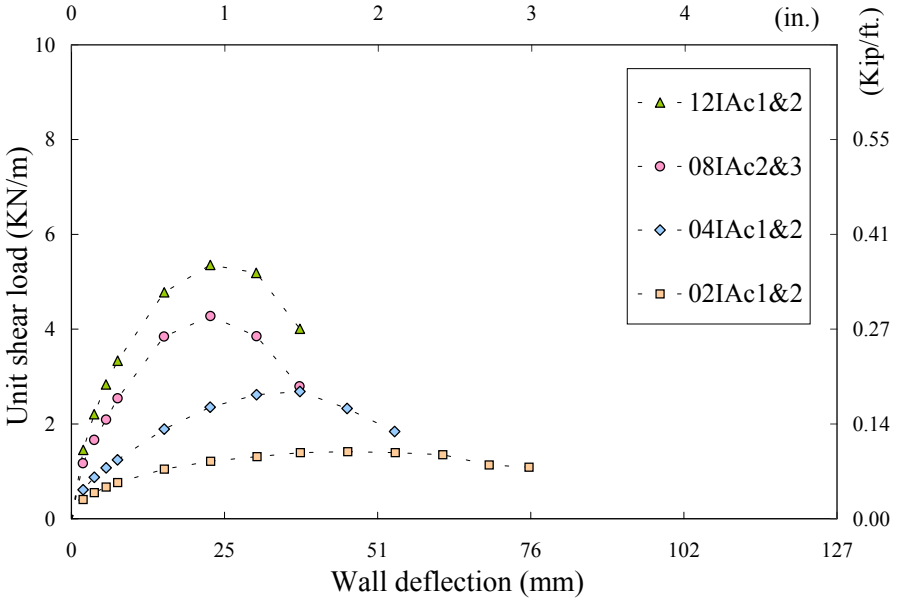

Figure 5. 28. Average initial envelope response curves of **IAc** walls.

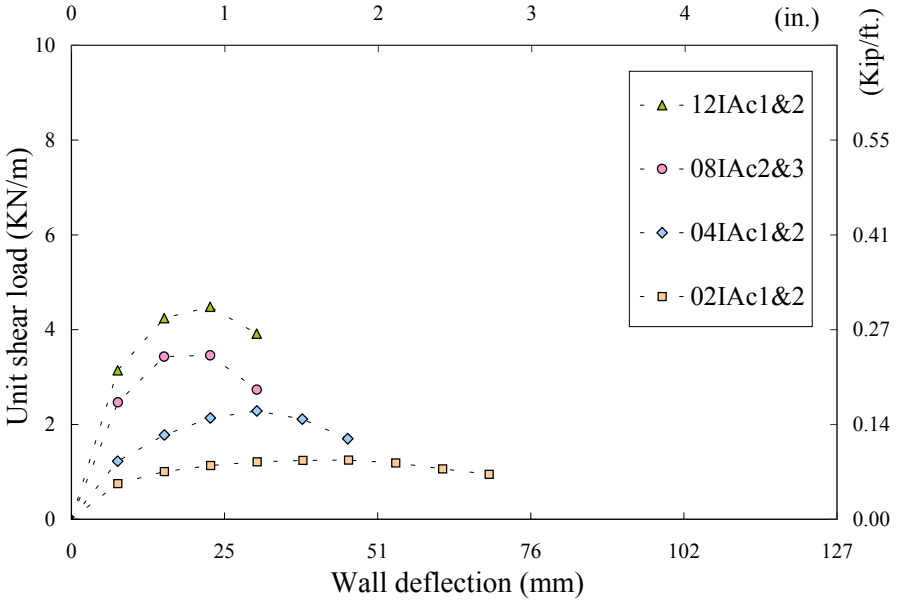

Figure 5. 29. Average stabilized envelope response curves of **IAc** walls.

Figure 5. 30 represents the initial envelopes of the vertical displacements of studs in a **12IAc** wall. It can be seen that the wall rotated symmetrically about the middle of

the bottom plate. The sheathing displacements of the first panel in this wall, shown in Figure 5. 31, illustrate that on the positive stroke, there was little racking (maximum 0.35 mm) except fast separation from the bottom plate. On the reverse stroke, the panel developed tenfold racking displacements. The combined information from these graphs suggested that the third panel produced an equal and opposite response of the first panel. These measurements prove the contribution of the third panel to the racking resistance. Similar contribution, but at a lower level, is provided by the second panel in **08IA** walls.

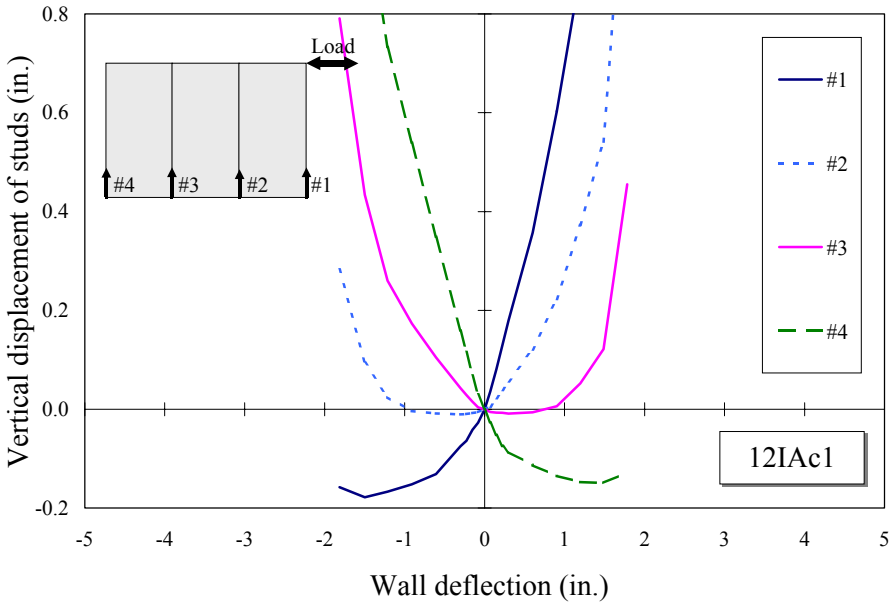

Figure 5. 30. Vertical displacements of studs in 12IAc walls (initial envelope).

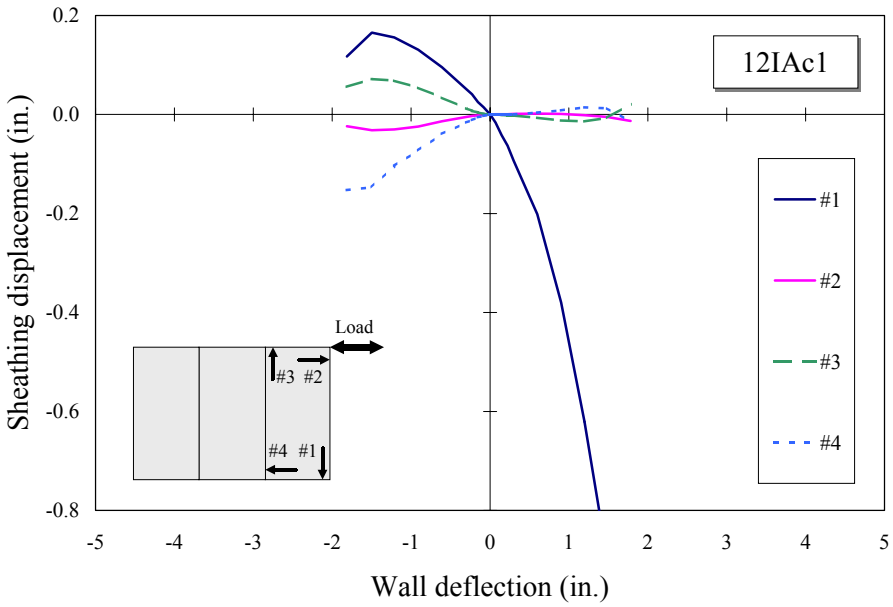

Figure 5. 31. Sheathing displacements in **12IAc** walls (initial envelope).

Figure 5. 32 shows the bottom part of **08IAm3** wall after the test. It illustrates a typical failure mode of **IAc** walls. There is no visible racking. The entire wall, as a rigid body, is separated from the bottom plate. There is no sign of nail fatigue, withdrawal, or bending if the edge distance is shorter than 19 mm (3/4 in.). When the nails were driven with 19-mm (3/4-in.) edge distance, the bottom plate ends experienced significant bending caused by the work of sheathing nails. The ends of the bottom plate were often split during the test. Remarkably, during **04IAc1** test, the bottom plate was ruptured from bending as is shown in Figure 5. 33.

Figure 5. 32. Failure mode of **IAc** wall with reduced edge distance.

Figure 5. 33. Failure of **04IAc1** wall.

The importance of the edge distance in sheathing-to-framing connections is evident from the comparison of monotonic and cyclic test results. Walls **08IAc2** and **08IAc3** exhibited similar performance to walls **08IAm3** and **08IAm4** with similar wood density of framing and similar edge distance of sheathing attachment. Despite the high wood density of the bottom plates in these walls (between 550 and 600 kg/m^3), the small edge distance effects dominated. The strength and stiffness of these walls were significantly lower than the observed for **08IAm1** and **08IAm2** walls with the lower wood density of the bottom plates (520 kg/m^3) but the larger edge distance.

Wood density of the bottom plates was the second important factor affecting the shear wall strength. Wall **12IAc1** with the wood density 450 kg/m^3 was stronger than wall **12IAc2** with the density 400 kg/m^3. For comparison, wall **12IAm1** (625 kg/m^3) was stronger than **12IAm2** (562 kg/m^3). Both **12IAm** walls were stronger than **12IAc** walls. Wood density of other framing elements in walls **IA** did not correlate with the wall strength. On the contrary, the strength of **FA** walls was dependent on wood density of studs and was not correlated to the density of the plates.

5.7.2 Repaired IAcr Walls with Regular Nailing Schedule

Walls **12IAc2**, **08IAc3**, and **02IAc2** were repaired after the tests by replacing the bottom plates and attaching the sheathing with the nails at 152-mm (6-in.) o. c. The edge distance was maintained at 19 mm (3/4 in.). The tests were conducted within one hour

after the repair. Figure 5. 34 shows the initial envelope response curves for these walls in comparison with the average initial envelopes obtained earlier.

The results show the increase in strength and stiffness of the repaired walls. Note, that the performance parameters of **12IAc2r** wall were nearly equal those of **12IAm** walls. The improved performance of **12IAc2r** wall was due to the higher wood density and the fresh nailing in the new bottom plate. The retrofit of **08IAc3r** wall was less effective because the density of the new bottom plate was only 488 kg/m^3 vs. original 600 kg/m^3. However, the effect of quality nailing appeared to be dominating. (Note: the original test for each specimen occurred after a minimum of two weeks storage. This allowed the wood fibers around the nails to relax. In other connection tests, the relaxation results in a 5 to 10% reduction in resistance.)

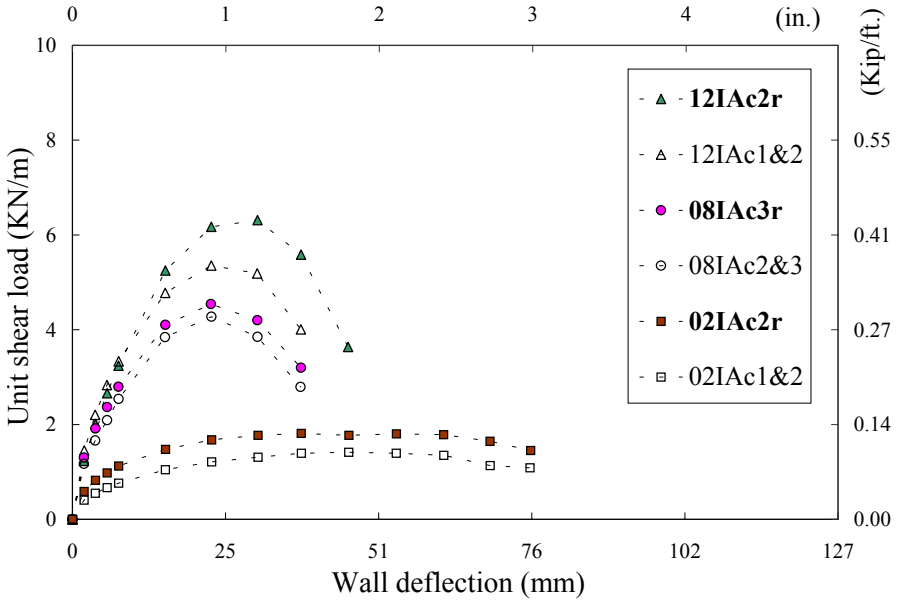

Figure 5. 34. Initial envelope response curves of **IAcr** walls.

5.7.3 Repaired IAcre Walls with Dense Nailing Schedule

Walls **12IAc1**, **08IAc2**, **04IAc1**, and **04IAc1** were repaired after the tests by replacing the bottom plates and attaching the sheathing to it with the nails at 76-mm (3-in.) o. c. The edge distance was maintained between 13 and 19 mm (1/2 and 3/4 in.). The tests were conducted within one hour after the repair. Figure 5. 35 shows the initial

envelope response curves for these walls in comparison with the average initial envelopes obtained for the original walls.

The graphs illustrate the dramatic increase in resistance of each wall. On the average, the initial cyclic strength was increased by 50%. The ultimate deflections of **08IAc** and **12IAc** walls almost doubled and the work to failure more than tripled. Note that the **12IAc** wall remained the strongest, on unit length basis, and **04IAc** wall was still half as strong as **08IAc** wall. The sheathing displacements shown in Figure 5. 36 illustrate that the dense nailing and panel interaction provided for larger racking displacements in the panels and, consequently, the higher racking resistance of the walls. At the peak loads, the sheathing displacements in the first panel of **12IAc1re** and **08Iacre** walls reached 4 mm (0.15 in.). Corresponding displacements in **04IAc2re** and **02IAc1re** walls remained negligible; therefore, the wall strength in the single-panel walls was controlled by the nails along the bottom plate.

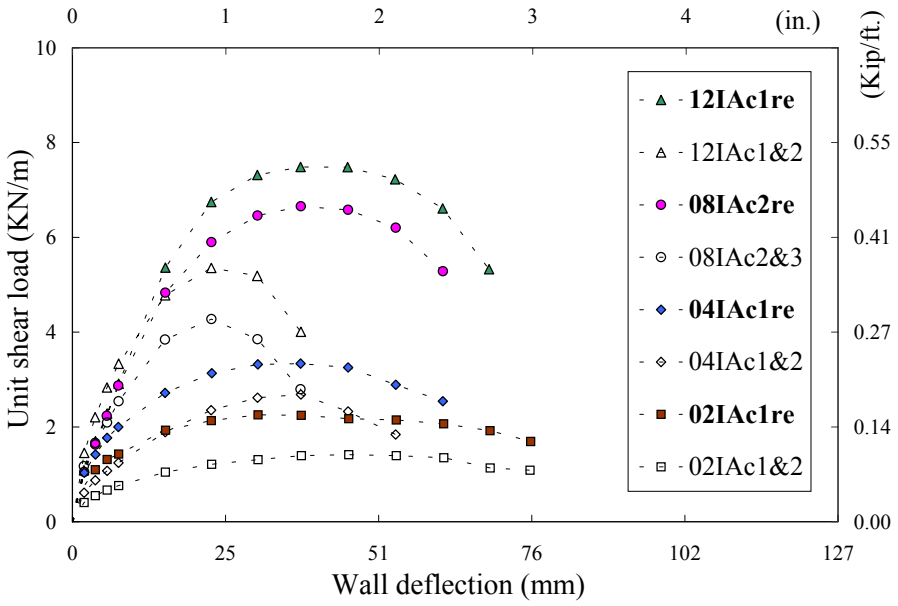

Figure 5. 35. Initial envelope response curves of **IAcre** walls.

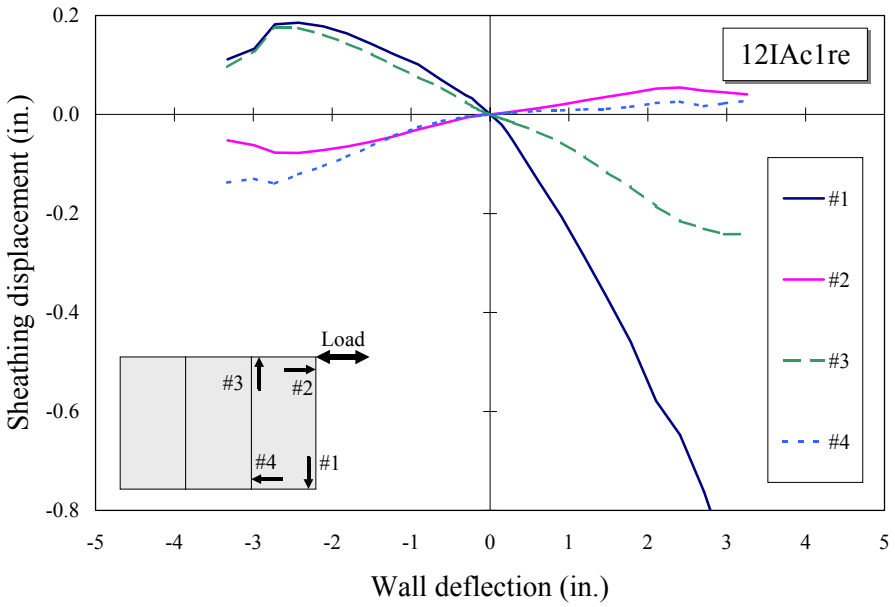

Figure 5. 36. Sheathing displacements in **12IAc1re** wall.

The dense nailing caused the change in the failure mode of the walls. Prior to the separation of the sheathing, the bottom plates split under the sheathing nails and often ruptured from bending as is shown in Figure 5. 37 and Figure 5. 38. The large edge distance allowed the sheathing nails along the bottom plate to develop their full capacity.

Figure 5. 37. Failure of **08Iac2re** wall.

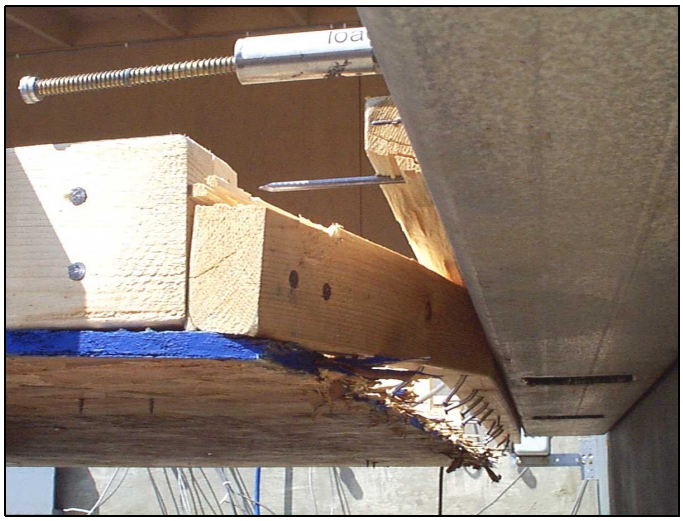

Figure 5. 38. Failure of **04IAc1re** wall.

5.8 Conclusions on Walls with Intermediate Anchorage

Combining the results of twenty-seven monotonic and cyclic tests on walls with the intermediate anchorage, the following conclusions were made:

1. The strength, shear modulus, and ductility of **IA** walls were dependent on the aspect ratio and the number of panels in the wall. **02IA** walls were the weakest but the most ductile. **04IA** walls were half as strong (on the unit length basis) as **08IA** walls but failed at 50% larger deflections. **12IA** walls were the strongest due to interaction of adjacent sheathing panels.

2. Because of small racking, the wall resistance was controlled by the quality of sheathing attachment at the bottom plate. When the edge distance along the bottom was reduced from 19 mm (3/4 in.) to 10 mm (3/8 in.), the strength, stiffness, and ductility of the wall reduced 20% and more. In addition, the strength of the wall was positively correlated with the wood density of the bottom plate.

3. There was no significant difference in wall performance under the cyclic (initial envelope) and the monotonic loading conditions because there was no fatigue or withdrawal of sheathing nails from the wood. During stabilization cycles, the load resistance of walls decreased on average 15%.

4. The repeated testing showed that the original wall resistance was restored with the replacement of the bottom plate after the first test. If the density of nailing along the bottom plate was doubled, the wall strength was increased approximately 50%. In addition, the deflection capacity of the repaired **08IA** and **12IA** walls increased more than 50%.

5.9 Monotonic and Cyclic Tests on Walls with Nailed Attachment (Walls NA)

Eleven tests were conducted in this series. First, the adequate nailing schedule for holding the specimens against overturning was determined in four monotonic tests on **04NAm1** wall. Then, three monotonic and three corresponding cyclic tests were conducted on walls **04NA**, **08NA,** and **12NA**. After the cyclic test on **04NAc2** wall, the specimen was repaired and re-tested. The test results are discussed in the following three subsections and comparisons are made between **IA** and **NA** walls in the conclusion.

5.9.1 Determine Adequate Nailing Schedule

5.9.1.1 Preliminary Estimates

The *International Residential Code* (ICC 2000) requires three 16d nails every 406 mm (16 in.) to attach the sole plate to underlying structures. According to this requirement, **04NAm** wall should be attached to the base with nine 16d nails. The following calculations and tests illustrate that this nailing schedule was not adequate to prevent the wall overturning under the racking load.

Recall that no dead load was applied in the wall plane. Therefore, only the withdrawal resistance of nails attaching the wall to the base provided the wall overturning resistance. This situation was similar to the real-life when the walls parallel to the floor joists carry minimal gravity loads.

The capacity of 16d common nails in withdrawal from the SPF lumber assuming dry conditions can be estimated as follows:

$$W' = W \cdot p / F_{safety} = 26 \cdot 2 \cdot 5 = 260 \text{ lbf. } (1.16 \text{ KN}) \quad (5.\ 10)$$

where W = 26 lbf./in., tabulated withdrawal design value from Table 12.2A (AF&PA 1993a),

p = 2 in., penetration depth of 16d nail,

F_{safety} = 1/5, safety factor (AF&PA 1993b).

The maximum overturning moment acting on the wall with the aspect ratio 2:1 is:

$$M = v \cdot L \cdot H = 175 \cdot 4 \cdot 8 = 5600 \text{ lbf.-ft. } (7.59 \text{ KN-m}) \quad (5.\ 11)$$

where v = 175 plf., maximum lateral load observed during the tests of **04IAm** walls,

L = 4 ft., wall length,

H = 8 ft., wall height,

If the wall pivots around the corner (point O in Figure 5. 39) and the withdrawal forces are uniformly distributed among the nails along the bottom plate at the strength limit state, the moment developed by the nails to resist the overturning equals:

$$M_O = u_w \cdot \frac{L^2}{2} \tag{5. 12}$$

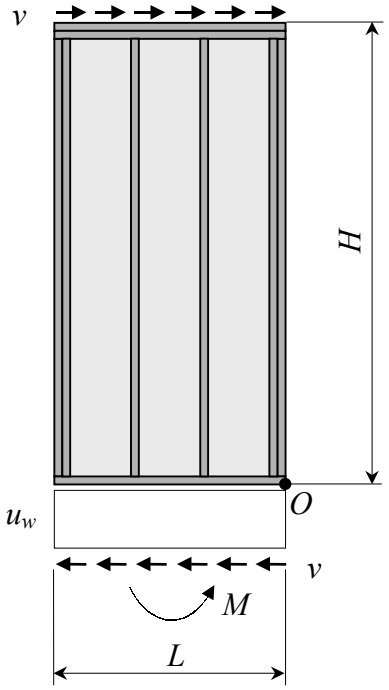

Figure 5. 39. Free body diagram of **NA** shear wall.

To satisfy the static moment equilibrium, it follows from Equations (5.11) and (5.12):

$$u_w = \frac{2H}{B} v \tag{5. 13}$$

Therefore, to allow **04NA** wall develop the maximum shear strength during the test, the number of 16d common nails attaching the bottom plate to the base should be at least

$$n = \frac{u_w B}{W'} = \frac{2H}{W'} v = \frac{2 \cdot 8}{260} \cdot 175 \approx 11 \quad (5.\ 14)$$

The lateral resistance of 16d nail can be estimated as follows:

$$Z' = Z \cdot C_D / F_{safety} = 120 \cdot 1.6 \cdot 2 = 384 \text{ lbf. (1.71 KN)} \quad (5.\ 15)$$

where Z = 120 lbf., tabulated lateral design value for single shear with 1-1/2 in. thick SPF side member from Table 12.3B (AF&PA 1993a),

C_D = 1.6, load duration factor for wind and seismic loading (AF&PA 1993a),

F_{safety} = 1.2, minimum safety factor for nail connections (Gutshall 1994).

Therefore, the resistance of the **NA** walls is governed by the withdrawal capacity of the nails because their lateral capacity is higher than the withdrawal capacity.

*5.9.1.2 Preliminary Experiments on **04NAm** walls*

Four preliminary tests were conducted to determine the nailing schedule that prevented specimen overturning failure due to the nail withdrawal. In these tests, the same specimen was reused because little or no visible damage occurred to the shear wall during the first few tests.

For the first test, **04NAm1** wall was secured to the base with twelve 16d common nails in one row at 76 mm (3 in.) o. c. At 4-mm (0.16-in.) deflection, the nails started withdrawing from the base, and soon the wall was overturned resisting less than 1.5 KN/m (0.10 Kip/ft.) load. From Figure 5. 40 and the sheathing displacement measurements, it can be seen that the wall rotated as a rigid body, and the bottom plate remained firmly attached to the wall.

For the next test, the specimen was attached to the base with twenty-four 16d common nails in two rows at 76 mm (3 in.) o. c. The wall was able to resist up to 1.9 KN/m (0.13 Kip/ft.) but it was also overturned due to the nail withdrawal from the base. The bottom plate separated from the studs 2.3 mm (0.09 in.) utmost, and remained firmly attached to the wall.

For the third test, the wall was attached to the base with thirty-six 16d common nails at 76 mm (3 in.) o. c. in three staggered rows. In this case, the attachment was sufficient to prevent the nail withdrawal from the base. The wall stiffness was low due to the previous loading history, but the load resistance increased to 2.3 KN/m (0.16 Kip/ft.), and the failure mode changed. As is shown in Figure 5. 41, the sheathing unzipped from the bottom plate similar to the failures observed in **IAm** wall tests.

Figure 5. 40. Wall attached with 12 nails in one row.

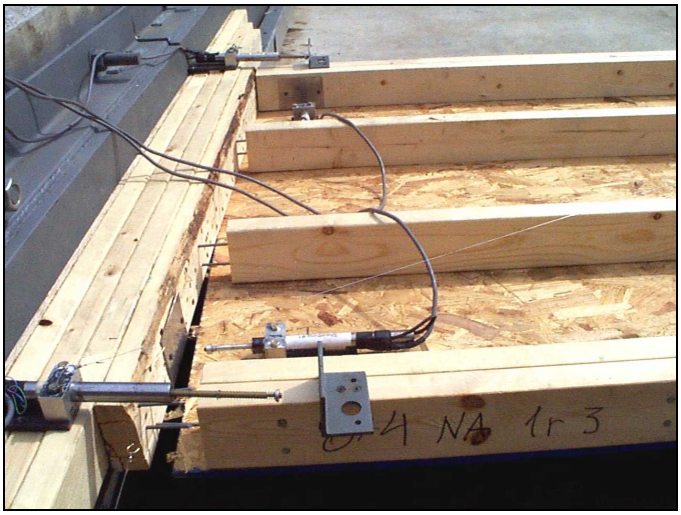

Figure 5. 41. Wall attached with 36 nails in three rows.

It was reasonable to assume that the nails near the corners contributed the withdrawal resistance the most, and that the nails in the mid-span were not necessary. This assumption was tested as follows. The bottom plate was replaced and the wall was attached to a newly installed base using nine 16d nails at each corner at 76 mm (3 in.)

o. c. in three staggered rows. The connection was able to resist overturning until the wall deflection reached 21 mm (0.85 in.). At that point, the separation between the base and the right end of the bottom plate reached 5.4 mm (0.21 in.), and it was the moment when the base connection failed (see the Appendix, Wall **04NAm1r4**). The assumption was not proved by the test: nine nails in the corner could not hold down the wall and it rocked away from the base as is shown in Figure 5. 42.

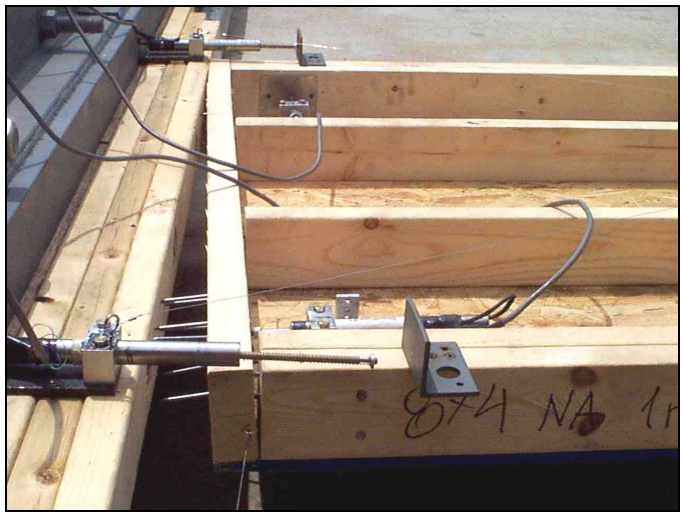

Figure 5. 42. Wall attached with 9 nails in each corner.

Based on the preliminary tests, the nailing schedule with three rows of 16d nails at 76 mm (3 in.) o. c. was used to attach all other **NA** specimens.

5.9.1.3 Potential Use of Improved Fasteners

Improved fasteners, such as threaded nails of high-carbon steel, have been developed for many years in the U.S. to improve performance of wood assemblies. Stern (1950) conducted numerous tests to compare performance of threaded nails and plain-shank nails in various applications. His tests demonstrated significant improvement in withdrawal and lateral resistance of the threaded nails relative to common nails in various wood species immediately after assembly and after seasoning. If threaded nails were used to attach the bottom plate of shear walls to the platform, the required number of the fasteners to prevent the wall overturning could be reduced.

Stern (1959) compared the racking strength of the lumber frames assembled with various types of fasteners. The frame built with green lumber and assembled with

annularly threaded nails carried 4.6 times the load of the frame assembled with plain-shank nails. These findings suggest a prospect for future research in improvement of the racking performance of shear walls using the improved fasteners.

5.9.2 Monotonic tests on NA Walls (Walls NAm)

The test **04NAm1r5** was performed on **04NAm1r4** wall with the bottom plate replaced and the sheathing attached to it at 76 mm (6 in.) o. c. with 19-mm (3/4-in.) edge distance. Both **08NAm1** and **12NAm1** walls were built with 76±3 mm (3/8±1/8 in.) edge distance.

Figure 5. 43 shows the response curves of **NAm** walls in comparison with the corresponding **IAm** walls. The comparison of these curves with consideration to the edge distance and wood density revealed similarities in response of **NAm** and **IAm** walls and confirmed previous conclusions. Walls **04NAm1r5** and **04IAm2,** having the equal wood density and 19-mm (3/4-in.) edge distance, produced equivalent responses. Walls **08IAm3&4** and **08NAm1** built with 10-mm (3/8-in.) edge distance might have produced responses similar of each other. However, the bottom plate of **08NAm1** wall had wood density only 505 kg/m3, while **08IAm3&4** walls had 590 kg/m^3 on the average. In **12NAm1** wall, the low quality nailing was coincidental with the low density of the bottom plate (398 kg/m^3) resulting in the lowest response of all 3.6-m (12-ft.) walls. Nevertheless, due to certain panel interaction, **12NAm1** wall was stronger than **08NAm1** wall, and the latter was stronger than **04NAm1r5** wall.

Figure 5. 44 shows how easily the sheathing is separated from the bottom plate if the edge distance requirements are violated.

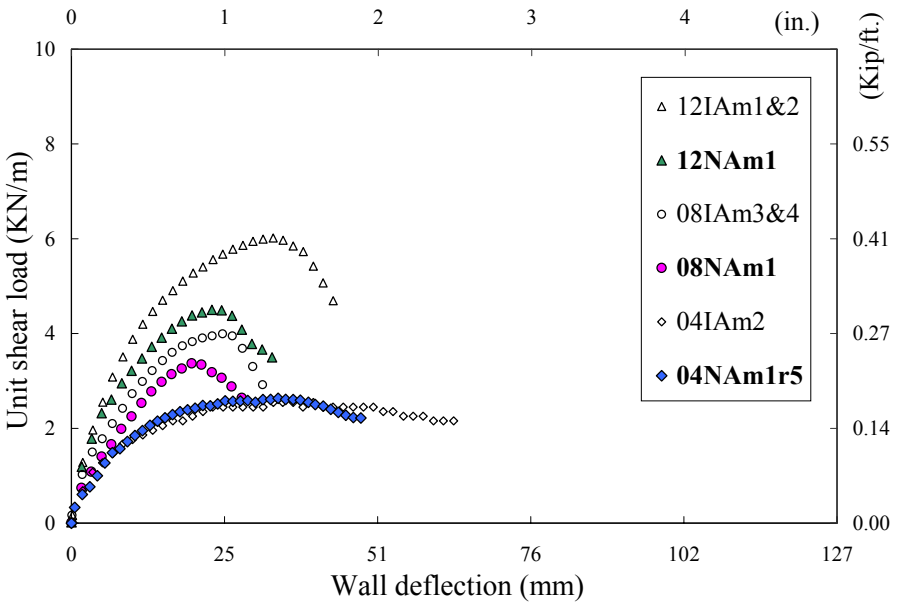

Figure 5. 43. Response curves of **NAm** and **IAm** walls.

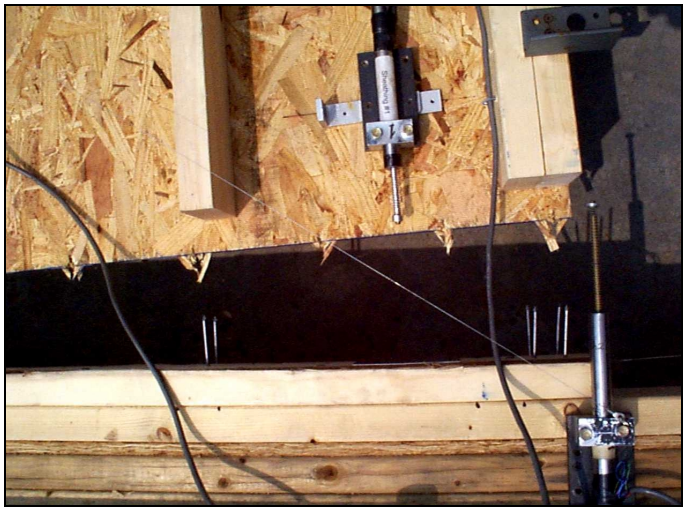

Figure 5. 44. Failure of **12NAm1** wall.

5.9.3 Cyclic tests on NA Walls (Walls NAc)

The only new wall in this series, **04NAc2**, was built with 10-mm (3/8-in.) edge distance. The other specimens were built of the previously tested walls, based on the assumption that repaired walls were capable of developing the original resistance. After **04NAc2** test, the specimen was repaired and re-tested as **04NAc2r** wall. Similarly, walls **08NAc1** and **12NAc1** were built of **08NAm1** and **12NAm1** specimens, respectively. In

the repaired walls, the bottom plates were replaced and the sheathing attached at 152 mm (6 in.) o. c. with 19-mm (3/4-in.) edge distance.

The response curves of **NAc** specimens are shown in Figure 5. 45 in comparison with the corresponding **IAc** tests. The comparison shows that the **NAc** and **IAc** walls performed equivalently provided the edge distance and the wood density were equal. As expected, the strength, stiffness, and ductility of **04NAc2** wall were low because of the small edge distance.

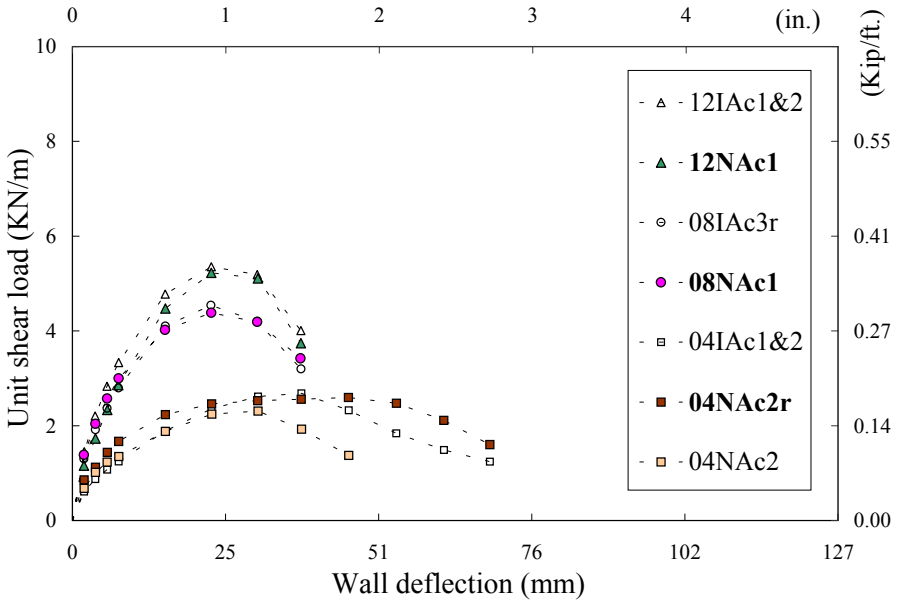

Figure 5. 45. Initial envelope response curves of **NAc** and **IAc** walls.

In the **NAc** tests, the sheathing displacements and failure modes followed the same patterns as in the corresponding **IAc** tests, with the exception of the bottom plate performance. Since the bottom plates were attached to the base starting at the wall corner with the density of nine nails per foot, there was no bending or splitting that was observed during the **IAm** tests. The bottom plate remained firmly attached at the base. Figure 5. 46 helps visualizing the density of the nailing and understanding that the second replications of the **NA** tests were considered unnecessary from the practical point of view.

Figure 5. 46. Wall **NAc1** after the test.

5.10 Conclusions on Walls with Nailed Attachment

Based on eleven monotonic and cyclic tests on walls with the nailed attachment, the following conclusions were made:

1. Overturning resistance of shear walls under the lateral load was governed by withdrawal resistance of the nails attaching the shear wall to the base. In the absence of dead load in the plane of the wall, it took unreasonably high density of nailing to prevent the specimen overturning during the test.

2. If attached to the base adequately, **NA** walls were capable of developing the equivalent resistance to **IA** walls. The performance characteristics and the patterns of sheathing displacements, similar to **IA** walls, were dependent on the wall size, quality of the sheathing attachment, and the wood density of the bottom plates.

3. During the cyclic loading, the stabilized load resistance was, on average, 12% lower than the initial cyclic resistance.

5.11 Summary

Fifty-six full-size shear walls with aspect ratios of 4:1, 2:1, 1:1, and 2:3 were tested monotonically and cyclically. Three overturning restraint conditions were applied: 1) Tie-down anchors at the end studs and shear bolts along the bottom plate, or 2) Shear

bolts along the bottom plate, or 3) Nailing along the bottom plate. To obtain conservative estimates, no dead load was applied in the wall plane during the tests. In eight specimens, the edge distance of sheathing attachment was reduced from 19 mm (3/4 in.) to 10 mm (3/8 in.). Twelve walls without tie-down anchors were repaired after the tests and re-tested. Combining the information obtained during the tests, the following conclusions were made:

1. The resistance of shear wall is positively correlated to the amount of racking displacements developed by the wall components. If shear wall is restrained from the uplift of studs, the racking is uniformly distributed along the perimeter of sheathing panels and the wall develops the maximum resistance independent of the number of full-size panels in the wall. If the uplift of studs is not restrained (by tie-down anchors or otherwise), the distribution of racking is not uniform and depends on the wall size. In this case, a shear wall with a single panel has the minimum racking resistance. The racking resistance increases with each additional panel.

2. Narrow walls, 0.6-m (2-ft.) long, are not capable of developing the uniform racking, even if fully restrained, which results in the lower resistance. The observed stiffness and strength were 50% lower relative to the long walls. Due to the low racking, the sheathing connections in these walls did not fail, which lead to the extraordinary ductility.

3. Low wood density reduces the nailed connection strength, and therefore, the shear wall strength and toughness. In fully-restrained walls, where the racking displacements are distributed along the panel perimeter, the wood density of each framing element is important for the wall resistance. In non-restrained walls, where the maximum work is done by the connections along the bottom, the density of the bottom plate is dominant.

4. The strength of the wall, as a function of the work done by the sheathing-to-framing connections, effectively decreases due to premature failure of individual connections if the edge distance is too short. In fully-restrained

walls, where the work is uniformly distributed among all connections, the effect of the short edge distance is diminished. In non-restrained walls, the edge distance along the bottom plate is imperative.

5. During the cyclic loading, the nails are pulled by sheathing from the wood. With each cycle, the resistance of the connection decreases. At the strength limit state, the resistance decreases 12% to 15% between the initial and the stabilized cycle. In fully-restrained walls, the effect of cycling is similar to the effect of the low-density wood. Therefore, the cycling leads to earlier strength limit state and failure. After many cycles at large amplitudes, nail fatigue is observed. In non-restrained walls, the effect of cycling is neutralized by shifting the center of wall rotation to the middle of the bottom plate, therefore reducing the displacement demand on the connections.

6. Due to small racking, little damage occurs to the shear wall without overturning restraint. It is easy to repair by replacing the bottom plate and attaching the sheathing to it at a regular or dense nailing schedule. The repaired wall is capable of restoring the original strength. Considerable improvement was achieved when the nailing density was increased.

7. To improve the overturning and racking resistance of shear walls, the use of improved fasteners in the frame assembly and attachment to the platform should be investigated.

Chapter 6. Analytical Models of Shear Walls

6.1 General

Analytical modeling can be used as a complementary tool in understanding performance and developing design methods of structural systems. Many shear wall models have been developed in the last twenty-five years to predict response of shear walls to lateral loads.

The chapter begins with an introduction of a simple mechanical model of shear wall action, which displays major assumptions of the approach. Then, a brief overview of closed-form models and finite element models proposed by other researchers is given. Previously developed models described the performance of engineered fully-anchored shear walls adequately. In this study, a simple mechanical model is proposed to predict load capacity of shear wall without tie-down restraint representative of conventional construction.

To predict failure mechanisms of structural systems, the analyst needs predictions of failure modes of the structural components in addition to the load capacity. For advanced analysis, one would need to know load-deflection relationships of shear walls, diaphragms, and other structural components contributing the building lateral force resisting system. Some structural elements have brittle failure modes, when the load resistance drops quickly after the load capacity is reached. Other elements yield without significant load decrease at large deflections. For future applications, it is useful to extend the predictions of shear wall performance beyond the load capacity levels. This has been done in this study by including the post-capacity load-deflection curve of the sheathing connections into the shear wall model.

Results of the shear wall tests described in Chapter 5 are used to derive load-deflection prediction models for walls with and without tie-down restraint. Conclusions are made about applicability of the models for design purposes and recommendations for further model development are made.

6.2 Simple Shear Wall Model with Tie-Down Anchors

Assume a shear wall with tie-down anchors attached at the end studs. A simple mechanical model representing the shear wall deformation under lateral load is shown in Figure 6. 1. Frame joints are considered pinned and their separation is prevented by the tie-down restraint. The lateral load applied at the top causes the framing to distort in the shape of parallelogram. Racking of the frame is prevented by the sheathing through fasteners connecting it to the frame. Due to the high rigidity, the sheathing panels deform less than the framing. The difference between sheathing and framing deformations is resisted by the fasteners (nails, screws or staples). Along with shear deformation of the sheathing, the shear strain of the wall is a function of the fasteners' slip. Vertical reactions act along the end studs, which are called chords, in proportion to the wall aspect ratio.

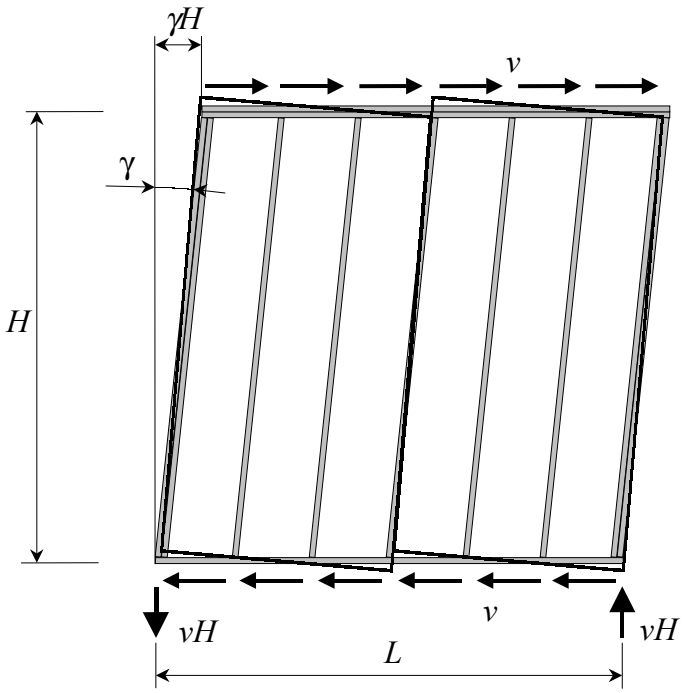

Figure 6. 1. Simple shear wall response to lateral load.

The model in Figure 6. 2 shows internal forces arising in the shear wall segment according to so-called simple shear-wall theory (Stewart 1987). There are axial forces along the edges of sheathing panel, which are induced by the racking load and are transferred by sheathing fasteners to the studs. In Figure 6. 2, the right chord is in

tension, which is the maximum at the bottom and zero at the top due to the action of the sheathing fasteners. The left chord is under compression at the bottom, which decreases to zero at the top. The maximum values of the axial forces in the chords equal the reactions in the anchors.

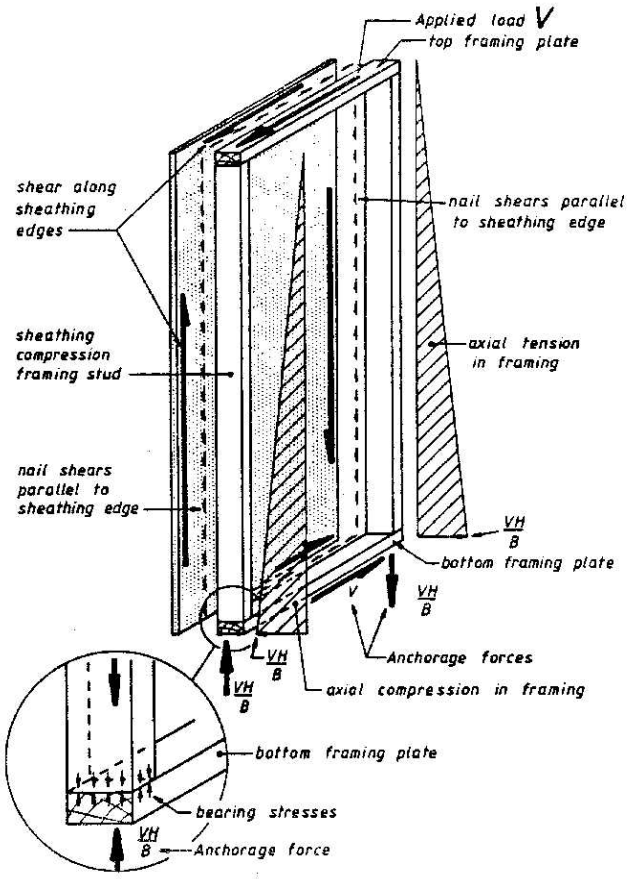

Figure 6. 2. Forces in shear wall segment (Stewart 1987).

During the last twenty-five years, many shear wall models have been developed describing the shear wall response in more detail. There are two basic categories of models used most often: models that allow closed-form solutions and finite element models. Closed-form models are simplistic: they describe overall response of a structure of a given configuration without a detailed analysis of its components. On the other hand, finite element models are complicated and versatile. They are capable of producing detailed analysis of any structure as long as components and connections are defined appropriately. Another tool used for prediction of shear wall performance involves empirical equations based on experiments. Such an approach is regarded as a

method rather than a model because it is limited to testing procedures and conditions used to derive them.

6.3 Closed-Form Models

Closed-form models are usually based on energy methods or strain-displacement relationships, which are relatively easy to solve. Since the models are derived for certain wall configurations, they correspond well with experimental results, which reproduce the assumed conditions. Several models most often cited in literature are presented below.

Tuomi and McCutcheon (1978) proposed an equation for predicting the response of a single-panel nailed wall assuming a parallelogram distortion of the frame. The strength equation was derived assuming all external energy from applied force being absorbed by sheathing nails around the perimeter of the wall. In this model, diagonals of the deformed frame coincide with the diagonals of the sheathing. Individual nails deform linearly following a certain load-distortion ratio; deformations are small; the strain energy of the nails equals a sum of the energy absorbed by each nail. Robertson (1980) argued that the model contradicted experimental results if a wall consisted of several panels. The nail movement pattern and unit racking resistance depend on many factors including length of the wall, presence of openings, varying nail spacing, vertical load, etc., which were not considered in the model (Robertson, 1980).

Another shear wall model was proposed by Easley *et al.* (1982). The closed-form equation was derived from a force and moment equilibrium for a particular panel. It was assumed that the sheathing only distorts relative to top and bottom plates, while the studs remain parallel to the panel edges. The wall is simply supported and the nail forces consist of vertical and horizontal components. The vertical nail force component is proportional to the distance from the vertical centerline of the panel. The force-slip relationship is linear. The model predicted experimental results of 2.4×3.7 m (8×12 ft.) walls under monotonic loading with reasonable accuracy, but Gupta and Kuo (1985) indicated that the model underestimated the overall stiffness.

A model proposed by Gupta and Kuo (1985) was based on the strain energy calculation, which included terms of elastic bending of studs and shear energy of

sheathing. Eliminating some assumptions and introducing additional unknowns, the authors were aiming at higher accuracy of the model, which would still produce a closed-form solution through an iterative process. They found that the bending stiffness of the studs and the shear stiffness of the sheathing did not contribute significantly to the load-deformation properties of shear walls. Later, Gupta and Kuo (1987) modified their model by taking into account stud and sheathing uplift. They verified the model applying it to test data from literature and found that vertical load and uplift restraint provide significant increase to the wall stiffness.

In 1985, McCutcheon revised his model by introducing a non-linear nail load-slip behavior and deformation of sheathing. First, he fit a power function to the test data of small-scale walls (McCutcheon 1985). Later, Patton-Mallory and McCutcheon (1987) applied four types of curves to fit the load-slip of nails and substituted each one in the racking resistance equation. An asymptotic curve was concluded the best to describe the nail behavior until the maximum load. Tests of two hundred small-scale walls proved the possibility of predicting the racking performance of walls sheathed on both sides with different materials by applying the equation to each side. However, the model still did not account for the uplift. The model was not validated through full-scale shear wall tests and reverse cyclic loading.

Stewart (1987) developed several models predicting the response of timber shear walls to static and dynamic loading. An elastic shear wall model was used to predict the wall stiffness, framing joint forces, and sheathing stresses in the elastic range (design level). An ultimate strength shear wall model was used to predict wall strength, the framing joint forces, framing stresses, and the sheathing stresses occurring at the ultimate strength of the wall. The proposed models verified that wall strength and stiffness were primarily governed by the load-slip characteristics of sheathing connections and their spacing. The bending of the studs and separation of the framing joints demonstrated little influence on the stiffness and strength of the wall. The strength of long walls was approximately proportional to wall length (Stewart 1987).

Murakami et al. (1999) proposed simple formulae to predict nonlinear performance of single-panel walls with any nailing arrangement pattern and any size of

sheathing panel. The method is based on the equilibrium of the internal moment of the sheathing nails and the external moment from the racking force. The nail load-slip relationship is approximated by bilinear elastic-plastic curve. The moment at yield threshold is found easily as a function of the yield strength of nails and their arrangement pattern. The inelastic calculation required iterative solution. The authors solved numerically 759 models with various nailing patterns and panel sizes to carry out the regression analysis. They formulated the approximate closed-form equations to calculate the applied inelastic moment as a function of rotation angles and the moments at the yield threshold (R_y, M_y) and at the plastic threshold (R_p, M_p). Comparisons with the experimental results showed satisfactory accuracy of the approximate formulae.

The advantage of the closed-form models is their simplicity. Based on simple assumptions and straightforward calculations, the models produce results of reasonable accuracy. However, all of the proposed models are valid only for fully-anchored shear walls with symmetric placement of anchors. Therefore, the symmetric actions and the distortion pattern around the center of the sheathing panel are assumed. These assumptions become invalid when analyzing shear walls without hold-down restraint. New assumptions and new models should be proposed for non-anchored walls, because their response is not symmetric.

6.4 Finite Element Models

Independently from the closed-form models, a number of finite element models were developed during the last two decades. The benefit of the finite element method is that it provides detailed information on performance of various components of the structure. However, the more information wanted, the higher the degree of sophistication needed for the analysis. Discretization should be balanced between accuracy and computational efficiency. Today, computers are powerful enough to allow analysis of problems with large number of equations, but it takes special training to formulate and apply such models in everyday design.

Foschi (1977) developed one of the first finite-element models for static analysis of light-frame shear walls. The non-linear model contained four components:

1) sheathing panels represented by linear-elastic orthotropic plane stress element; 2) framing members represented by linear beam elements; 3) connections between frame members represented by three-degree-of freedom spring elements; and 4) connection between sheathing and framing represented by two-degree-of-freedom spring element. The load-slip relationship for the connections was represented by an exponential function, which reproduced the non-linear behavior observed in the connection tests. It was found that almost all of the non-linearity in shear wall performance was due to the non-linear behavior of connections between sheathing and framing.

Subsequently, other researchers proposed a number of models. Finite elements representing sheathing and connections were modified in different ways. Among these are models proposed by Itani and Cheung (1984), Gutkowski and Castillo (1988), Falk and Itani (1989). None of these models accounted for cyclic or dynamic response of shear walls.

Dolan (1989) extended the formulation of the model presented by Foschi (1977) to predict the dynamic response of walls to earthquakes and implemented the model in two finite element programs (SHWALL and DYNWALL). He modified the model by adding out-of-plane degrees of freedom to the plate element and sheathing connector, introducing the modified load-displacement curve for the connector, which included hysteretic behavior. Also, a bilinear sheathing bearing connector was included by Dolan to model the bearing effects between adjacent sheathing panels. Both programs (static and dynamic) allowed predicting the ultimate load capacity of shear walls without limitations to wall configurations but of limited size due to memory limitations on the computers of that time.

After the model was examined and verified by an extensive experimental program, Dolan (1989) concluded that it could be simplified and improved by eliminating variables, which were of minor significance, and by adding ability to calculate member forces in the program. White (1995) implemented the modifications in his program WALSEIZ. He verified and validated the model using experimental results obtained earlier by Dolan (1989).

The major modification made by White (1995) to Dolan's model was reduction of the degrees-of-freedom (DOF) of the sheathing element, which in turn reduced the DOF associated with the connector and bearing elements. This was done based on Dolan's (1989) conclusion that out-of-plane deflections of the sheathing are not significant when the sheathing thickness is 9.5 mm (3/8 in.) or greater and stud spacing is no more than 610 mm (24 in.). This change significantly reduced the computation time and made possible a larger wall size to be analyzed. Another modification enabled computation of forces and stresses in framing and sheathing elements at any time during analysis. The framing-to-framing connectors were replaced by hinges. This is a more accurate and conservative way to represent connections between studs and horizontal members, because they act more like pins than rigid connections in shear walls. Some procedures in the program were modified to enhance its efficiency.

After the modifications, WALSEIZ attained the capability to analyze shear walls up to 4.9×12.2 m (16×40 ft.) in size, calculate actions and stresses and determine their extreme magnitudes for all nodes and elements. White (1995) performed a parametric study in order to determine the effects of aspect ratio and openings on the response of shear walls subjected to monotonic or dynamic loads. Twenty-five shear wall models with or without openings were analyzed using the WALSEIZ.

None of the described studies included the effects of various overturning restraints. Anchorage conditions used in the standard testing procedures for single shear walls were simulated. In the models, the anchorage connections were assumed rigid, with no vertical displacements. As indicated in Chapter 2, real-world situations present a variety of restraint conditions that affect performance of shear walls in various ways depending on the length of the wall and amount of openings in it. The validity of a model is limited if these conditions are ignored. In order to study the effect of hold-down restraint on shear wall response, the modifications to shear wall mechanical model have been proposed in the next section.

6.5 Shear Wall Strength Models without Tie-Down Anchors

6.5.1 Introduction

As is shown in Section 6.2 and assumed in more sophisticated models, reactions in shear walls with tie-down anchors act along the chords as in a vertical cantilever I-beam. The shear wall action changes when it is not anchored at the end studs. It depends on the amount of dead load applied to the wall. Modifications of the simple mechanical model for shear walls without tie-down anchors are described in this section. Some of the assumptions for the model development were discussed with Mr. Phillip Line (2000) prior to implementation.

The following sections present a step-by-step derivation of the mechanical model of a shear wall without tie-down anchors, beginning with the elastic model of a single-panel segment without dead load. Then, an ultimate strength model of a single-panel segment is introduced. Although the simple shear wall theory neglects shear forces in the chords, each section presents the comparison with the wall model that accounts for the shear forces.

The assumptions used in the derivation of the single-panel elastic model can be applied in the elastic analysis of multiple-panel shear walls. Results can be easily obtained using commercial software. The examples of the elastic solutions obtained using the finite-element program SAP 2000 are presented in Section 6.5.4. These results are used in Section 6.6 for calculation of shear wall deflections.

Section 6.5.5 starts with the derivation of the ultimate strength models for multi-panel shear walls assuming shear forces in the chords and uneven distribution of forces along the bottom plate. Then, to simplify the model, these assumptions are eliminated, and the model is shown to be sufficiently accurate. The simple ultimate strength model is of interest for designers, because it allows designing the shear walls with a hand calculator or spreadsheet. In the end of the section, it is shown how the effect of dead load on the shear wall resistance can be estimated using the strength model.

6.5.2 Shear Wall Segment without Dead Load. Elastic Model

Consider a shear wall segment consisting of one panel attached to the base at the bottom plate with shear bolts or with adequate nailing to prevent the wall overturning. Assuming rigid top and bottom plates, the applied lateral load and the horizontal reaction, v, are uniformly distributed along the plates as is shown in Figure 6. 3a, and the exact placement of the shear connectors is not important for the analysis. The wall, with the height-to-length aspect ratio $\alpha = H / B$, resists an overturning moment:

$$M = BHv = \alpha B^2 v \tag{6.1}$$

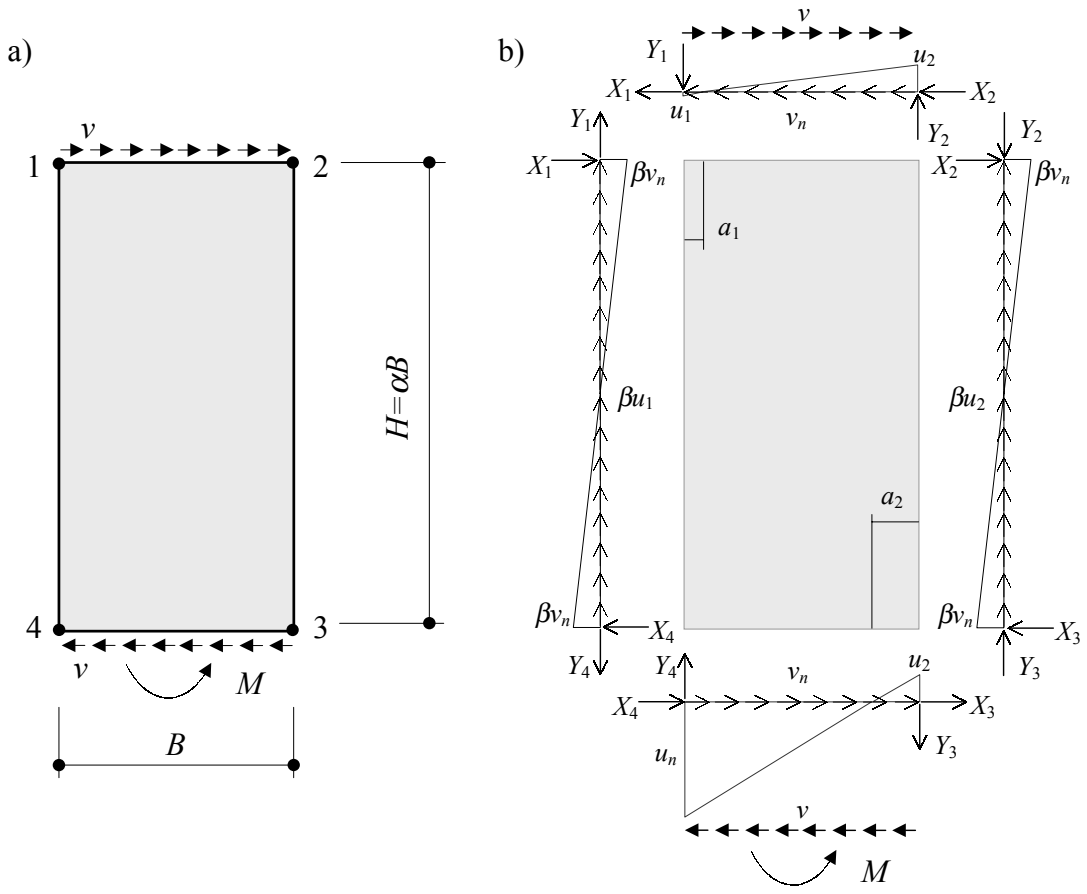

Figure 6. 3. Elastic model of unrestrained shear wall segment with rigid chords.

a) External equilibrium, b) Internal equilibrium.

In the absence of tie-down anchors or dead load, the overturning moment applied at the bottom plate is transferred to the wall via the framing fasteners and sheathing-to-

framing attachment. Effective withdrawal resistance of framing nails driven into the end grain of the studs is negligible. Therefore, it is safe to assume the vertical tension forces at the framing joints equal zero. For example, shown in Figure 6. 3b, the joint force $Y_4 = 0$.

The shear force resisted by the individual sheathing fastener can be represented by two orthogonal components:

$$F_n = \sqrt{F_{nx}^2 + F_{ny}^2} \tag{6.2}$$

Similarly, the shear resistance of the row of sheathing fasteners can be expressed as follows:

$$v_{\max} = \sqrt{v_n^2 + u_n^2} \tag{6.3}$$

The relationship between the resistance of a single fastener, F_n, and the resistance of the row of fasteners depends on the fastener spacing, s. Often, the shear resistance is determined as $v_n = F_n / s$. This approximation can introduce significant errors in the analysis, especially when the spacing is large. For example, the shear strength of the row of fasteners along the 1.2-m (4-ft.) panel with 150-mm (6-in.) spacing would be estimated as $Bv_n = BF_n / s = 8F_n$, while in fact it is $9F_n$ (i.e., 12.5% higher). To minimize the errors during the transition from the strength of the individual fastener to the strength of the row, the following relationship is proposed. Assume for the plates:

$$v_n = \frac{F_n n_p}{B} \tag{6.4}$$

where, $n_p = \frac{B}{s} + 1$, the number of fasteners along the top plate.

For the chords:

$$v_{nc} = \frac{F_n n_c}{\alpha B} \tag{6.5}$$

where, $n_c = \frac{\alpha B}{s} + 1$, the number of fasteners along the chord.

Then, the relationship between v_n and v_{nc}:

$$\beta = \frac{v_{nc}}{v_n} = \frac{\alpha B + s}{\alpha(B + s)} \tag{6.6}$$

Shear resistance of the wall as a function of the shear resistance of the sheathing fasteners can be determined from the static equilibrium of the framing members and the sheathing panel. Two approaches are shown in the further analysis: 1) the chords are assumed rigid (i.e., resisting axial and shear forces) and 2) the chords are assumed non-rigid (i.e., resist only axial forces).

6.5.2.1 Elastic Model with Rigid Chords

Assume rigid chords that allow developing the orthogonal components in resistance of the sheathing fasteners. The free body diagrams of the framing elements are shown in Figure 6. 3b. The forces along the sheathing edges are equal and opposite of the forces in the framing members and are not shown.

The following equations determine the static equilibrium of the system:

Left chord:

$$X_1 - X_4 = 0 \tag{6.7}$$

$$Y_1 + (\alpha B - 2s) \cdot \beta u_1 - Y_4 = 0 \tag{6.8}$$

$$\alpha B X_4 - \frac{(\alpha B)^2}{6} \cdot \beta v_n = 0 \tag{6.9}$$

Right chord:

$$X_2 - X_3 = 0 \tag{6.10}$$

$$Y_3 - (\alpha B - 2s) \cdot \beta u_2 - Y_2 = 0 \tag{6.11}$$

$$\alpha B X_2 - \frac{(\alpha B)^2}{6} \cdot \beta v_n = 0 \tag{6.12}$$

Top plate:

$$Bv - X_1 - X_2 - (B - 2s)v_n = 0 \tag{6.13}$$

$$Y_2 - Y_1 + \frac{a_1}{2}u_1 - \frac{B - a_1}{2} \cdot u_2 = 0 \tag{6.14}$$

$$-BY_1 + \frac{a_1}{2}\left(B - \frac{a_1}{3}\right) \cdot u_1 - \frac{(B - a_1)^2}{6} \cdot u_2 = 0 \tag{6.15}$$

Bottom plate:

$$X_4 + X_3 + (B - 2s)v_n - Bv = 0 \tag{6.16}$$

$$Y_4 - Y_3 + \frac{B - a_2}{2} \cdot u_n - \frac{a_2}{2}u_2 = 0 \tag{6.17}$$

$$BY_4 + \frac{B - a_2}{2}\left(B - \frac{B - a_2}{3}\right) \cdot u_n - \frac{a_2^2}{6} \cdot u_2 - M = 0 \tag{6.18}$$

Distances a_1 and a_2 are determined from the following ratios:

$$u_2 = \frac{B - a_1}{a_1} \cdot u_1 \tag{6.19}$$

$$u_n = \frac{B - a_2}{a_2} \cdot u_2 \tag{6.20}$$

Setting the joint force $Y_4 = 0$ and using Equation (6.1), the system of Equations (6.7) - (6.20) is solved. Results are shown in Table 6. 1 for the standard aspect ratio $\alpha = 2$ and for various spacing of sheathing fasteners. The last column shows the solution if the spacing s is ignored (i.e., the corner nails are counted twice). The last row in Table 6. 1 shows the reduction factor r, which reflects the ratio of the shear wall resistance to the resistance of the sheathing fasteners:

$$r = \frac{v}{v_{\max}} \tag{6.21}$$

Table 6. 1. Elastic response of unrestrained single-panel shear wall with rigid chords.

Parameters[1)]	Spacing of sheathing fasteners, s			
	$s = B / 8$	$s = B / 12$	$s = B / 16$	$s = 0$ (ignored)
a_1 / B	0.077	0.074	0.074	0.067
a_2 / B	0.168	0.162	0.159	0.151
u_1 / v_n	0.156	0.151	0.148	0.139
u_2 / v_n	1.863	1.896	1.910	1.944
$c = u_n / v_n$	9.209	9.794	10.088	10.972
X / Bv_n	0.315	0.321	0.324	0.333
Y_1 / Bv_n	-0.258	-0.266	-0.269	-0.278
Y_2 / Bv_n	0.595	0.607	0.612	0.625
Y_3 / Bv_n	3.673	3.949	4.089	4.514
v / v_n	1.380	1.474	1.522	1.667
v_n / v_{max}	0.108	0.102	0.099	0.091
$r = v / v_{max}$	0.149	0.150	0.150	0.151

[1)] $\alpha = 2$

It can be seen from Table 6. 1 that the elastic resistance of the single-panel shear wall is only 15% of the sheathing connections' resistance. Note that the reduction factor similarly calculated for the wall with tie-down anchors equals 0.956. Therefore, it can be concluded that the elastic resistance of an unrestrained shear wall is less than 16% of the elastic resistance of anchored shear wall.

To verify the proposed method of calculating the shear resistance of the row of fasteners, the elastic analysis was performed using the commercial finite element program SAP 2000 for the spacing s = 150 mm (6 in.). In the finite element model, the same assumptions were used: pin-connected framing members, rigid sheathing and rigid framing members connected with elastic link elements, and the axial release in the left chord at joint 4. Table 6. 2 shows the comparison between the proposed method and the finite element analysis.

The most important fact in Table 6. 2 is more accurate prediction of the ratio c, using the proposed method. It is shown later that the ratio determines the shear wall resistance and the distribution of forces in the rest of the wall.

Table 6. 2. Comparison with finite element analysis[1)].

Parameters[1)]	Proposed	SAP 2000	Proposed / SAP 2000	*s* ignored	*s* ignored / SAP 2000
a_1 / B	0.077	0.067	115%	0.067	99%
a_2 / B	0.168	0.166	101%	0.151	91%
u_1 / v_n	0.156	0.131	119%	0.139	106%
u_2 / v_n	1.863	1.820	102%	1.944	107%
$c = u_n / v_n$	9.209	9.131	101%	10.972	120%
v / v_n	1.380	1.485	93%	1.667	112%
$v_n / v_{\max}$	0.108	0.109	99%	0.091	83%
$r = v / v_{\max}$	0.149	0.161	93%	0.151	94%

[1)] $s = B/8$, $\alpha = 2$

Although the reduction factors, *r*, have similar values in both methods, the calculation of the wall resistance can yield different results during transition from the resistance of the individual fasteners. From Equation (6.4), the shear wall resistance is expressed via the strength of the individual fastener and the reduction factor as follows:

$$v = \frac{rF_n}{B}\left(\frac{B}{s}+1\right) \tag{6.22}$$

As was mentioned in the beginning of the section, if the number of fasteners is determined as B/s, the wall resistance will be underestimated up to 12.5%.

6.5.2.2 Elastic Model with Non-Rigid Chords

Derivation of the elastic resistance of an unrestrained shear wall can be simplified assuming that the chords resist only axial forces. Then, the shear resistance of the wall, *v*, equals the horizontal resistance of the sheathing-to-framing connections along the plates, v_n. The free body diagram of the system is shown in Figure 6. 4. The forces along the sheathing edges are equal and opposite of the forces in the framing members and are not shown.

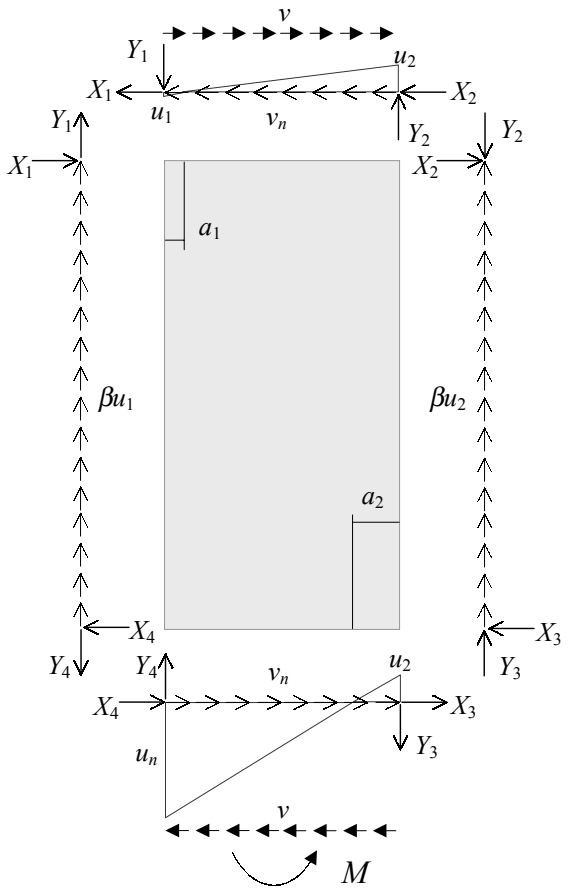

Figure 6. 4. Elastic model of unrestrained shear wall segment with non-rigid chords.

The static equilibrium of the framing members is determined as follows:

Left chord:

$$Y_1 + (\alpha B - 2s)\cdot \beta u_1 - Y_4 = 0 \tag{6.23}$$

Right chord:

$$Y_3 - (\alpha B - 2s)\cdot \beta u_2 - Y_2 = 0 \tag{6.24}$$

Top plate:

$$Bv - Bv_n = 0 \tag{6.25}$$

$$Y_2 - Y_1 + \frac{a_1}{2}u_1 - \frac{B - a_1}{2}\cdot u_2 = 0 \tag{6.26}$$

$$-BY_1 + \frac{a_1}{2}\left(B - \frac{a_1}{3}\right)\cdot u_1 - \frac{(B-a_1)^2}{6}\cdot u_2 = 0 \tag{6.27}$$

Bottom plate:

$$Y_4 - Y_3 + \frac{B-a_2}{2}\cdot u_n - \frac{a_2}{2}u_2 = 0 \tag{6.28}$$

$$BY_4 + \frac{B-a_2}{2}\left(B - \frac{B-a_2}{3}\right)\cdot u_n - \frac{a_2^2}{6}\cdot u_2 - M = 0 \tag{6.29}$$

Distances a_1 and a_2 are determined from Equations (6.19) and (6.20). Setting the joint force $Y_4 = 0$ and using Equation (6.1), the system of Equations (6.23) - (6.29) is solved. Results are shown in Table 6. 3 for the standard aspect ratio $\alpha = 2$ and for various spacing of sheathing fasteners.

In the simplified method, the reduction factor can be derived from Equation (6.3), setting $v_n = v$:

$$r = \frac{v}{v_{\max}} = \frac{1}{\sqrt{1+c^2}} \tag{6.30}$$

where, $c = \frac{u_n}{v_n}$, the ratio of the orthogonal components of the fasteners' resistance.

Table 6. 3. Elastic response of unrestrained single-panel shear wall with non-rigid chords.

Parameters	Spacing of sheathing fasteners, *s*			
	s = B/8	*s* = B/12	*s* = B/16	*s* = 0 (ignored)
a_1 / B	0.077	0.074	0.072	0.067
a_2 / B	0.168	0.162	0.159	0.151
u_1 / v_n	0.113	0.102	0.097	0.083
u_2 / v_n	1.350	1.286	1.255	1.167
$c = u_n / v_n$	6.675	6.643	6.628	6.583
Y_1 / Bv_n	-0.187	-0.180	-0.177	-0.167
Y_2 / Bv_n	0.431	0.412	0.402	0.375
Y_3 / Bv_n	2.662	2.679	2.686	2.708
$r = v / v_{\max}$	0.148	0.149	0.149	0.150

[1)] $\alpha = 2$.

Comparison of the reduction factors in Table 6. 1 and Table 6. 3 shows that there is no practical difference between the shear wall resistance determined by either method. Therefore, the simplified method can be used conservatively in design.

Note that in both cases, the left chord experiences slight compression at the top due to the work of sheathing fasteners. Recall that in fully-anchored walls, this chord is completely in tension (Figure 6. 2).

Two important results of the elastic analysis are related to the ratio c. The large ratio between the vertical and the horizontal components of the fastener resistance at the bottom plate indicates that the fasteners work predominantly perpendicular-to-grain and that they will yield first. The other fasteners are significantly under-loaded, and they will likely remain elastic. These conclusions lead to the assumptions used for derivation of the plastic model described in the next section.

6.5.3 Shear Wall Segment without Dead Load. Ultimate Strength Model

From the elastic analysis shown in the previous section, it can be assumed that the strength limit state occurs in the unrestrained shear wall when the sheathing fasteners along the bottom plate develop their ultimate capacity. Other fasteners along the perimeter are assumed to remain elastic. Therefore, the same assumptions used in the elastic model are valid with the exception of the shear force (u_n) distribution along the bottom plate. These assumptions are supported by experimental results.

During the tests (Section 5.7), single-panel shear walls developed the ultimate strength at deflections between 28 and 39 mm (1.10 and 1.55 in.). The measured nail-slip along the bottom plate at peak loads did not exceed 15 mm (0.6 in.) as can be seen in Figures 04IAm1-d and 04IAm2-d in Appendix. From the tests on the sheathing-to-framing connections (Section 4.5), it follows that the fasteners along the bottom plate at these deflections work in the plastic region shown in Figure 4. 11. Therefore, it is assumed that with the plastic yielding of the fasteners, the force distribution changes as is shown in Figure 6. 5 while the distance a_2 decreases.

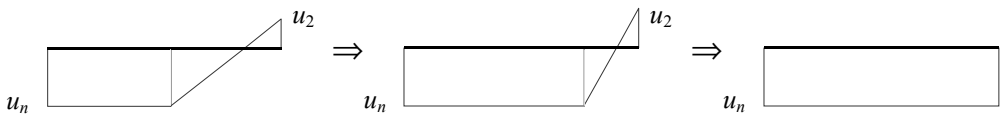

Figure 6. 5. Plastic yielding of fasteners along the bottom plate.

Solution of the equilibrium shows that at the ultimate limit state the distance $a_2 = 0$. Therefore, in the ultimate strength model, u_n is considered uniformly distributed along the length of the panel. Similar to the elastic models, consider two cases: 1) rigid chords resisting axial and shear forces and 2) non-rigid chords resisting only axial forces.

6.5.3.1 Ultimate Strength Model with Rigid Chords

The free body diagram of the system with the rigid chords at the strength limit state is shown in Figure 6. 6. The static equilibrium of the chords and the top plate is described by Equations (6.5) through (6.15). The equilibrium equations of the bottom plate change as follows:

$$X_4 + X_3 + (B - 2s)v_n - Bv = 0 \tag{6.31}$$

$$Y_4 - Y_3 + Bu_2 = 0 \tag{6.32}$$

$$BY_4 + \frac{B^2}{2} \cdot u_n - M = 0 \tag{6.33}$$

Substituting the moment from Equation (6.1), the distance a_1 from the Equation (6.19), and setting the joint force $Y_4 = 0$, the equilibrium is solved. Results are shown in Table 6. 4 for the standard aspect ratio $\alpha = 2$ and for various spacing of sheathing fasteners.

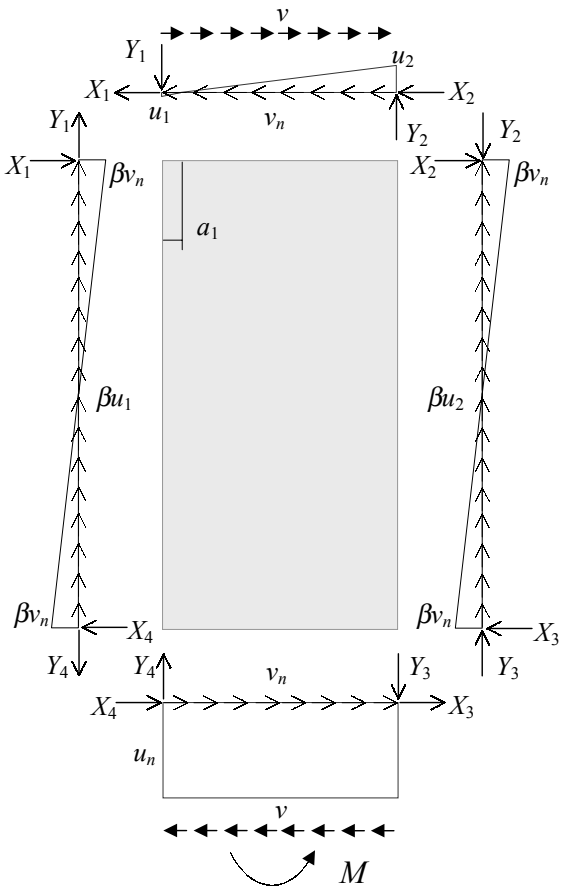

Figure 6. 6. Ultimate strength model of unrestrained shear wall with rigid chords.

Table 6. 4. Plastic response of unrestrained single-panel shear wall with rigid chords.

Parameters[1)]	Spacing of sheathing fasteners, s			
	$s = B / 8$	$s = B / 12$	$s = B / 16$	$s = 0$ (ignored)
a_1 / B	0.077	0.074	0.072	0.067
u_1 / v_n	0.235	0.225	0.220	0.205
u_2 / v_n	2.798	2.831	2.845	2.872
$c = u_n / v_n$	5.519	5.897	6.088	6.667
X / Bv_n	0.315	0.321	0.324	0.333
Y_1 / Bv_n	-0.388	-0.397	-0.401	-0.410
Y_2 / Bv_n	0.894	0.906	0.911	0.923
Y_3 / Bv_n	5.519	5.897	6.088	6.667
v / v_n	1.380	1.474	1.522	1.667
v_n / v_{max}	0.178	0.167	0.162	0.148
$r = v / v_{max}$	0.246	0.246	0.247	0.247

[1)] $\alpha = 2$.

The reduction factor in Table 6. 4 indicates that the strength of the wall is approximately 25% or the sheathing fasteners' strength, which agrees with the test results (Chapter 5) very closely.

Because forces in the chords are assumed elastic, the ratio v / v_n remains the same as in the elastic model (i.e., the contribution of the shear components in the chords does not change). This result can be used for further simplification of the model.

6.5.3.2 Ultimate Strength Model with Non-Rigid Chords

To simplify the derivation of the ultimate strength of unrestrained shear wall, assume that the chords resist only axial forces. Then, the shear resistance of the wall, v, equals the horizontal resistance of the sheathing connections along the plates, v_n. The free body diagram of the system is shown in Figure 6. 7.

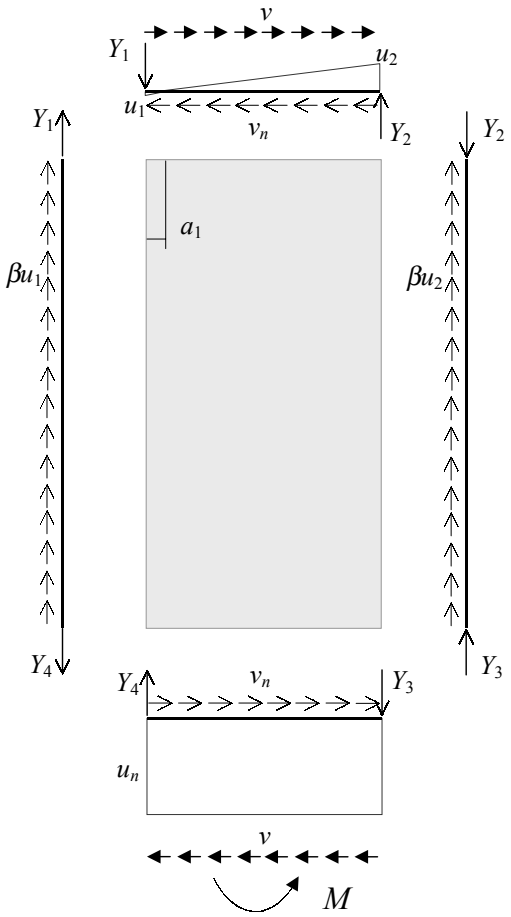

Figure 6. 7. Ultimate strength model of unrestrained shear wall with non-rigid chords.

Equations (6.23) through (6.27) describe the static equilibrium of the chords and the top plate without changes. However, the shear wall strength can be easily determined from the equilibrium of the bottom plate only:

$$BY_4 + \frac{B^2}{2} \cdot u_n - M = 0 \tag{6.34}$$

Assuming $Y_4 = 0$ and the moment from Equation (6.1), the ratio c becomes:

$$c = \frac{u_n}{v_n} = \frac{u_n}{v} = 2\alpha \tag{6.35}$$

According to Equation (6.30), the reduction factor becomes:

$$r = \frac{v}{v_{\max}} = \frac{1}{\sqrt{1+4\alpha^2}} \tag{6.36}$$

Equation (6.36) is a simple and conservative way of estimating the shear capacity of a single-panel shear wall of any size. For example, if $\alpha = 2$, $r = \frac{1}{\sqrt{17}} = 0.243$.

Other parameters of the shear wall at the strength limit state are found by solving the static equilibrium equations. Results for the standard aspect ratio $\alpha = 2$ and for various spacing of sheathing fasteners are shown in Table 6. 5.

Table 6. 5. Plastic response of unrestrained single-panel shear wall with rigid chords.

Parameters	Spacing of sheathing fasteners, s			
	s = B/16	s = B/12	s = B/8	s = 0 (ignored)
a_1 / B	0.077	0.074	0.072	0.067
u_1 / v_n	0.170	0.153	0.145	0.123
u_2 / v_n	2.028	1.920	1.869	1.723
$c = u_n / v_n$	4.000	4.000	4.000	4.000
Y_1 / Bv_n	-0.281	-0.269	-0.263	-0.246
Y_2 / Bv_n	0.648	0.615	0.599	0.554
Y_3 / Bv_n	4.000	4.000	4.000	4.000
$r = v / v_{\max}$	0.243	0.243	0.243	0.243

[1)] $\alpha = 2$.

6.5.4 Multiple-Panel Shear Wall without Dead Load - Elastic Response

The assumptions discussed in Section 6.5.2 were applied in the elastic analysis of multiple-panel shear walls using commercial finite-element program SAP 2000. This section presents examples of the shear walls representative of the specimens described in Chapters 3 and 5. Shear walls composed of two, three, and four panels with aspect ratio $\alpha = 2$ and spacing of sheathing fasteners $s = B/8$ were analyzed. The stiffness of the sheathing panel and the framing elements were taken sufficiently high to represent an infinite shear rigidity. Sheathing connections were modeled using the elastic link elements with the stiffness taken from the test results (Chapter 4). Framing elements were pin-connected and the axial releases were placed at the bottom of each stud except for the compression (right) chord.

Two cases were analyzed for each wall configuration: 1) assuming rigid studs, when the moment releases were placed only at the ends of the studs, and 2) assuming non-rigid studs, when the moment releases were placed at the ends of each finite element of the studs. The length of the elements was equal the spacing of the sheathing connectors.

Figure 6. 8 through Figure 6. 10 and Table 6. 6 through Table 6. 11 illustrate the distribution of forces among the sheathing connectors in each panel. The following conclusions can be made from the results of the elastic analysis:

1) Unlike anchored shear walls, the resistance of multiple-panel unrestrained walls is not proportional to the resistance of the single panel. Resistance of a two-panel wall is 66% higher than the resistance of two single panel walls. Resistance of a three-panel wall is 211% higher than the resistance of three single panel walls. Resistance of a four-panel wall is 240% higher than the resistance of four single panel walls. This conclusion is in full agreement with the experimental results.
2) Similar to the single-panel wall, the sheathing connections along the bottom plate in each panel are overloaded relative to the connections along the studs and the top plates. This allows extending the ultimate strength model of the

single-panel wall onto the multi-panel walls assuming the yielding of fasteners along the bottom plate only.

3) The distribution of forces (v_{ni}) along the plates in multi-panel walls is not uniform. The longer the wall, the higher the variation. In a two-panel wall, the difference is less than 4%. In a three-panel wall the variation exceeds 10%, and in a four-panel wall the difference in the forces between the first and the fourth panels reaches 20%.
4) With increasing number of panels, the pivot point of the panel (distance a_i) shifts towards the center of the panel. In the fourth panel, it almost reaches the middle, so that the panel rotates symmetrically. That means that the fourth panel acts like a fully-restrained wall, developing its maximum available capacity.

Analysis results given in this section can serve to estimate design shear strength for unrestrained walls of n panels as a fraction of the design strength of fully-restrained shear walls of the same size. If design shear strength of a fully-restrained wall, based on the elastic response, equals v_{design}, then shear strength of single-panel wall is 0.15 v_{design}, two-panel wall – 0.27 v_{design}, three-panel wall – 0.34 v_{design}, and four-panel wall – 0.39 v_{design}, assuming rigid chords.

If the fourth panel in unrestrained wall acts similar to a fully-restrained wall in the elastic range, it is assumed that the plastic performance and failure modes are also similar. Therefore, the next section provides the derivation of the ultimate strength model for two-and three-panel unrestrained shear walls only.

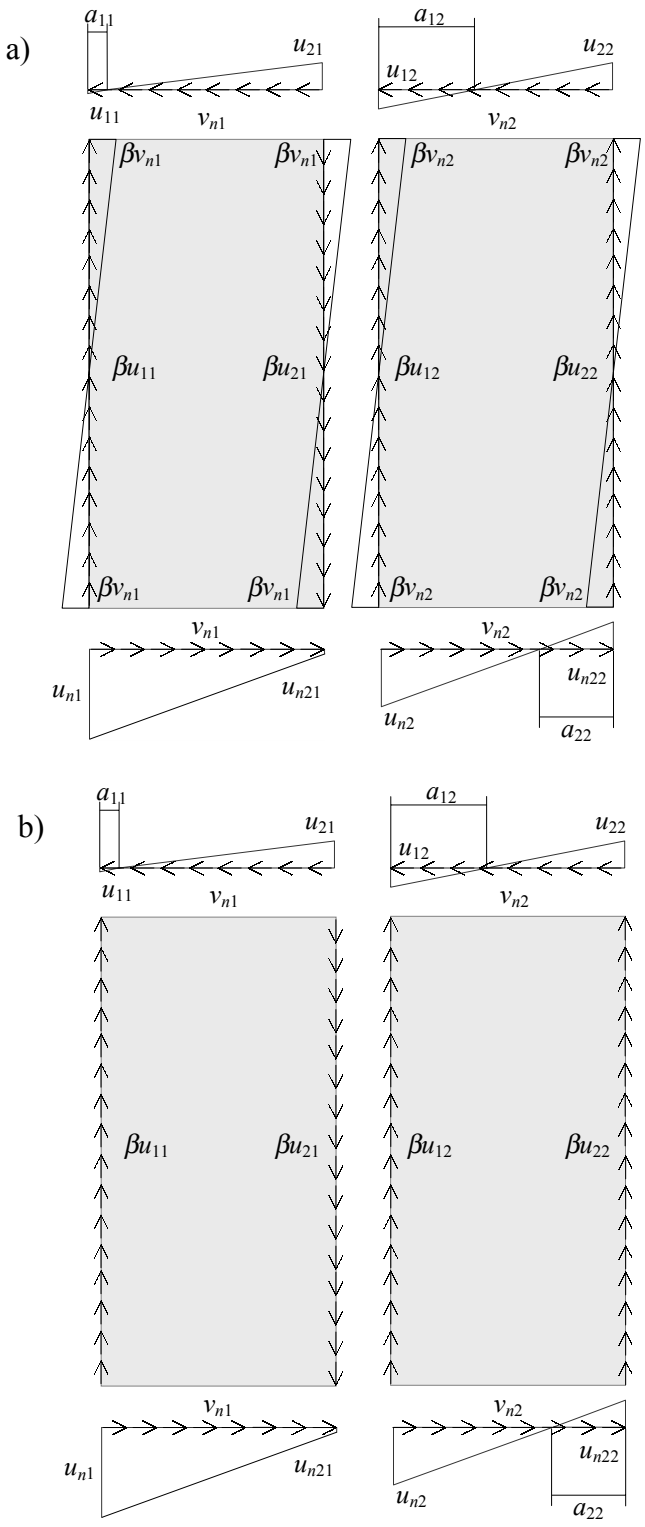

Figure 6. 8. Elastic response of unrestrained two-panel shear wall:
a) Rigid chords, b) Non-rigid chords.

Table 6. 6. Elastic response of unrestrained two-panel shear wall. Rigid chords[1)].

Panel 1		Panel 2	
a_{11} / B	0.233	a_{21} / B	0.417
		a_{22} / B	0.310
v / v_{n1}	1.513	v_{n2} / v_{n1}	1.037
u_{11} / v_{n1}	0.603	u_{12} / v_{n1}	1.133
u_{21} / v_{n1}	1.990	u_{22} / v_{n1}	1.584
u_{n21} / v_{n1}	0.411	u_{n22} / v_{n1}	1.584
$c_1 = u_{n1} / v_{n1}$	5.579	u_{n2} / v_{n1}	3.534
$v_{n1} / v_{\max}$	0.176	$v_{n2} / v_{\max}$	0.183
$r_1 = v / v_{\max}$	0.267		

[1)] $s = B/8$, $\alpha = 2$

Table 6. 7. Elastic response of unrestrained two-panel shear wall. Non-rigid chords[1)].

Panel 1		Panel 2	
a_{11} / B	0.233	a_{21} / B	0.417
		a_{22} / B	0.309
v / v_{n1}	1.014	v_{n2} / v_{n1}	1.029
u_{11} / v_{n1}	0.405	u_{12} / v_{n1}	0.759
u_{21} / v_{n1}	1.335	u_{22} / v_{n1}	1.061
u_{n21} / v_{n1}	0.275	u_{n22} / v_{n1}	1.062
$c_1 = u_{n1} / v_{n1}$	3.742	u_{n2} / v_{n1}	2.369
$v_{n1} / v_{\max}$	0.258	$v_{n2} / v_{\max}$	0.266
$r_1 = v / v_{\max}$	0.262		

[1)] $s = B/8$, $\alpha = 2$

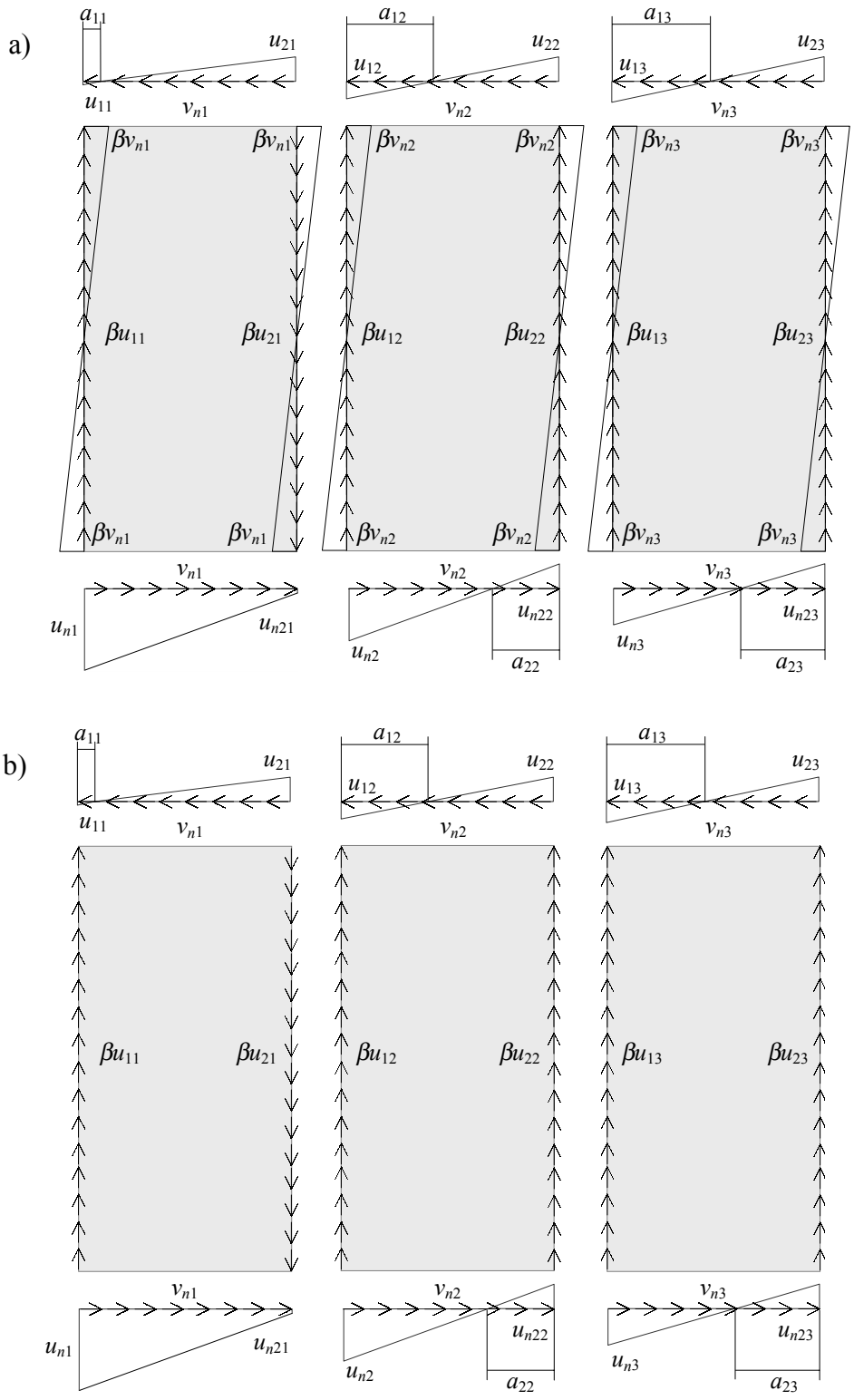

Figure 6. 9. Elastic response of unrestrained three-panel shear wall:
a) Rigid chords, b) Non-rigid chords.

Table 6. 8. Elastic response of unrestrained three-panel shear wall. Rigid chords[1)].

Panel 1		Panel 2		Panel 3	
a_{11} / B	0.294	a_{21} / B	0.395	a_{31} / B	0.470
		a_{22} / B	0.186	a_{32} / B	0.401
v / v_{n1}	1.572	v_{n2} / v_{n1}	1.062	v_{n3} / v_{n1}	1.114
u_{11} / v_{n1}	0.794	u_{12} / v_{n1}	1.149	u_{13} / v_{n1}	1.445
u_{21} / v_{n1}	1.908	u_{22} / v_{n1}	1.756	u_{23} / v_{n1}	1.631
u_{n21} / v_{n1}	0.304	u_{n22} / v_{n1}	0.769	u_{n23} / v_{n1}	1.631
$c_1 = u_{n1} / v_{n1}$	4.494	u_{n2} / v_{n1}	3.360	u_{n3} / v_{n1}	2.432
$v_{n1} / v_{\max}$	0.217	$v_{n2} / v_{\max}$	0.231	$v_{n3} / v_{\max}$	0.242
$r_1 = v / v_{\max}$	0.341				

[1)] $s = B/8$, $\alpha = 2$

Table 6. 9. Elastic response of unrestrained three-panel shear wall. Non-rigid chords[1)].

Panel 1		Panel 2		Panel 3	
a_{11} / B	0.295	a_{21} / B	0.395	a_{31} / B	0.470
		a_{22} / B	0.186	a_{32} / B	0.401
v / v_{n1}	1.048	v_{n2} / v_{n1}	1.050	v_{n3} / v_{n1}	1.093
u_{11} / v_{n1}	0.533	u_{12} / v_{n1}	0.766	u_{13} / v_{n1}	0.960
u_{21} / v_{n1}	1.276	u_{22} / v_{n1}	1.171	u_{23} / v_{n1}	1.083
u_{n21} / v_{n1}	0.198	u_{n22} / v_{n1}	0.513	u_{n23} / v_{n1}	1.084
$c_1 = u_{n1} / v_{n1}$	3.001	u_{n2} / v_{n1}	2.240	u_{n3} / v_{n1}	1.617
$v_{n1} / v_{\max}$	0.316	$v_{n2} / v_{\max}$	0.332	$v_{n3} / v_{\max}$	0.346
$r_1 = v / v_{\max}$	0.331				

[1)] $s = B/8$, $\alpha = 2$

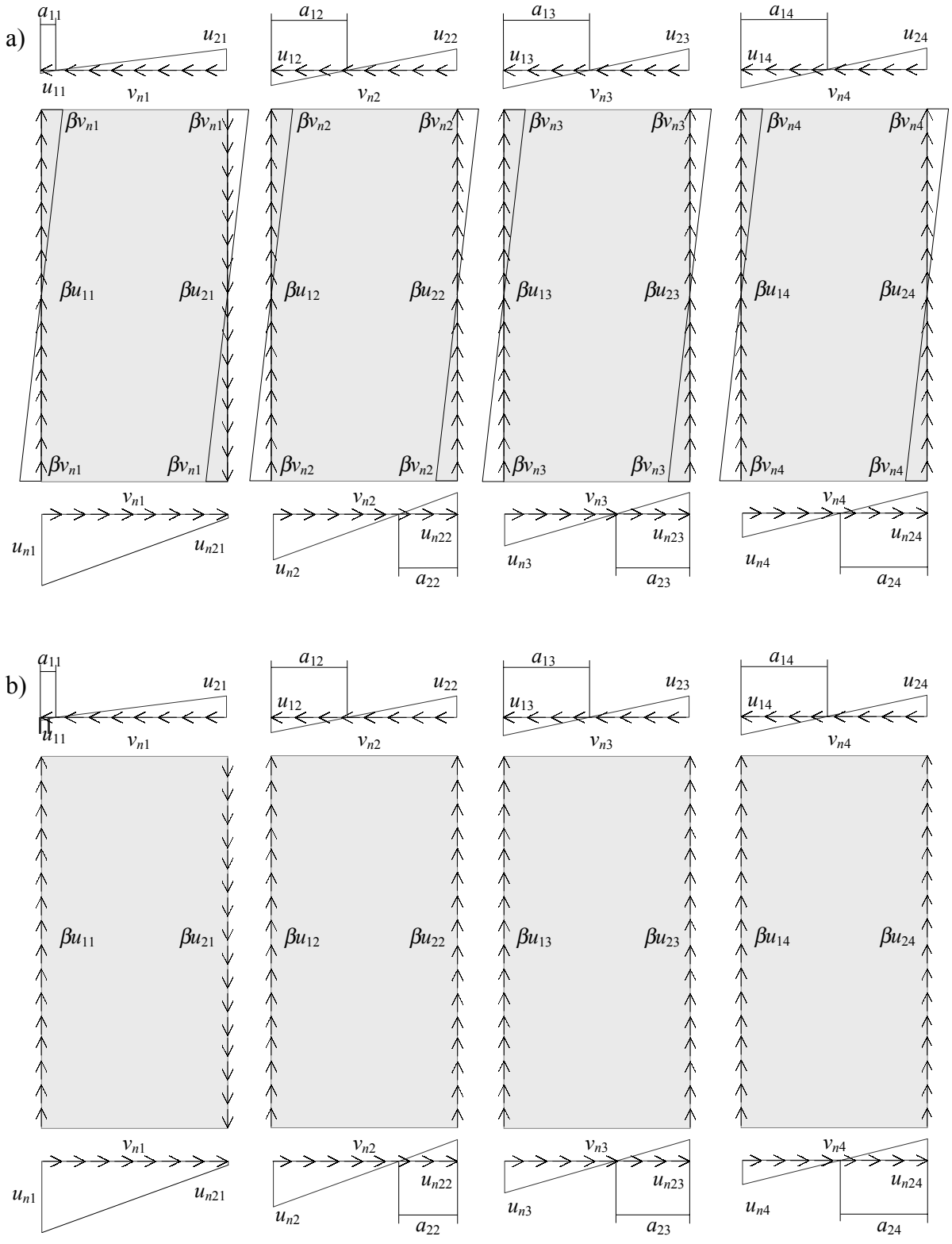

Figure 6. 10. Elastic response of unrestrained four-panel shear wall:
a) Rigid chords, b) Non-rigid chords.

Table 6. 10. Elastic response of unrestrained four-panel shear wall. Rigid chords[1)].

Panel 1		Panel 2		Panel 3		Panel 4	
a_{11} / B	0.317	a_{21} / B	0.402	a_{31} / B	0.457	a_{41} / B	0.456
		a_{22} / B	0.188	a_{32} / B	0.349	a_{42} / B	0.489
v / v_{n1}	1.642	v_{n2} / v_{n1}	1.073	v_{n3} / v_{n1}	1.153	v_{n4} / v_{n1}	1.200
u_{11} / v_{n1}	0.864	u_{12} / v_{n1}	1.190	u_{13} / v_{n1}	1.472	u_{14} / v_{n1}	1.651
u_{21} / v_{n1}	1.859	u_{22} / v_{n1}	1.769	u_{23} / v_{n1}	1.750	u_{24} / v_{n1}	1.727
u_{n21} / v_{n1}	0.142	u_{n22} / v_{n1}	0.737	u_{n23} / v_{n1}	1.342	u_{n24} / v_{n1}	1.728
u_{n1} / v_{n1}	4.141	u_{n2} / v_{n1}	3.191	u_{n3} / v_{n1}	2.505	u_{n4} / v_{n1}	2.058
$v_{n1} / v_{\max}$	0.235	$v_{n2} / v_{\max}$	0.252	$v_{n3} / v_{\max}$	0.271	$v_{n4} / v_{\max}$	0.282
$r_1 = v / v_{\max}$	0.386						

[1)] $s = B/8$, $\alpha = 2$

Table 6. 11. Elastic response of unrestrained four-panel shear wall. Non-rigid chords[1)].

Panel 1		Panel 2		Panel 3		Panel 4	
a_{11} / B	0.319	a_{21} / B	0.403	a_{31} / B	0.457	a_{41} / B	0.456
		a_{22} / B	0.189	a_{32} / B	0.348	a_{42} / B	0.488
v / v_{n1}	1.090	v_{n2} / v_{n1}	1.060	v_{n3} / v_{n1}	1.129	v_{n4} / v_{n1}	1.170
u_{11} / v_{n1}	0.581	u_{12} / v_{n1}	0.793	u_{13} / v_{n1}	0.974	u_{14} / v_{n1}	1.088
u_{21} / v_{n1}	1.241	u_{22} / v_{n1}	1.176	u_{23} / v_{n1}	1.158	u_{24} / v_{n1}	1.141
u_{n21} / v_{n1}	0.085	u_{n22} / v_{n1}	0.493	u_{n23} / v_{n1}	0.885	u_{n24} / v_{n1}	1.141
u_{n1} / v_{n1}	2.756	u_{n2} / v_{n1}	2.119	u_{n3} / v_{n1}	1.658	u_{n4} / v_{n1}	1.361
$v_{n1} / v_{\max}$	0.341	$v_{n2} / v_{\max}$	0.362	$v_{n3} / v_{\max}$	0.385	$v_{n4} / v_{\max}$	0.399
$r_1 = v / v_{\max}$	0.372						

[1)] $s = B/8$, $\alpha = 2$

6.5.5 Multiple-Panel Shear Wall without Dead Load. Ultimate Strength Model

6.5.5.1 Distribution of Forces in the Bottom Plate

Further derivation of the ultimate strength model depends on the assumptions for the distribution of forces along the bottom plate. Elastic analysis showed that there is some variation between the forces even though the framing elements are assumed infinitely rigid. First, consider a general case with a non-uniform distribution. Assume a free-body diagram of the bottom plate of multi-panel wall with n panels at the strength limit state as is shown in Figure 6. 11.

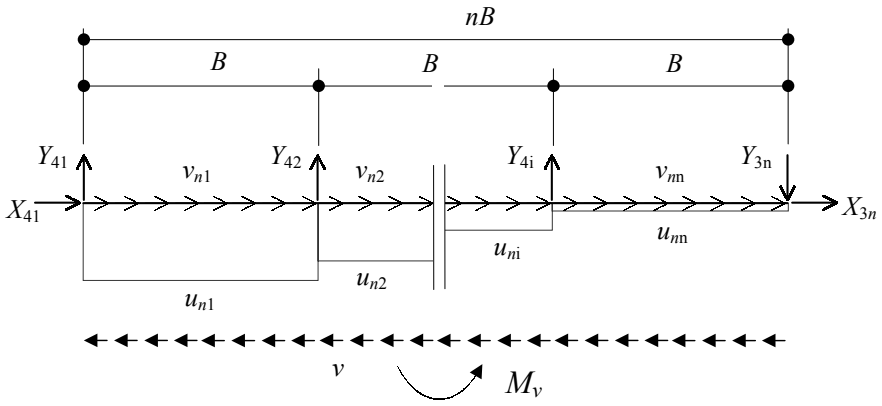

Figure 6. 11. Bottom plate of multi-panel unrestrained wall at strength limit state. Non-uniform distribution of forces.

The static equilibrium of the bottom plate is described as follows:

$$X_{41} + X_{3n} + \sum_{i=1}^{n} v_{ni} - nBv = 0 \tag{6.37}$$

$$\sum_{i=1}^{n-1} Y_{4i} + B\sum_{i=1}^{n} u_{ni} - Y_{3n} = 0 \tag{6.38}$$

$$\sum_{i=1}^{n} M_{ni} + \sum_{i=0}^{n-1} BY_{4i}(n-i) - M_v = 0 \tag{6.39}$$

where, $M_{ni} = B\left(\frac{B}{2} + B(n-i)\right)u_{ni}$ and $M_v = \alpha B^2 nv$

The elastic analysis shows that for simplicity, the horizontal joint forces can be conservatively neglected. These forces are collected from the horizontal forces in the sheathing fasteners along the chords, and can be accounted anytime later because they are assumed elastic. Also, neglecting the resistance of the framing fasteners in the end-grain withdrawal, assume vertical joint forces Y_4 equal zero. Then, from Equations (6.37) and (6.39):

$$nv = \sum_{i=1}^{n} v_{ni} \tag{6.40}$$

$$2\alpha B^2 \sum_{i=1}^{n} v_{ni} = B^2 \sum_{i-1}^{n} (1 + 2(n-i)) u_{ni} \tag{6.41}$$

Let

$$c_i = \frac{u_{ni}}{v_{ni}} \tag{6.42}$$

and

$$r_i = \frac{1}{\sqrt{1 + c_i^2}} \tag{6.43}$$

Then,

$$2\alpha \sum_{i=1}^{n} v_{ni} = \sum_{i=1}^{n} (1 + 2(n-i)) c_i v_{ni} \tag{6.44}$$

From Equation (6.43) it can be written:

$$\frac{v_{ni}}{v_{n1}} = \frac{r_i}{r_1} = \frac{\sqrt{1 + c_1^2}}{\sqrt{1 + c_i^2}} \tag{6.45}$$

To find ratio c_{i+1} for each consecutive panel, assume that the ratio c_i in the previous panel remains unchanged. Thus, assuming

$$c_1 = 2\alpha \tag{6.46}$$

Equation (6.44) becomes:

$$\sum_{i=1}^{n} r_i = \sum_{i=1}^{n} \left(1 + 2\left(n - i\right)\right) \frac{c_i}{c_1} r_i \tag{6.47}$$

Then, for the second panel in a two-panel wall:

$$c_2 = \frac{c_1\left(c_1^2 - 3\right)}{3c_1^2 - 1} = \frac{2\alpha\left(4\alpha^2 - 1\right)}{12\alpha^2 - 1} \tag{6.48}$$

Knowing c_1 and c_2, one can find c_3, and so forth. The average shear wall resistance as a function of the maximum resistance of sheathing fasteners is derived from Equations (6.40) and (6.45):

$$\frac{v}{v_{\max}} = \frac{1}{n}\sum_{i=1}^{n} \frac{v_{ni}}{v_{\max}} = \frac{1}{n}\sum_{i=1}^{n} r_i \tag{6.49}$$

where $v_{\max} = \frac{v_{n1}}{r_1}$

Table 6. 12 shows the solutions for one-, two-, three-, and four-panel walls with the aspect ratio $\alpha = 2$.

Table 6. 12. Ultimate strength of unrestrained multi-panel shear wall[1)].

Non-uniform force distribution.

n	c_i	r_i	$\frac{v_{ni}}{v_{n1}}$	$\frac{v}{v_{\max}}$
1	4	0.2425	1	0.2425
2	1.1064	0.6705	2.7647	0.4565
3	0.3604	0.9408	3.8789	0.6180
4	-0.1451	0.9896	4.0804	0.7109

[1)] $\alpha = 2$

Two important conclusions are drawn from the data in Table 6. 12:

1) The ratio r shows that the sheathing connections in the fourth panel develop their full capacity. The same conclusion was made during the elastic analysis. The accuracy of the prediction appears to decrease with increasing number of panels. When the panel acts like the anchored wall, the nail forces at the bottom of the wall, u_{ni}, are not uniform. For higher accuracy, a different shape of the diagram should be assumed, where the sign of the diagram changes within the panel.

2) The distribution of forces in sheathing connections between the panels is significantly less uniform than it was shown during the elastic analysis. It is unlikely that the connection forces in two adjacent panels increase two- or three-fold, as data in Table 6. 12 suggest. Therefore, the assumption used in this solution is not accurate.

Based on these conclusions, assume an unrestrained n-panel shear wall with the uniform distribution of forces in the sheathing fasteners along the bottom plate until the n-th panel. For the n-th panel, consider three cases shown in Figure 6. 12:

a) The diagram of u_n forces changes the sign within the n-th panel in triangular form. This is the most conservative assumption, which allows only elastic performance of the sheathing connections along the top plate and the chords, while most of the fasteners yield along the bottom plate. However, if $a_n \to B/2$, the assumption may become overly conservative and underestimate the contribution of other fasteners on perimeter. In this case, the diagram b is considered.

b) The diagram of u_n forces changes the sign within the n-th panel in rectangular form. According to this assumption, all sheathing connections along the bottom plate develop full plastic capacity. In this case, the plastic yielding of connections along the top plate is allowed.

c) The diagram of u_n forces remains rectangular along the entire wall length. This is the least conservative assumption; however it allows the simplest estimation or the shear wall ultimate strength.

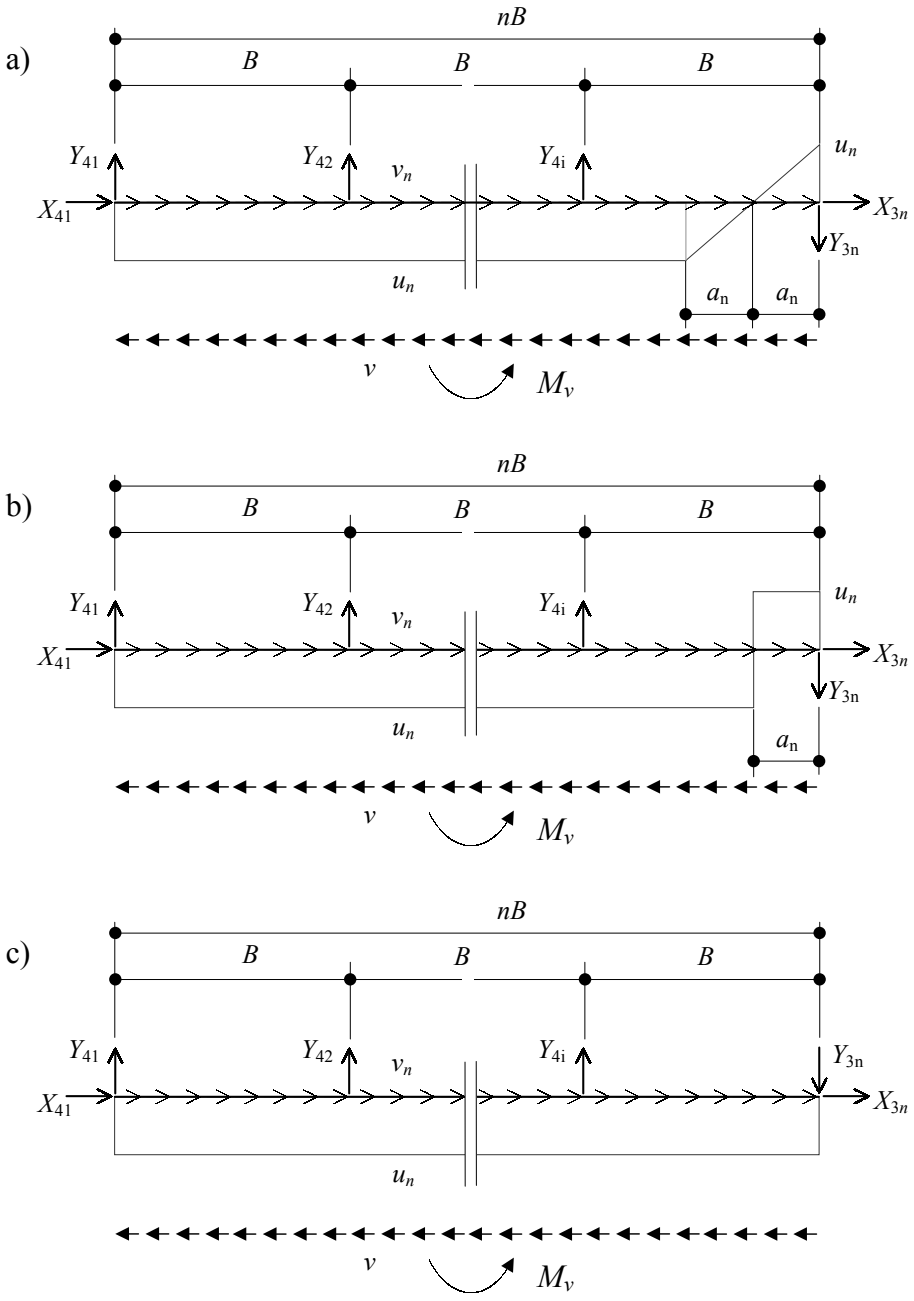

Figure 6. 12. Bottom plate of multi-panel unrestrained wall at strength limit state.

a) Uniform and triangular distribution of forces,

b) Uniform and rectangular distribution of forces,

c) Uniform distribution of forces.

First, consider the triangular force distribution in the *n*-th panel assuming that these nails do not develop full plastic yielding at the wall strength limit state. Neglecting the joint forces Y_{4i} and X_{41}, the moment equilibrium is expressed as follows:

$$M = \alpha B^2 nv = \left(Bn - 2a_n\right)\left(Bn - \frac{Bn - 2a_n}{2}\right) + \left(\frac{a_n}{2}\left(2a_n - \frac{a_n}{3}\right) - \frac{a_n^2}{6}\right)u_n \tag{6.50}$$

$$\alpha B^2 nv = \left(\frac{B^2 n^2}{2} - \frac{4a_n^2}{3}\right)u_n \tag{6.51}$$

Therefore,

$$c = \frac{u_n}{v} = \frac{2\alpha B^2 n}{B^2 n^2 - \frac{8}{3}a_n^2} \tag{6.52}$$

Similarly, for the rectangular force distribution in the *n*-th panel:

$$M = \alpha B^2 nv = \left(\left(Bn - a_n\right)\left(Bn - \frac{Bn - a_n}{2}\right) - \frac{a_n^2}{2}\right)u_n \tag{6.53}$$

$$c = \frac{2\alpha B^2 n}{B^2 n^2 - 2a_n^2} \tag{6.54}$$

To determine the distance a_n, the equilibrium of the entire wall should be considered. Considering the previous results, note that the solution is accurate while $a_n \le B$. The solutions for two- and three-panel walls are shown in Sections 6.5.5.2 and 0.

If uniform force distribution is assumed along the entire wall length (case c), the ultimate strength of the wall can be determined from the equilibrium of the bottom plate only:

$$M = \alpha B^2 nv = \frac{(Bn)^2}{2}u_n \tag{6.55}$$

$$c = \frac{2\alpha}{n} \tag{6.56}$$

Neglecting the shear forces in the studs ($X_{3n} = 0$), the reduction factor becomes:

$$r = \left(1 + \left(\frac{2\alpha}{n}\right)^2\right)^{-\frac{1}{2}} \tag{6.57}$$

Table 6. 13 shows the ratio *c* and the reduction factor *r* for shear walls with up to four panels. Examples are given for the aspect ratio $\alpha = 2$.

Table 6. 13. Ultimate strength of unrestrained multi-panel shear wall.

n	α		$\alpha = 2$	
	c	*r*	*c*	*r*
1	2α	$\left(1+4\alpha^2\right)^{-\frac{1}{2}}$	4	0.2425
2	α	$\left(1+\alpha^2\right)^{-\frac{1}{2}}$	2	0.4472
3	$\frac{2\alpha}{3}$	$\left(1+\frac{4}{9}\alpha^2\right)^{-\frac{1}{2}}$	1.333	0.6000
4	$\frac{\alpha}{2}$	$\left(1+\frac{\alpha^2}{9}\right)^{-\frac{1}{2}}$	1	0.7071

The reduction factor *r* in Table 6. 13 can serve to estimate the design shear strength of an unrestrained wall as a fraction of the design shear strength of fully-restrained wall if the design values are based on the ultimate shear wall strength. Note that the reduction factors in Table 6. 13 are significantly higher than the corresponding values shown in Section 6.5.4 for the elastic response. The differences can be explained by the influence of the shear wall stiffness on the elastic response: Restrained walls are not only stronger; they are significantly stiffer than unrestrained walls.

Table 6. 14 shows the comparison between the two methods derived in this section and the experimental results obtained during the shear wall tests discussed in Chapter 5. The shear strength of unrestrained walls (**IAm**) is related to the shear strength of the fully-anchored walls (**FAm**). During the tests, the anchored walls developed the average shear strength 9.9 KN/m (0.68 Kip/ft.). Assuming that the sheathing connections in the anchored walls develop 0.956 of their ultimate capacity:

$$v_{\max} = \frac{9.9}{0.956} = 10.36 \text{ KN/m (0.71 Kip/ft.)} \tag{6.58}$$

It appears from the comparison that both methods produce reasonably accurate predictions. Note, however, that the accuracy decreases with increasing number of panels, as was expected. It is encouraging that the simple uniform distribution method produces more accurate and conservative results than the non-uniform method.

In the following sections, the more accurate than discussed above solutions are shown for two- and three-panel shear walls.

Table 6. 14. Ultimate strength of unrestrained shear walls.
Comparison of experimental and predicted values.

n	Experimental		Non-uniform distribution method		Uniform distribution method	
	v Kip/ft.	r_i	r_i	Predicted / experimental	r_i	Predicted / experimental
1	0.168	0.236	0.243	1.027	0.243	1.027
2	0.309	0.434	0.457	1.051	0.447	1.029
3	0.413	0.581	0.618	1.064	0.600	1.033

6.5.5.2 Two-Panel Unrestrained Shear Wall

It was shown in the previous section that assuming one-sided diagrams of the force distribution among the fasteners in the bottom plate is not conservative. The most conservative estimate of the shear wall strength can be obtained assuming that the diagram u_n changes the sign in the n-th panel and that the shape of the diagram at the right end of the panel is triangular.

Consider the free body diagram of the two-panel wall with rigid chords shown in Figure 6. 13. Assume all horizontal joint forces in perimeter framing members equal X. Then, for all chords and plates:

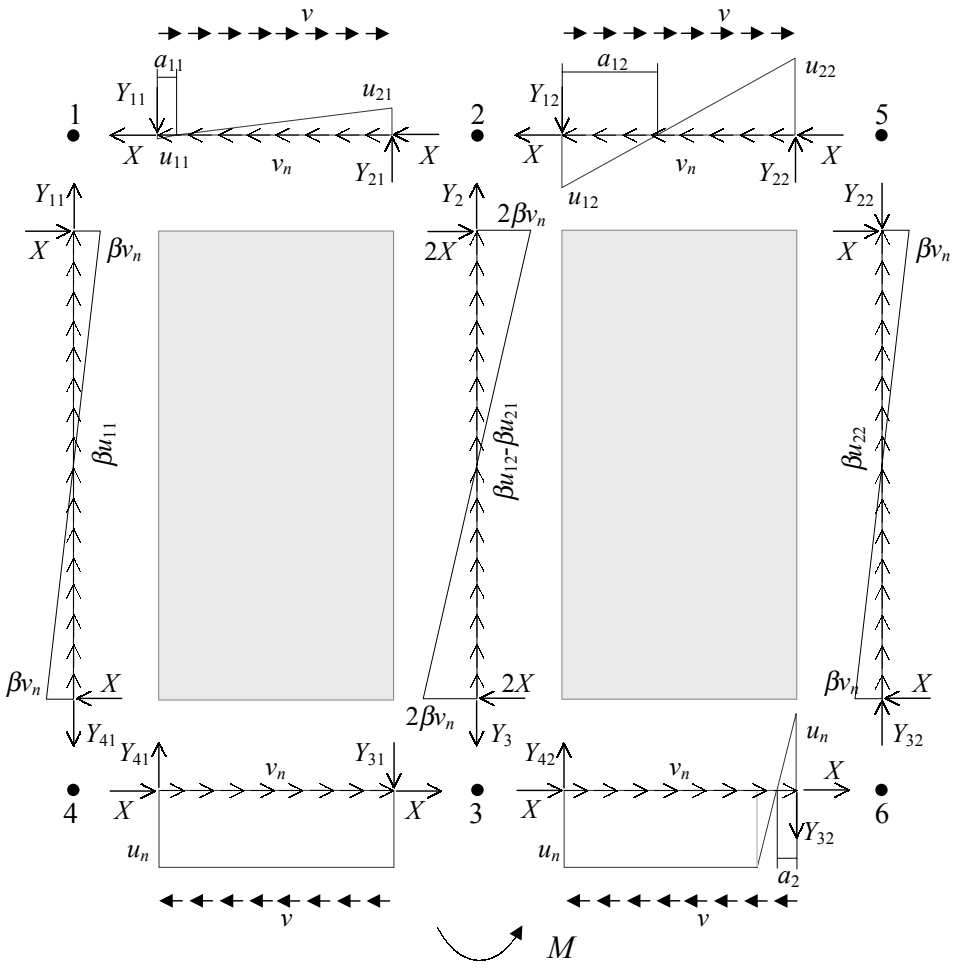

Figure 6. 13. Two-panel unrestrained wall at the strength limit state. Case a.

$$\alpha BX - \frac{(\alpha B)^2}{6} \cdot \beta v_n = 0 \tag{6.59}$$

$$Bv - 2X - (B - 2s)v_n = 0 \tag{6.60}$$

The other equations of the static equilibrium are written as follows:

Chord 1-4:

$$Y_{11} + (\alpha B - 2s) \cdot \beta u_{11} - Y_{41} = 0 \tag{6.61}$$

Chord 2-3:

$$Y_2 + (\alpha B - 2s) \cdot \beta (u_{12} - u_{21}) - Y_3 = 0 \tag{6.62}$$

Top plate 1-2:

$$Y_{21} - Y_{11} + \frac{a_{11}}{2} u_{11} - \frac{B - a_{11}}{2} \cdot u_{21} = 0 \tag{6.63}$$

$$-BY_{11} + \frac{a_{11}}{2}\left(B - \frac{a_{11}}{3}\right) \cdot u_{11} - \frac{(B - a_{11})^2}{6} \cdot u_{21} = 0 \tag{6.64}$$

Bottom plate 4-3:

$$Y_{41} - Y_{31} + Bu_n = 0 \tag{6.65}$$

Chord 5-6:

$$Y_{32} - (\alpha B - 2s) \cdot \beta u_{22} - Y_{22} = 0 \tag{6.66}$$

Top plate 2-5:

$$Y_{22} - Y_{12} + \frac{a_{12}}{2} u_{12} - \frac{B - a_{12}}{2} \cdot u_{22} = 0 \tag{6.67}$$

$$-BY_{12} + \frac{a_{12}}{2}\left(B - \frac{a_{12}}{3}\right) \cdot u_{12} - \frac{(B - a_{12})^2}{6} \cdot u_{22} = 0 \tag{6.68}$$

Bottom plate 3-6:

$$Y_{42} - Y_{32} + (B - 2a_2)u_n = 0 \tag{6.69}$$

Joint 2:

$$Y_{12} - Y_2 - Y_{21} = 0 \tag{6.70}$$

Joint 3:

$$Y_3 + Y_{31} - Y_{42} = 0 \tag{6.71}$$

Distances a_{11} and a_{12} are determined from the following ratios:

$$u_{21} = \frac{B - a_{11}}{a_{11}} \cdot u_{11} \tag{6.72}$$

$$u_{22} = \frac{B - a_{12}}{a_{12}} \cdot u_{12} \tag{6.73}$$

Distance a_2 is determined from Equation (6.52) with $n = 2$:

$$a_n = B\sqrt{\frac{3}{4}n\left(\frac{n}{2} - \alpha\frac{v}{u_n}\right)} = B\sqrt{\frac{3}{2}\left(1 - \alpha\frac{v}{u_n}\right)} \tag{6.74}$$

To solve the system of Equations (6.59) through (6.72), the following assumptions are made:

$$Y_{41} = Y_3 = 0 \tag{6.75}$$

$$u_{22} = u_n \tag{6.76}$$

$$Y_{31} - (\alpha B - 2s)\cdot \beta u_{21} - Y_{21} = 0 \tag{6.77}$$

Equation (6.77) is derived from Equation (6.24) assuming that the pattern of force distribution in the first panel remains the same as in the single-panel wall.

Now, consider the free body diagram with the rectangular distribution at the end of the top and bottom plates in the second panel as is shown in Figure 6. 14. Assume the same distance a_2 at the top and the bottom, which is found from Equation (6.54):

$$a_n = B\sqrt{n\left(\frac{n}{2} - \alpha\frac{v}{u_n}\right)} = B\sqrt{1 - \alpha\frac{v}{u_n}} \tag{6.78}$$

Equations (6.67) and (6.68) for the top plate transform into:

$$Y_{22} - Y_{12} + \frac{a_{12}}{2}u_{12} - \frac{B - a_{12} + a_2}{2}\cdot u_{22} = 0 \tag{6.79}$$

$$-BY_{12} + \frac{a_{12}}{2}\left(B - \frac{a_{12}}{3}\right)\cdot u_{12} - \left((B - a_{12} - a_2)\frac{(B - a_{12} + 2a_2)}{3} - \frac{a_2^2}{2}\right)\cdot u_{22} = 0 \tag{6.80}$$

If the shear forces in the studs are neglected, then Equations (6.59) and (6.60) are eliminated, and $v = v_n$. Table 6. 15 shows the solutions of the equilibrium for two-panel shear wall with $\alpha = 2$ and $s = B/8$. The results show that the pivot point (distance a_2)

moved to the right from $0.3B$ in elastic solution to $0.05B$ at the strength limit state. Because the distance is so small, the differences between the triangular and rectangular distributions are negligible. As expected, the results are more conservative when the shear forces in the chords are neglected. However, the differences between the solutions in Table 6. 15 and Table 6. 14 are less than 2%, which justifies again the applicability of the simplified method shown in Equation (6.57).

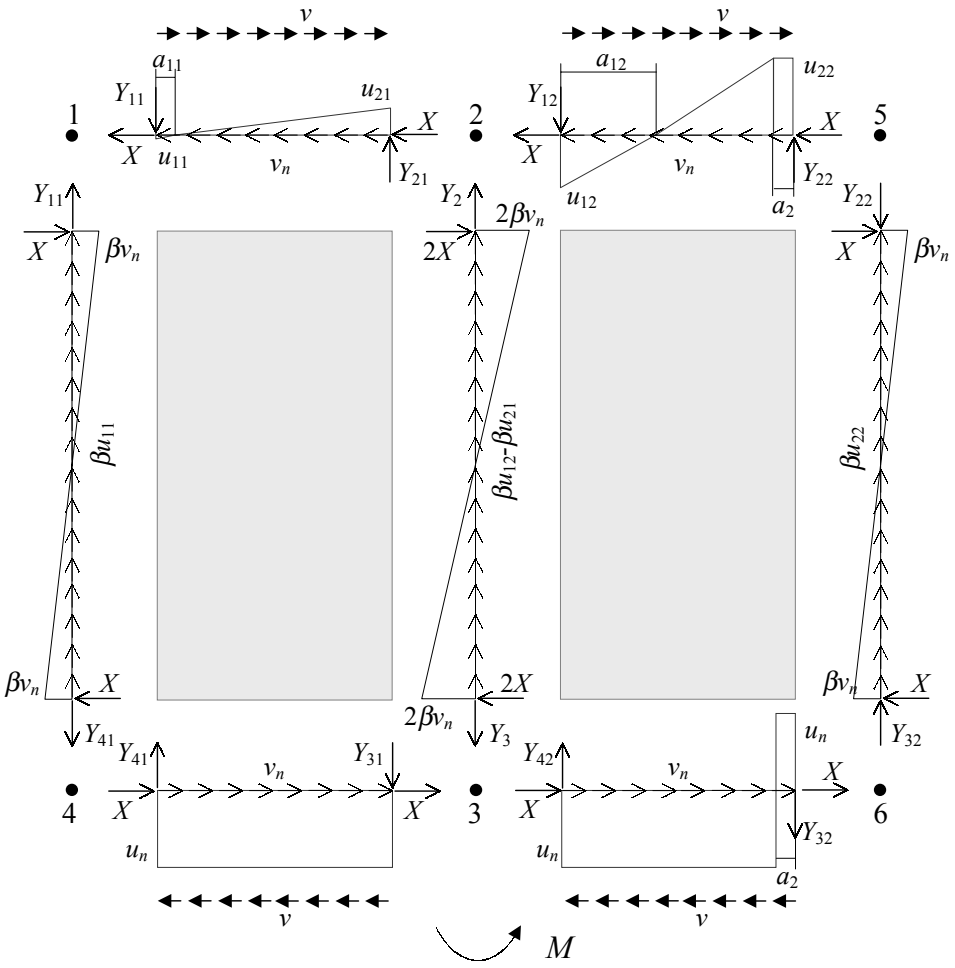

Figure 6. 14. Two-panel unrestrained wall at the strength limit state. Case b.

Table 6. 15. Strength limit state response of unrestrained two-panel shear wall.

Parameters	Rigid chords		Non-rigid chords	
	Triangular distribution	Rectangular distribution	Triangular distribution	Rectangular distribution
v / v_n	1.065	1.190	1.000	1.000
u_n / v_n	2.134	2.382	2.004	2.002
$v_n / v_{\max}$	0.424	0.387	0.446	0.447
$\boldsymbol{r = v / v_{max}}$	**0.452**	**0.461**	**0.446**	**0.447**
a_{11} / B	0.077	0.077	0.077	0.077
u_{11} / v_n	0.091	0.101	0.085	0.085
u_{21} / v_n	1.082	1.208	1.016	1.015
a_{12} / B	0.370	0.356	0.370	0.356
u_{12} / v_n	1.254	1.414	1.177	1.189
a_2 / B	0.056	0.045	0.056	0.045

6.5.5.3 Three-Panel Unrestrained Shear Wall

Because the distance a_2 is small (and it decreases with increasing density of the sheathing fasteners), it is safe to assume that forces u_n in the bottom plate change the sign only once, in the third panel. The free body diagram of the second and the third panels with the assumed triangular force distribution at the end of the third panel is shown in Figure 6. 15. The force distribution in the first and the second panels is assumed to follow the same pattern as in the two-panel wall.

Equations (6.59) through (6.65), (6.67), (6.68), (6.70) through (6.73), (6.75), and (6.77) remain the same as for the two-panel wall. Equation (6.66) for Chord 2-3 transforms into:

$$Y_5 + (\alpha B - 2s) \cdot \beta (u_{13} - u_{22}) - Y_6 = 0 \tag{6.81}$$

Equation (6.69) for the Bottom plate 3-6 transforms into:

$$Y_{42} - Y_{32} + B u_n = 0 \tag{6.82}$$

Equation (6.76) transforms into:

$$u_{23} = u_n \tag{6.83}$$

Equation (6.74) with $n = 3$ determines the distance a_3:

$$a_n = B\sqrt{\frac{3}{4}n\left(\frac{n}{2}-\alpha\frac{v}{u_n}\right)} = B\sqrt{\frac{9}{4}\left(\frac{3}{2}-\alpha\frac{v}{u_n}\right)} \tag{6.84}$$

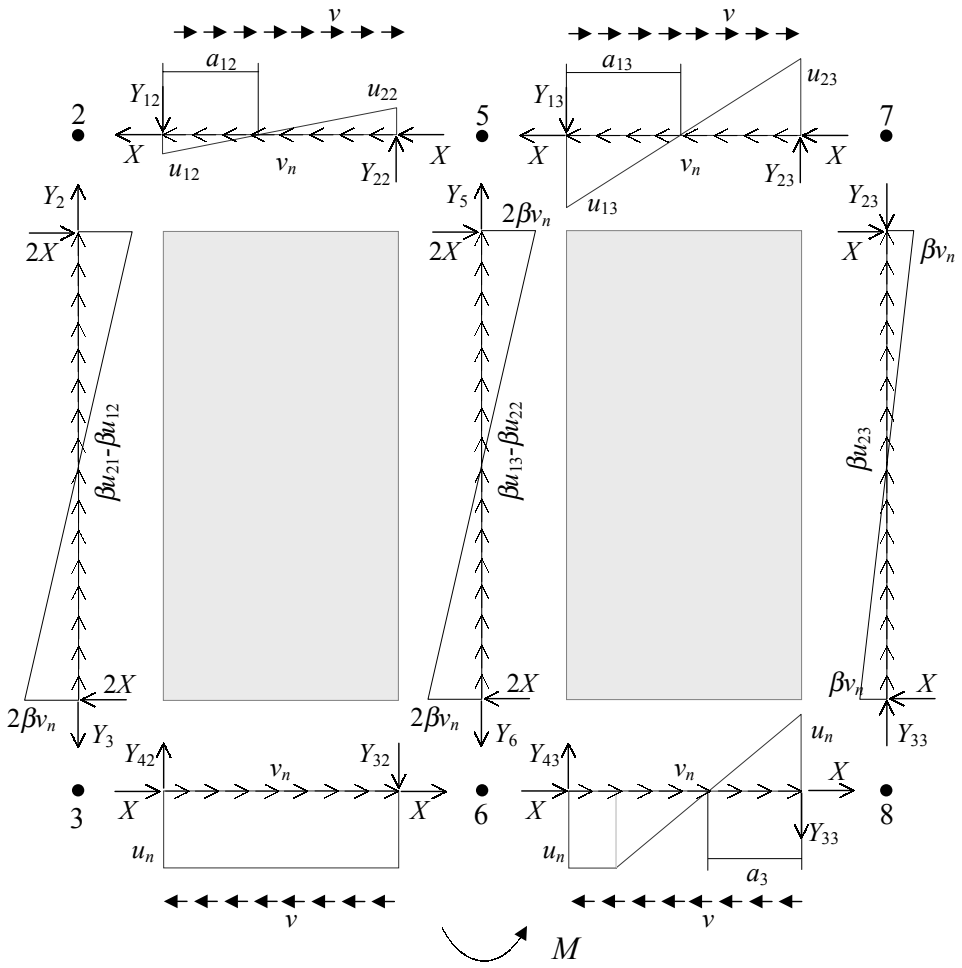

Figure 6. 15. Three-panel unrestrained wall at the strength limit state. Case a (The first panel is not shown).

The following equations are added to describe the equilibrium of the third panel:

Top plate 5-7:

$$Y_{23} - Y_{13} + \frac{a_{13}}{2}u_{13} - \frac{B-a_{13}}{2}\cdot u_{23} = 0 \tag{6.85}$$

$$-BY_{13}+\frac{a_{13}}{2}\left(B-\frac{a_{13}}{3}\right)\cdot u_{13}-\frac{(B-a_{13})^2}{6}\cdot u_{23}=0 \tag{6.86}$$

Bottom plate 6-8:

$$Y_{43}-Y_{33}+(B-2a_3)u_n=0 \tag{6.87}$$

Cord 7-8:

$$Y_{33}-(\alpha B-2s)\cdot \beta u_{23}-Y_{23}=0 \tag{6.88}$$

Joint 5:

$$Y_{13}-Y_5-Y_{22}=0 \tag{6.89}$$

Joint 6:

$$Y_6+Y_{32}-Y_{43}=0 \tag{6.90}$$

Distance a_{13} is determined from:

$$u_{23}=\frac{B-a_{13}}{a_{13}}\cdot u_{13} \tag{6.91}$$

Similar to the two-panel wall, assume

$$Y_6=0 \tag{6.92}$$

$$Y_{32}-(\alpha B-2s)\cdot \beta u_{22}-Y_{22}=0 \tag{6.93}$$

Results of the analysis for the three-panel shear wall with $\alpha=2$ and $s=B/8$ are shown in Table 6. 16. Note that the distance $a_3>B/2$ and force u_{13} is 9% higher than u_n. Therefore, the assumption of triangular force distribution is not accurate for this aspect ratio and spacing of fasteners. It means, that at the strength limit state, the fasteners along the perimeter of the third panel develop plastic yielding and the rectangular force distribution would represent the wall performance more accurately.

It can be shown that the rectangular force distribution, similar to the two-panel wall shown in Section 6.5.5.2, is also not accurate for $\alpha=2$ and $s=B/8$. Therefore,

consider the force distribution as is shown in Figure 6. 16, where the distances $a_3 = a_{13} = B/2$. Therefore, forces $u_{13} = u_{23} = u_n$. For simplicity, the plastic yielding of the fasteners along the studs in the third panel is neglected. Results of analysis for the three-panel shear wall with $\alpha = 2$ and $s = B/8$ are shown in Table 6. 16. Also, Table 6. 16 shows the results of analysis when the shear forces in the studs are neglected.

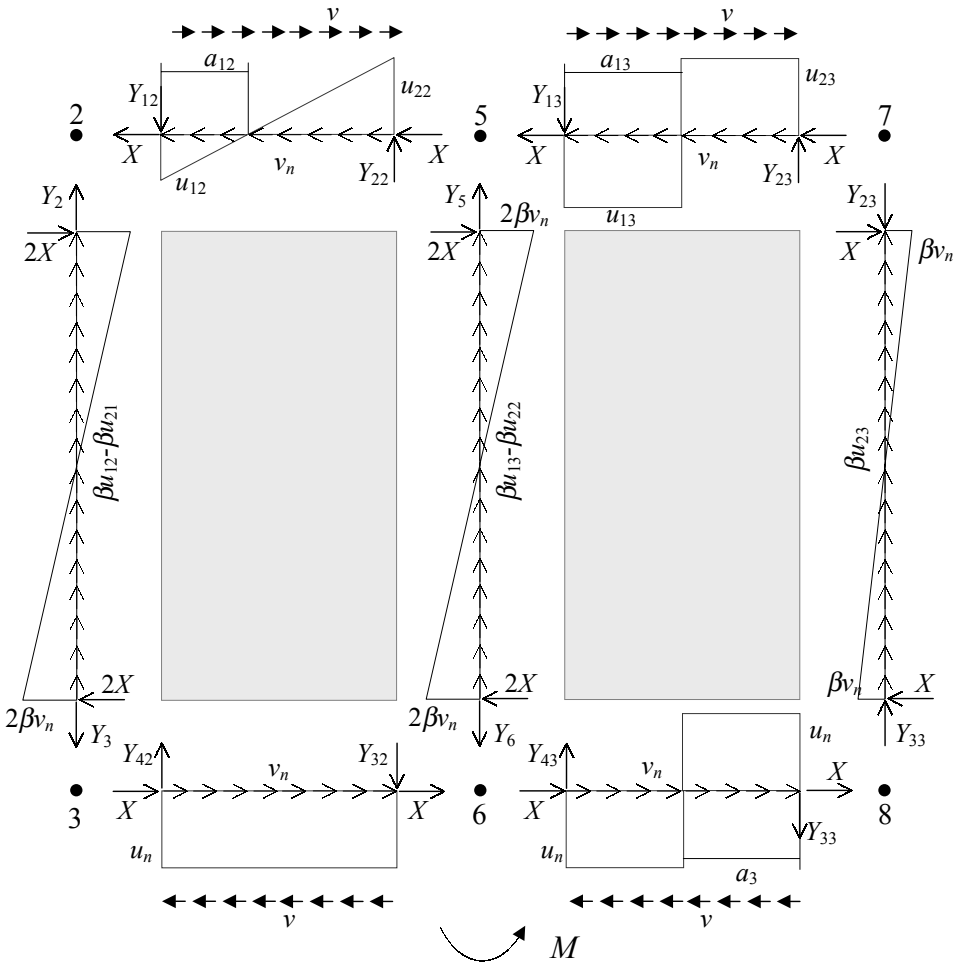

Figure 6. 16. Three-panel unrestrained wall at the strength limit state. Case b (The first panel is not shown).

It can be seen from Table 6. 16 that the solution with the rectangular force distribution is more precise: the difference between forces u_{22} and u_n is approximately 5%. The error is likely due to the neglecting of the plastic yielding of the fasteners along the studs. In the future, the precision of the model can be improved by eliminating this assumption. However, would it improve the accuracy? Comparing the data in

Table 6. 16 with the experimental results (Table 6. 14), the solution neglecting shear forces in studs appears more accurate, or at least conservative. Experimental observations suggest that due to the high length of the wall, the sheathing at the left-bottom corner separated from the framing earlier than the fasteners in the third panel could develop their plastic capacity. Overturning of the wall can be restrained by dead load, which is the subject of the next section. Note again the satisfactory accuracy of the simple method given in Equation (6.57) relative to the sophisticated predictions.

Table 6. 16. Strength limit state response of unrestrained three-panel shear wall.[1)]

Parameters	Rigid chords		Non-rigid chords	
	Triangular distribution	Rectangular distribution	Triangular distribution	Rectangular distribution
v / v_n	1.065	1.380	1.000	1.000
u_n / v_n	2.057	1.948	1.491	1.412
$v_n / v_{\max}$	0.437	0.457	0.557	0.578
$\boldsymbol{r = v / v_{max}}$	**0.603**	**0.630**	**0.557**	**0.578**
a_{11} / B	0.077	0.077	0.077	0.077
u_{11} / v_n	0.163	0.155	0.119	0.112
u_{21} / v_n	1.948	1.844	1.412	1.337
a_{12} / B	0.359	0.359	0.359	0.359
u_{12} / v_n	1.218	1.153	0.883	0.836
u_{22} / v_n	2.174	2.058	1.576	1.492
a_{13} / B	0.522	0.500	0.522	0.500
u_{13} / v_n	2.244	1.948	1.627	1.412
a_3 / v_n	0.598	0.500	0.598	0.500

[1)] $\alpha = 2$, $s = B/8$

Data in Table 6. 16 suggest that the third panel can develop the full plastic capacity similar to the fully-restrained panels. Recall that in the elastic region, only the fourth panel acted as the fully restrained (see Section 6.5.4). The ratio between the vertical and the horizontal components of the fastener' resistance equals $\alpha = 2$ in each corner of the third panel, which is the same ratio as assumed in the Tuomi and McCutcheon model (1978). When the shear forces in the studs are neglected (i.e., the bending stiffness approaches zero), the ratio is between 1.41 and 1.49, which is similar to the ratio assumed in the simple shear wall theory for anchored walls (Stewart 1987). This information is used for predicting the shear wall deflections in Section 6.6.

6.5.6 Shear Wall Segment with Dead Load. Elastic Model

Consider the shear wall segment discussed in Section 6.5.2 with dead load applied to the chords as is shown in Figure 6. 17. Values of dead load forces W_1 and W_2 vary depending on the location of the wall segment, stiffness of the upper structural elements, and the method of construction. It is often assumed that dead load from the upper structure is uniformly distributed along the wall top plate and then transmitted to the studs. Then, if the segment is located at the wall corner, the force W_1 is no more than half of the force W_2. If the segment is in the middle of the wall, say, between the windows, then the forces W_1 and W_2 may be equal. For the analysis of the single-panel wall segment, the value W_2 is not important, because only the force W_1 provides the overturning restraint. Therefore, the value of the force W_1 is estimated as a fraction of the floor dead load *w*, e.g.:

$$W_1 = m \cdot B \cdot w \tag{6.94}$$

It is up to the designer to estimate what fraction of the floor dead load is transmitted to the shear wall, and to the corner segments, in particular. Here, the method of accounting for the dead load is presented only theoretically.

Equations (6.1) and (6.7) through (6.20), and the equilibrium equations of the joints (6.94) through (6.97) describe the equilibrium of the shear wall segment.

$$-W_1 - Y_{1c} + Y_{1p} = 0 \tag{6.95}$$

$$-W_2 + Y_{2c} - Y_{2p} = 0 \tag{6.96}$$

$$W_2 - Y_{3c} + Y_{3p} = 0 \tag{6.97}$$

$$W_1 + Y_{4c} - Y_{4p} = 0 \tag{6.98}$$

Under the assumptions discussed in Section 6.5.2, the force in Joint 4: $Y_4 = W_1$. To determine the effect of the dead load on the wall resistance, solve for equilibrium, setting the distance a_2 from B/2 to the minimum found in Table 6. 1. Solving for equilibrium for various aspect ratios and fastener spacing, the relationship between the strength reduction factor *r* and the ratio of the dead load to the racking load *w*/*v* can be

established. For example, solutions for the aspect ratio $\alpha = 2$ and various spacing of sheathing fasteners showed that the reduction factor *r* could be described as a hyperbolic function of *w/v*. The function is independent of the spacing of the sheathing fasteners and the method of analysis (rigid or non-rigid chords). The following expression was found for the aspect ratio $\alpha = 2$:

$$r = \left(6.5 - 5.7\frac{mw}{v}\right)^{-1} \tag{6.99}$$

where *m* is found from Equation (6.94) using the engineering judgement. For example, if $m = 0.5$ and the ratio $w/v = 0.5$, then $r = 0.2$. On one hand, it is a 33% increase in the resistance relative to the unrestrained wall (see Table 6. 1). On the other hand, it is just 5% increase relative to the sheathing connections' resistance.

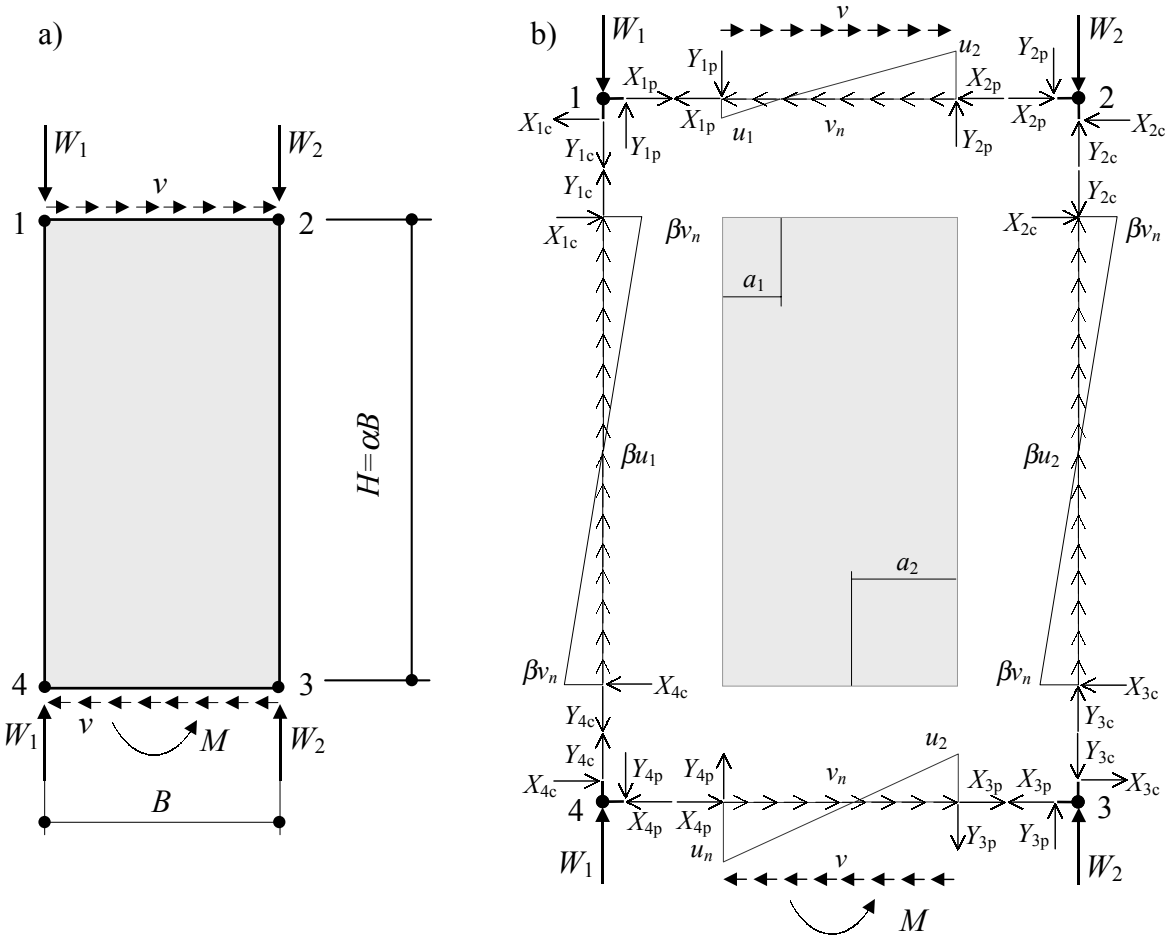

Figure 6. 17. Elastic model of shear wall segment with dead load:
a) External equilibrium, b) Internal equilibrium.

Figure 6. 18 shows the strength reduction factor for various values of *m*. Theoretically, if the shear wall segment is restrained with significant amount of the dead load, there could be a significant increase in the shear resistance. However, if the corner segment carries 12.5% of the floor dead load, the resistance of the segment is practically not affected within the realistic range of the dead load. This simple analysis opposes the speculations about the possible restraining effect of the adjacent transverse corner walls and shows that the use of dead load as restraining force is not practical in design. Unless the adjacent shear wall is tied-down to the base, the resistance cannot be improved due to the dead load only.

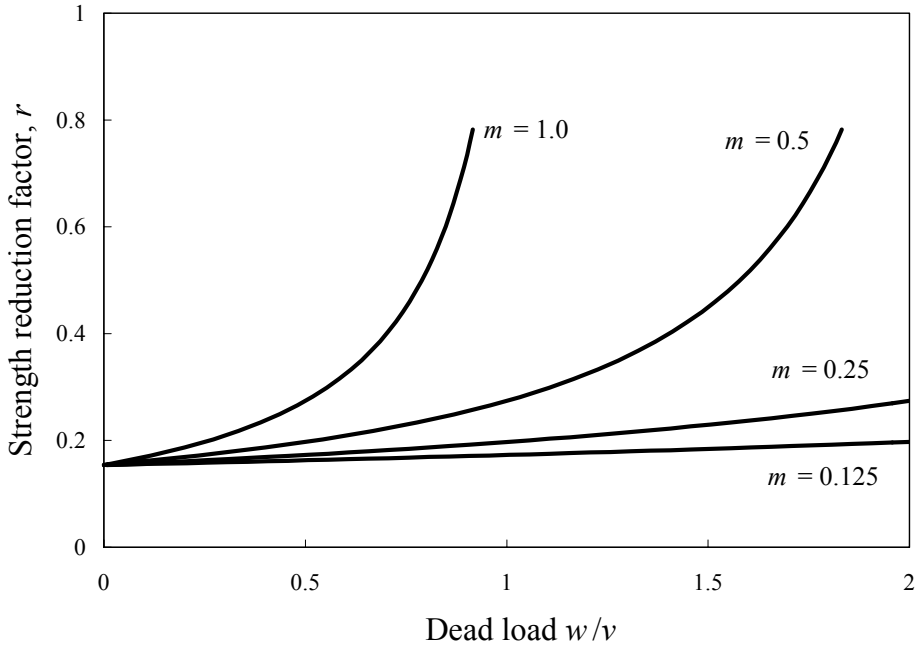

Figure 6. 18. Resistance of shear wall segment with dead load:

6.5.7 Summary on the Strength Models

This section presented the derivation of the mechanical models for elastic and strength limit state responses of multi-panel shear walls without overturning restraint. The derivation is based on the assumption that the joint tension forces between the studs and the bottom plate equal zero. According to this assumption, the single-panel segment develops only a small fraction of the resistance of an anchored wall depending on the height-to-length aspect ratio.

The static equilibrium of the multi-panel walls proved that the adjacent segments provide the restraining effect to each other, increasing the wall shear resistance. The example analyses of shear walls with the aspect ratio of sheathing panels $\alpha = 2$ demonstrated that in the elastic range the fourth segment already acts as the fully restrained shear wall. Therefore, the modeling of the strength limit state for only two- and three-panel unrestrained walls was of interest. Experimental results and the elastic analyses suggested that the plastic yielding of the sheathing fasteners along the bottom plate controlled the wall strength. Therefore, in derivation of the ultimate strength model it was assumed that the fasteners along the bottom plate develop the full plastic strength while the other fasteners remain elastic.

Analysis of the two-panel walls with the aspect ratio of panels $\alpha = 2$ indicated that the assumption was reasonable. However, the analyses of the three-panel walls with the same panels indicated yielding of the fasteners along the top plate in the third panel. Although the yielding of fasteners along the studs was neglected for simplicity during the analysis, it was concluded that the third panel acts as the fully restrained wall at the strength limit state.

At each step of the model derivations, simplified assumptions were tested, such as neglecting shear forces in the studs and the uniform distribution of the fastener forces along the bottom plate. The simplified approach produced remarkably accurate predictions, which correlate well with the test results of full-size shear walls and are sufficient for most design purposes. The simple Equation (6.57) allows estimating the ultimate shear strength of the unrestrained multi-panel wall based on the aspect ratio of the sheathing panel and the number of panels in the wall.

In the end, the elastic response of a single-panel shear wall segment under the dead load was considered. The correlation between the shear resistance and the amount of the dead load on the wall segment was determined. The correlation demonstrated that there is little or no restraining effect of the dead load on the corner wall segments if the amount of the dead load is estimated realistically.

6.6 Shear Wall Deflections

6.6.1 Introduction

Currently, it is accepted in research and design practices (e.g., Deam 1997, ICBO 1997, etc.) that shear wall deflections consist of four components. Chord bending, sheathing shear, rigid body rotation, and slip of sheathing fasteners contribute overall lateral deformation of the wall. The first three components linearly increase the wall deflection and contribute a small fraction to the deformation of a typical fully-restrained wall with small aspect ratio. Highly nonlinear slip of sheathing fasteners determines the shape of the load-deflection relationship of the entire wall. Numerous methods were proposed by researchers to model the non-linear performance of sheathing connections to predict deflections of shear walls. Some of these studies were discussed in Sections 6.3 and 6.4.

This section presents the combined closed-form and empirical models for calculating the load-deflection curves of walls with and without overturning restraint. In addition to mechanics-based sheathing shear and chord flexural deflections, the models include empirical rigid body rotation and sheathing fastener nonlinear slip determined from the tests. The contribution of the sheathing fastener slip in fully-restrained walls is based on the Tuomi and McCutcheon (1978) assumptions. A similar approach is proposed for calculating deflections of unrestrained shear walls assuming the distribution of forces among the sheathing fasteners at the strength limit state discussed in Section 6.5. In both models, the asymptotic curve represents the nailed connection deflections up to the nail peak load. To estimate the deflection at capacity and post-capacity performance of shear walls, the strength degradation portion is added to the nail-slip curve. Comparisons of the predicted and experimental deflection curves are shown, and future directions of the model development are outlined.

6.6.2 Shear Walls with Tie-Down Anchors

Total deflection of a shear wall can be expressed as a sum of the four components:

$$\Delta = \Delta_b + \Delta_s + \Delta_r + \Delta_n \tag{6.100}$$

where, Δ_b = deflection due to the chord bending;

Δ_s = deflection due to sheathing shear;

Δ_r = deflection due to rigid body rotation (due to hold-down displacements);

Δ_n = deflection due to slip of sheathing fasteners;

6.6.2.1 Chord Bending

Flexural deformation of the chords can be determined from the moment-area method assuming the wall frame as a vertical cantilever as is shown in Figure 6. 19:

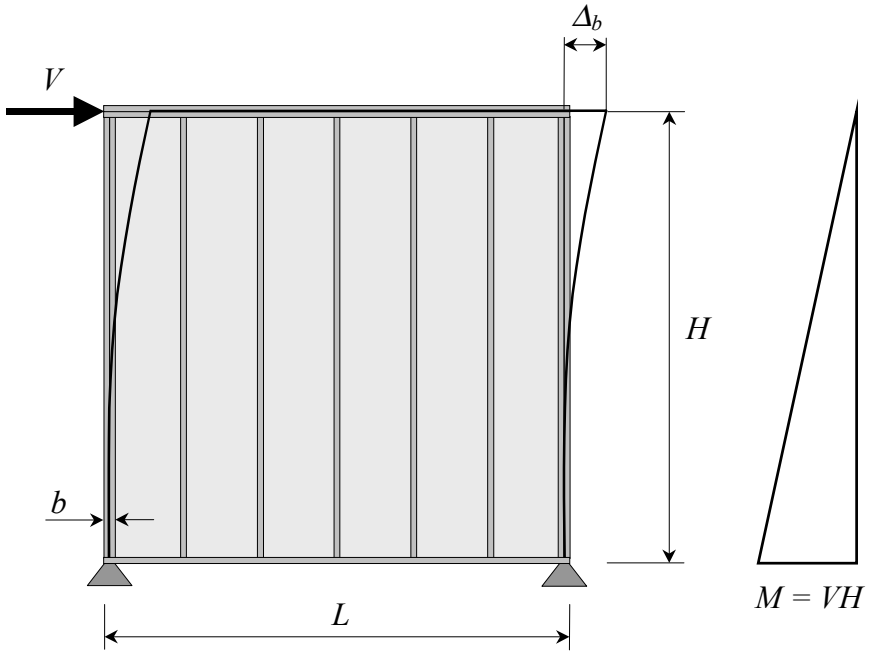

Figure 6. 19. Flexural deformation of cords in shear wall.

$$\Delta_b = \frac{MH^2}{3EI_{ef}} = \frac{VH^3}{3EI_{ef}} \tag{6.101}$$

where, $M = VH$, moment acting on the frame,

E = modulus of elasticity,

I_{ef} = effective moment of inertia of the chords.

Usually, cords are made of double 2×4 studs connected with two 16d nails every 0.6 m (2 ft.). The effective moment of inertia of the composite cross-section is less than a solid 4×4 stud would have. The amount of reduction can be estimated using the theory of built-up beams (e.g. Wheat and Calixto 1994). In this study, the factor k_J from the Russian Timber Design Code (Gosstroy 1983) was chosen as a reasonable and simple adjustment for most practical purposes:

$$I_{ef} = I \cdot k_J = 2A\left(\frac{L-b}{2}\right)^2 \cdot k_J = \frac{A(L-b)^2}{2} \cdot k_J \tag{6.102}$$

where, A = area of cross-section of the chord;

L = wall length;

b = width of the chord;

k_J = 0.49, adjustment factor for composite cross-section of two members 2.4-m (8-ft.) long (Table 13, Gosstroy 1983).

At peak load, the chord flexural deformation typically contributes approximately 2.5 mm (0.1 in.) to the deflection of a 2.4-m (8-ft.) tall and 1.2-m (4-ft.) or longer fully-anchored wall. In narrow walls with the aspect ratio 4:1, the deflection is twice as high.

6.6.2.2 Sheathing Shear

Although structural sheathing is rigid and contributes the least portion to the wall deflection, it is included into the model for accuracy. It provides the opportunity to compare the influence of various types and thicknesses of sheathing on the wall stiffness. The shear deformation of the sheathing and framing is shown in Figure 6. 20.

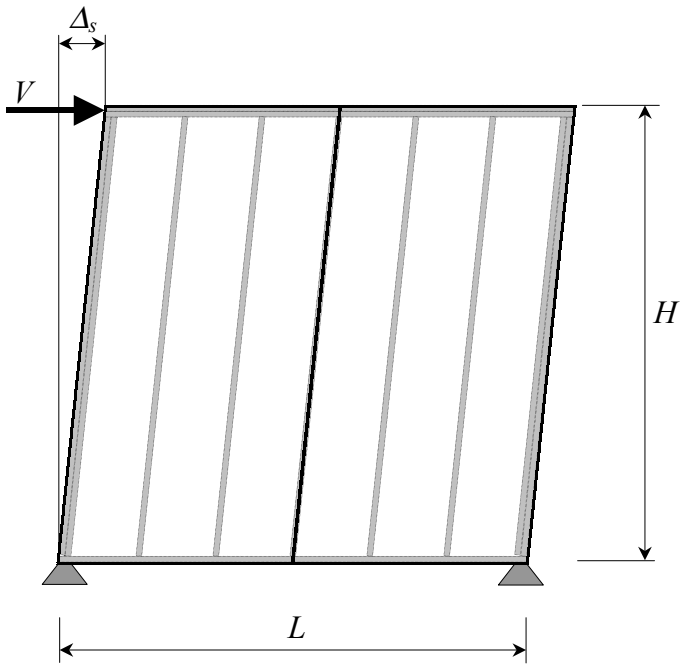

Figure 6. 20. Shear deformation of sheathing and framing.

Since the framing joints are considered pinned, the contribution of the frame to the racking force is ignored. Therefore, the shear deflection of the wall is determined by the shear rigidity of the sheathing only:

$$\Delta_s = \frac{VH}{G_v t_v L} \tag{6.103}$$

where, $G_v t_v$ = panel rigidity through the thickness.

APA (1995) provides values of the shear rigidity for rated structural sheathing panels of various types. For example, for the 11-mm (7/16-in.) OSB used in the experimental program (Chapter 5), $G_v t_v$ = 14657 N/mm depth (83700 lb./in. depth). Typically, the shear deformation of the OSB panel contributes 1.6 mm (0.06 in.) to the wall deflection at the peak load.

6.6.2.3 Rigid Body Rotation

In walls with tie-down anchors, some rigid body rotation occurs due to hold-down displacements. On the tension side, the displacements are due to axial elongation of the anchor, deformation of the tie-down device, and slip of the fasteners attaching it to the

chord. On the compression side, the displacement is due to compression perpendicular-to-grain of the bottom plate under the chord. Figure 6. 21 is a simplified illustration of these effects on the wall deflection. For the purposes of this study, the contribution of the hold-down deformations on the wall rotation was determined from the vertical displacements of chords measured during the shear wall tests (Chapter 5). As illustrated in Figure 6. 22, the measurements revealed almost symmetrical upward and downward movements of the chords in linear proportion to the total wall deflection. The relationship between the total vertical displacement and the axial force in the chord was fit as an asymptotic equation (6.104) for each wall, and then, the average equation parameters A_0 and A_1 were found.

$$F_{chord} = \frac{A_0 \cdot (\delta_t + \delta_c)}{A_1 + (\delta_t + \delta_c)} \tag{6.104}$$

where, $F_{chord} = V \cdot H / L_c$, and L_c = distance between the forces in the chords.

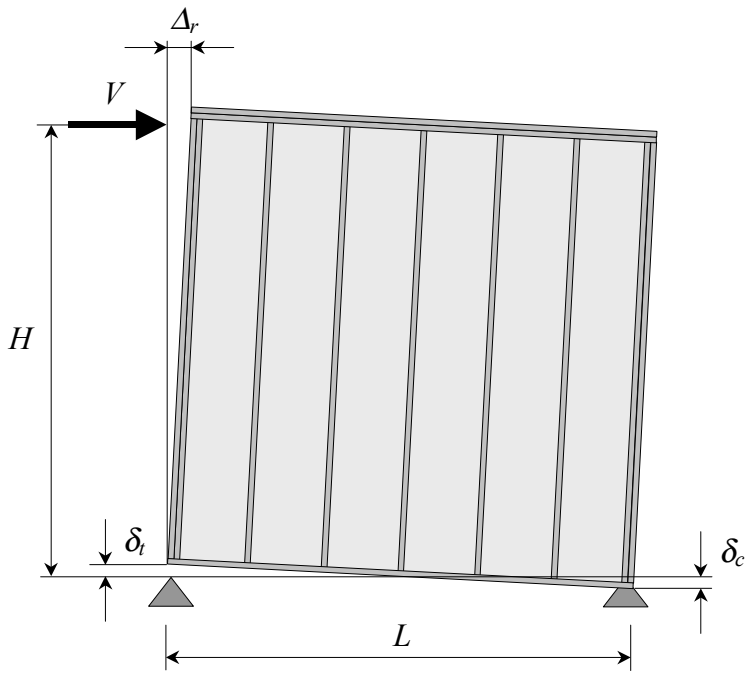

Figure 6. 21. Rigid body rotation of shear wall with tie-down anchors.

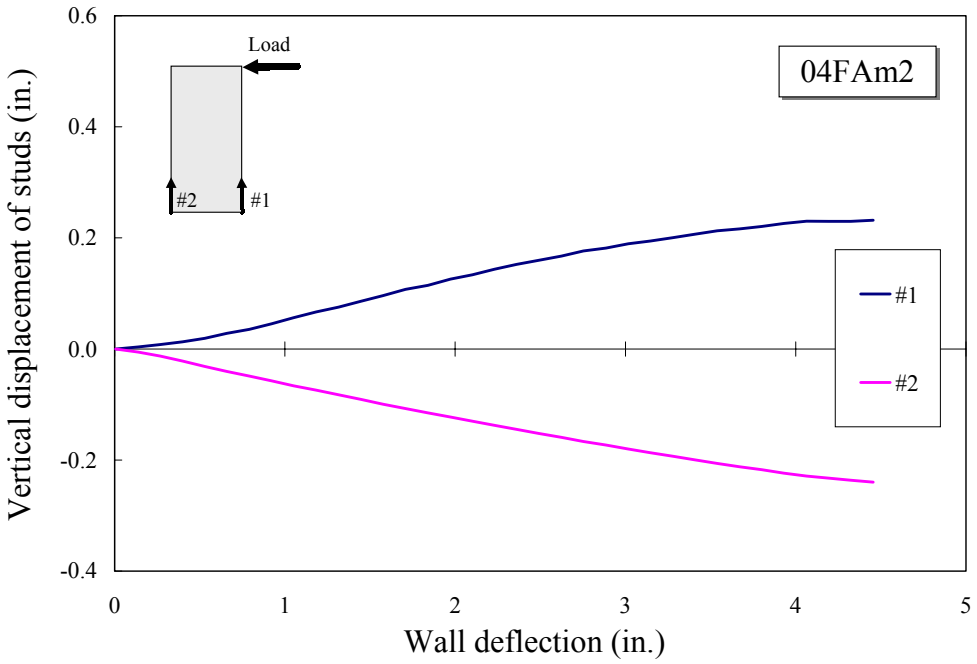

Figure 6. 22. Typical vertical displacements of chords in walls with the tie-down anchors.

The observed and predicted relationships are shown in Figure 6. 23. The regression parameters are shown in the U.S. customary units (lbf. and in.).

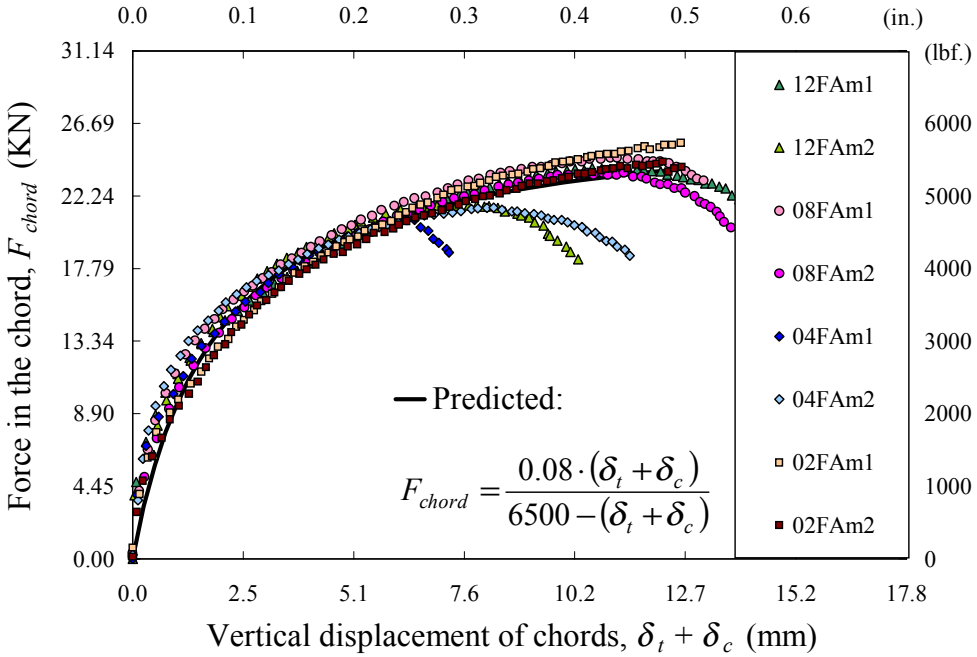

Figure 6. 23. Chord forces vs. vertical displacements of chords for walls tested in this study.

To estimate the vertical displacement of the chords during the analysis, the reciprocal function is used:

$$(\delta_t + \delta_c) = \frac{A_1 \cdot F_{chord}}{A_0 - F_{chord}} \tag{6.105}$$

Then, the deflection due to the rigid body rotation is determined:

$$\Delta_r = \frac{H}{L}(\delta_t + \delta_c) = \frac{H}{L} \cdot \frac{A_1 \cdot VH / L_c}{A_0 - VH / L_c} \tag{6.106}$$

In longer walls, L_c can be assumed equal L, for simplicity. However, in the narrow 0.6-m (2-ft.) walls, the magnitude of the chord forces is sensitive to L_c. Note that in fact, L_c is the distance between the resultant forces arising from the reactions in the anchors. From the experiments (Chapter 5), it was determined that for the relationship to comply with the other walls, L_c equals 610 - 90×2 = 430 mm (17 in.). Apparently, the rigid body rotation is the main reason for developing large deflections under low loads in the 0.6 –m (2-ft.) walls. For example, Δ_r exceeded 50 mm (2 in.) at the peak loads in **02FAm** walls.

6.6.2.4 Slip of Sheathing Fasteners

Sheathing fasteners resist the distortion of framing, and performance of the sheathing fasteners controls the load resistance and the load-deflection relationship of shear walls. By calculating the work of fasteners at a given wall deflection, the resisted load can be estimated. Two major assumptions are needed to assess the work of fasteners. One is the distortion pattern of the sheathing relative to the framing, and the other is the load-deflection relationship of the individual connection.

6.6.2.4.1 Distortion Pattern of Sheathing Connections

Tuomi and McCutcheon (1978) have assumed that the sheathing panel rotates about the center while the framing distorts as a parallelogram. Therefore, the slip of each fastener is proportional to its distance from the center of the panel. Numerous researchers (see Section 6.3) examined this assumption, and currently it is considered the simplest,

yet accurate, way of predicting deflections for fully-restrained shear walls. Figure 6. 24 illustrates the slip of sheathing fasteners in a single panel according to the McCutcheon's method.

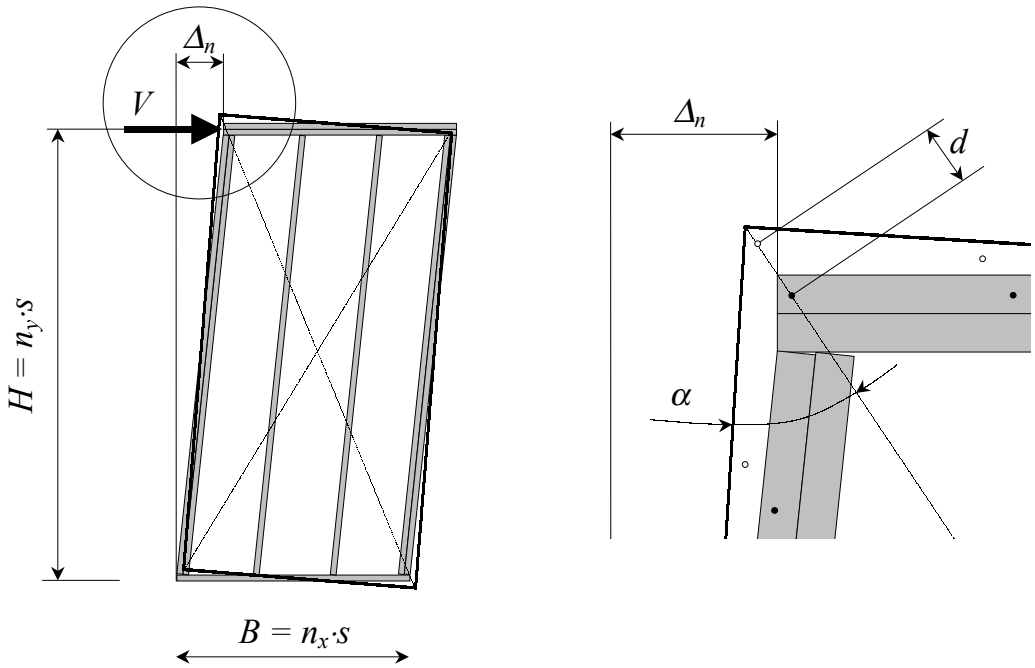

Figure 6. 24. Slip of sheathing fasteners.

Fasteners in the panel corners have the largest deformation, denoted as d. From the geometry of the panel distortion, it follows that the wall deflection can be expressed via the slip of these fasteners:

$$\Delta_n = \frac{2d}{\sin\alpha} \tag{6.107}$$

where, $\alpha = \arctan\left(\frac{B}{H}\right)$, the angle between the diagonal and the vertical edge of the panel.

Slip of fasteners, δ, is represented by two orthogonal components:

$$\delta = \sqrt{\delta_x^2 + \delta_y^2} \tag{6.108}$$

Given the spacing of fasteners along the perimeter, *s*, the number of spaces between the fasteners along the horizontal and vertical edges of the panel is $n_x = \frac{B}{s}$ and $n_y = \frac{H}{s}$, respectively. Then the slip of each fastener in the perimeter can be expressed as a portion of *d*:

$$\delta_{ij} = 2d\sqrt{\left(\frac{x_i}{B}\cos\alpha\right)^2 + \left(\frac{y_j}{H}\sin\alpha\right)^2} \tag{6.109}$$

where, $x_i = \frac{B}{2}\left(\frac{2i}{n_x} - 1\right)$ and $y_j = \frac{H}{2}\left(\frac{2j}{n_y} - 1\right)$, coordinates of the fastener relative to the center of the panel; $i = 0, 1, \ldots, n_x$ and $j = 0, 1, \ldots, n_y$.

Tuomi and McCutcheon (1978) also proposed that the distortions of the interior (field) fasteners follow the same pattern as the perimeter fasteners. For the 'rectangle' of the interior fasteners with sides $r_x B \times r_y H$, the coordinates are also found using Equation (6.109), where $x_i = \frac{r_x B}{2}\left(\frac{2i}{n_{rx}} - 1\right)$ and $y_j = \frac{r_y H}{2}\left(\frac{2j}{n_{ry}} - 1\right)$ and n_{rx}, n_{ry} are the number of horizontal and vertical spaces between the interior fasteners.

6.6.2.4.2 Load-Slip Relationship of Sheathing Connections

Patton-Mallory and McCutcheon (1987) compared four load-slip relationships for sheathing-to-framing nailed connections and concluded that the asymptotic curve was the best to describe the connection behavior until maximum load:

$$F_n = \frac{A_0 \cdot \delta}{A_1 + \delta} \tag{6.110}$$

Parameters A_0 and A_1 have physical meanings: A_0 represents the asymptotic strength of the connection and A_1 represents the slip at half the asymptotic strength. A_1 can also be represented as a factored service slip (Deam 1997) as is shown in Figure 6. 25:

$$F_n = \frac{F_a \cdot \delta}{1.5\delta_s + \delta} \tag{6.111}$$

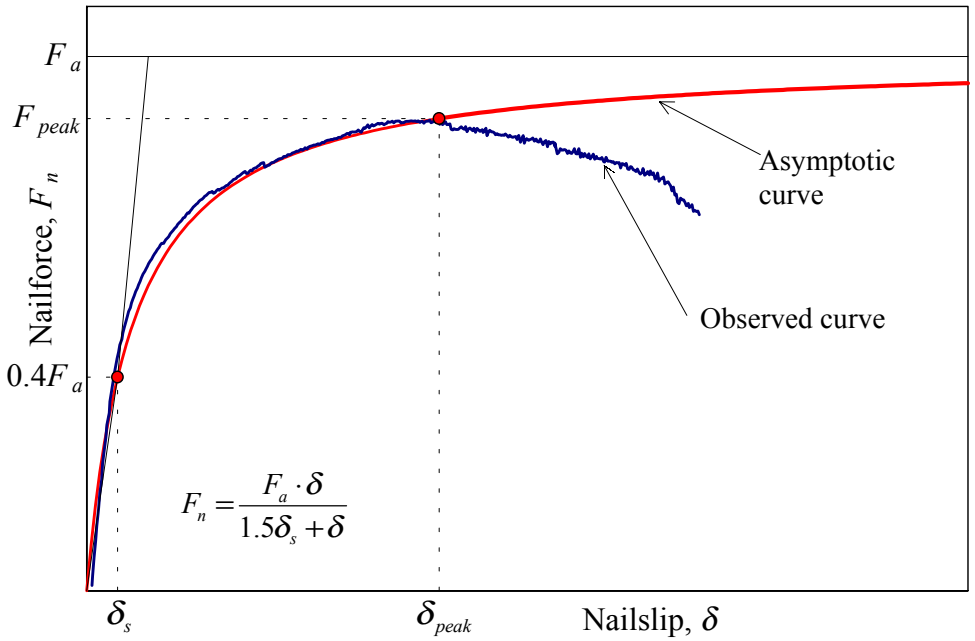

Figure 6. 25. Asymptotic approximation of load-slip curve.

If the connection slip is not limited by the peak deflection, predictions of the connection and shear wall capacities are overestimated. Furthermore, deflections at the maximum load and failure of the wall cannot be predicted. To describe connection performance more accurately, the degradation portion is added to the load-slip curve. The form of the degradation portion is not important as long as it does not complicate the integration of the equation for use in shear wall analysis. The circular curve shown in Figure 6. 26 meets this requirement and fits the test results with sufficient accuracy (Chapter 4):

$$F_n = F_{peak}\sqrt{1 - \frac{(\delta - \delta_{peak})^2}{\delta_0^2}} \tag{6.112}$$

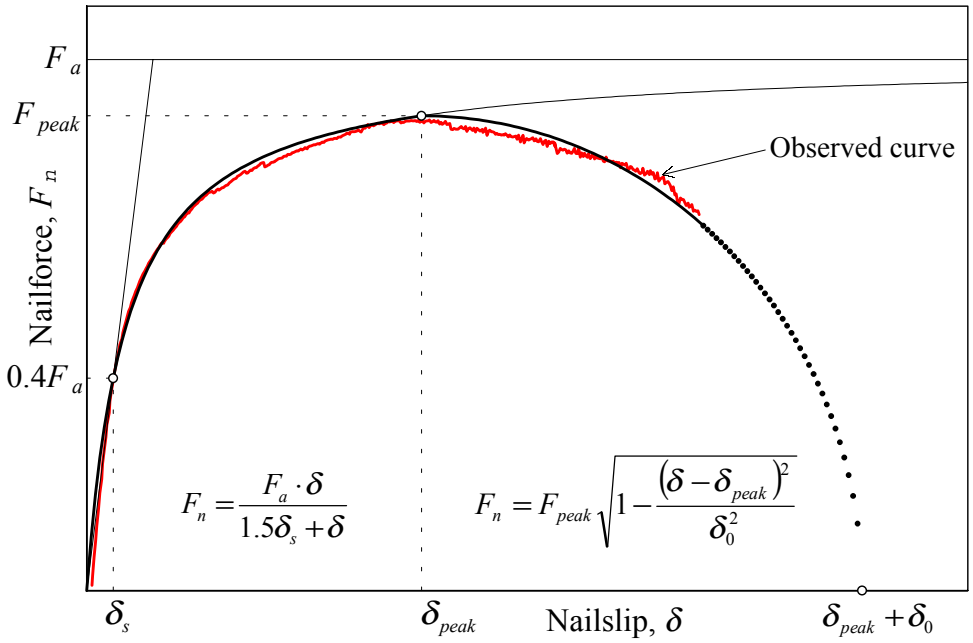

Figure 6. 26. Asymptotic-circle approximation of load-slip curve.

The physical meaning of δ_0 is the additional slip of the connection beyond δ_{peak} until zero force is reached. Therefore, the connection slip is limited by the following condition:

$$\delta \le \delta_{peak} + \delta_0 \tag{6.113}$$

For example, it was found that δ_0 = 12.7 mm (0.5 in.) produced a reasonable estimate of the post-capacity performance for the nailed connections described in Chapter 4. Then, in the U.S. customary units the tail curve is expressed as follows:

$$F_n = F_{peak}\sqrt{1 - 4(\delta - \delta_{peak})^2} \tag{6.114}$$

6.6.2.4.3 Work of Sheathing Connections in Shear Wall

To estimate the force resisted by sheathing connections in shear wall, the energy method is used as described by McCutcheon (1985). The external energy applied to the wall is defined as the area under the load-deflection curve, V-Δ_n:

$$E = \sum \int_0^{\Delta_n} V dx \tag{6.115}$$

Similarly, the internal energy absorbed by the fasteners is the sum of the areas under their individual load-slip curves:

$$I = \sum \int_0^{\delta} F_n dx \tag{6.116}$$

When the external and internal energies are equal, the external racking load is found. After differentiation of the internal energy:

$$V = \frac{\partial E}{\partial \Delta_n} = \frac{\partial I}{\partial \Delta_n} = \frac{\partial}{\partial \Delta_n} \sum \int_0^{\delta} F_n dx \tag{6.117}$$

The area under the asymptotic curve described by Equation (6.110), is found as:

$$\int_0^{\delta} F_n dx = \int_0^{\delta} \frac{A_0 x}{A_1 + x} dx = A_0 \left(\delta + A_1 \ln \left(\frac{A_1}{A_1 + \delta} \right) \right) \tag{6.118}$$

From Equations (6.107) and (6.109), the slip of each fastener is expressed as a portion of the wall deflection Δ_n:

$$\delta_{ij} = K_{ij} \Delta_n \tag{6.119}$$

where, $$K_{ij} = \sin\alpha \sqrt{\left(\frac{x_i}{B} \cos\alpha \right)^2 + \left(\frac{y_j}{H} \sin\alpha \right)^2} \tag{6.120}$$

Therefore, the internal energy can be expressed in terms of Δ_n as

$$I = A_0 \sum \left(K_{ij} \Delta_n + A_1 \ln \left(\frac{A_1}{A_1 + K_i \Delta_n} \right) \right) \tag{6.121}$$

After differentiation:

$$V = A_0 \sum \left(K_{ij} - \frac{A_1 K_{ij}}{A_1 + K_i \Delta_n} \right) = A_0 \sum \left(\frac{K_{ij}^2 \Delta_1}{A_1 + K_{ij} \Delta_n} \right) \tag{6.122}$$

It follows from Equation (6.122) that the asymptotic load capacity of shear wall can be estimated simply as:

$$V_a = A_0 \sum K_{ij} \tag{6.123}$$

V_a depends only on aspect ratio of the panel ($\alpha = H/B$), the spacing of fasteners (s), and the asymptotic strength of the sheathing connections ($A_0 = F_a$). If F_{peak} is used instead of F_a, the approximate shear wall capacity V_{peak} can be found without overestimation. The shear load capacity of a multiple-panel wall is determined as:

$$V_{peak} = nF_{peak} \sum K_{ij} \tag{6.124}$$

where, n = number of panels in shear wall,

$\sum K_{ij}$ = constant value characterizing the fastener' schedule.

To estimate the shear wall strength more accurately and to determine the deflections at the peak load and failure, the degradation portion of the sheathing fasteners' load-slip curve is added to the formulation of the model. Integration of Equation (6.112) with δ substituted from Equation (6.117) and further differentiation gives:

$$\frac{\partial}{\partial \Delta_n} \int_0^{\Delta_n} F_{peak} \sqrt{1 - \frac{\left(K_{ij} x - \delta_{peak}\right)^2}{\delta_0^2}} = K_{ij} F_{peak} \sqrt{1 - \frac{\left(\delta_{peak} - K_{ij} \Delta_n\right)^2}{\delta_0^2}} \tag{6.125}$$

Now, the external racking load is found as a sum of contributions from each fastener depending on the fastener slip under the following conditions:

$$V = \sum v_{nij} \tag{6.126}$$

where, $v_{nij} = \dfrac{K_{ij}^2 F_a \Delta_n}{1.5\delta_s + K_{ij} \Delta_n}$, if $K_{ij} \Delta_n \le \delta_{peak}$,

$$v_{nij} = K_{ij} F_{peak} \sqrt{1 - \frac{\left(\delta_{peak} - K_{ij}\Delta_n\right)^2}{\delta_0^2}}\ , \text{ if } \frac{\delta_{peak} - K_{ij}\Delta_n}{\delta_0} \le 1 \text{, else}$$

$$v_{nij} = 0\ .$$

6.6.2.5 Computational Algorithm

Now, after all components of shear wall deflection have been presented, the computational algorithm can be formulated. Figure 6. 27 presents the flowchart of the load-deflection calculation for shear walls with tie-down anchors at the wall ends.

For shear walls with sheathing panels of equal size, the input requires the number of panels (n), height (H) and width (B) of the panels and their rigidity ($G_v t_v$), and stiffness of chords (EA). Parameters of rigid body rotation (as a function of tie-down restraint) and sheathing connections are input as described in Sections 6.6.2.3 and 6.6.2.4. Then, the racking force exerted by the sheathing connections is calculated for each increment of deflection Δ_n as described in Section 6.6.2.4.3. Next, the deflection components due to chord bending (Δ_b), sheathing shear (Δ_s), and rigid body rotation (Δ_r) are calculated and added to the deflection caused by the slip of sheathing connections (Δ_n). Values of the racking force and the corresponding total deflection are stored. The process is repeated incrementally until the racking force equals zero or another criterion is imposed. The output can include the entire load-deflection curve and/or characteristic parameters determined from the curve, such as the peak load and corresponding deflection, secant or tangent stiffness at any point, etc.

For shear walls with the sheathing panels of different sizes, the algorithm can be modified such that the racking forces V_i in the i-th panel are calculated and added to determine (Δ_b), (Δ_s), and (Δ_r).

Since the algorithm includes closed-form equations, the formalizing and computing are easily performed using a spreadsheet or programmable calculator. The computation time is virtually instantaneous for any reasonable number of deflection increments.

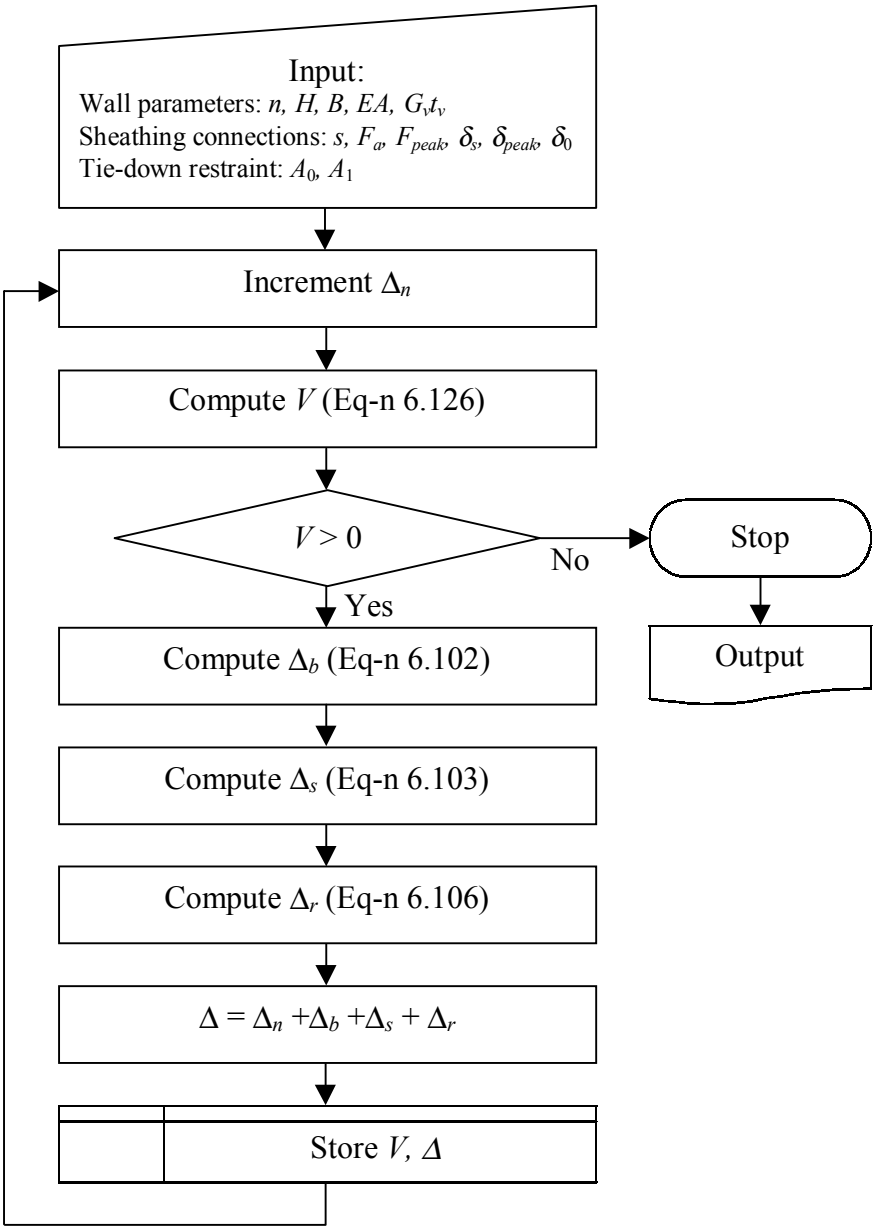

Figure 6. 27. Flowchart of load-deflection calculation.

6.6.2.6 Comparative Analysis of the Model Predictions and Experimental Results

The proposed method was applied to predict the racking performance of shear wall specimens discussed in Chapter 5. The mechanical properties of the shear wall components were determined as described in Chapter 4. The sheathing panel rigidity was taken from the APA publication (APA 1995). The bending stiffness of studs was taken from the Metriguard tests, although the contribution of the flexural deformations in the

total wall deflection was not significant. For the sheathing nailed connections, parameters from Table 4. 7 were used. To account for the rigid body rotation, the parameters A_0 and A_1 in Equation (6.106) were used as is shown in Figure 6. 23 for all shear walls. Note that these parameters are valid only for the tie-down connectors used in these tests. For other types of connectors, the manufacturers should provide similar information or physical tests would be needed to obtain accurate predictions.

Figure 6. 28 through Figure 6. 31 illustrate the load-deflection curves for each of the tested shear walls. As discussed in Chapter 5, framing elements with the lowest density governed the shear wall performance, because the nailed connections in these elements were less strong and served as a weak link in a chain. This observation was confirmed by the model analysis because the best predictions were achieved when the lower limits of the observed parameters for the perpendicular-to-grain connections with 19-mm (3/4 in.) edge distance were used. The predicted curves illustrated in Figure 6. 28 through Figure 6. 31 are remarkably similar in shape with the observed curves.

Note that the predicted curves are somewhat steeper than the experimental curves. If the stiffness parameters of the sheathing connections were reduced by approximately 15%, a perfect match with the experimental shear wall deflection curves could be achieved. The most likely cause was the test fixture for the sheathing connections provided more restraint to the nail-slip than it was present in the shear wall tests.

Table 6. 17 shows load capacities of the shear walls determined experimentally and from using Equations (6.124) and (6.126). The capacities of the two-and three-panel walls were predicted with 5% accuracy. The racking performance of these walls was governed by the properties of the sheathing connections and was only slightly sensitive to the variations in other components of the deflection.

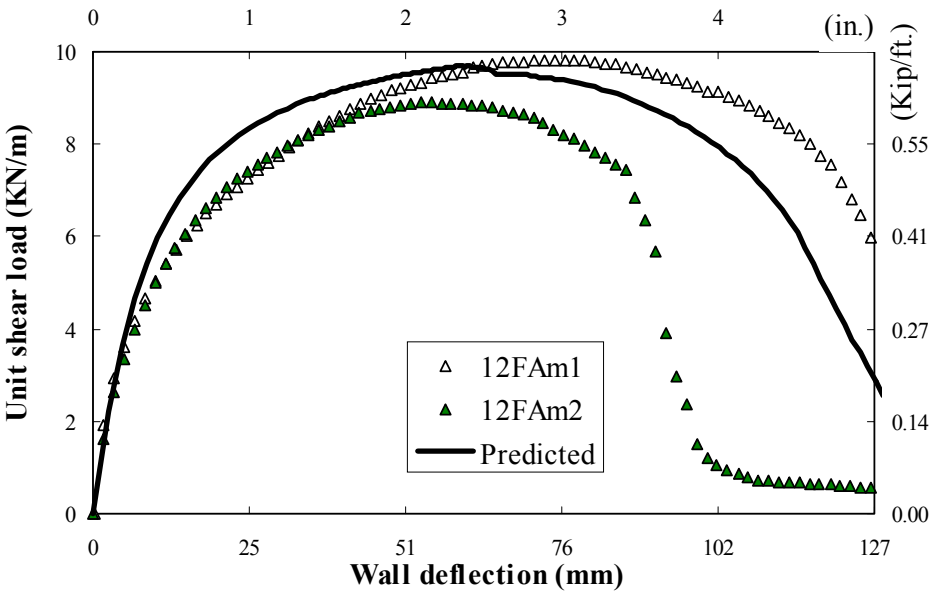

Figure 6. 28. Experimental and predicted load-deflection curves for 3.6-m (12-ft.) walls.

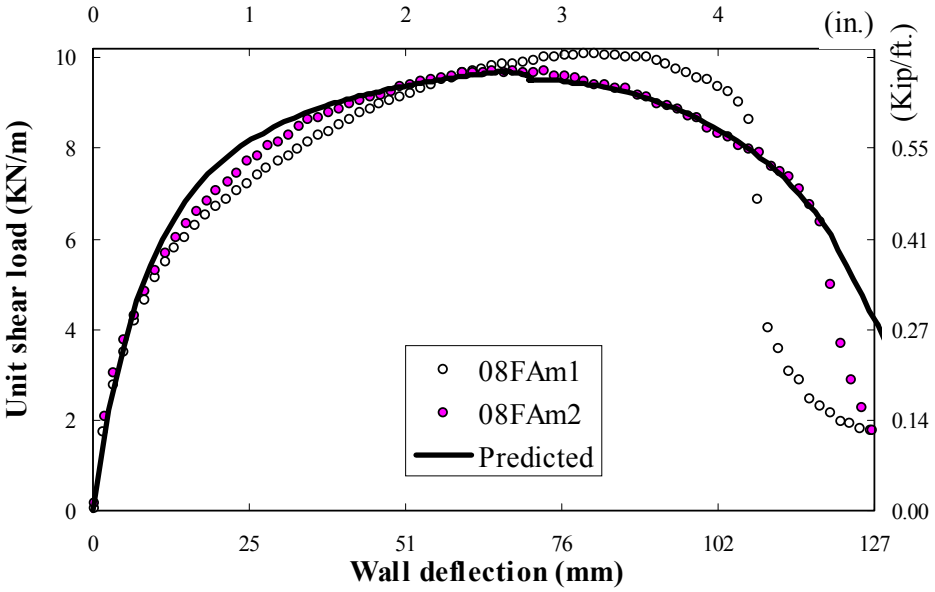

Figure 6. 29. Experimental and predicted load-deflection curves for 2.4-m (8-ft.) walls.

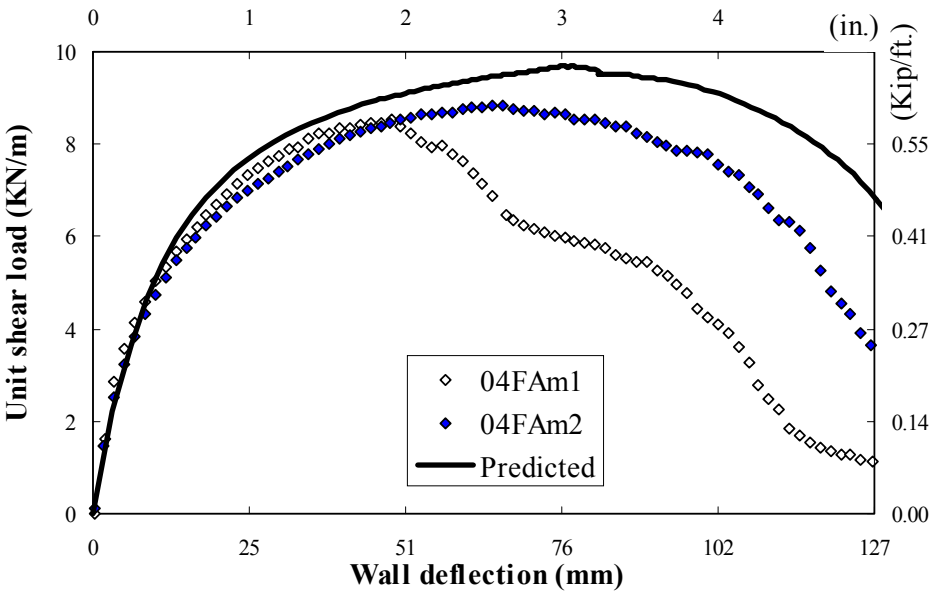

Figure 6. 30. Experimental and predicted load-deflection curves for 1.2-m (4-ft.) walls.

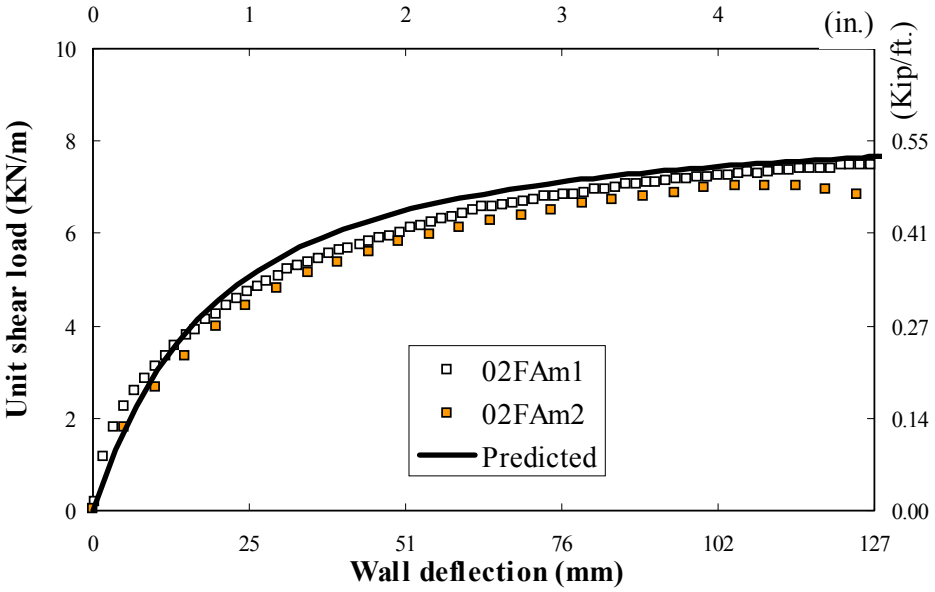

Figure 6. 31. Experimental and predicted load-deflection curves for 0.6-m (2-ft.) walls.

Both experimental and analytical parameters of the single-panel walls were significantly different from the multi-panel walls. Experimental results of the 1.2-m (4-ft.) walls were on average 12% lower then those of the two- and three-panel walls, which was originally attributed to the lower density of the framing in these walls (see Chapter 5). Equations (6.124) and (6.126) overestimated the load capacity of these walls by approximately the same amount. By inputting the lower parameters for the sheathing connections, this overestimation of wall performance could be reduced. But there is another reason for the lower performance of the single-panel walls. Due to the smaller distance between the chords, the wall deflections become extremely sensitive to the anchor forces.

The capacity of the 0.6-m (2-ft.) walls was also overestimated if based on the sheathing nail strength. Apparently, the performance of the narrow walls was governed by the large deflections associated with rigid body rotation and/or yielding of fasteners attaching the anchors to the chords. As is shown in Figure 6. 23, the axial forces in the chords of 1.2-m (4-ft.) walls reached maximum before the sheathing nails developed their full capacity. Therefore, the sheathing connections in these walls did not develop the full nail strength within the practical deflection range. If the capacity is determined within some limited deflection range, the predictions are no less accurate than for the other walls.

Table 6. 17. Experimental and predicted load capacities of shear walls, Kips.

Wall length Ft.	**Experimental**		**Equation (6.124)**		**Equation (6.126)**	
	FAm1	FAm2	Predicted	Predicted / Avg. Experim	Predicted	Predicted / Avg. Experim
12	8.143	7.353	7.883	1.017	7.975	1.029
8	5.559	5.344	5.255	0.964	5.317	0.975
4	2.342	2.425	2.628	1.102	2.658	1.115
2	1.045	0.978	1.126	1.113	1.329	1.314

Note: 1 ft. = 305 mm, 1 Kip. = 4.45 KN

As opposed to multi-panel walls, deflections of single-panel walls were extremely sensitive to the rigid body rotation parameters of Equation (6.106). At the same time, 0.6-m (2-ft.) walls were only slightly sensitive to the parameters of the sheathing

connections. Performance of 1.2-m (4-ft.) walls was highly sensitive to the both forces in the anchors and in sheathing nails. This explains the high variation in the experimental parameters of these walls.

6.6.2.7 Simple Calculation of the Shear Wall Deflections. Example

Note that the approximate Equation (6.124) produced slightly more conservative yet accurate load capacity predictions relative to the exact calculations. Therefore, it could be implemented for the design purposes. Since $\sum K_{ij}$ is a constant geometric characteristic of a particular nailing pattern, it could be tabulated for typical panel sizes and fastener' schedules. To determine the shear wall capacity, the designer only needs to multiply this number from the table by the appropriate fastener's strength and the number of panels in the wall. If the wall consists of different size segments, then the shear capacities are calculated for each segment independently and then superimposed.

The analysis of shear wall deflections and the distribution of forces among the nails indicated that wall capacity was reached when the corner nails reached their capacity. This allows a simple and accurate estimation of the peak shear wall deflection due to nail-slip from Equation (6.107), where $d = \delta_{peak}$ is the nail-slip at peak load, determined from the tests of individual fasteners. Then, the total shear wall deflection at the peak load is determined from Equation (6.100).

For example, in this analysis the nail characteristics were taken from Table 4.7:

δ_{peak} = (25.4)·(0.42) in. = 10.69 mm, and

F_{peak} = (4.45)·(0.258) Kip = 1.148 KN.

Then, from Equation (6.107):

$$\Delta_n = \frac{2d}{\sin\alpha} = \frac{(2)\cdot(10.69)}{0.4472} = 47.71\,\text{mm} = 1.878\ \text{in.} \tag{6.127}$$

Then, for the two-panel shear wall, from Equation (6.124):

$$V_{peak} = nF_{peak}\sum K_{ij} = (2)\cdot(1.148)\cdot(10.69) = 23.40\,\text{KN} = 5.26\ \text{Kip} \tag{6.128}$$

where, $\sum K_{ij} = 10.19$.

The other deflection components are found from Equations (6.101), (6.103), and (6.106):

$$\Delta_b = \frac{VH^3}{3EI_{ef}} = \frac{(23.40)\cdot(2438)^2}{(3)\cdot(14.7\times10^6)\cdot(2.467\times10^9)} = 1.53\,\text{mm}, = 0.078\ \text{in.} \qquad (6.129)$$

$$\text{where, } I_{ef} = \frac{A(L-b)^2}{2}\cdot k_J = \frac{(2)\cdot(89\times38)\cdot(2438-1219)^2}{2}\cdot 0.49 = 2.467\times10^9\ \text{mm}^4$$

$$= 2963\ \text{in.}^4 \qquad (6.130)$$

$$\Delta_s = \frac{VH}{G_v t_v L} = \frac{(23.40)\cdot(2438)}{(83.70)\cdot(2438)} = 1.60\,\text{mm} = 0.063\ \text{in.} \qquad (6.131)$$

$$\Delta_r = \frac{H}{L}\cdot\frac{A_1\cdot V\,H/L_c}{A_0 - VH/L_c} = \frac{2438}{2438}\cdot\frac{(28900)\cdot(23400)\cdot(2438)/(2438-178)}{2-(23400)\cdot(2438)/(2438-178)} =$$

$$= 8.75\ \text{mm} = 0.549\ \text{in.} \qquad (6.132)$$

$$\Delta_{peak} = \Delta_b + \Delta_s + \Delta_r + \Delta_n = 1.53 + 1.60 + 8.75 + 47.71 = 59.59\ \text{mm} = 2.568\ \text{in.} \qquad (6.133)$$

Similarly, the deflection at the design load can be predicted. For example, assuming the design load 40% of V_{peak} from Table 4.7:

δ_s = (25.4)·(0.035) in. = 0.89 mm, and

$0.4F_{peak}$ = (0.4)·(4.45)·(0.258) Kip = 0.459 KN.

Substituting these values into Equations (6.127) through (6.133), one can get the total elastic deflection of the shear wall:

$$\Delta_{elastic} = \Delta_b + \Delta_s + \Delta_r + \Delta_n = 0.61 + 0.64 + 0.98 + 3.98 = 6.20\ \text{mm} = 0.256\ \text{in.} \qquad (6.134)$$

at 0.4 V_{peak} = 9.358 KN = 2.104 Kips.

6.6.2.8 Conclusions on the Deflections of Shear Walls with Tie-Down Anchors

In this section, the method of estimating the nonlinear racking deflections of the anchored shear walls is introduced. The total deflection is represented as a superposition of the four components: a) deflection due to the chord bending, b) deflection due to sheathing shear, c) deflection due to rigid body rotation (due to hold-down displacements, and d) deflection due to slip of sheathing fasteners.

Racking performance of the multiple-panel shear walls can be accurately predicted via the calculating work of the sheathing fasteners on the racking displacement. Deflections and the load capacity of these walls can be accurately predicted using simple formulae presented in this section. Introducing the limitations on the strength and deflection in the sheathing fastener load-deflection curve allows accurate approximation of the shear wall load via calculating the work of the sheathing fasteners.

Performance of single-panel walls is largely dependent on the rigid body rotation and performance of the tie-down restraint. It was found that the resistance of the tie-down restraint introduces an additional non-linearity in the shear wall deflections. In this study, the non-linear rigid body rotation was approximated by an empirically fit asymptotic function. However, more accurate approximations can be suggested in the future research to properly account for the effect of the tie-down restraint on the performance of single-panel shear walls. Various types of tie-down devices should be tested on narrow walls to make their performance parameters available to the design profession. This is an important task, because many historical failures during earthquakes occurred due to structural damage to narrow walls.

One of the steps in studying the effects of overturning restraint on the shear wall performance is to study the racking response of unrestrained shear walls. A method of predicting deflections of the unrestrained shear walls is presented in the next section.

6.6.3 Shear Walls without Tie-Down Restraint

If the bottom framing plate is attached to the platform or foundation adequately to prevent the plate from uplifting, deflections of shear walls without tie-down restraint include the same four components as discussed in Section 6.6.2 and given by Equation (6.100). The deflections due to chord bending (Δ_b) and sheathing shear (Δ_s) can be determined using Equations (6.101) and (6.103), respectively. The magnitudes and the contribution of Δ_b and Δ_s into the total wall deflection are significantly smaller, because the unrestrained walls resist lower loads. Deflections due to rigid body rotation (Δ_r) and slip of sheathing fasteners (Δ_n) are determined differently as discussed in the following paragraphs.

6.6.3.1 Rigid Body Rotation

It was shown experimentally (Chapter 5) that the rigid body rotation of shear walls without tie-down restraint was significantly higher than the rotation of fully-restrained walls. Uplift displacement of the unrestrained tension chord exceeded the downward displacement of the compression chord as is shown in Figure 6. 32.

In fact, the nature of the wall rotation was totally different from that observed in the anchored walls, where rotation was due to hold-down displacements as a function of the axial forces in the chords and was slightly dependent of the wall aspect ratio (see Figure 6. 23). In unrestrained walls, the rotation appeared as a function of the aspect ratio and the number of panels in the wall. Apparently, the total vertical movement of the chords was in linear proportion to the total wall deflection as is shown in Figure 6. 33:

$$(\delta_t + \delta_c) = A_0 \cdot \Delta \tag{6.135}$$

Assuming that the relationship between the vertical displacements of chords and rigid body deflection holds true (see Figure 6. 21):

$$\Delta_r = \frac{H}{L}(\delta_t + \delta_c) = \frac{H}{L} \cdot A_0 \cdot \Delta, \tag{6.136}$$

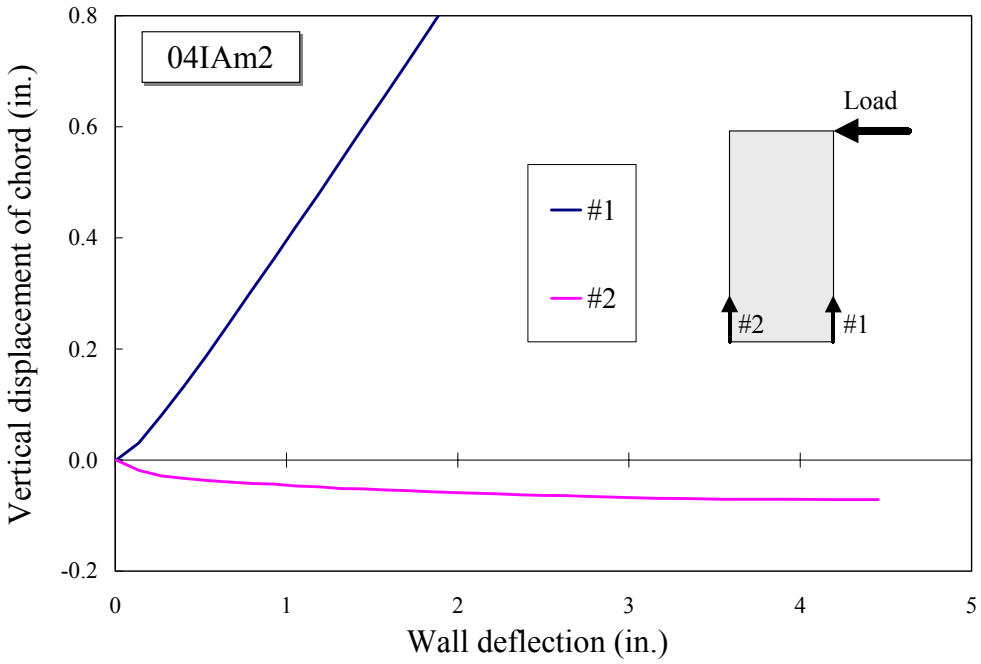

Figure 6. 32. Vertical displacements of chords in unrestrained walls.

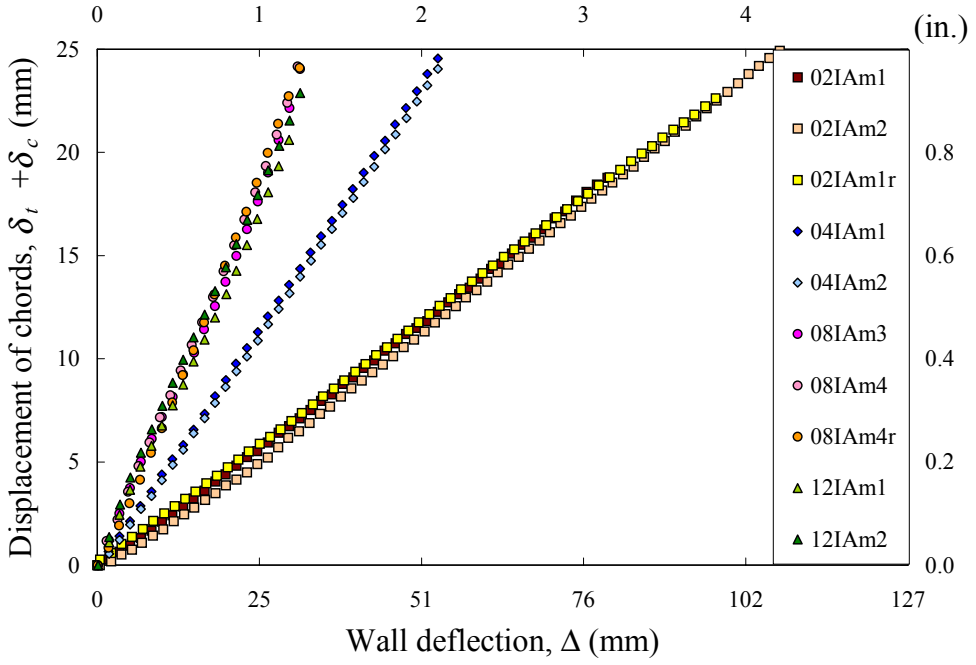

Figure 6. 33. Vertical displacements of chords in unrestrained walls.

Therefore, from Equation (6.100):

$$\left(1 - A_0 \frac{H}{L}\right)\Delta = \Delta_n + \Delta_s + \Delta_b, \tag{6.137}$$

Table 6. 18 shows the average ratios between the components of shear wall deflection for the tested walls (Chapter 5) determined from these assumptions.

Table 6. 18. Ratios between components of shear wall deflection.

Wall	$\frac{H}{L}$	A_0	$\frac{\Delta_r}{\Delta}$	$\frac{\Delta_n + \Delta_s + \Delta_b}{\Delta}$
02IAm	4	0.24	0.96	0.04
04IAm	2	0.46	0.92	0.08
08IAm	1	0.74	0.74	0.26
12IAm	2/3	0.75	0.50	0.50

As is seen from Table 6. 18, 96% of the 0.6-m (2-ft.) shear wall is due to the rigid body rotation. Resistance of the sheathing fasteners along the bottom plate governs the resistance of the wall. Sheathing panel distortion, chord bending, and the slip of sheathing fasteners along the chords and the top plate contribute only 4% to the total wall deflection of 0.6-m (2-ft.) walls. In 1.2-m (4-ft.) walls, the combined contribution of Δ_n, Δ_s, and Δ_b is twice that associated with 0.6-m (2-ft.) walls, but it is still no more than 8% of the total wall deflection. These assumptions are confirmed by the measurements of the sheathing displacements during the tests (Chapter 5). Sheathing displacements relative to the framing did not exceed 0.25 mm (0.01-in.) in **02IAm** walls and 0.78 mm (0.03 in.) in **04IAm** walls in all locations except along the bottom plate.

In shear walls with two and three panels, the contribution of Δ_n, Δ_s, and Δ_b increased considerably. In **08IAm** walls, the contribution was 26% and in **12IAm** walls the contribution was 50%. Recall that the derivation of the strength model (Section 6.5) arrived at the similar conclusions: the second and the third panels develop significant racking due to restraining effect of the adjacent panels.

To estimate the contribution of the rigid body rotation to the wall deflection analytically, it is assumed to be entirely due to the work of the sheathing fasteners along the bottom plate. Assuming the distribution of the forces in the fasteners from the elastic

analysis, the following relationship between the displacement of the sheathing bottom edge and the Δ_r is assumed

$$\Delta_r = \alpha\left(c + \frac{u_{21}}{v_{n1}}\right)\delta_y\,, \tag{6.138}$$

where, c and $\frac{u_{21}}{v_{n1}}$ = relationships from Table 6. 2, Table 6. 6, and Table 6. 8.

δ_y = vertical component of the sheathing fastener slip in the bottom-left corner of the first panel.

6.6.3.2 Slip of Sheathing Fasteners

To estimate the contribution of the sheathing fasteners into the wall deflection and resistance, a similar approach is used as discussed in Section 6.6.2.4. However, it is convenient to relate the displacement and work of all the fasteners to Δ_r, because it is a function of the fasteners' slip at the bottom plate as discussed in Section 6.6.3.1. The contribution of other sheathing fasteners into the wall deflection, Δ_n, is then found from the following relationship (in place of Equation (6.107))

$$\Delta_n = \frac{d}{c} \tag{6.139}$$

where,

$$d = \sqrt{\delta_x^2 + \delta_y^2} = \delta_y\sqrt{1 + \frac{1}{c^2}} \tag{6.140}$$

Then, from Equation (6.138)

$$\Delta_n = \frac{\sqrt{1 + \frac{1}{c^2}}}{\alpha c\left(c + \frac{u_{21}}{v_{n1}}\right)}\Delta_r \tag{6.141}$$

Equation (6.119) is then replaced by

$$\delta_{ij} = K_{ij}\Delta_r \tag{6.142}$$

The distortion pattern of the fasteners is taken from the elastic analysis (see Table 6. 2, Table 6. 6, and Table 6. 8) and the geometric constant K_{ij} is found as follows:

For the *i*-th fastener in the first bottom plate

$$\delta_{bi} = \sqrt{\delta_x^2 + \delta_{yi}^2} \tag{6.143}$$

where, $\delta_x = \dfrac{\delta_y}{c}$ and $\delta_{yi} = B\left(1 - \dfrac{a_1}{B} - \dfrac{i}{n_i}\right)\delta_y$.

Therefore,

$$K_{b1i} = \frac{\delta_{bi}}{\Delta_r} = \frac{1}{\alpha\left(c + \dfrac{u_{21}}{v_{n1}}\right)} \cdot \sqrt{\left(\frac{1}{c}\right)^2 + B^2\left(1 - \frac{a_1}{B} - \frac{i}{n_i}\right)^2} \tag{6.144}$$

For the *i*-th fastener in the *k*-th bottom plate

$$\delta_{bki} = \sqrt{\delta_{xk}^2 + \delta_{yki}^2} \tag{6.145}$$

where, $\delta_{xk} = \dfrac{v_{nk}}{v_{n1}}\delta_x$ and $\delta_{yki} = B\dfrac{u_{nk}}{cv_{n1}}\left(1 - \dfrac{a_k}{B} - \dfrac{i}{n_i}\right)\delta_y$.

Therefore,

$$K_{bki} = \frac{\delta_{bki}}{\Delta_r} = \frac{1}{\alpha c\left(c + \dfrac{u_{21}}{v_{n1}}\right)} \cdot \sqrt{\left(\frac{v_{nk}}{v_{n1}}\right)^2 + B^2\left(\frac{u_{nk}}{v_{n1}}\right)^2\left(1 - \frac{a_k}{B} - \frac{i}{n_i}\right)^2} \tag{6.146}$$

Similarly, the slip of fasteners in the *k*-th top plate

$$\delta_{xk} = \frac{v_{nk}}{v_{n1}}\delta_x \text{ and } \delta_{yki} = B\frac{u_{1k}}{cv_{n1}}\left(1 - \frac{a_{1k}}{B} - \frac{i}{n_i}\right)\delta_y \tag{6.147}$$

$$K_{tki} = \frac{\delta_{tki}}{\Delta_r} = \frac{1}{\alpha c\left(c + \dfrac{u_{21}}{v_{n1}}\right)} \cdot \sqrt{\left(\frac{v_{nk}}{v_{n1}}\right)^2 + B^2\left(\frac{u_{1k}}{v_{n1}}\right)^2\left(1 - \frac{a_k}{B} - \frac{i}{n_i}\right)^2} \tag{6.148}$$

For the *j*-th fastener in the left chord of the *k*-th panel

$$\delta_{xkj} = \frac{2\delta_{xk}}{\alpha B}\left(\frac{\alpha B}{2} - \frac{j}{n_j}\alpha B\right) = \frac{2v_{nk}}{cv_{n1}}\left(\frac{1}{2} - \frac{j}{n_j}\right)\delta_y \text{ and } \delta_{yk1} = \frac{u_{1k}}{cv_{n1}}\delta_y \tag{6.149}$$

$$K_{ck1j} = \frac{\delta_{ck1j}}{\Delta_n} = \frac{1}{\alpha c\left(c + \dfrac{u_{21}}{v_{n1}}\right)}\sqrt{4\left(\frac{v_{nk}}{v_{n1}}\right)^2\left(\frac{1}{2} - \frac{j}{n_j}\right)^2 + \left(\frac{u_{1k}}{v_{n1}}\right)^2} \tag{6.150}$$

Similarly, for the right chord of the *k*-th panel

$$K_{ck2j} = \frac{\delta_{ck2j}}{\Delta_n} = \frac{1}{\alpha c\left(c + \dfrac{u_{21}}{v_{n1}}\right)}\sqrt{4\left(\frac{v_{nk}}{v_{n1}}\right)^2\left(\frac{1}{2} - \frac{j}{n_j}\right)^2 + \left(\frac{u_{2k}}{v_{n1}}\right)^2} \tag{6.151}$$

In Equations (6.143) through (6.151)

$i = 0, 1, \ldots, n_x$ and $j = 1, 2, \ldots, n_y\text{-}1$,

where, n_x = number of spaces between the fasteners in the plate,

n_y = number of spaces between the fasteners in the chord.

Then, the work of the sheathing connections is calculated from Equation (6.126).

6.6.3.3 Computational Algorithm

The computation of deflections for unrestrained shear walls follows the algorithm shown in Figure 6. 34. Basically, the algorithm is similar to that of anchored shear walls presented in Section 6.6.2.5. The racking force is calculated for the increments of Δ_r instead of Δ_n. Then, Δ_n, Δ_b, and Δ_s are calculated from Equations (6.141), (6.101), and (6.103), respectively. The total deflection is found from Equation (6.100). Note that the method produces the racking force on the entire wall for a given Δ_r.

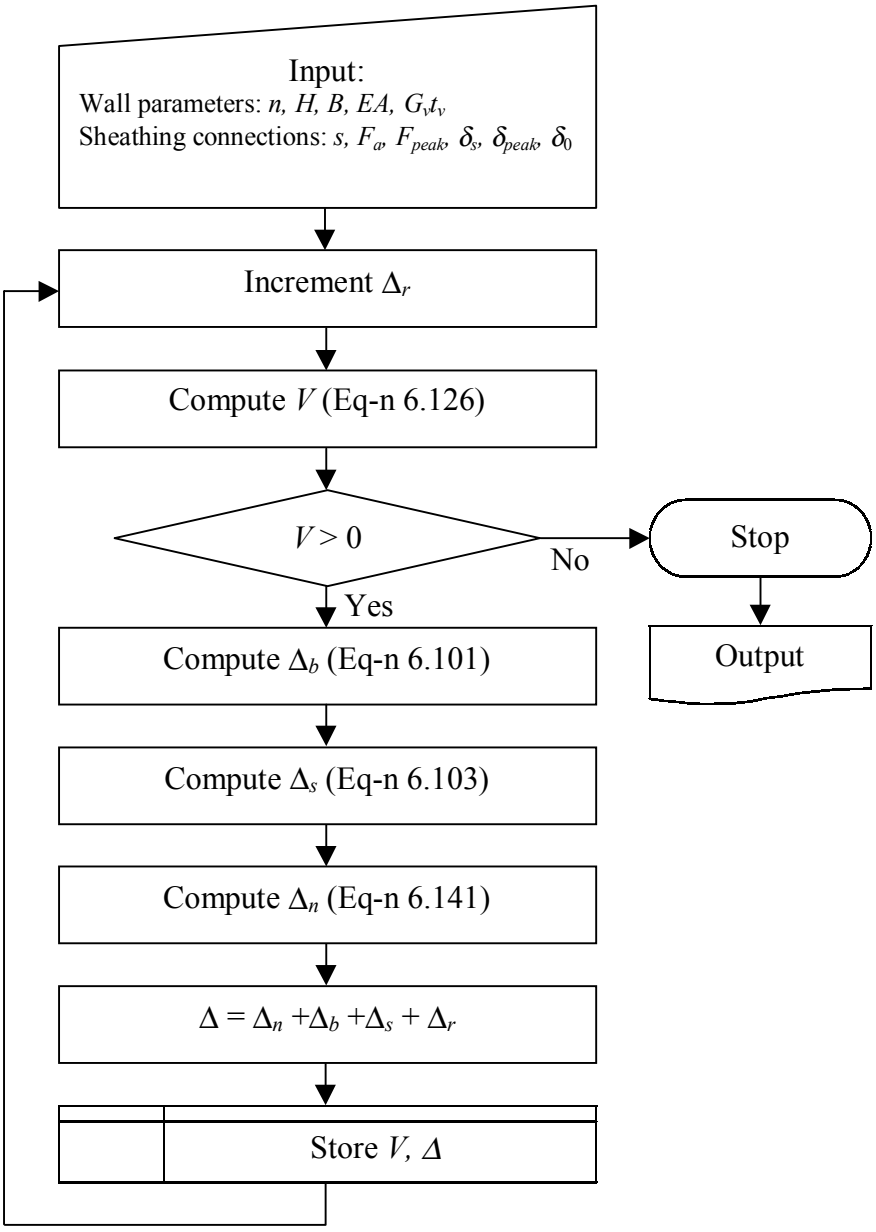

Figure 6. 34. Flowchart of load-deflection calculation. Unrestrained walls.

Although, the algorithm consists of the closed-form equations, the formalizing of the computational process is more complicated than for the anchored walls. First, it requires the elastic solution to determine the distortion pattern of the wall, which depends on the number and aspect ratio of the panels and spacing of the sheathing fasteners. Even if the patterns are determined and tabulated for typical wall configurations without dead load, the distortion patterns will change if the dead load is applied.

6.6.3.4 Alternative Method to Predict Deflections of Unrestrained Walls

The complicated computational procedure constitutes the major drawback of the above-proposed method, because it is difficult to apply in everyday design. To develop a convenient design method, at least two ways can be chosen. First is to simulate various wall configurations under various load conditions and derive a simple empirical equation relating the basic wall parameters with the wall deflection, if possible. The other way is to simplify the calculation of the work of sheathing fasteners by introducing simplifying assumptions. For example, it can be assumed that the slip at the bottom plate contributes the same portion to the total shear wall deflection as the rigid body rotation estimated from experimental tests (Table 6. 18). The mode of the load-deflection curve can be estimated by calculating the work of sheathing fasteners at the bottom plate. It is assumed that performance of these fasteners governs the nonlinear shape (mode) of the load-deflection curve, and the fasteners along the top plate and studs increase the wall resistance linearly. Therefore, to approximate the load-deflection curve, a fudge factor can be applied to the modal curve that would account for the linear response of the sheathing connections.

The second approach was validated using parameters of the tested specimens. Deflection due to nail-slip at the bottom was found from Equation (6.137) and the corresponding force was found from Equation (6.126). The ultimate strength of the wall was found using equations from Section 6.5.5. The fudge factor was determined as a ratio of the ultimate strength of the wall to the force developed by the connections at the bottom plate. Results of the analysis are shown in Figure 6. 35 through Figure 6. 38 together with the observed load-deflection curves. For comparison purposes, the graphs include predicted and observed load-deflection curves of anchored shear walls.

It can be seen from the graphs that initial deflections are predicted with sufficient accuracy using the simplified method. Deflections in the yield region are extremely sensitive to the assumed force distribution among the fasteners. The analysis assuming the force distribution from elastic analysis tends to underestimate the wall load and overestimate the deflections; the force distribution at the strength limit state tends to overestimate the load and underestimate the deflections.

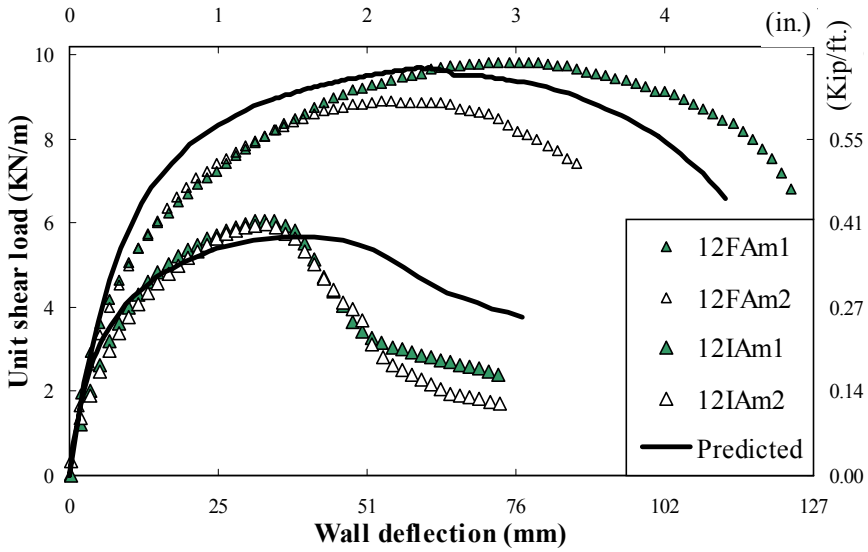

Figure 6. 35. Experimental and predicted load-deflection curves for 3.6-m (12-ft.) walls.

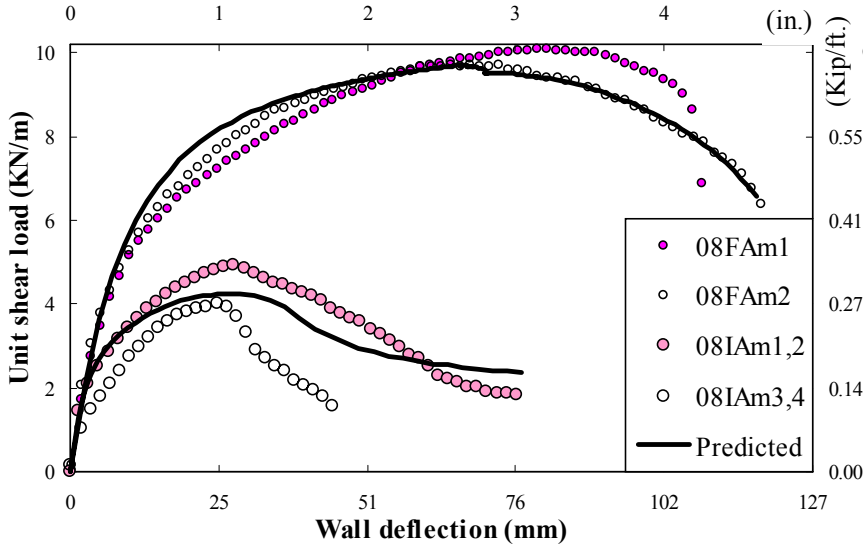

Figure 6. 36. Experimental and predicted load-deflection curves for 2.4-m (8-ft.) walls.

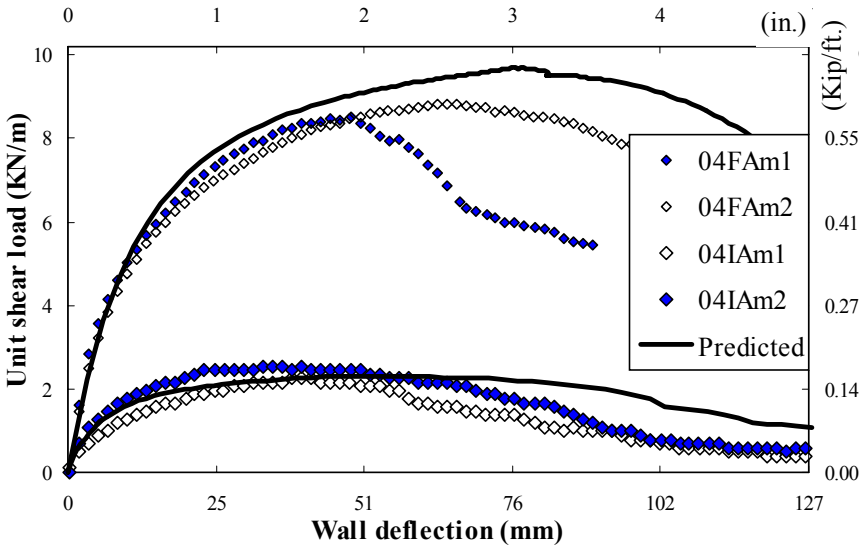

Figure 6. 37. Experimental and predicted load-deflection curves for 1.2-m (4-ft.) walls.

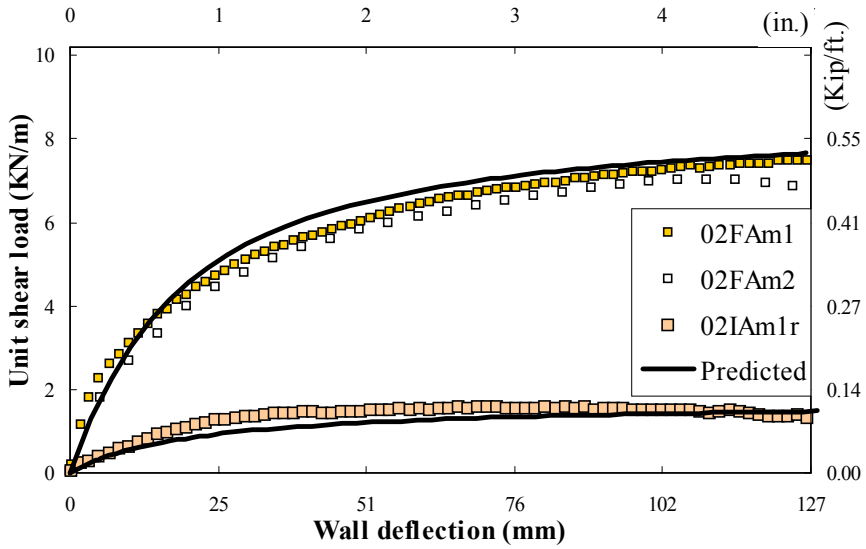

Figure 6. 38. Experimental and predicted load-deflection curves for 0.6-m (2-ft.) walls.

Chapter 7. Summary and Conclusions

7.1 Summary

Racking performance of light-frame timber shear walls was the focus of this dissertation. The objective of the study was to obtain performance characteristics of shear walls with various aspect ratios and overturning restraint via experimental testing and analytical modeling. If a building is designed to resist high wind and/or seismic forces, shear walls at each story often require mechanical fasteners, such as tie-down anchors and shear bolts, to provide continuous and complete load paths from the top of the building to the foundation. In this study, the fully-anchored shear walls represented the engineered walls. Unlike the engineered walls, conventionally-built walls are often secured to underlying structures only by nails that provide minimum overturning restraint. Sometimes, in construction practice an intermediate solution is applied: the bottom plates of the first story walls are attached to the foundation by shear bolts while tie-down devices at the end studs are omitted.

During this study, fifty-six full-size shear wall specimens with aspect ratios 4:1, 2:1, 1:1, and 2:3 were tested under unidirectional monotonic and reversed cyclic loading. Three overturning restraint conditions were applied: 1) Tie-down anchors at the end studs and shear bolts along the bottom plate, 2) Shear bolts along the bottom plate, and 3) Nailing along the bottom plate. The first condition represented engineered or segmented construction; the second and the third represented conventional construction practices (assuming attachment of the bottom plate was sufficient to prevent slippage or overturning of the wall as a rigid body). To obtain conservative estimates the specimens were tested in horizontal position, so that no dead load was applied in the wall plane. The sheathing – 11-mm (7/16in.) OSB - was attached on one wall side with 8d common nails. The nail-edge distance across the top and bottom plates varied from 10 mm (3/8 in.) to 19 mm (3/4 in.). Twelve walls were repaired after the initial tests and re-tested.

A mechanics-based model was advanced to predict the racking resistance of conventional multi-panel shear walls. A simple formula was proposed that produced

estimates of shear wall strength in good agreement with the experimental results. The effect of dead load on the shear wall strength was shown for a single-panel wall.

Deflections of engineered shear walls were predicted using the energy method combined with empirical formulae to account for load-deformation characteristics of sheathing-to-framing connections and overturning restraint. To obtain the nail-slip characteristics of the sheathing connections, thirty specimens with single fasteners were tested monotonically. The degradation part of the load-deflection curve was modeled to estimate the shear wall strength and deflections at the strength limit state and failure. Simple formulae were proposed to estimate the shear wall deflections at the design and the ultimate strength levels. The proposed formulae were validated through comparison with test results obtained during this study.

The following paragraphs provide a summary on performance of engineered and conventional shear walls observed during experimental tests and predicted using analytical models.

7.1.1 Engineered Walls

Based on eighteen monotonic and cyclic tests on walls with the full anchorage and analytical modeling, the following observations were made:

1. Two- and three- panel walls had the same shear modulus and strength, on unit length basis, provided the wood density of studs was equal. Mutual support of adjacent panels and the uniform wood density allowed the symmetrical distribution of sheathing displacements relative to the framing.

2. The monotonic strength of 1.2-m (4-ft.) single-panel walls was on average 12% lower and occurred at lower deflections than multi-panel walls. Low wood density of chords and/or compression perpendicular-to-grain at the end of the bottom plate due to higher axial forces in the chords was the reason for the earlier shear wall degradation.

3. Walls 0.6-m (2-ft.) long had 50% lower stiffness and strength relative to the long walls. However, their strength did not degrade at high deflections due to small displacement demand on sheathing-to-framing connections.

4. The sheathing nails withdrew from the low-density wood reducing the shear wall ductility and energy dissipation up to 50%. Similar nail withdrawal effect was observed during cyclic loading.

5. Under the cyclic loading, the initial stiffness and strength of the walls were not significantly different from the corresponding monotonic parameters. However, the load resistance of walls decreased on average 13% between the initial and stabilized cycles.

7.1.2 Conventional Walls

In the absence of tie-down anchors or dead load, the overturning moment applied at the bottom plate is transferred to the wall via the framing fasteners and sheathing-to-framing attachment. Effective resistance of framing nails driven into the end grain of the studs is negligible. Therefore, the walls act as unrestrained walls. Combining the results of twenty-seven monotonic and cyclic tests on walls with the intermediate anchorage, eleven monotonic and cyclic tests on walls with the nailed attachment, and analytical modeling, the following observations were made:

1. In the absence of dead load in the plane of the wall, unreasonably high density of nailing is required to prevent the specimen overturning during the test. If attached to the platform adequately, these walls were capable of developing the equivalent resistance to walls with intermediate anchorage.

2. Single-panel walls with aspect ratio 4:1 were the weakest but the most ductile. Single panel-walls with aspect ratio 2:1 were half as strong (on the unit length basis) as two-panel walls but failed at 50% larger deflections. Three-panel walls were 33% stronger than the two-panel walls.

3. Because of small edge distance, the wall resistance was controlled by the quality of sheathing attachment at the bottom plate. When the edge distance

along the bottom was reduced from 19 mm (3/4 in.) to 10 mm (3/8 in.), the strength, stiffness, and ductility of the wall was reduced 20% and more. In addition, the strength of the wall was positively correlated with the wood density of the bottom plate.

4. There was no significant difference in wall performance under the cyclic (initial envelope) and the monotonic loading conditions because there was no fatigue or withdrawal of sheathing nails from the wood. During stabilization cycles, the load resistance of walls decreased on average 15% when compared to the initial cycle resistence.

5. Repeated testing showed that the original wall resistance was restored with the replacement of the bottom plate after the first test. If the density of nailing along the bottom plate was doubled, the wall strength and deflection capacity was increased approximately 50%.

7.1.3 Strength Models

In the past, many models have been developed that predict the strength of fully-anchored shear walls with reasonable accuracy. Resistance of conventional shear walls has not been studied before. Therefore, the resistance of unrestrained shear walls became the focus of the analytical modeling in this study. The following observations were advanced:

1. Racking resistance of shear walls without dead load was considered. The static equilibrium of shear wall components was analyzed with the assumption that the joint tension forces between the studs and the bottom plate equal zero. The elastic strength model of a single-panel wall was derived and compared with the prediction of the commercial finite-element program SAP2000. According to these solutions, the single-panel segment of an unanchored wall develops only a small fraction of the resistance of the anchored wall depending on the height-to-length aspect ratio.

2. Static equilibrium of the multi-panel walls proved that the adjacent segments provide restraining effect to each other, increasing the wall shear resistance. Example analyses of shear walls with the aspect ratio of sheathing panels $\alpha = 2$ demonstrated that that in the elastic range the fourth segment of unrestrained wall already acts as a fully restrained shear wall. Therefore, the modeling of the strength limit state for only two- and three-panel unrestrained walls was of interest. Experimental results and the elastic analyses suggested that plastic yielding of the sheathing fasteners along the bottom plate controlled the wall strength. Therefore, in derivation of the ultimate strength model it was assumed that the fasteners along the bottom plate develop the full plastic strength while the other fasteners remain elastic.

3. The ultimate strength model of single-panel and multi-panel shear walls without dead load was derived assuming uniform and non-uniform distributions of forces between the sheathing fasteners along the bottom plate. The analysis of the two-panel walls with the aspect ratio of panels $\alpha = 2$ indicated that the assumption of the elastic performance of the nails along the studs and the top plate was reasonable. However, the analyses of the three-panel walls with the same panels indicated yielding of the fasteners along the top plate in the third panel. Although, the yielding of fasteners along the studs was neglected for simplicity during the analysis, {it was concluded that the third panel acts as the fully restrained wall at the strength limit state}.

4. At each step of the model derivations, simplified assumptions were tested, such as neglecting shear forces in the studs and the uniform distribution of the fastener forces along the bottom plate. The simplified approach produced remarkably accurate predictions, which correlate well with the test results of full-size shear walls. {The simple Equation (6.57) allows estimating the ultimate shear strength of the unrestrained multi-panel wall based on the aspect ratio of the sheathing panel and the number of panels in the wall.}

5. The elastic response of a single-panel shear wall segment under the dead load was considered. The correlation between the shear resistance and the amount

of dead load on the wall segment was determined. {The correlation demonstrated that there is little or no restraining effect of the dead load on the corner wall segments if the amount of dead load is estimated realistically.}

7.1.4 Predicting Shear Wall Deflections

To estimate nonlinear racking deflections of shear walls, the total deflection is represented as a superposition of the four components: a) deflection due to the chord bending, b) deflection due to sheathing shear, c) deflection due to rigid body rotation, and d) deflection due to slip of sheathing fasteners. The first two components are in linear proportion with the racking force developed by the sheathing fasteners. The other two components are non-linear and are determined using empirical data. The following observations were advanced for anchored walls:

1. The contribution of the sheathing fasteners' slip to the wall deflection was calculated using the energy method assuming the symmetrical distortion of shear wall according to McCutcheon's (1985) model. The nonlinear slip of individual fasteners until peak load was approximated by the asymptotic function; the post-capacity slip was approximated by a circular curve.

2. The parameters of the sheathing connections were determined via thirty experimental tests on single-fastener connections. {During the experiments on connections loaded perpendicular-to-grain of framing members, the deformations at peak load and at failure were reduced more than 40% when the edge distance was reduced from 19 to 10 mm (3/4 to 3/8 in.). This reduction was the reason for the decreased strength and deformation capacity of unrestrained shear walls.}

3. The contribution of the rigid body rotation into the wall deflection was determined from experimental tests. It was found that the resistance of the tie-down restraint introduced an additional non-linearity in the shear wall deflections. In this study, the non-linear rigid body rotation was approximated by an empirically fit asymptotic function. When real anchor forces do not exceed the asymptotic strength assumed in this relationship, the shear wall

performance is governed by the slip of the sheathing connections. Otherwise, the strength and deformation of the anchor connection is the controlling factor. To properly account for the effect of the tie-down restraint on the performance of single-panel shear walls, more accurate approximations can be suggested in the future research.

4. {The racking resistance of the multiple-panel shear walls can be accurately predicted via calculating the work of the sheathing fasteners on the racking displacement.} The deflections and the load capacity of these walls can be accurately predicted using simple formulae presented in Section 6.6.2.7. Introducing the limitations on the strength and deflection in the sheathing fastener load-deflection curve allows accurate approximation of the shear wall load via calculating the work of the sheathing fasteners.

5. To predict deflections of unrestrained shear walls, a similar approach was used as for the anchored walls. It was found that the shape of the load-deflection curve is governed by the slip of the sheathing connections along the bottom plate. The contribution of the sheathing connections along the top plate and studs was accounted for using a fudge factor assuming that these connections work in elastic region. The method was validated using experimental results.

7.2 Conclusions

Based on the observations and results of the analysis, the following conclusions were made about racking performance of light-frame shear walls:

7.2.1 Engineered (Fully-Anchored) Walls

1. The development of full-load capacity of the sheathing-to-framing connections was the governing factor of the shear wall racking performance.

2. Rigid body rotation had significant effect on the shear wall racking performance of single-panel walls.

3. Rigid body rotation contributed to the high deflections of narrow (0.6-m (2-ft.)) walls and was the controlling factor of the shear wall performance.
4. Chords with low wood density influenced the resistance of the walls.
5. Under the cyclic loading, the initial stiffness and strength of the walls were not significantly different from the corresponding monotonic parameters.

7.2.2 Conventional (Unrestrained) Walls

1. Withdrawal resistance of the nails attaching the shear wall to the base governed overturning resistance of shear walls with nailed attachment.
2. Current prescriptive requirements for the nailed attachment of walls to the underlying structures are not adequate and should be revised.
3. Strength, shear modulus, and ductility of the unrestrained walls were dependent on the aspect ratio and the number of panels in the wall.
4. Results of the study warrant a revision of current minimum requirements on the sheathing edge distances.
5. There was no significant difference in wall performance under the cyclic (initial envelope) and the monotonic loading conditions.
6. Repeated testing showed that the original wall resistance was restored with the replacement of the bottom plate after the first test.
7. If the density of nailing along the bottom plate was doubled, the wall strength and deflection capacity was increased approximately 50%.

7.2.3 Strength Models

1. Single-panel segments of an unanchored wall develop only a small fraction of the resistance of the anchored wall depending on the height-to-length aspect ratio.

2. Static equilibrium of the multi-panel walls proved that the adjacent segments provide the restraining effect to each other, increasing the wall shear resistance. In the elastic range the fourth segment of unrestrained wall acts as a fully-restrained shear wall segment. In the strength limit state, the third panel acts as a fully restrained shear wall segment.

3. Experimental results and the elastic analyses suggested that plastic yielding of the sheathing fasteners along the bottom plate controlled the strength of unrestrained walls.

4. A simplified equation was proposed that provides accurate estimate of ultimate shear strength of the unrestrained multi-panel wall based on the aspect ratio of the sheathing panel and the number of panels in the wall.

5. Correlation between dead load and shear resistance of the wall demonstrated that there is little or no restraining effect of the dead load on the corner wall segments if the amount of dead load resisted by the wall segment is estimated realistically.

7.2.4 Predicting Shear Wall Deflections

1. Increasing the minimum edge distance from 10 mm (3/8 in.) to 19 mm (3/4 in.) increases the displacement capacity (toughness) of the nailed connections leading to the higher strength and toughness of unrestrained shear walls.

2. When real anchor capacity exceeded the wall strength, the shear wall performance was governed by the slip of the sheathing connections. Otherwise, the strength and deformation of the anchor connection was the controlling factor.

3. The deflections and the load capacity of multi-panel shear walls can be accurately predicted using simple formulae.

4. For unrestrained shear walls, further development of the method or development of another method is needed.

7.3 Future Research

During this study, a limited number of shear wall configurations were tested. The fully-anchored conditions were represented by one type of tie-down device; one type and size of framing, sheathing, and fastener schedule was used in the experimental tests. The sheathing was attached on one side of the wall; effects of double-sided sheathing and interaction of different types of sheathing were not considered. (Currently, effects of gypsum wallboard sheathing on the racking performance of shear walls are being conducted for the City of Los Angeles at the University of California at Irvine.) Hold-down effect of adjacent transverse walls or corner walls was neglected.

Results of this study revealed the need for further research to investigate a number of different issues related to light-frame shear walls.

1. To predict the racking performance of shear walls with various sheathing types and sheathing fastener schedules, the experimental tests on various types of the sheathing connections are needed.

2. The test setup for the individual connections used in this study restrained the separation of the elements during the test, providing conditions for the connection performance that were more rigid than in shear wall specimens. Consequently, the stiffness of the tested connections might be overestimated. In future tests, the setup should be improved to reflect the conditions close to reality.

3. Further cyclic tests on the sheathing connections similar to those conducted by Gutshall (1994) should be conducted to estimate the influence of the cyclic loading on the connection performance parameters. The protocols for the cyclic tests on connections and shear walls should be similar and satisfy the following requirements: a) contain sufficient number of cycles to estimate the major events (yield, strength, and failure), b) be sufficiently short to eliminate the fasteners' fatigue at the large displacement amplitudes.

4. Performance of tie-down devices should become the subject of thorough investigation, because it often controls both strength and stiffness of single-panel shear wall segments. Various types of tie-down devices should be tested on the narrow walls to make their performance parameters available to the design profession. This is an important task, because many historical failures during earthquakes occurred due to structural damage at the narrow walls.

5. Analytical and experimental studies of conventional shear walls should be continued, and the effect of the dead load and other means of restraint should be investigated. Adequate nailed (or other fastener) attachment of these walls to the underlying structures should be determined and validated experimentally.

6. The analytical modeling of the unrestrained shear walls should be continued to enable the prediction of nonlinear shear wall deflections.

These are some of the topics that should be addressed before significant improvement of the design methodology can be achieved. Results of this study are one of the steps in this direction.

Literature Cited

[1] American Forest and Paper Association (AF&PA). 1993a. *National Design Specification® for Wood Construction, 1991 Edition*. ANSI/NF&PA NDS 1991. AF&PA, Washington, D.C.

[2] _____. 1993b. *Commentary on the National Design Specification® for Wood Construction, Commentary on the 1991 Edition*. AF&PA, Washington, D.C.

[3] _____. 1996. *Wood Frame Construction Manual for One- and Two-family Dwellings. 1995 SBC High Wind Edition.* AF&PA, Washington, D.C.

[4] APA – The Engineered Wood Association. 1995. *Design Capacities of APA Performance Rated Structural-Use Panels*. Technical Note No. 375B. APA, Tacoma, WA.

[5] American Society for Testing and Materials. 1995. Proposed Standard Method for Dynamic Properties of Connections Assembled with Mechanical Fasteners (*4th Draft*). ASTM, Philadelphia, PA.

[6] _____. 1998a. ASTM D 1761 – 88 Standard Test Methods for Mechanical Fasteners in Wood. *Annual Book of ASTM Standards*. ASTM, Philadelphia, PA.: 268-279.

[7] _____. 1998b. ASTM E 564 – 95 Standard Practice for Static Load Test for Shear Resistance of Framed Walls for Buildings. *Annual Book of ASTM Standards*. ASTM, Philadelphia, PA: 556-559.

[8] _____. 1998c. ASTM E 72 – 95 Standard Test Methods of Conducting Strength Tests of Panels for Building Construction. *Annual Book of ASTM Standards*. ASTM, Philadelphia, PA: 392-402.

[9] _____, 1998d. ASTM F 1575 – 95 Standard Test Method for Determining Bending Yield Moment of Nails. *Annual Book of ASTM Standards*. ASTM, Philadelphia, PA: 365-368.

[10] _____. 1998e. ASTM F 1667 – 95 Standard Specification for Driven Fasteners: Nails, Spikes, and Staples. *Annual Book of ASTM Standards*. ASTM, Philadelphia, PA: 369-378.

[11] Andreason, K. R. and J. D. Rose. 1994. *Northridge, California Earthquake.* APA Report T94-5. American Plywood Association, Tacoma, WA.

[12] Applied Technology Council (ATC). 1980. Proceedings of Workshop on Design of Horizontal Wood Diaphragms. ATC-7-1. ATC, Redwood City, CA.

[13] Birch, J. 1998. *Personal Communication.* Statistical Consulting Center, Virginia Polytechnic Institute and State University, Blacksburg, VA.

[14] Building Seismic Safety Council. 1998. NEHRP Recommended Provisions for Seismic Regulations for New Buildings and Other Structures. 1997 Edition. BSSC, Washington, D.C.

[15] Carney, J. M. 1975. Bibliography on Wood and Plywood Diaphragms. *Journal of Structural Division,* ASCE, Vol. 101, No. ST11: 2423-2436.

[16] Ceccotti, A. (Ed.) 1990. *Structural Behavior of Timber Constructions in Seismic Zones*. Commission of the European Communities and Florence University, Florence, Italy.

[17] Ceccotti, A. and A. Vignoli. 1990. Engineered timber structures: an evaluation of their seismic behavior. Proceedings of 1990 International Timber Engineering Conference, Tokyo, Japan: 946-953.

[18] Chui, Y.H., Ni, C. and L. Jiang. 1998. Finite element model for nailed wood joints under reversed cyclic load. *Journal of Structural Engineering*, ASCE, Vol. 124 (1): 98-103.

[19] Chui, Y. H. and C. Ni. 1997. Load-Embedment Response of Timber to Reversed Cyclic Load. *Wood and Fiber Science*, SWST, 29(2): 148-160.

[20] Commins, A. D. and R. C. Gregg. 1994. Cyclic Performance of Tall-Narrow Shearwall Assemblies. Simpson strong-Tie Co., Pleasanton, CA.

[21] Commins, A. D. and R. C. Gregg. 1996. Effect of Hold-downs and Stud-Frame Systems on the Cyclic Behavior of Wood Shear Walls. Simpson strong-Tie Co., Pleasanton, CA.

[22] Comite' European de Normalization (CEN). 1995. "Timber Structures – Test Methods – Cyclic Testing of Joints Made with Mechanical Fasteners (*Draft*)." EN TC 124.117, European Committee for Standardization, Brussels, Belgium.

[23] Computers and Structures, Inc. (CSI). 1997. SAP®2000. Integrated Structural Analysis and Design Software. SCI, Berkeley, CA.

[24] Deam, B. L. 1997. Seismic Ratings for Residential Timber Buildings. Building Research Association of New Zealand, Study Report SR 73. Judgeford, Wellington, New Zealand.

[25] Dean, J. A., W. G. Stewart, and A. J. Carr. 1986. The Seismic Behavior of Plywood Sheathed Shearwalls. *Bulletin of the New Zealand National Society for Earthquake Engineering*, Vol. 19, No. 1: 48-63.

[26] Dean, J. A. 1988. *The Ductility of Nailed Sheathing Joints in Timber Frame Shear Walls.* Civil Engineering Report CE 88/14, University of Canterbury, New Zealand.

[27] Diekmann, E. F. 1995. Diaphragms and Shearwalls. In: *Wood Engineering and Construction Handbook.* K. F. Faherty and T. G. Williamson (Eds.), McGraw-Hill, New York, NY.

[28] Diekmann, E. F. 1997. Design and Design Code issues in the design of Diaphragms and Sheawalls. In: *Earthquake Performance and Safety of Timber Structures*. G. C. Foliente (Ed.), Forest Products Society, Madison, WI.

[29] Dinehart, D. W. and H. W. Shenton III. 1998. Comparison of Static and Dynamic Response of Timber Shear Walls. *Journal of Structural Engineering*, ASCE, 124(6): 686-695.

[30] Dolan, J. D. 1989. *The Dynamic Response of Timber Shear Walls*. Thesis submitted in partial fulfillment of the requirements for the degree of Doctor of Philosophy, University of British Columbia, Vancouver, Canada.

[31] Dolan, J. D. 1994. Proposed Test Method for Dynamic Properties of Connections Assembled with Mechanical Fasteners. *ASTM Journal of Testing and Evaluation.* 22(6): 542-547.

[32] Donea, J., G. Magonette, P. Negro, P. Pegon, A. Pinto, and G. Verzeletti. 1996. Pseudodynamic Capabilities of the ELSA Laboratory for Earthquake Testing of Large Structures. *Earthquake Spectra.* 12(1): 163-180.

[33] Douglas Fir Plywood Association. 1948. The lateral Bearing Strength of Nailed Plywood Joints. Technical Data on Douglas Fir Plywood for Engineers and Architects. Douglas Fir Plywood Association, Tacoma, WA.

[34] Easley, J. T., M. Foomani, and R. H. Dodds. 1982. Formulas for Wood Shear Walls. *Journal of Structural Division*, ASCE, 108(11): 2460-2478.

[35] Ehlbeck, J. 1979. *Nailed Joints in Wood Structures. Bulletin No.166.* Virginia Polytechnic Institute and State University Wood Research and Wood Construction Laboratory, Blacksburg, VA.

[36] Falk, R. H. and R. Y. Itani. 1989. Finite Element Modeling of Wood Diaphragms. *Journal of Structural Engineering*, ASCE, 115(3): 543-559.

[37] Ficcadenti, S. J., T. A. Castle, D. A. Sandercock, and R. K. Kazanjy. 1995. Laboratory Testing to Investigate Pneumatically Driven Box Nails for the Edge Nailing of 3/8" Thick Plywood Shear Walls. In: *Proceedings, 64th SEAOC Annual Convention; October 19-21*, Structural Engineers Association of California, Indian Wells, CA.

[38] Foliente, G. C. (Ed.) 1994. Analysis, Design and Testing of Timber Structures under Seismic Loads. Proceedings of a Research Needs Workshop. University of California, Forest Products Laboratory, Richmond, CA.

[39] Foliente, G. C. 1994. Summary of Research Needs. In: *Analysis, Design and Testing of Timber Structures under Seismic Loads. Proceedings of a Research Needs Workshop*. University of California, Forest Products Laboratory, Richmond, CA.: 111-120.

[40] Foliente, G.C. 1995. Hysteresis modeling of wood joints and structural systems. *Journal of Structural Engineering*, ASCE, Vol. 121 (6): 1013-1022.

[41] Foliente, G. C. 1996. Issues in Seismic Performance Testing and Evaluation of Timber Structural Systems. In: *Proceedings of the 1996 International Wood Engineering Conference, New Orleans,* 1:29-36.

[42] Foliente, G. C. (Ed.) 1997. *Earthquake Performance and Safety of Timber Structures*. Forest Products Society, Madison, WI.

[43] Foliente, G. C. and E. G. Zacher. 1994. Performance Tests of Timber Structural Systems under Seismic Loads. In: Foliente, G.C. ed., *Analysis, Design and Testing of Timber Structures under Seismic Loads. Proceedings of a Research Needs Workshop.* University of California Forest Products Laboratory, Richmond, CA.: 21-86.

[44] Foschi, R. O. 1974. Load-slip characteristic of nails. *Wood Science*. Vol. 7 (1): 69-76.

[45] Foschi, R. O. 1977. Analysis of Wood Diaphragms and Trusses, Part One: Diaphragms. *Canadian Journal of Civil Engineering*, 4(3): 345-352.

[46] Forest Products Society. 1998. *Recent Advances in Understanding Full-scale Behavior of Wood Buildings*. Forest Products Society, Madison, WI.

[47] Gopu, V. K. A. (Ed.). 1996. Proceedings of the 1996 International Wood Engineering Conference, New Orleans, LA.

[48] Gosstroy USSR. 1983. Standard for Design of Timber Structures. Building Code II-25-80. Stroyizdat, Moscow, USSR.

[49] Gray, R. G. and E. G. Zacher. 1988. Dynamic Testing of Wood Shear Panels. *Architecture*, 77(3): 121-124.

[50] Gupta, A. K. (Ed.). 1981. *Seismic Performance of Low-Rise Buildings – State-of-the-Art and Research Needs*. American Society of Civil Engineers, New York, NY.

[51] Gupta, A. K. and G. P. Kuo. 1985. Behavior of Wood-Frame Shear Walls. *Journal of Structural Engineering*, ASCE, 111(8): 1722-1733.

[52] Gupta, A. K. and G. P. Kuo. 1987. Wood-Frame Shear Walls with Uplifting. *Journal of Structural Engineering*, ASCE, 113(2): 241-259.

[53] Gutkowski, R. M. and A. L. Castillo. 1988. Single- and Double- Sheathed Wood Shear Wall Study, *Journal of Structural Engineering*, ASCE, 114(6): 1268-1284.

[54] Gutshall, S. T. 1994. *Monotonic and Cyclic Short-term Performance of Nailed and Bolted Timber Connections*. Master's Thesis. Virginia Polytechnic Institute and State University, Blacksburg, VA.

[55] Hanson, D. 1990. *Shear Wall and Diaphragm Cyclic Load Testing, Cyclic Shear Fastener Testing, and Panel Durability Performance Testing of Weyerhaeuser Sturdy-Wood Oriented Strandboard.* Report submitted to the chief Structural Engineer, State of California Office of the State Architect, Structural Safety Section.

[56] He, M. 1997. *A Study of Wood Based Shear Walls Sheathed with Oversize Oriented Strand Board Panels.* Master's Thesis. University of British Columbia, Vancouver, Canada.

[57] Heine, C. P. 1997. *Effect of Overturning Restraint on the Performance of Fully Sheathed and Perforated Timber Framed Shear Walls*. Master's Thesis. Virginia Polytechnic Institute and State University, Blacksburg, VA.

[58] International Code Council (ICC) .2000. *International Building Code for One- and Two-Family Dwellings*. ICC, Falls Church, VA.

[59] International Conference of Building Officials. 1997. *Uniform Building Code*. ICBO, Whittier, CA.

[60] ISO. 1998. Timber structures – Joints made with mechanical fasteners – Quasi-static reversed-cyclic test method. WG7 Draft. ISO TC 165 Secretariat, Standards Council of Canada.

[61] Itani, R. Y. and C. K. Cheung. 1984. Nonlinear Analysis of Sheathed Wood Diaphragms. *Journal of Structural Engineering,* Vol. 110(9): 2137-2147.

[62] Itani, R. Y. and K. F. Faherty (Eds.). 1984. Structural Wood Research – State-of-the-Art and Research Needs. American Society of Civil Engineers, New York, NY.

[63] Johnson, A. C. 1997. *Monotonic and Cyclic Performance of Long Shear Walls with Openings*. Master's Thesis. Virginia Polytechnic Institute and State University, Blacksburg, VA.

[64] Kamia, F. 1988. Nonlinear Earthquake Response Analysis of Sheathed Walls by a Computer-Actuator on-line System. In: *Proceedings, International Conference on Timber Engineering,* Vol. 1: 838-847.

[65] Kamia, F., K. Sugimoto, and N. Mii. 1996. Pseudo Dynamic Test of Sheathed Wood Walls. *Proceedings of the 1996 International Wood Engineering Conference, New Orleans,* 2: 187-194.

[66] Karacabeyli, E. 1996. Quasi-Static Reversed-Cyclic Testing of Nailed Joints. *International Council for Building Research Studies and Documentation,* Working Commission W18 – Timber Structures, Meeting Twenty-Nine. Bordeaux, France.

[67] Karacabeyli, E. and A. Ceccotti. 1996. Test Results on the Lateral Resistance of Nailed Shear Walls. *Proceedings of the 1996 International Wood Engineering Conference, New Orleans,* 2: 179-186.

[68] Leiva, L. 1994. The influence of Boundary Conditions on the Racking Resistance of Timber-Framed Shear Walls. Proceedings IUFRO/S5.02 Timber Engineering Meeting, 05-07 July 1994, Sydney, Australia.

[69] Line, P. 1998-2000. American Wood Council, American Forest and Paper Association. *Personal Communication.*

[70] Medearis, K. and D. H. Young. 1964. Energy Absorption of Structures under Cyclic Loading. *Journal of Structural Division ASCE* 90(ST1): 61-91.

[71] Merrick, D. S. 1999. Cyclic Comparison Testing of Light Wood Framed Shear Walls. San Jose State University. http://www.engr.sjsu.edu/dmerrick/shearwalls/.

[72] McCutcheon, W. J. 1985. Racking Deformations in Wood Shear Walls. *Journal of Structural Engineering*. ASCE. Vol. 111(2), 257-269.

[73] Murakami, M., P. J. Moss, A. J. Carr, and M. Inayama. 1999. Formulae to Predict Non-Linear Behavior of Sheathed Walls with Any Nailing Arrangement Pattern. *In*: Walford, G. B. and Gaunt, D. J. (Ed.) Proceedings of the Pacific Timber Engineering Conference. Rotorua, New Zealand, Vol. 3: 189-196.

[74] National Association of Homebuilders (NAHB). 1990. Manufactured Housing Shearwall Tests Using ASTM Methods E72 and E564. NAHB Research Center, Upper Marlboro, MD.

[75] _____. 1996. Builder Practices Database. NAHB Research Center, Upper Marlboro, MD.

[76] Oliva, M. G. 1990. Racking behavior of wood-framed gypsum panels under dynamic load. Report No.UCB/EERC-85/06, Earthquake Research Center, University of California, Berkeley, CA.

[77] Ott, R. L. 1992. *An Introduction to Statistical Methods and Data Analysis*. Duxbury Press, Belmont, CA.

[78] Patton-Mallory, M., R. M. Gutkowski, and L. A. Soltis. 1984. Racking Performance of Light-Frame Walls Sheathed on Two Sides. *Research Paper FPL 448,* U.S. Department of Agriculture, Forest Service, Forest Products Laboratory, Madison, WI.

[79] Patton-Mallory, M. and W. J. McCutcheon. 1987. Predicting Racking Performance of Walls Sheathed on Both Sides. *Forest Products Journal*, Vol. 37(9): 27-32.

[80] Peterson, J. 1983. Bibliography on Lumber and Wood Panel Diaphragms. *Journal of Structural Engineering*, ASCE, 111(10): 2227-2239.

[81] Polensek, A. 1976. Finite Element Analysis of Wood-Stud Walls. *Journal of Structural Engineering*, ASCE, 102(7): 1317-1335.

[82] Porter, M. L. 1987. Sequential Phase Displacement (SPD) Procedure for TCCMAR testing. In: *Proceedings, 3rd Meeting of the Joint Technical Coordination Committee on Masonry Research.* U.S. - Japan Coordinated Earthquake Research Program, Tomamu, Japan.

[83] Reyer, E. and O. A. Oji. 1991. Background Document on Test Methods for Timber Structures under seismic actions. *Paper prepared for RILEM TC 109 TSA Group Meeting*, London, UK.

[84] RILEM TC 109-TCA. 1994. *Timber Structures in Seismic Regions: RILEM State-of-the-Art Report. Materials and Structures.* 27:157-184.

[85] Robertson, G. F. 1980. Discussion of "Racking Strength of Light-Frame Nailed Walls" by Tuomi, R. L. and W. J. McCutcheon. *Journal of Structural Engineering*, ASCE, 106(9), 1981-1985.

[86] Rose, J. D. 1998. *Preliminary Testing of Wood Structural Panel Shear Walls under Cyclic (Reversed) Loading. APA Research Report 158*. APA – The Engineered Wood Association, Tacoma, WA.

[87] Skaggs, T. D. and J. D. Rose. 1996. Cyclic Load Testing of Wood Structural Panel Shear Walls. *Proceedings of the 1996 International Wood Engineering Conference, New Orleans,* 2:195-200.

[88] Schmidt, B. L., R. J. Nielsen and R. R. Linderman. 1994. Narrow Plywood Shear Panels. *Earthquake Spectra* 10(3): 569-588.

[89] Southern Building Code Congress International, Inc. 1991. *Standard Building Code*. SBCC, Birmingham, AL.

[90] Soltis, L. A., D. S. Gromala, and K. L. Tuomi. 1981. Seismic Performance of Low-Rise Wood Buildings. In: Gupta, A. K. (Ed.) *Seismic Performance of Low-Rise Buildings – State-of-the-Art and Research Needs*. American Society of Civil Engineers, New York, NY.:78-91.

[91] Soltis, L. A. and R. H. Falk. 1992. "Seismic Performance of Low-Rise Wood Buildings. Literature Review". In: *The Shock and Vibration Digest*. USDA, Forest Service, Forest Product Laboratory. Madison, WI. 24(12): 3-6.

[92] Stern, E. G. 1950. Deterioration of Green Wood Along Steel-Nail Shank and Its Influence in the Nail-Holding Properties. *The Virginia Journal of Science*, July 1950: 200-218.

[93] Stern, E. G. 1950. *Better Utilization of Wood through Assembly with Improved Fasteners. Bulletin No.38.* Virginia Polytechnic Institute Wood Research Laboratory, Blacksburg, VA.

[94] Stewart, W. G. 1987. *The Seismic Design of Plywood Sheathed Shearwalls.* Thesis submitted in partial fulfillment of Ph.D. degree, University of Canterbury, New Zealand.

[95] Structural Engineers Association of Southern California. 1996. *Standard Method of Structural Connector or Sub-Assembly*. SEAOSC, Whittier, CA.

[96] Structural Engineers Association of California. 1997. *Guidelines for Wood Diaphragms and Shear Walls.* Ed.: Vaughn, W.B., SEAOC, Sacramento, CA.

[97] Structural Engineers Association of Southern California. 1997a. *Standard Method of Cyclic (Reversed) Load Test for Shear Resistance of Framed Walls for Buildings*. SEAOSC, Whittier, CA.

[98] Structural Engineers Association of Southern California. 1997b. *Standard Method of Cyclic (Reversed) Load Test for Anchors in Concrete or Grouted Masonry*. SEAOSC, Whittier, CA.

[99] Sugiyama, H. and S. Suzuki. 1975a. Experimental Study of the effect of Racking Test Methods, Sheathing Materials and Nailing upon the Strength properties of the Platform Construction Wall Subjected to Lateral Force (Part 1). Transactions of A.I.J. No. 232.

[100] Sugiyama, H. and S. Suzuki. 1975b. Experimental Study of the effect of Racking Test Methods, Sheathing Materials and Nailing upon the Strength properties of

the Platform Construction Wall Subjected to Lateral Force (Part 2). Transactions of A.I.J. No. 232.

[101] Sugiyama, H., T. Uchako, N. Andoh, T. Arima, S. Hirano, and N. Nakamura. 1988. Comparison of lateral stiffness of frame obtained from full-scale test and that estimated by racking tests in Japanese type of wooden frame construction. Proceedings of 1988 International Conference on Timber Engineering, Seattle, WA, 1:804-810.

[102] Sugiyama, H. and T. Matsumoto. 1994. Empirical Equations for the Estimation of Racking Strength of a Plywood Sheathed Shear Wall with Openings. *Mokuzai Gakkaishi,* Vol. 39, No. 8: 924-929.

[103] Takanashi, K. 1975. Nonlinear earthquake response analysis of structures by a computer-actuator on-line system. Bulletin of Earthquake Resistance Construction, No. 8., Institute of Industrial Science, University of Tokyo, Tokyo, Japan.

[104] Thurston, S. J. and Flack, P. F. 1980. Cyclic Load Performance of Timber Sheathed Bracing Walls. Central Laboratories Report 5-80/10, Ministry of Works and Development, Wellington, New Zealand.

[105] Tissell, J. R. 1990. *Structural Panel Shear Walls*. *APA Research Report 154*. American Plywood Association, Tacoma, WA.

[106] Tissell, J. R. and J. Rose. 1994. *Wood Structural Panel Sheathing for Narrow-Width Wall Bracing*. *APA Research Report 156*. American Plywood Association, Tacoma, WA.

[107] Tuomi, R. L. and W. J. McCutcheon. 1978. Racking Strength of light-frame nailed walls. *Journal of Structural Engineering*, ASCE, 104(7): 1131-1140.

[108] Wheat, L. and J. M. Calixto. 1994. Nonlinear Analysis of Two-Layered Wood Members with Interlayer Slip. *Journal of Structural Engineering*, ASCE, 120(6): 1909-1921.

[109] Wen, Y. K. 1976. Method for Random Vibration of Hysteretic Systems, *Journal of Engineering Mechanics Division,* ASCE, Vol.102, No. EM2: 249-263.

[110] Wen, Y. K. 1980. Equivalent Linearization for Hysteretic Systems under Random Excitation. *Journal of Applied Mechanics*. Vol. 47: 150-154.

[111] White, M. W. 1995. *Parametric Study of Timber Shear Walls*. Ph.D. Dissertation. Virginia Polytechnic Institute and State University. Blacksburg, VA.

[112] White, M. W. and J. D. Dolan. 1995. Nonlinear Shear-Wall Analysis. *Journal of Structural Engineering*, ASCE, 121(11): 1629-1635.

[113] Wolfe, R. W. 1983. *Research Paper FPL 439 – Contribution of Gypsum Wallboard to Racking Resistance of Light-Frame Walls.* United States Department of Agriculture, Forest products Laboratory, Madison, WI.

[114] Wolfe, R. W. and R. C. Moody. 1991. North American Structural Performance Tests of Low-Rise Wood-Frame Building Systems. Proceedings of Workshop on Full-Scale Behavior of Wood-Framed Buildings in Earthquakes and High Winds, Walford, UK, XXII-1-19.

[115] Zacher, E. G. and R. G. Gray. 1989. Lessons Learned from Dynamic Tests of Shear Panels. In: A.H-S. Ang, (Ed.) *Structural Design, Analysis and Testing*, American Society of Civil Engineers, New York, NY.: 134-142.

[116] Zacher, E. G. 1994. "Past Seismic Performance of Timber Buildings". In: *Analysis, Design and Testing of Timber Structures under Seismic Loads. Proceedings of a Research Needs Workshop*. University of California, Forest Products Laboratory, Richmond, CA.: 3-8.

Vita

(July 2000)

Alexander Salenikovich is a native of Kirov, Russia. He graduated with honors from Kirov Polytechnic Institute in 1983 with a master's degree in Civil Engineering. After graduation, he worked at industrial and residential construction sites. In 1985, Alexander returned to Kirov Polytechnic Institute to serve on the faculty as a research engineer in the Department of Structural Engineering. His duties included laboratory and field tests, analysis, design, and practical implementation of various structural products, preservation of historical wood structures, and teaching a lab course in Wood Engineering.

In 1995, Salenikovich came to Virginia Tech for one year to act as a faculty advisor for a group of ten Russian exchange students. After the completion of the exchange program, he enrolled in the graduate school at Virginia Tech and began his work on a Ph.D. in Timber Engineering.

In 1999, Salenikovich received the first-place Wood Award from the Forest Products Society and the first place in the SWST Student Poster competition for the outstanding graduate research in the field of wood science and forest products. In March 2000, he received the A. B. Massey Award in recognition of superior performance and professionalism while a graduate student in the College of Natural Resources at Virginia Tech. Salenikovich is a member of the SWST Committee on International Relations (since 1996), the Forest Products Society (since 1997), and the Honor Societies of Phi Kappa Phi (since 1997) and Gamma Sigma Delta (since 2000).

Starting August 2000, Salenikovich is appointed as a postdoctoral research assistant in the Department of Forest Products at the Mississippi State University.